

CALIFORNIA INSTITUTE OF TECHNOLOGY

EARTHQUAKE ENGINEERING RESEARCH LABORATORY

**DEVELOPMENT OF
FINITE ELEMENT PROCEDURES
FOR FLUID-STRUCTURE INTERACTION**

By

Wing Kam Liu

EERL 80-06

A Report on Research Conducted Under Grants
from the National Science Foundation and
the Electric Power Research Institute

Pasadena, California
August, 1980

This investigation was sponsored by Grants No. PFR79-00712 and PFR77-23687 from the National Science Foundation, Division of Problem-Focused Research Applications and the Electric Power Research Institute under the supervision of Professor Thomas J.R. Hughes. Any opinions, findings, and conclusions or recommendations expressed in this publication are those of the author and do not necessarily reflect the views of the National Science Foundation or the Electric Power Research Institute.

DEVELOPMENT OF FINITE ELEMENT PROCEDURES
FOR FLUID-STRUCTURE INTERACTION

Thesis by
Wing Kam Liu

In Partial Fulfillment of the Requirements
for the Degree of
Doctor of Philosophy

California Institute of Technology
Pasadena, California
1981

(Submitted August 27, 1980)

-ii-

To my Parents

ACKNOWLEDGMENTS

I wish to extend my deepest gratitude to the following:

- to my advisor: Professor T.J.R. Hughes for his assistance, understanding, careful guidance and encouragement in all aspects of my thesis;
- to my undergraduate advisor: Professor A. B. Schultz for his motivation of my pursuing this degree;
- to my former excellent teacher: Professor T. B. Belytschko for his motivation of my interest in finite element methods;
- to my colleague: Dr. T. K. Zimmermann for his advice and encouragement in the development of part of this thesis;
- to the Caltech SOPS (Society of Professional Students), the staff, and faculty for their help and sharing;
- to the Computing Center of the California Institute of Technology for providing computing services;
- to Ruth Stratton for expending so much care and energy in the typing of the manuscript;
- to the Electric Power Research Institute and the National Science Foundation for their interest and support of this study; and finally,
- to my Parents whose unending support and encouragement have brought me this far.

ABSTRACT

In this thesis the development of finite element procedures for fluid-structure interaction problems is presented. The areas upon which attention is focused are: numerical transient algorithms which emphasize implicit-explicit finite element concepts; finite element kinematical descriptions for modelling fluid subdomains in fluid-structure interaction problems; finite element methodology for nearly incompressible fluids and solids, and beam, plate and shell structures based upon theories which include transverse shear deformations; and finite rotation effects in numerical integration of rate constitutive equations arising in large-deformation analysis. All these nonlinear methodologies have been integrated into a working finite element computer code. A number of numerical examples are presented to demonstrate the effectiveness of these approaches.

TABLE OF CONTENTS

<u>Chapter</u>	<u>Page</u>
1. INTRODUCTION	
I. General Remarks and Previous Studies	1
I-A. Introduction	1
I-B. Structural/Solid Mechanics	2
I-C. Fluid Mechanics	3
I-D. Interface Techniques	3
I-E. Transient Analysis	4
II. Scope of the Present Investigation	7
References for Chapter 1	10
2. FUNDAMENTAL CONTINUUM MECHANICS THEORY AND FINITE ELEMENT FORMULATION	16
I. General Description of Governing Equations	16
I-A. General Theory of Mixed Lagrangian-Eulerian Description	17
I-B. Balance Laws (Mass and Momentum)	23
II. Formal Statement of the Initial/Boundary-Value Problem	27
II-A. Mixed Description	27
III. Linearized Equations of Motion Using Lagrangian Description	29
III-A. Constitutive Equation	29
III-B. Linearized Variational Equation	34
IV. Galerkin/Finite Element Formulation and Matrix Equations	36
IV-A. Generalized Mixed Lagrangian-Eulerian Linearized Variational Equation	36
IV-B. Matrix equations	37
IV-C. Definition of \hat{d}_{ijkl} for Incompressible Fluid and Slightly Compressible Fluid	44

<u>Chapter</u>		<u>Page</u>
	References for Chapter 2	47
3.	NUMERICAL SOLUTION TECHNIQUES	50
	I. Numerical Integration of the Variational Equations	50
	I-A. Selective Integration	50
	I-B. "Upwind" Finite Elements by Modifying the Standard Gauss-Legendre Rules	58
	I-C. Mass Matrix	63
	II. Implementation of Lagrangian-Eulerian Finite Elements	64
	II-A. Generalized Description Using Isoparametric Finite Elements	65
	III. Numerical Integration of Rate Constitutive Equations	67
	III-A. Numerical Algorithms for Rotational Term	68
	III-B. Numerical Algorithms for Integration of Equation (IIIA-10)	70
	IV. Transient Analysis Techniques for the Variational Equations	76
	IV-A. Temporal Integration of the Variational Equations	78
	IV-B. Computer Implementation of Equations (IVA-1) through (IVA-29)	81
	References for Chapter 3	84
4.	NONLINEAR FINITE ELEMENT ANALYSIS OF SHELLS	92
	I. Introduction	92
	II. Geometric and Kinematic Descriptions	94
	II-A. Geometry	94
	II-B. Kinematics	99
	II-C. Laminar Coordinate Systems	102
	II-D. Fiber Coordinate Systems	102
	III. Integration of Constitutive Equations	107
	III-A. Numerical Algorithms	107

<u>Chapter</u>	<u>Page</u>
IV. Element Arrays	109
IV-A. Material Tangent Matrix	109
IV-B. Strain-Displacement Matrix	110
IV-C. Transformation Matrices	111
IV-D. Tangent Stiffness Matrix and Internal Force Vector	112
IV-E. External Force Vector	113
IV-F. Stress Resultants	115
IV-G. Mass Matrix	117
V. Shell Elements	118
V-A. Reduced Integration Lagrangian Elements and Heterosis Elements	118
VI. Sample Problems	121
References for Chapter 4	140
5. NUMERICAL EXAMPLES OF FINITE ELEMENT ANALYSIS OF INCOMPRESSIBLE VISCOUS FLOWS BY THE PENALTY FUNCTION FORMULATION	144
I. Introduction	144
II. Sample Problems	147
III. Remark on Slightly Compressible Formulation for Viscous Fluid Flow	192
References for Chapter 5	193
6. APPLICATION TO FLUID-STRUCTURE INTERACTION	196
I. Introduction	196
II. Contact/Sliding Element	198
III. Numerical Examples	201
References for Chapter 6	218
7. SUMMARY AND SUGGESTIONS FOR FURTHER DEVELOPMENT	220
References for Chapter 7	223

Chapter 1

INTRODUCTION

I. General Remarks and Previous Studies

I-A. Introduction

Significant attention has been devoted to the development of fluid-structure interaction procedures over the last two decades. However, many fluid-structure interaction problems are of such complexity that the method of analysis must be numerical in nature. Finite element methods enable the modelling of such complicated problems.

The term "fluid-structure interaction" refers to either (1) fluids contained within structures, or (2) structures surrounded by fluids. Examples of (1) are the seismic response of ground supported, cylindrical liquid storage tanks, aerospace applications such as rocket fuel tanks, and the response of a dam due to sudden acceleration into a contiguous reservoir. Examples of (2) are the transient motion of submerged or partially submerged structures, flow-induced vibrations, normal and abnormal operations of light water reactor and pressurized water reactor cores.

The applications of finite element methods to fluid-structure interaction problems have been made by several investigators. One of the related current research areas is seismic analysis and design procedures for ground supported, cylindrical liquid storage tanks [1,2]. Another application is the use of toroidal tanks as pressure-suppression pools in certain designs of boiling water reactors [3]. Presently used methods are mostly based on linear small motion response and do not take satisfactory account of nonlinear effects. For example, in the response

of tanks to strong earthquakes, lift-off, finite-amplitude sloshing, and nonlinear and inelastic response are important.

Nonlinear fluid-structure finite element procedures have been proposed by Belytschko et al. [4-9] and Donea et al. [10,11] among others. However, most of these studies are oriented to particular applications, specifically nuclear reactors, and these procedures are not flexible enough for a wide class of engineering applications.

The ability to solve general classes of fluid-structure interaction problems involving finite deformations depends upon the ability to solve the corresponding uncoupled fluid and structural problems, and also the ability to "interface" fluid and structural subdomains. Even though the development of general finite element procedures for fluid-structure interactions is obviously too complicated to handle as one thesis topic, the author's goal is to make significant strides in this direction.

I-B. Structural/Solid Mechanics

The success of finite element methods in structural/solid mechanics is well known. The main thrusts of research herein were directed toward both low- and higher-order, two- and three-dimensional continuum elements with particular reference to nearly incompressible materials [12-15,19-21] and the development of effective general thick/thin shell elements based upon theories accounting for transverse shear deformation [16-18]. Attention is also focused on reduced/selective integration and allied concepts which have facilitated the development of simple yet effective "displacement" models for these constrained media applications [12-21]. For general nonlinear material models, the

numerical integration of constitutive equations requires special attention since it is a major cost in the finite element calculations. Many new techniques have been proposed [22-29] for this task. For nonlinear shell analysis this is complicated by the fact that the stress components are referred to a rotating basis, and a zero normal stress constraint needs to be enforced with respect to the normal direction of this basis [18].

I-C. Fluid Mechanics

In the fluid mechanics area, finite element research is just coming of age. Although much effort has been exerted in recent years, it is fair to say that transient finite element, Navier-Stokes algorithms have not achieved the speed and versatility of existing finite difference methods [30-32]. The basic problems of fluid mechanics involve non-symmetric "convection" operators. In most physical problems of engineering interest, convection is dominant. Unlike solid and structural mechanics which involve well-understood symmetric, positive, spatial differential operators, nonsymmetric "convection" operators are still not fully understood [19,33,34]. Due to the ability to eliminate the incompressibility constraints and pressure unknowns [19], and also to the better understanding of the convection operators [33,35-37], it is hoped that the finite element technique, due primarily to its geometric versatility, will soon equal, and eventually surpass the better finite-difference methods.

I-D. Interface Techniques

The simplest Eulerian-Lagrangian interfacing technique goes under the name of "arbitrary Lagrangian-Eulerian" (ALE) technique in the finite

difference literature [38]. Donea et al. [10] and Belytschko and Kennedy [9] generalized the procedure in straightforward fashion to finite elements. Hughes et al. [39] proposed an alternative mixed Lagrangian-Eulerian description in which each degree-of-freedom may be assigned to move at a fraction of the fluid particle velocity. Many problems, such as sloshing and surface waves, may be handled by these procedures. To illustrate the basic idea, consider a cylindrical liquid storage tank, under the action of a strong earthquake. Field observations after strong earthquakes indicate: (1) large amplitude free surface sloshing, which often results in roof damage, (2) nonlinear inelastic tank response such as the well-known elephant's foot bulge phenomenon, and (3) lift-off of tank from foundations. In order to model fluid-structure problems of this type, the following description may be employed: Lagrangian for the shell structure, Eulerian for the main core of the fluid, a split or mixed description for the free surface, and an interpolated description between the Lagrangian and Eulerian subdomains (see Fig. I-C.1). In this way the motion of the fluid may be represented without gross distortions of the mesh.

I-E. Transient Analysis

Basically, there are two general classes of algorithms for transient nonlinear problems: implicit and explicit [40,41]. Implicit algorithms tend to be numerically stable, permitting large time steps, but the cost per step is high and storage requirements tend to increase dramatically with the size of the mesh. On the other hand, explicit algorithms tend to be inexpensive per step, and require less storage than the implicit algorithms, but numerical stability requires that small steps be employed. There are some problems for which implicit

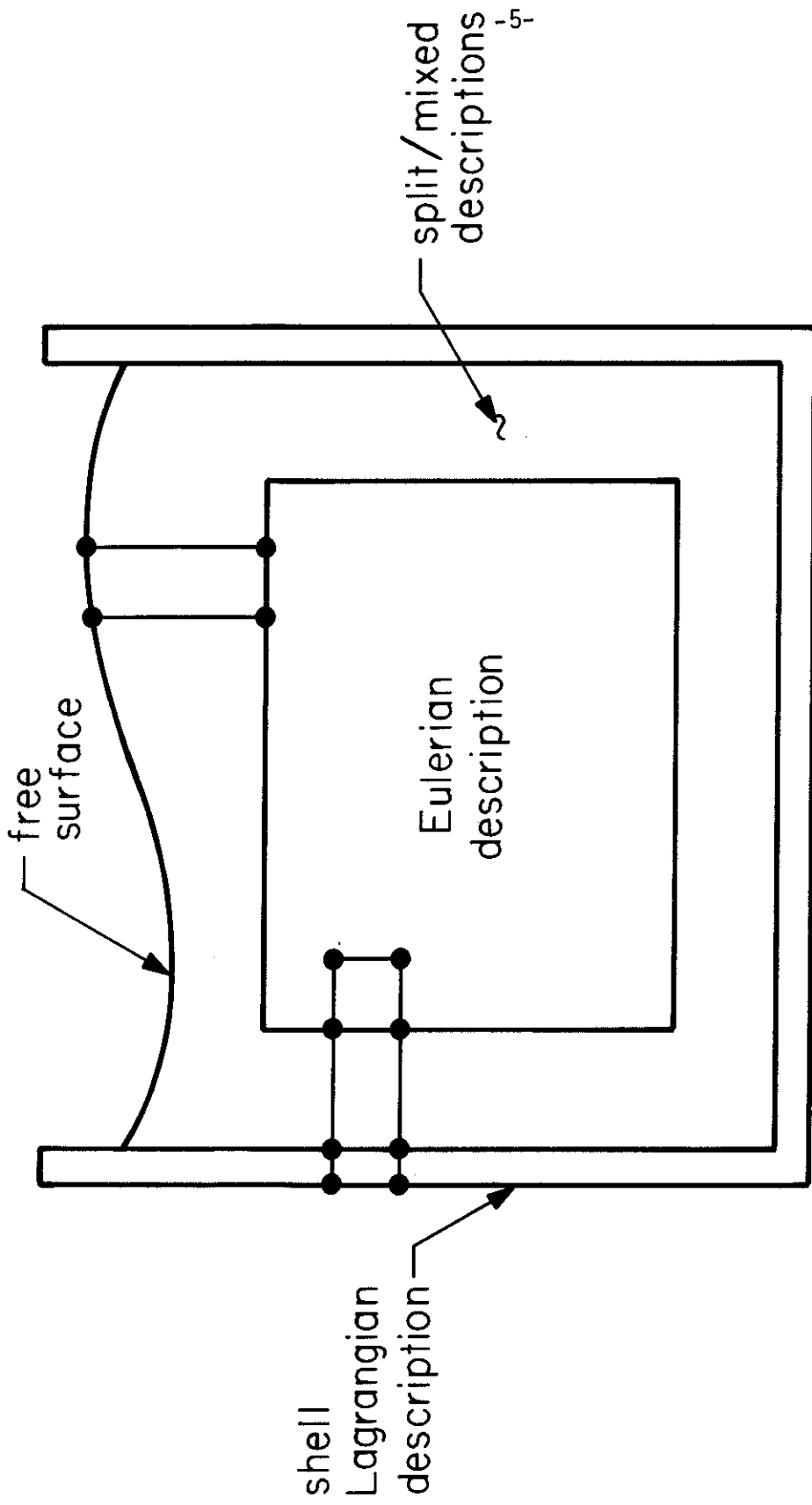


Fig. IC-1 Lagrangian - Eulerian mesh description of shell-like structure containing a fluid

algorithms are very efficient and others for which explicit algorithms are very efficient. However, the direct time integration of the equations resulting from fluid-structure interaction problems presents computational difficulties that are not normally encountered in single-field problems (structural and fluid).

To overcome these difficulties, methods have been developed in which it is attempted to simultaneously achieve the attributes of both classes of algorithms. Belytschko and Mullen [42,43] proposed an implicit-explicit nodal partition in which the explicit nodes are integrated first in each time step and the results are used subsequently as "boundary conditions" for the integration of the implicit nodes. Hughes and Liu [44,45] proposed an alternate element-by-element implicit-explicit partition which is amenable to stability and accuracy analysis, and, at the same time, can be simply and concisely implemented. In this approach the mesh is divided into implicit and explicit finite element groups only. The notions of "strong coupling," "weak coupling," "interface elements," explicit and implicit nodes [46,47] are completely avoided. The coupling between the groups is fully accounted for by the standard finite element assembly procedures. The convergence, extension to nonlinear problems, and implicit-explicit finite element techniques for symmetric and nonsymmetric systems have been developed in [19,50,51, 54]. A general partitioned transient analysis procedure is proposed by Park [48], which is amenable to a unified stability analysis and incorporates the mentioned algorithms as special cases.

Various other improvements in transient algorithms have also been recently achieved [49,52,53,55-57]. The applications of these ideas in different branches of engineering problems has proven to be

successful [19,39,42,53,55].

II. Scope of the Present Investigation

This report deals with the developments of finite element procedures in fluid-structure interactions. Both geometrical and material nonlinearities are accounted for.

In Chapter 2, the fundamental theories in continuum mechanics are reviewed. A general theory of mixed Lagrangian-Eulerian descriptions will be derived. The definitions of convective velocity and referential or mesh time derivative are given. The balance laws, such as conservation of mass and balances of linear and angular momentum are derived within the mixed-Lagrangian-Eulerian concept. The formal statements of the initial/boundary-value problem for the mixed description, Eulerian description and Lagrangian description and their corresponding variational equations will be discussed. A class of rate-type constitutive equations is introduced which represents a wide class of material models. The Galerkin/finite element formulation and matrix equations, as well as the incremental constitutive equations are derived. The elimination of the continuity equation and pressure unknown for a viscous incompressible fluid is achieved within the framework of the penalty function formulation. A related idea for slightly compressible fluids is also discussed.

In Chapter 3, the numerical solution techniques are discussed. The integrals appearing in the variational equations are carried out by numerical integration. Selective/reduced integration procedures are discussed in detail. "Upwind" finite elements are developed based upon modification of standard Gauss-Legendre quadrature rules and also Petrov-Galerkin techniques. These enable stable finite element

approximations to highly convective flows. Consistent, lumped and "row-summed" mass matrices are discussed. The implementation of Lagrangian-Eulerian finite elements is done by introducing a "Lagrange-Euler parameter." The numerical integration of rate constitutive equations is reviewed, and finally, different transient analysis techniques for the variational equations are presented.

In Chapter 4, the nonlinear finite element analysis of shells is discussed. The geometry and kinematic descriptions are first defined. "Laminar" coordinate systems and "fiber" coordinate systems are then introduced in order to account for the zero-normal stress condition and to eliminate the "torsional" degree of freedom, respectively. The numerical algorithms for integrating the constitutive equations for shells are then discussed. The avoidance of "mesh-locking" in the thin shell limit is achieved by a simple modification of the strain-displacement matrix via selective/reduced integration. Different transformation matrices as well as the tangent stiffness matrix, internal force vector, and mass matrix are defined. Different shell elements, such as the selective/reduced Lagrangian elements and heterosis elements are also discussed. Numerical examples involving a number of the elements are presented to demonstrate the effectiveness of the proposed shell procedures.

Numerical examples of incompressible viscous flows by the penalty function formulation are presented in Chapter 5 to demonstrate the effectiveness and accuracy of the proposed formulation. A free-surface wave generation problem is used to demonstrate the mixed Lagrangian-Eulerian theory in Chapter 6. Also presented is an example of practical interest concerning a nonlinear analysis of an inclined cylindrical liquid storage tank. In addition, the axisymmetric buckling of

circular cylinders under different boundary conditions due to a uniformly applied axial load is presented. Finally a dynamic analysis of a liquid storage tank is presented. A summary of the present study and suggestions for further developments are discussed in Chapter 7.

References

1. N. Edwards, "A procedure for the dynamic analysis of thin-walled cylindrical liquid storage tanks," Ph.D. thesis, U. of Michigan, Ann Arbor, Michigan, 1969.
2. M. A. Haroun, "Dynamic analysis of liquid storage tanks," Ph.D. thesis, California Institute of Technology, Pasadena, Ca., 1979.
3. M. Aslan, W. G. Godden, D. T. Scalise, "Sloshing of water in torus pressure-suppression pool of boiling water reactors under earthquake ground motions," Lawrence-Berkeley Laboratory reports #7984 and 6754, NUREG/CR-1082-1083, Oct. 1979.
4. T. Belytschko, J. M. Kennedy, and D. F. Schoeberle, "Quasi-Eulerian finite element for fluid-structure interactions," J. Pressure Vessel Tech. 102, 62-69 (1980).
5. T. Belytschko and U. Schumann, "Fluid-structure interaction in light water reactor systems," preprint.
6. T. Belytschko, ed. "Fluid-structure interactions in LWR systems," First International Seminar on Fluid-Structure Interaction in LWR Systems (International Congress Center, Berlin (West), Germany, August 20-21, 1979), pp. 29-54.
7. T. Belytschko and R. Mullen, "Two-dimensional fluid structure impact computation," preprint.
8. J. M. Kennedy and T. Belytschko, "Finite element method of above core structures," Argonne National Laboratory, ANL/RAS 79-19, 1979.
9. T. Belytschko and J. M. Kennedy, "Computer models for subassembly simulation," preprint.
10. J. Donea, P. Fasoli-Stella, S. Giuliani, J. P. Halleux, and A. V. Jones, "The computer code EURDYN-1M for transient dynamic fluid-structure interaction," EUR6751EN. Commission of the European Communities Joint Research Center Ispra Establishment, Italy 1980.
11. J. Donea, P. Fasoli-Stella, and S. Giuliani, "Lagrangian and Eulerian finite element techniques for transient fluid structure interaction problems," Trans. Fourth Internat. Conf. on Structural Mechanics in Reactor Technology, San Francisco, August, 1977.

12. D. S. Malkus and T.J.R. Hughes, "Mixed finite-element methods-- reduced and selective integration techniques: a unification of concepts," *Computer Meth. in Appl. Mech. and Eng.* 15, 63-81 (1978).
13. I. Fried, "Finite element analysis of incompressible material by residual energy balancing," *Internat. J. Solids and Structures* 10, 993-1002 (1974).
14. J. C. Nagtegaal, D. M. Parks, and J. R. Rice, "On numerically accurate finite element solutions in the fully plastic range," *Computer Meth. in Appl. Mech. and Eng.* 4, 153-178 (1974).
15. D. S. Malkus, "Finite element analysis of incompressible solids," Ph.D. thesis, Boston University, Boston, Mass., 1975.
16. T.J.R. Hughes, M. Cohen, and M. Haroun, "Reduced and selective integration techniques in the finite element analysis of plates," *Nucl. Eng. and Design* 46, 203-222 (1978).
17. T.J.R. Hughes and M. Cohen, "The 'heterosis' finite element for plate bending," *Computers and Structures* 9, 445-450 (1978).
18. T.J.R. Hughes and W. K. Liu, "Nonlinear finite element analysis of shells: Part I. Three-dimensional shells; Part II. Two-dimensional shells," *Computer Meth. in Appl. Mech. and Eng.*, in press.
19. T.J.R. Hughes, W. K. Liu, and A. Brooks, "Review of finite element analysis of incompressible viscous flows by the penalty function formulation," *J. Computational Phys.* 30, 1-60 (1979).
20. T.J.R. Hughes, "Generalization of selective integration procedures to anisotropic and nonlinear media," *Internat. J. Numerical Meth. in Eng.*, in press.
21. D. S. Malkus, "A finite element displacement model valid for any value of the compressibility," *Internat. J. Solids and Structures* 12, 731-738 (1976).
22. T.J.R. Hughes and J. H. Prevost, "DIRT II --A nonlinear quasistatic finite element analysis program," California Institute of Technology, 1979.
23. R. D. Krieg, "An efficient numerical method for time independent plasticity," SAND 77-0943, Sandia Labs., Albuquerque, N.M., 1977.

24. J. O. Hallquist, "NIKE2D: An implicit, finite-deformation, finite-element code for analyzing the static and dynamic response of two-dimensional solids," Lawrence-Livermore Laboratory, Report UCRL-52678, University of California, Livermore, March 3, 1979.
25. R. M. McMeeking and J. R. Rice, "Finite element formulation for problems of large elastic-plastic deformation," *Internat. J. Solids and Structures* 11, 601-616 (1975).
26. H. L. Schreyer, R. F. Kulak, and J. M. Kramer, "Accurate numerical solutions for elastic and plastic models," *J. Pressure Vessel Technol.* 101, 226-234 (1979).
27. R. D. Krieg and D. B. Krieg, "Accuracies of numerical solution methods for the elastic perfectly plastic model," *ASME J. Pressure Vessel Technol.* 99, 510-515 (1977).
28. S. W. Key, "Hondo, a finite element computer program for large deformation dynamic response of axisymmetric solids," Sandia Laboratories, Albuquerque, N.M., SLA-74-0039, April, 1974.
29. T.J.R. Hughes and J. Winget, "Finite rotation effects in numerical integration of rate constitutive equations arising in large-deformation analysis," *Internat. J. Numerical Meth. in Eng.*, in press.
30. A. A. Amsden and C. W. Hirt, "YAQUI, an arbitrary Lagrangian-Eulerian computer program for fluid flow at all speeds," Report LA-5100, Los Alamos Scientific Laboratory, Los Alamos, N.M., March, 1973.
31. B. Alder (ed.), "Methods in computational physics," in Advances in Research and Applications 3 (Academic Press, New York, 1964).
32. T. Belytschko (ed.), *First International Seminar on Fluid-Structure Interaction in LWR Systems* (International Congress Center, Berlin (West), Germany, August 20-21, 1979) pp. 29-54.
33. T.J.R. Hughes (ed.), Finite Element Methods for Convection Dominated Flows, AMD--vol. 34 (ASME, New York, 1979).
34. T.J.R. Hughes, "Current trends in finite element research, Feature article to appear in *Applied Mechanics Reviews*.

35. T.J.R. Hughes, "A simple scheme for developing 'upwind' finite elements," *Internat. J. for Numerical Meth. in Eng.* 12, 1359-1365 (1978).
36. T.J.R. Hughes and J. Atkinson, "A variational basis for 'upwind' finite elements," *IUTAM Symposium on Variational Meth. in Mech. of Solids*, Northwestern University, Evanston, Ill, Sept., 1978.
37. A. Brooks and T.J.R. Hughes, "Streamline-upwind/Petrov-Galerkin methods for advection dominated flows," *Third Internat. Conf. on Finite-Element Methods in Fluid Flow*, Banff, Canada, 1980.
38. C. W. Hirt, A. A. Amsden, and J. L. Cook, "An arbitrary Lagrangian-Eulerian computing method for all flow speeds," *J. Computational Phys.* 14, 227-253 (1974).
39. T.J.R. Hughes, W. K. Liu, and T. K. Zimmermann, "Lagrangian-Eulerian finite element formulation for incompressible viscous flows." Presented at the U.S.-Japan Conf. on Interdisciplinary Finite Element Analysis, Cornell University, August 7-11, 1978.
40. O. C. Zienkiewicz, The Finite-Element Method, 3d edition (McGraw-Hill Book Co., 1977).
41. K-J. Bathe and E. L. Wilson, Numerical Methods in Finite-Element Analysis (Prentice-Hall, Inc., 1976).
42. T. Belytschko and R. Mullen, "Mesh partitions of explicit-implicit time integration," in Formulation and Computational Algorithms in Finite-Element Analysis, K. J. Bathe, J. T. Oden, and W. Wunderlich, eds. (M.I.T. Press, Cambridge, Mass., 1977).
43. T. Belytschko and R. Mullen, "Stability of explicit-implicit mesh partitions in time integration," *Internat. J. for Numerical Meth. in Eng.* 12, 1575-1586 (1978).
44. T.J.R. Hughes and W. K. Liu, "Implicit-explicit finite elements in transient analysis: Stability theory," *J. Appl. Mech.* 45, 371-374 (1978).
45. T.J.R. Hughes and W. K. Liu, "Implicit-explicit finite elements in transient analysis: Implementation and numerical examples," *J.*

- Appl. Mech. 45, 375-378 (1978).
46. C. A. Felippa, K. C. Park, and H. C. Yee, "Synthesis of staggered solution procedures for coupled field analysis," 2d International Conf. on Appl. Numerical Modeling, Polytechnical University of Madrid, Madrid, Spain, Sept. 11-15, 1978.
 47. K. C. Park, C. A. Felippa, and J. A. DeRuntz, "Stabilization of staggered solution procedures for fluid-structure interaction analysis," in Computational Methods for Fluid-Structure Interaction Problems (T. Belytschko and T. L. Geers, eds.), Applied Mechanics Symposia Series (ASME, New York, 1977).
 48. K. C. Park, "Partitioned transient analysis procedures for coupled-field problems," presented at the 2d Conf. on Numerical Meth. in Nonlinear Mech., TICOM, University of Texas, Austin, Tex., March 1979.
 49. K. C. Park and P. G. Underwood, "A variable-step central difference method for structural dynamics analysis--Part I: Theoretical aspects," ASME Paper No. 79-PVP-120, presented at the Pressure Vessels and Piping Conf., San Francisco, Ca., June 25-29, 1979.
 50. T.J.R. Hughes, K. S. Pister, and R. L. Taylor, "Implicit-explicit finite elements in nonlinear transient analysis," Computer Meth. in Appl. Mech. and Eng. 17/18, 159-182 (1979).
 51. T.J.R. Hughes and R. A. Stephenson, "Convergence of implicit-explicit algorithms in nonlinear transient analysis," International Journal of Engineering Science, in press.
 52. H. M. Hilber, T.J.R. Hughes, "Collocation, dissipation, and 'overshoot' for time integration schemes in structural dynamics," Earthquake Eng. Struct. Dyn. 6, 99-118 (1978).
 53. T.J.R. Hughes, T. K. Caughey, and W. K. Liu, "Finite element methods for nonlinear elastodynamics which conserve energy," J. Appl. Mech. 45, 366-370 (1978).
 54. T.J.R. Hughes, "Implicit-explicit finite element techniques for symmetric and nonsymmetric systems," Proc. Conf. on Nonlinear Problems

in Mechanics, University of Swansea, Swansea, U.K., Sept. 2-5, 1980.

55. T. Belytschko, H. J. Yen, and R. Mullen, "Mixed methods for time integration," Computer Meth. in Appl. Mech. and Eng. 17/18, 259-275 (1979).
56. P. G. Underwood and K. C. Park, "A variable-step central difference method for structural dynamics analysis, Part II: Implementation and performance evaluation," ASME Paper No. 79-PVP-121, presented at the Pressure Vessels and Piping Conf., San Francisco, CA., June 25-29, 1979.
57. J. P. Wright, "Mixed time integration schemes," Computers and Structures 10, 235-238 (1979).

Chapter 2

FUNDAMENTAL CONTINUUM MECHANICS THEORY
AND FINITE ELEMENT FORMULATION

I. General Description of Governing Equations

"A continuum is an abstraction applied to a large collection of material particles. Continuum mechanics deals with deformations and motions of these particles in space and time, under a variety of external conditions such as mechanical and thermal processes. The theory of continuum mechanics serves to establish the mathematical formulation of any physical phenomenon that takes place in a material body. This is tantamount to replacement of the actual body with an idealized 'mathematical body' in the sense that it is not an atomistic view of matter; rather, it associates material bodies with regions of Euclidean space," K. S. Pister [2].

Equations describing the behavior of a continuum can generally be divided into four major categories: (1) kinematic, (2) kinetic (balanced laws), (3) thermodynamic, and (4) constitutive. Detailed treatments of the subject can be found in many standard texts and articles [1-6]. However, the two classical descriptions of motion, Lagrangian and Eulerian [3,5,6], are not adequate for many free-surface flows and problems of fluid-solid-structure interaction involving finite deformation. The Lagrangian description is generally not suitable for the fluid undergoing large displacements since the mesh will become highly contorted. In addition, when the Eulerian description is used for the fluid it is not compatible with the large displacement of the structure for which the geometries of the boundary are altered.

It is the purpose of this section to develop a more versatile description of motion based on the previous developments by Amsden and Hirt [7], Donea et al. [8], Belytschko and Kennedy [9], Hughes et al. [10], and references therein.

I-A. General Theory of Mixed Lagrangian-Eulerian Description

Suppose a body B occupies a region $R_Z \subset \mathbb{R}^{n_{sd}}$. We describe the motion of B by a mapping $\underline{\phi}: R_Z \times [t_0, t_1] \rightarrow \mathbb{R}^{n_{sd}}$. The image of R_Z at time t is denoted by R_Y , and the image of $\underline{z} \in R_Z$ is denoted by \underline{y} , i.e.,

$$\underline{y} = \underline{\phi}(\underline{z}, t) \quad (\text{IA.1})$$

Here R_Z is thought to be the region occupied at $t = t_0$ by the "material particles" which occupy R_Y at time t, so we wish to think of R_Y as the "spatial" region. In order to describe the mixed formulation, we have to introduce a "reference" region. To this end, let us introduce $R_X \subset \mathbb{R}^{n_{sd}}$ which is fixed throughout. Its motion is defined by the mapping $\hat{\phi}: R_X \times [t_0, t_1] \rightarrow \mathbb{R}^{n_{sd}}$. We assume that R_Y is the image of R_X at t under the mapping $\hat{\phi}$, and that \underline{y} is the image of $\underline{x} \in R_X$. Therefore,

$$\underline{y} = \hat{\phi}(\underline{x}, t) \quad (\text{IA.2})$$

By composition we may define a third mapping $\underline{\psi}$ by

$$\underline{x} = \underline{\psi}(\underline{z}, t) \quad ; \quad \underline{\psi}(\cdot, t) = \hat{\phi}^{-1}(\underline{\phi}(\cdot, t), t) \quad (\text{IA.3})$$

The set-up is illustrated in Figure IA-1.

We may obtain the classical kinematic descriptions by specializing the definition of R_X and $\hat{\phi}$. The Lagrangian description is obtained by picking $R_X = R_Z$ and $\hat{\phi} = \underline{\phi}$, whereas if $R_X = R_Y$ and $\hat{\phi} = \underline{1}$, we have the

Eulerian description. By appropriate selection of R_x and $\hat{\phi}$, more general kinematic descriptions, which are useful for many free-surface and fluid-solid-structure interaction problems, may be obtained. In order to describe this formulation, it is helpful to introduce coordinate systems. For simplicity, let us restrict ourselves to proper orthogonal coordinate frames and let x_i , y_i , and z_i , $1 \leq i \leq n_{sd}$ denote the Cartesian components of \underline{x} , \underline{y} , and \underline{z} , respectively. Partial differentiation operators will be indicated by the following shorthand notation [10]:

$$\begin{aligned}
 'i &= \frac{\partial}{\partial x_i} & ; & & ' &= \frac{\partial}{\partial t} \Big|_{x_i \text{ fixed}} & & \text{("referential derivatives")} \\
 ,i &= \frac{\partial}{\partial y_i} & ; & & ,t &= \frac{\partial}{\partial t} \Big|_{y_i \text{ fixed}} & & \text{("spatial derivatives")} \\
 \cdot i &= \frac{\partial}{\partial z_i} & ; & & \cdot &= \frac{\partial}{\partial t} \Big|_{z_i \text{ fixed}} & & \text{("material derivatives")}
 \end{aligned} \tag{IA.4}$$

It follows from (IA.4) that:

$$x_i' = 0 \quad ; \quad y_{i,t} = 0 \quad ; \quad \dot{z}_i = 0 \tag{IA.5}$$

$$x_i' j = y_{i,j} = z_{i \cdot j} = \delta_{ij} \tag{IA.6}$$

where δ_{ij} is the Kronecker delta.

A summary of useful kinematic definitions, associated with the mappings defined above, is given as follows:

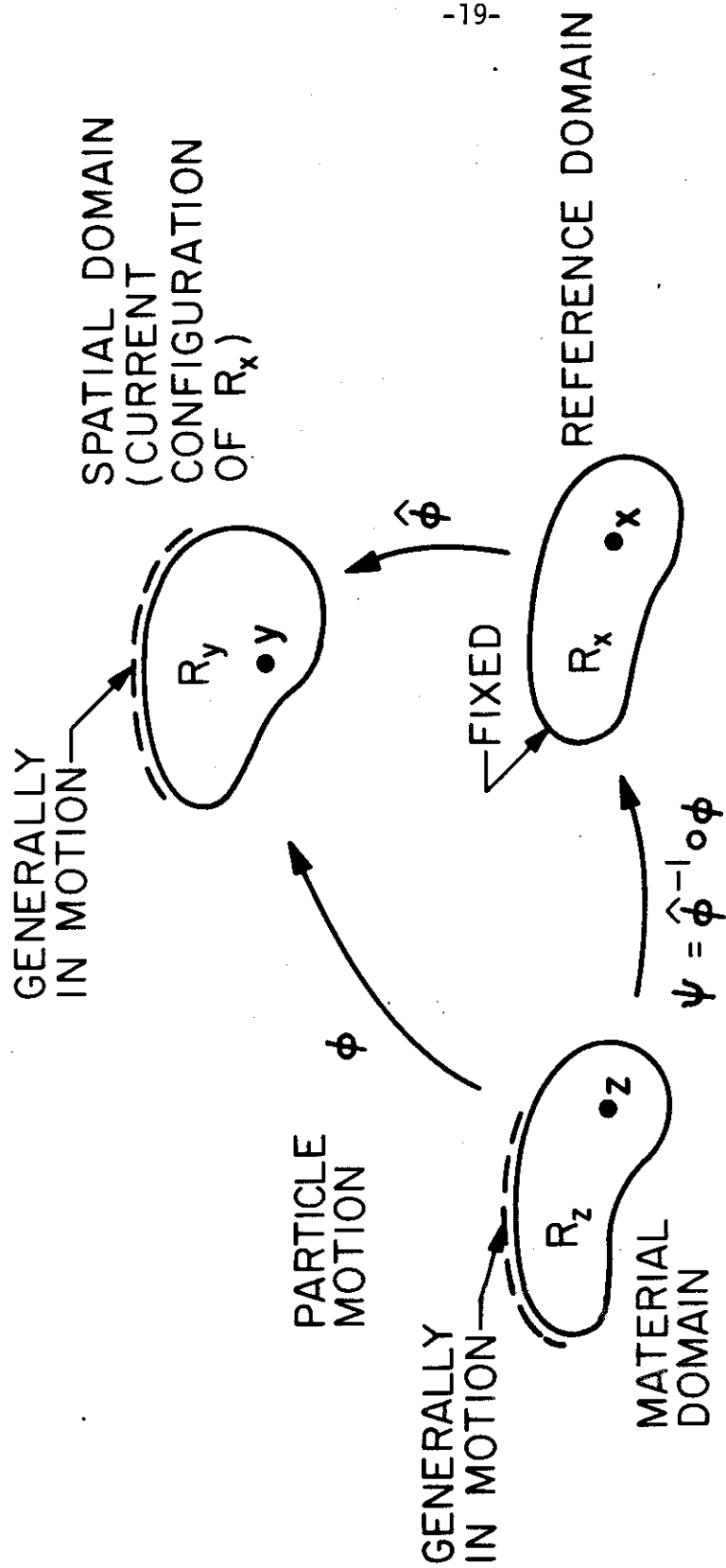


Fig. IA -1 Schematic diagram of domains and mappings for mixed Lagrangian - Eulerian description

$$\tilde{\phi} \left\{ \begin{array}{ll} y_i = \phi_i(\tilde{z}, t) & \text{(motion)} \quad \text{(IA.7)} \\ u_i = y_i - z_i & \text{(displacement)} \quad \text{(IA.8)} \\ \dot{u}_i = \dot{y}_i = \partial \phi_i / \partial t & \text{(velocity)} \quad \text{(IA.9)} \\ \ddot{u}_i = \ddot{y}_i = \partial^2 \phi_i / \partial t^2 & \text{(acceleration)} \quad \text{(IA.10)} \\ y_{i \cdot j} = \partial \phi_i / \partial z_j = \delta_{ij} + u_{i \cdot j} & \text{(deformation gradient)} \quad \text{(IA.11)} \end{array} \right.$$

$$\hat{\phi} \left\{ \begin{array}{ll} y_i = \hat{\phi}_i(\tilde{x}, t) & \text{(motion)} \quad \text{(IA.12)} \\ \hat{u}_i = y_i - x_i & \text{(displacement)} \quad \text{(IA.13)} \\ \hat{u}'_i = y'_i = \partial \hat{\phi}_i / \partial t & \text{(velocity)} \quad \text{(IA.14)} \\ \hat{u}''_i = y''_i = \partial^2 \hat{\phi}_i / \partial t^2 & \text{(acceleration)} \quad \text{(IA.15)} \\ y_{i'j} = \partial \hat{\phi}_i / \partial x_j = \delta_{ij} + \hat{u}_{i'j} & \text{(deformation gradient)} \quad \text{(IA.16)} \end{array} \right.$$

$$\psi \left\{ \begin{array}{ll} x_i = \psi_i(\tilde{z}, t) & \text{(motion)} \quad \text{(IA.17)} \\ w_i = x_i - z_i & \text{(displacement)} \quad \text{(IA.18)} \\ \dot{w}_i = \dot{x}_i = \partial \psi_i / \partial t & \text{(velocity)} \quad \text{(IA.19)} \\ \ddot{w}_i = \ddot{x}_i = \partial^2 \psi_i / \partial t^2 & \text{(acceleration)} \quad \text{(IA.20)} \\ x_{i \cdot j} = \partial \psi_i / \partial z_j = \delta_{ij} + w_{i \cdot j} & \text{(deformation gradient)} \quad \text{(IA.21)} \end{array} \right.$$

Equations (IA.7) - (IA.11) are the classical kinematic relations of the Lagrangian description of a continuum (e.g., u_i is the particle displacement, \dot{u}_i is the particle velocity, and \ddot{u}_i is the particle acceleration).

Convective velocity and material time derivatives

Differentiating (IA.12) with respect to t , holding \underline{z} fixed, and using (IA.17), yields

$$\dot{u}_i = y_{i,j} \dot{w}_j + \hat{u}_i \quad (\text{IA.22})$$

from which it follows that

$$\dot{w}_i = x_{i,j} c_j \quad (\text{IA.23})$$

where

$$c_j = \dot{u}_j - \hat{u}_j \quad (\text{IA.24})$$

is called the convective velocity.

The material time derivative, which appears in continuum conservation laws, is the time derivative with the material coordinates (\underline{z}) held constant as in equation (IA.4). We assume, however, if f is a scalar function defined on any one of the regions R_x , R_y , or R_z , via composition, f can be expressed in terms of the other two functions. Without loss of generality, if $f: R_x \times [t_0, t_1] \rightarrow \mathbb{R}$, then we can define $g: R_y \times [t_0, t_1] \rightarrow \mathbb{R}$ and $h: R_z \times [t_0, t_1] \rightarrow \mathbb{R}$ (using (IA.2) and (IA.3)), by:

$$g(\underline{y}, t) = g(\hat{\phi}(\underline{x}, t), t) = f(\underline{x}, t) \quad (\text{IA.25})$$

$$h(\underline{z}, t) = h(\psi^{-1}(\underline{x}, t), t) = f(\underline{x}, t)$$

In order to avoid introducing new variables (i.e., instead of writing (IA.25)) we will simply write

$$\underbrace{f(\underline{x}, t)}_{\text{referential}} = \underbrace{f(\underline{y}, t)}_{\substack{\text{spatial} \\ \text{or} \\ \text{Eulerian}}} = \underbrace{f(\underline{z}, t)}_{\substack{\text{material} \\ \text{or} \\ \text{Lagrangian}}} \quad (\text{IA.26})$$

with the understanding that the second and third f's in (IA.26) are actually g and h, respectively. Differentiating (IA.26) with respect to t and holding \underline{z} fixed, we get

$$\underbrace{f' + f_{,i} \dot{w}_i}_{\text{referential}} = \underbrace{f_{,t} + f_{,i} \dot{u}_i}_{\substack{\text{spatial} \\ \text{or} \\ \text{Eulerian}}} = \underbrace{\dot{f}}_{\substack{\text{material} \\ \text{or} \\ \text{Lagrangian}}} \quad (\text{IA.27})$$

Since R_x is fixed throughout in this formulation, it is convenient to express the material time derivative (\dot{f}) in referential form. Combining (IA.27) and (IA.23), and by the chain rule, we have the important relation

$$\dot{f} = f' + f_{,i} c_i \quad (\text{IA.28})$$

Strain measures

Let $\underline{a} = (1-\alpha)\underline{z} + \alpha\underline{y}$, where $0 \leq \alpha \leq 1$. Also, let ds_z, ds_y be the differential distances between points in R_z and R_y , respectively. We can write

$$ds_z^2 = d\underline{z} \cdot d\underline{z} \quad (\text{IA.29})$$

$$ds_y^2 = d\underline{y} \cdot d\underline{y} \quad (\text{IA.30})$$

Consider:

$$\underline{z} = \hat{\underline{z}}(\underline{a}) \quad \text{and} \quad \underline{y} = \hat{\underline{y}}(\underline{a})$$

and define:

$$ds_y^2 - ds_z^2 = 2d\underline{a}^T \cdot \underline{E} \cdot d\underline{a} \quad (\text{IA.31})$$

Letting $d\tilde{z} = \tilde{F}_z da$ and $d\tilde{y} = \tilde{F}_y da$, where $\tilde{F}_z = \partial\tilde{z}/\partial a$, $\tilde{F}_y = \partial\tilde{y}/\partial a$, we have:

$$\tilde{E} = \frac{1}{2} \left\{ \left(\frac{\partial\tilde{y}}{\partial a} \right) + \left(\frac{\partial\tilde{y}}{\partial a} \right)^T + (1 - 2\alpha) \left(\frac{\partial\tilde{y}}{\partial a} \right)^T \left(\frac{\partial\tilde{y}}{\partial a} \right) \right\} \quad (\text{IA.32})$$

If $\alpha = 0$, \tilde{E} is called Green or Lagrangian strain tensor.

If $\alpha = 1$, \tilde{E} is called Almansi or Eulerian strain tensor.

If the motion of B is rigid, then this is equivalent to saying $\tilde{E} = \underline{0}$ [5]. Also, for $\alpha = 1/2$ it was shown by Hallquist [14] and by Hughes and Winget [13] that \tilde{E} has certain useful numerical calculation properties as will be discussed later.

I-B. Balance Laws (Mass and Momentum)

Mass density, conservation of mass (equation of continuity)

We assume there exists a scalar-valued function $\rho(\cdot, t)$ called mass density defined on R_y and $t_0 \leq t \leq t_1$ with the properties [5]:

(i) $\rho(\tilde{y}, t) > 0 \quad \forall \tilde{y} \in R_y \quad (t_0 \leq t \leq t_1)$

(ii) If $P_x \subset R_x$ is a bounded subregion of R_x , and if $P_y = \hat{\phi}(P_x, t)$, then

$$m(P_y) = \int_{P_y} \rho(\tilde{y}, t) dP_y$$

is the mass of material occupying P_y at time t .

We call $\rho_0(\tilde{x})$ the initial mass density, viz.

$$\rho_0(\tilde{x}) = \rho(\hat{\phi}(\tilde{x}, t_0), t_0)$$

(iii) If $P_z \subset R_z$ is a bounded subregion of R_z , and if $P_y = \phi(p_z, t)$, then

$$m(P_y) = \int_{P_y} \rho(y, t) dP_y = \int_{P_z} \rho(\tilde{y}, t) J_{yz} dP_z$$

where $J_{yz} = \det(\partial \tilde{y} / \partial z)$.

The principle of conservation of mass states that mass cannot be created nor destroyed if we follow the motion of the given mass [12],

i.e.,

$$\frac{d}{dt} m(P_y) = \frac{d}{dt} \int_{P_y} \rho(\tilde{y}, t) dP_y = 0 \quad (\text{IB.1})$$

Equivalently:

$$\dot{[\rho J_{yz}]} = 0 \quad (\text{IB.2})$$

Carrying out the material time derivative, (IB.2) becomes

$$\dot{\rho} J_{yz} + \rho \dot{J}_{yz} = 0 \quad (\text{IB.3})$$

As $\dot{J}_{yz} = J_{yz} \dot{u}_{k,k}$ [5], conservation of mass says:

$$\dot{\rho} + \rho(\dot{u}_k)_{,k} = 0 \quad (\text{IB.4})$$

If the material is incompressible so that the density of each material particle remains constant as it moves, the continuity equation takes the simpler form

$$\dot{u}_{k,k} = 0 \quad (\text{IB.5})$$

This is the condition of incompressibility, which has been important in classical hydrodynamics and in plasticity theories.

Body forces and contact forces, surface tractions [5]

Body forces

We assume there exists a vector-valued function $\underline{b}(\cdot, t)$ (body-force density per unit current volume) defined on R_y such that the resultant force and resultant moment about the origin, 0, of an n_{sd} -dimensional Euclidean space due to the body force acting on the material in R_y are given by

$$\int_{P_y} \underline{b}(\underline{y}, t) dP_y \quad ; \quad \int_{P_y} \underline{y} \times \underline{b}(\underline{y}, t) dP_y$$

Here \times is a "cross product" or "vector product."

Contact forces

We assume there exists a vector-valued function $\underline{T}(\cdot, \cdot, t)$ (surface-force density per unit current area, actual surface traction, or Cauchy-traction) defined on $R_y \times U$, where U is the set of all unit vectors, such that the resultant force and resultant moment about 0 due to the surface forces acting on the boundary of P_y , denoted ∂P_y , are given by:

$$\int_{\partial P_y} \underline{T}(\underline{y}, \underline{n}(\underline{y}, t), t) dA_y \quad ; \quad \int_{\partial P_y} \underline{y} \times \underline{T}(\underline{y}, \underline{n}(\underline{y}, t), t) dA_y$$

where $\underline{n}(\underline{y}, t)$ is the unit outer normal vector at $\underline{y} \in \partial P_y$.

The principles of linear and angular momentum (postulates) [12]

Newton's law states that the time rate of change of linear momentum of a given mass is equal to the force exerted upon the mass, i.e.,

$$\int_{P_y} \underline{b}(\underline{y}, t) dP_y + \int_{\partial P_y} \underline{T}(\underline{y}, \underline{n}, t) dA_y = \frac{d}{dt} \int_{P_y} \rho(\underline{y}, t) \dot{\underline{u}}(\underline{y}, t) dP_y \quad (\text{IB.6})$$

Also, conservation of moment of linear momentum states that the time rate of change of angular momentum of a given mass with respect to a given point is equal to the applied torque referred to the same point, i.e.,

$$\int_{P_y} \underline{y} \times \underline{b}(\underline{y}, t) dP_y + \int_{\partial P_y} \underline{y} \times \underline{T}(\underline{y}, \underline{n}, t) dA_y = \frac{d}{dt} \int_{P_y} \underline{y} \times \rho(\underline{y}, t) \dot{\underline{u}}(\underline{y}, t) dP_y \quad (\text{IB.7})$$

Before deriving the mixed Lagrangian-Eulerian equation of motion we have to introduce a very important lemma.

Lemma IB-1

Let $\underline{\phi}: R_z \times [t_0, t_1] \rightarrow \mathbb{R}^{nd}$ be sufficiently regular. Let P_y and ρ be defined as previously. Suppose \underline{g} is vector-valued, and

$$\underline{g}(\underline{y}, t) = \underline{g}(\underline{\phi}(\underline{z}, t), t) = \underline{g}(\underline{z}, t)$$

then

$$\frac{d}{dt} \int_{P_y} \rho(\underline{y}, t) \underline{g}(\underline{y}, t) dP_y = \int_{P_y} \rho(\underline{y}, t) \dot{\underline{g}}(\underline{y}, t) dP_y$$

Following [5], we can define a second order tensor $\underline{\tau}(\underline{y}, t)$ called Cauchy, or actual, stress-tensor field on R_y . $\tau_{ij}(\underline{y}, t)$ are the Cartesian components of the two-tensor $\underline{\tau}(\underline{y}, t)$. If $\underline{n}(\underline{y}, t)$ is the unit outer normal vector of ∂P_y at \underline{y} , then the surface traction vector \underline{T} is related to the Cauchy stress-tensor $\underline{\tau}$ by:

$$T_i = \tau_{ji} n_j \quad (\text{IB.8})$$

Substituting (IB.8) into (IB.6), using lemma IB-1, and invoking the divergence theorem, we get

$$\int_{P_y} (\tau_{ji,j} + b_i - \rho \ddot{u}_i) dP_y = 0 \quad \forall P_y \subset R_y$$

Continuity of integrand implies

$$\tau_{ji,j} + b_i = \rho \ddot{u}_i \quad \text{on } R_y \quad \forall t \in [t_0, t_1] \quad (\text{IB.9})$$

Using (IA.28) on the right-hand side term of (IB.9) yields the equations of motion in the mixed Lagrangian-Eulerian description.

$$\begin{aligned} \tau_{ji,j} + b_i &= \rho [(\dot{u}_i)' + (\dot{u}_i)_{,j} c_j] \\ &\text{on } R_y \quad \forall t \in [t_0, t_1] \end{aligned} \quad (\text{IC.10})$$

Using (IB.7) and following [5], we have the symmetry of the Cauchy stress tensor, i.e., $\tau_{ji} = \tau_{ij}$.

II. Formal Statement of the Initial/Boundary-Value Problem

II-A. Mixed Description

We will restrict ourselves to fluid flow problems if the mixed description is being used.

The object of the initial/boundary-value problem is to find functions $\hat{u}_i: R_x \times [t_0, t_1] \rightarrow \mathbb{R}$, $\dot{u}_i: \bar{R}_y \times [t_0, t_1] \rightarrow \mathbb{R}$, and $p: \bar{R}_y \times [t_0, t_1] \rightarrow \mathbb{R}$ (pressure) (where \bar{R} is the closure of R), such that

$$\left. \begin{aligned} \rho \ddot{u}_i &= \tau_{ij,j} + b_i & (\text{IIA.1}) \\ (\dot{u}_i)_{,i} &= 0 & (\text{IIA.2}) \\ \tau_{ij} &= -p \delta_{ij} + \mu [(\dot{u}_i)_{,j} + (\dot{u}_j)_{,i}] & (\text{IIA.3}) \\ \dot{u}_i &= g_i & \text{on } \partial R_y^g \times [t_0, t_1] & (\text{IIA.4}) \end{aligned} \right\} \text{on } R_y \times [t_0, t_1]$$

$$\tau_{ij}n_j = h_i \quad \text{on } \partial R_Y^h \times [t_0, t_1] \quad (\text{IIA.5})$$

$$\dot{u}_i = \dot{u}_{oi} \quad \text{on } R_Y \times [t_0] \quad (\text{IIA.6})$$

$$\hat{u}_i = \text{a given representation} \quad \text{on } R_X \times [t_0, t_1] \quad (\text{IIA.7})$$

depending on $\hat{\phi}$, as will
be discussed in the
next chapter

$$\hat{u}_i = \hat{u}_{oi} \quad \text{on } R_X \quad (\text{IIA.8})$$

where $\rho > 0$ is the density, b_i is the prescribed body force (per unit volume R_Y); μ is the dynamic viscosity; g_i and h_i are prescribed boundary velocities and tractions, respectively; n_i is the unit outward normal vector to ∂R_Y ; and \dot{u}_{oi} and \hat{u}_{oi} are the given initial data.

In order to eliminate the pressure unknown and the continuity equation, we employ a penalty-function formulation of the incompressibility condition in which (IIA.2) is dropped and the pressure is determined from

$$p = -\lambda(\dot{u}_i)_{,i} \quad (\text{IIA.9})$$

where $\lambda > 0$ is the penalty parameter; see [15] for a discussion.

An alternative is to use a "slightly compressible formulation" in which it is assumed that

$$0 = \rho_{,t} + \dot{u}_i \rho_{,i} + \rho \dot{u}_{k,k} \approx \rho_{,t} + \rho \dot{u}_{k,k} \quad (\text{IIA.10})$$

Then by using the equation of state for an isothermal process,

$$F(p, \rho) = 0$$

it follows that

$$\rho_{,t} = \frac{\partial p}{\partial \rho} \rho_{,t} \approx - \frac{\partial p}{\partial \rho} \rho \dot{u}_{k,k}$$

We further assume $\partial p / \partial \rho \approx \text{constant} = \beta$. Then

$$\dot{p}_{,t} = -\beta \rho \dot{u}_{k,k}$$

and the constitutive equation (IIA.3) becomes

$$\tau_{ij} = -(p_0 - \int_0^t \beta \rho \dot{u}_{k,k} dt) \delta_{ij} + \mu [(\dot{u}_i)_{,j} + (\dot{u}_j)_{,i}] \quad (\text{IIA.11})$$

where p_0 is the pressure at $t=0$.

With the continuity equation eliminated, the variational equation corresponding to (IIA.1) through (IIA.8) is

$$\int_{R_y} (\rho \ddot{u}_i \bar{u}_i + \tau_{ij} \bar{u}_{i,j}) dR_y = \int_{R_y} b_i \bar{u}_i dR_y + \int_{\partial R_y^h} h_i \bar{u}_i dA_y \quad (\text{IIA.12})$$

in which

$$\bar{u}_i = 0 \quad \text{on } \partial R_y^g \quad (\text{IIA.13})$$

By virtue of R_x being fixed throughout, we recall

$$\ddot{u}_i = (\dot{u}_i)_{,t} + (\dot{u}_i)_{,j} c_j$$

III. Linearized Equations of Motion Using Lagrangian Description

III-A. Constitutive Equation

In many engineering applications it is found convenient to put constitutive equations into rate form. A wide class of plastic, visco-elastic, and viscoplastic models can be put into this form.

Nonlinear elasticity can be put into this form by time-differentiating the more usual forms. We will restrict our attention here to linear elasticity, the Saint-Venant-Kirchhoff nonlinear elastic

model, and the Krieg-Key combined isotropic/kinematic hardening plasticity model [21].

A class of rate-type constitutive equations for inviscid materials

For discussion purposes, consider rate-type constitutive equations of the following form:

$$\tau_{ij}^* = \dot{\tau}_{ij} - S_{ijkl} \dot{u}_{[k,\ell]} - C_{ijkl}^* \dot{u}_{(k,\ell)} \quad (\text{IIIA.1})$$

where

$$\tau_{ij}^* = C_{ijkl} \dot{u}_{(k,\ell)} \quad (\text{IIIA.2})$$

$$C_{ijkl} = C_{ijkl}(\underline{\tau}, \underline{F}) \quad (\text{IIIA.3})$$

$$S_{ijkl} = (\tau_{i\ell} \delta_{jk} + \tau_{j\ell} \delta_{ik} - \tau_{ik} \delta_{j\ell} - \tau_{jk} \delta_{i\ell}) / 2 \quad (\text{IIIA.4})$$

$$\dot{u}_{(k,\ell)} = (\dot{u}_{k,\ell} + \dot{u}_{\ell,k}) / 2 \quad (\text{IIIA.5})$$

$$\dot{u}_{[k,\ell]} = (\dot{u}_{k,\ell} - \dot{u}_{\ell,k}) / 2 \quad (\text{IIIA.6})$$

Here C_{ijkl} is the material constitutive tensor which is a function of Cauchy stress $\underline{\tau}$ and deformation gradient \underline{F} . $\dot{u}_{(k,\ell)}$ is the symmetric part of the velocity gradient, whereas $\dot{u}_{[k,\ell]}$ is the skew-symmetric part. Without loss of generality, we further assume the C_{ijkl} 's possess the minor symmetries:

$$C_{ijkl} = C_{jikl} = C_{ijlk} \quad (\text{IIIA.7})$$

The tensors S_{ijkl} and C_{ijkl}^* possess the following symmetries:

$$S_{ijkl} = S_{jikl} = -S_{ijlk} \quad (\text{IIIA.8})$$

$$C_{ijkl}^* = C_{jikl}^* = C_{ijlk}^* \quad (\text{IIIA.9})$$

The second term on the right-hand side of equation (IIIA.1) (i.e., the

$S_{ijkl}\dot{u}_{[k,\ell]}$ term) is the "rotational part" of the rate and is fixed once and for all by the so-called "objectivity" or "material frame indifference" as it is now often called [22,23]. As has been discussed in the paper by Hughes and Winget [13], there are several ways to account for this rotational term numerically; for details see [13] and [16]. The third term on the right-hand side of equation (IIIA.1) (i.e., the $C_{ijkl}^*\dot{u}_{(k,\ell)}$ term) is required to be an "objective tensor," but is otherwise arbitrary. We find it is convenient to employ the Truesdell rate of τ_{ij} in which C_{ijkl}^* has the following form:

$$C_{ijkl}^* \stackrel{\text{def}}{=} -\tau_{ik}\delta_{kl} + (\tau_{il}\delta_{jk} + \tau_{jl}\delta_{ik} + \tau_{ik}\delta_{jl} + \tau_{jk}\delta_{il}) / 2 \quad (\text{IIIA.10})$$

For further discussion of the "objective tensor," C_{ijkl}^* , the reader is urged to consult [17,24].

Combining (IIIA.1), (IIIA.2) and (IIIA.10), we can write the constitutive equation as follows:

$$\dot{\tau}_{ij} = \bar{C}_{ijkl}\dot{u}_{(k,\ell)} + S_{ijkl}\dot{u}_{[k,\ell]} \quad (\text{IIIA.11})$$

in which

$$\bar{C}_{ijkl} = C_{ijkl} + C_{ijkl}^* \quad (\text{IIIA.12})$$

Examples of C_{ijkl} for particular materials under consideration

1. Linear elasticity

A wide class of engineering problems can be studied by linear elastic material behavior. However, if finite rotations are involved, the analyst must generalize the small strain linear elastic model to account for these effects. In this way (IIIA.11) will yield a symmetric

stiffness matrix due to the choice of Truesdell rate. The choice $C_{ijkl}^* \equiv 0$ (Jaumann rate) results in a nonsymmetric stiffness. As has been mentioned in the paper by McMeeking and Rice [19], the C_{ijkl}^* 's will have a non-negligible effect on material response in the high-stress, finite deformation regime. Use of this model in this regime is clearly speculative.

If we consider the isotropic linear elastic model, the material constitutive tensor takes the following form:

$$C_{ijkl} = \lambda \delta_{ij} \delta_{kl} + \mu (\delta_{ik} \delta_{jl} + \delta_{il} \delta_{jk}) \quad (\text{IIIA.13})$$

where λ, μ are the Lamé parameters.

2. Saint Venant-Kirchhoff model

The second (symmetric) Piola-Kirchhoff stress tensor P_{pq} is related to the Lagrangian strain tensor E_{rs} by the following relation:

$$\begin{aligned} P_{pq} &= [\lambda \delta_{pq} \delta_{rs} + \mu (\delta_{pr} \delta_{qs} + \delta_{ps} \delta_{qr})] E_{rs} \\ &= D_{pqrs} E_{rs} \end{aligned} \quad (\text{IIIA.14})$$

where λ, μ are the Lamé parameters. The C_{ijkl} 's are defined by [18,20]:

$$C_{ijkl} = J^{-1} F_{ip} F_{jq} F_{kr} F_{ls} D_{pqrs} \quad (\text{IIIA.15})$$

where F_{ij} are the Cartesian components of the deformation gradient tensor and J is the determinant of $\underline{\underline{F}}$. Carrying out the algebra and defining $\underline{\underline{b}} = \underline{\underline{F}} \underline{\underline{F}}^T$ (the Finger tensor), (IIIA.15) becomes:

$$C_{ijkl} = J^{-1} \{ \lambda b_{ij} b_{kl} + \mu (b_{ik} b_{jl} + b_{il} b_{jk}) \} \quad (\text{IIIA.16})$$

3. Krieg-Key combined isotropic-kinematic hardening plasticity model [21]

Using the assumption made in the paper by Krieg and Key [21], we can write the C_{ijkl} 's as follows:

$$C_{ijkl} = \lambda \delta_{ij} \delta_{kl} + \mu (\delta_{ik} \delta_{jl} + \delta_{jk} \delta_{il}) - 2\mu \zeta n_{ij} n_{kl} \quad (\text{IIIA.17})$$

where λ, μ are Lamé parameters. ζ is set to one during plastic loading, that is, when $\phi > 0$; otherwise, ζ is set to zero. ϕ is the Von Mises yield function defined by:

$$\phi = \frac{1}{6} [(\epsilon_{11} - \epsilon_{22})^2 + (\epsilon_{22} - \epsilon_{33})^2 + (\epsilon_{33} - \epsilon_{11})^2] + \epsilon_{12}^2 + \epsilon_{13}^2 + \epsilon_{23}^2 - k^2 \quad (\text{IIIA.18})$$

in which

$$\xi_{rs} = \tau_{rs} - \alpha_{rs} \quad (\text{IIIA.19})$$

and the tensor α_{rs} is the location of the center of the Von Mises yield surface, and k is its radius. The plastic hardening rules are:

$$\alpha_{rs}^* = \frac{2}{3} (1 - \beta) B \dot{u}_{(r,s)}^P \quad (\text{IIIA.20})$$

and

$$k^* = \frac{1}{\sqrt{3}} \beta B d^P \quad (\text{IIIA.21})$$

with the effective plastic stretching, d^P , defined by

$$d^P = \int \left\{ \frac{2}{3} \dot{u}_{(r,s)}^P \dot{u}_{(r,s)}^P \right\}^{1/2} \quad (\text{IIIA.22})$$

An associated flow rule is used to give:

$$\dot{u}_{(r,s)}^P = \lambda \xi_{rs}' \quad (\text{IIIA.23})$$

where $\xi'_{rs} = \xi_{rs} - \delta_{rs} \xi_{kk} / 3$ is the deviatoric part of ξ_{rs} ,

$$\lambda = \frac{\dot{u}(r,s) \xi'_{rs}}{2k^2(1+B/3\mu)} \quad (\text{IIIA.24})$$

and

$$n_{rs} = \xi'_{rs} / [2k^2(1+B/3\mu)]^{1/2} \quad (\text{IIIA.25})$$

β is a kinematic variable. If β is equal to one, we have the case of isotropic hardening; if β is equal to zero, kinematic hardening, and if β is in between, it is combined isotropic-kinematic hardening. B is the plastic modulus and it is related to the elastic modulus, E , and plastic modulus, E_T , in the uniaxial true stress-strain curve by:

$$E_T = \frac{EB}{E+B} \quad (\text{IIIA.26})$$

III-B. Linearized Variational Equation

Before we can derive the appropriate form of the variational equation, we have to write the constitutive equation in incremental form. Express $\dot{\tau}$ as $\Delta\tau/\Delta t$ and \dot{u} as $\Delta u/\Delta t$, where Δt is the time increment. Equation (IIIA.11) becomes:

$$\Delta\tau_{ij} = \bar{C}_{ijkl} \Delta u_{(k,\ell)} + S_{ijkl} \Delta u_{[k,\ell]} \quad (\text{IIIB.1})$$

Following techniques in [17-20] for deriving linearized variational equations, the linearized version of equation (IIA.27) is given as follows:

$$\begin{aligned}
 & \int_{R_y} \rho \Delta \ddot{u}_i \bar{u}_i \, dR_y \\
 & + \int_{R_y} (\Delta \tau_{ij} + \tau_{ij} (\Delta u_k)_{,k} - (\Delta u_j)_{,k} \tau_{ki}) \bar{u}_{i,j} \, dR_y \\
 & = \int_{R_y} b_i \bar{u}_i \, dR_y + \int_{\partial R_y^h} h_i \bar{u}_i \, dA_y \quad \text{external force} \\
 & - \int_{R_y} \tau_{ij} \bar{u}_{(i,j)} \, dR_y \quad \text{internal force} \\
 & - \int_{R_y} \rho \ddot{u}_i \bar{u}_i \, dR_y \quad \text{inertial force}
 \end{aligned} \quad \left. \vphantom{\int_{R_y}} \right\} \text{(IIIB.2)}$$

in which

$$\bar{u}_i = 0 \quad \text{on } R_y^g \quad \text{(IIIB.3)}$$

Substituting the incremental constitutive equation (IIIB.1) into (IIIB.2) yields:

$$\int_{R_y} \rho \Delta \ddot{u}_i \bar{u}_i \, dR_y + \int_{R_y} \bar{u}_{i,j} d_{ijkl} \Delta u_{k,\ell} \, dR_y = \text{external force} \quad \text{(IIIB.4)}$$

- internal force
 - inertial force

where

$$d_{ijkl} = c_{ijkl} + \tau_{j\ell} \delta_{ik} \quad \text{(IIIB.5)}$$

We observe that d_{ijkl} will possess the major symmetry if the c_{ijkl} 's do, which leads to a symmetric (tangent) stiffness matrix in a Galerkin/finite element formulation as will be discussed in the next section.

This is due to the fact that the Truesdell rate definition of C_{ijkl}^* in (IIIA.10) is employed. (There are other rate definitions which give a

symmetric tangent stiffness matrix.)

Equation (IIIB.1), together with (IIIB.4) and (IIIB.5), constitute a very general formulation which is applicable to arbitrarily large deformations. If large rotations can be precluded, we set

$$S_{ijkl} = C_{ijkl}^* = 0 \quad (\text{IIIB.6})$$

Consequently,

$$d_{ijkl} = c_{ijkl} \quad (\text{IIIB.7})$$

IV. Galerkin/Finite Element Formulation and Matrix Equations

IV-A. Generalized Mixed Lagrangian-Eulerian Linearized Variational Equation

Combining the results that have been developed in the previous two sections, we can write the general form of the linearized mixed Lagrangian-Eulerian variational equation as follows:

$$\begin{aligned}
 & \underbrace{\int_{R_y} \rho \bar{u}_i \Delta(\dot{u}'_i) dR_y}_{\text{linearized part of time derivative term}} + \underbrace{\int_{R_y} \rho \bar{u}_i c_j (\Delta \dot{u}_i)_{,j} dR_y + \int_{R_y} \rho \bar{u}_i \Delta c_j (\dot{u}_i)_{,j} dR_y}_{\text{linearized part of convective force}} \\
 & + \underbrace{\int_{R_y} \bar{u}_{i,j} d_{ijkl} \Delta u_{k,l} dR_y}_{\text{linearized part of internal force}} + \underbrace{\int_{R_y} \bar{u}_{i,j} \hat{d}_{ijkl} \Delta \dot{u}_{k,l} dR_y}_{\text{linearized part of viscosity and penalty terms}} \\
 & = \int_{R_y} b_i \bar{u}_i dR_y + \int_{\partial R_y^h} h_i \bar{u}_i dA_y \quad \text{external force}
 \end{aligned}$$

$$\left. \begin{aligned}
 & - \int_{R_y} \tau_{ij} \bar{u}_{(i,j)} dR_y && \text{internal force} \\
 & - \int_{R_y} \rho(\dot{u}_i) \bar{u}_i dR_y \\
 & - \int_{R_y} \rho c_j(\dot{u}_i)_{,j} \bar{u}_i dR_y
 \end{aligned} \right\} \text{inertial force} \quad (IVA.1)$$

in which

$$\bar{u}_i = 0 \quad \text{on } \partial R_y^g \quad (IVA.2)$$

The first term corresponds to the linearized part of the time-derivative term and the second two terms correspond to the linearized part of the convective force. If we select the Lagrangian description, the latter terms are equal to zero. The third term is the tangential stiffness matrix, as described in Section III-B. The fourth term is the linearized part of the viscosity and penalty terms. We will define \hat{d}_{ijkl} later in this section.

IV-B. Matrix Equations

Background information on Galerkin/finite element formulations may be found in [18,25,26]. Review articles and current trends in finite element research can be found in [27,28,29].

The Galerkin/finite element method consists of the discretization of a region, say R_x , into non-overlapping subregions called "elements." We label each element by an element number "e", e.g., the e^{th} element is denoted by R_x^e , $e = 1, 2, \dots, \text{Numel}$. The discretization of

R_x also consists of $Numnp$ "nodal points." The position vector of the a^{th} node, $a = 1, 2, \dots, Numnp$ is denoted by \underline{x}_a . The "shape function" associated with node a is denoted by N_a and it satisfies the relation $N_a(\underline{x}_b) = \delta_{ab}$. We employ the isoparametric concept [25] that the same shape functions are used for both geometric interpolation and kinematic variables. Specifically, we assume for a typical element ("e"), with n_{en} nodes, that:

$$x_i = \sum_{a=1}^{n_{en}} N_a x_{ia}^e \quad (IVB.1)$$

$$y_i = \sum_{a=1}^{n_{en}} N_a y_{ia}^e \quad (IVB.2)$$

$$u_i = \sum_{a=1}^{n_{en}} N_a u_{ia}^e \quad (IVB.3)$$

$$\hat{u}_i = \sum_{a=1}^{n_{en}} N_a \hat{u}_{ia}^e \quad (IVB.4)$$

$$\dot{u}_i = \sum_{a=1}^{n_{en}} N_a \dot{u}_{ia}^e \quad (IVB.5)$$

$$\hat{\dot{u}}_i = \sum_{a=1}^{n_{en}} N_a \hat{\dot{u}}_{ia}^e \quad (IVB.6)$$

where x_{ia}^e , y_{ia}^e , u_{ia}^e , \hat{u}_{ia}^e , \dot{u}_{ia}^e , and $\hat{\dot{u}}_{ia}^e$ are the a^{th} nodal values of the coordinates in R_x and R_y , particle displacements and "mesh" displacements, particle velocities and "mesh" velocities, respectively. Also for programming purposes, it is convenient to introduce matrix counterparts of the variational equations (IVA.1) and the corresponding constitutive equations (IIIB.1). These are summarized as follows.

Variational equations

$$\begin{aligned}
 & \sum_{b=1}^{n_{en}} \sum_{e=1}^{Nume\ell} \bar{u}^e T \left[\int_{R_y^e} \rho N_a^T N_b dR_y \Delta(\bar{u}')_b^e \right. \\
 & + \int_{R_y^e} (B_a^1)^T E^1 (B_b^1) dR_y \Delta c_b^e \\
 & + \int_{R_y^e} (B_a^1)^T E^2 (B_b^2) dR_y \Delta \dot{u}_b^e \\
 & + \int_{R_y^e} B_a^T D B_b dR_y \Delta u_b^e \\
 & + \left. \int_{R_y^e} B_a^{\gamma T} \hat{D} B_b^{\gamma} dR_y \Delta \dot{u}_b^e \right. \\
 & = \int_{R_y^e} N_a^T b dR_y + \int_{\partial R_y^e} N_a^T h dA_y \\
 & - \int_{R_y^e} B_a^{\gamma T} \tau dR_y - \int_{R_y^e} \rho N_a^T (\dot{u}') dR_y \\
 & \left. - \int_{R_y^e} \rho N_a^T \eta dR_y \right]
 \end{aligned} \tag{IVB.7}$$

where

$$\tilde{B}_a^1 = \begin{bmatrix} N_a & 0 & 0 \\ 0 & N_a & 0 \\ 0 & 0 & N_a \end{bmatrix} = \tilde{N}_a \tag{IVB.8}$$

$$\tilde{E}^1 = \begin{bmatrix} \rho \dot{u}_{1,1} & \rho \dot{u}_{1,2} & \rho \dot{u}_{1,3} \\ \rho \dot{u}_{2,1} & \rho \dot{u}_{2,2} & \rho \dot{u}_{2,3} \\ \rho \dot{u}_{3,1} & \rho \dot{u}_{3,2} & \rho \dot{u}_{3,3} \end{bmatrix} \tag{IVB.9}$$

$$\tilde{B}_a^2 = \begin{bmatrix} N_{a,1} & 0 & 0 \\ N_{a,2} & 0 & 0 \\ N_{a,3} & 0 & 0 \\ 0 & N_{a,1} & 0 \\ 0 & N_{a,2} & 0 \\ 0 & N_{a,3} & 0 \\ 0 & 0 & N_{a,1} \\ 0 & 0 & N_{a,2} \\ 0 & 0 & N_{a,3} \end{bmatrix} \quad (\text{IVB.10})$$

$$\tilde{E}^2 = \rho \begin{bmatrix} c_1 & c_2 & c_3 & 0 & 0 & 0 & 0 & 0 & 0 \\ 0 & 0 & 0 & c_1 & c_2 & c_3 & 0 & 0 & 0 \\ 0 & 0 & 0 & 0 & 0 & 0 & c_1 & c_2 & c_3 \end{bmatrix} \quad (\text{IVB.11})$$

$$\tilde{B}_a = \begin{bmatrix} B_a^Y \\ B_a^\theta \end{bmatrix} \quad (\text{IVB.12})$$

$$\tilde{D} = \begin{bmatrix} \tilde{C} & \tilde{O}_{63} \\ \tilde{O}_{36} & \tilde{O}_{33} \end{bmatrix} + \tilde{T} \quad (\text{IVB.13})$$

$$\tilde{B}_a^Y = \begin{bmatrix} N_{a,1} & 0 & 0 \\ N_{a,2} & N_{a,1} & 0 \\ 0 & N_{a,2} & 0 \\ 0 & 0 & N_{a,3} \\ 0 & N_{a,3} & N_{a,2} \\ N_{a,3} & 0 & N_{a,1} \end{bmatrix} \quad (\text{IVB.14})$$

$$\underline{B}_a^\theta = \begin{bmatrix} N_{a,2} & -N_{a,1} & 0 \\ 0 & N_{a,3} & -N_{a,2} \\ -N_{a,3} & 0 & N_{a,1} \end{bmatrix} \quad (\text{IVB.15})$$

$$\underline{\hat{D}} = [\hat{D}_{IJ}] = [\hat{D}_{ijkl}] \quad (\text{the components will be defined in the next section}) \quad (\text{IVB.16})$$

$$\underline{\eta} = \begin{bmatrix} c_1 \dot{u}_{1,1} + c_2 \dot{u}_{1,2} + c_3 \dot{u}_{1,3} \\ c_1 \dot{u}_{2,1} + c_2 \dot{u}_{2,2} + c_3 \dot{u}_{2,3} \\ c_1 \dot{u}_{3,1} + c_2 \dot{u}_{3,2} + c_3 \dot{u}_{3,3} \end{bmatrix} \quad (\text{IVB.17})$$

where 0_{mn} denotes the $m \times n$ zero matrix, \underline{C} is a 6×6 matrix of material tangent moduli whose components are given by $C_{IJ} = C_{ijkl}$ in which the relationships between the indices are given by:

I \ J	i \ k	j \ l
1	1	1
2	1	2
3	2	2
4	3	3
5	2	3
6	3	1

(IVB.18)

The ordering convention in (IVB.18) may seem strange at first, but it is quite convenient for reducing to two-dimensional and axisymmetric theories (see Part II of [16]).

The initial-stress matrix, \underline{T} , is defined as follows:

$$\tilde{T} = \begin{bmatrix}
 \tau_1 & \frac{\tau_2}{2} & 0 & 0 & 0 & \frac{\tau_6}{2} & \frac{\tau_2}{2} & 0 & -\frac{\tau_6}{2} \\
 \frac{\tau_1+\tau_3}{4} & \frac{\tau_2}{2} & 0 & 0 & \frac{\tau_6}{4} & \frac{\tau_5}{4} & \frac{\tau_3-\tau_1}{4} & \frac{\tau_6}{4} & -\frac{\tau_5}{4} \\
 \tau_3 & 0 & \frac{\tau_5}{4} & 0 & -\frac{\tau_2}{2} & \frac{\tau_5}{2} & 0 & 0 & 0 \\
 \tau_4 & \frac{\tau_5}{2} & \frac{\tau_6}{2} & 0 & -\frac{\tau_5}{2} & \frac{\tau_6}{2} & 0 & -\frac{\tau_5}{2} & \frac{\tau_6}{2} \\
 \frac{\tau_3+\tau_4}{4} & \frac{\tau_2}{4} & -\frac{\tau_6}{4} & \frac{\tau_4-\tau_3}{4} & \frac{\tau_2}{4} & 0 & -\frac{\tau_6}{4} & \frac{\tau_4-\tau_3}{4} & \frac{\tau_2}{4} \\
 \tau_4+\tau_1 & \frac{\tau_5}{4} & -\frac{\tau_2}{4} & \frac{\tau_1-\tau_4}{4} & 0 & 0 & 0 & 0 & 0 \\
 \frac{\tau_1+\tau_3}{4} & -\frac{\tau_6}{4} & -\frac{\tau_5}{4} & 0 & 0 & 0 & 0 & 0 & 0 \\
 \frac{\tau_3+\tau_4}{4} & -\frac{\tau_2}{4} & 0 & 0 & 0 & 0 & 0 & 0 & 0 \\
 \frac{\tau_4+\tau_1}{4} & 0 & 0 & 0 & 0 & 0 & 0 & 0 & 0
 \end{bmatrix}$$

SYMMETRIC

(IVB.19)

where

$$\tau_I = \tau_{ij} \tag{IVB.20}$$

The \tilde{D} matrix is arranged to be compatible with the following ordering of strain and rotation components:

$$\gamma_{11}, 2\gamma_{12}, \gamma_{22}, \gamma_{33}, 2\gamma_{23}, 2\gamma_{31}, 2\omega_{12}, 2\omega_{23}, 2\omega_{31} \tag{IVB.21}$$

in which

$$\left. \begin{aligned}
 \gamma_{ij} &= (\Delta u_{i,j} + \Delta u_{j,i}) / 2 \\
 \omega_{ij} &= (\Delta u_{i,j} - \Delta u_{j,i}) / 2
 \end{aligned} \right\} \tag{IVB.22}$$

and

Incremental constitutive equation

The following definitions are used to derive the tangential initial stress matrix, but an improved representation can be used to integrate the constitutive equation (see Chapter 3, Sect. III).

$$\Delta \underline{\tau} = \underline{\bar{C}} \underline{\gamma} + \underline{S} \underline{\omega} \quad \text{Incremental Constitutive Equation (IVB.23)}$$

$$\Delta \underline{\tau} = \{\Delta \tau_I\} \quad \text{(IVB.24)}$$

$$\underline{\bar{C}} = \underline{C} + \underline{C}^* \quad \text{(IVB.25)}$$

$$\underline{C} = [C_{IJ}] \quad \text{(IVB.26)}$$

$$C_{IJ} = C_{ijkl} \quad \text{(IVB.27)}$$

$$\underline{\bar{C}}^* = \begin{bmatrix} \tau_1 & \tau_2 & -\tau_1 & -\tau_1 & 0 & \tau_6 \\ 0 & \frac{\tau_1 + \tau_3}{2} & 0 & -\tau_2 & \frac{\tau_6}{2} & \frac{\tau_5}{2} \\ -\tau_3 & \tau_2 & \tau_3 & -\tau_3 & \tau_5 & 0 \\ \hline -\tau_4 & 0 & -\tau_4 & \tau_4 & \tau_5 & \tau_6 \\ -\tau_5 & \frac{\tau_6}{2} & 0 & 0 & \frac{\tau_3 + \tau_4}{2} & \frac{\tau_2}{2} \\ 0 & \frac{\tau_5}{2} & -\tau_6 & 0 & \frac{\tau_2}{2} & \frac{\tau_4 + \tau_1}{2} \end{bmatrix} \quad \begin{array}{l} \text{Truesdell-} \\ \text{Rate Stress} \\ \text{Matrix} \end{array} \quad \text{(IVB.28)}$$

$$\underline{\gamma} = \begin{bmatrix} \Delta u_{1,1} \\ \Delta u_{1,2} + \Delta u_{2,1} \\ \Delta u_{2,2} \\ \Delta u_{3,3} \\ \Delta u_{2,3} + \Delta u_{3,2} \\ \Delta u_{3,1} + \Delta u_{1,3} \end{bmatrix} = \sum_{a=1}^{n_{en}} B_{\sim a}^Y \Delta u_{\sim a}^e \quad \text{Incremental Strain Vector} \quad \text{(IVB.29)}$$

$$\tilde{S} = \begin{bmatrix} \tau_2 & 0 & -\tau_6 \\ \frac{\tau_3 - \tau_1}{2} & \frac{\tau_6}{2} & -\frac{\tau_5}{2} \\ -\tau_2 & \tau_5 & 0 \\ \hline 0 & -\tau_5 & \tau_6 \\ -\frac{\tau_6}{2} & \frac{\tau_4 - \tau_3}{2} & \frac{\tau_2}{2} \\ \frac{\tau_5}{2} & -\frac{\tau_2}{2} & \frac{\tau_1 - \tau_4}{2} \end{bmatrix} \quad (\text{IVB.30})$$

$$\tilde{\omega} = \begin{bmatrix} \Delta u_{1,2} - \Delta u_{2,1} \\ \Delta u_{2,3} - \Delta u_{3,2} \\ \Delta u_{3,1} - \Delta u_{1,3} \end{bmatrix} = \sum_{a=1}^{N_{en}} B_a^\theta \Delta u_a^e \quad (\text{IVB.31})$$

Incremental Rotation Vector

$$\Delta u_a^e = \begin{bmatrix} \Delta u_{a1}^e \\ \Delta u_{a2}^e \\ \Delta u_{a3}^e \end{bmatrix} \quad \begin{array}{l} \text{Element Nodal Displacement} \\ \text{Increment Vector} \end{array} \quad (\text{IVB.32})$$

IV-C. Definition of \hat{d}_{ijkl} for Incompressible Fluid and Slightly Compressible Fluid

We restrict ourselves to incompressible or slightly compressible fluids. In this way \tilde{S} , \tilde{C}^* , and \tilde{T} can be set to zero, so that:

$$d_{ijkl} = c_{ijkl} = \hat{d}_{ijkl} \quad (\text{IVC.1})$$

Recall from equation (IIA.3) that

$$\tau_{ij} = -p\delta_{ij} + 2\mu \dot{u}_{(i,j)} \quad (\text{IVC.2})$$

For the penalty function formulation [15], we let

$$p = -\lambda(\dot{u}_{i,i}) \quad (\text{IVC.3})$$

where $\lambda > 0$ is the penalty parameter. Substituting (IVC.3) into (IVC.2) yields

$$\tau_{ij} = \lambda \delta_{ij} \dot{u}_{k,k} + 2\mu \dot{u}_{(i,j)} \quad (\text{IVC.4})$$

and therefore

$$\hat{D}_{IJ} = [\hat{d}_{ijkl}] \quad (\text{IVC.5})$$

and

$$\hat{D} \sim \begin{bmatrix} \lambda+2\mu & 0 & \lambda & \lambda & 0 & 0 \\ 0 & \mu & 0 & 0 & 0 & 0 \\ \lambda & 0 & \lambda+2\mu & \lambda & 0 & 0 \\ \lambda & 0 & \lambda & \lambda+2\mu & 0 & 0 \\ 0 & 0 & 0 & 0 & \mu & 0 \\ 0 & 0 & 0 & 0 & 0 & \mu \end{bmatrix} \quad (\text{IVC.6})$$

(Note that the \hat{D} is formally the same as the matrix for classical linear isotropic elasticity.)

If we consider the slightly compressible formulation, recall equation (IIA.11),

$$\tau_{ij} = -(p_0 - \int_0^t \beta \rho \dot{u}_{k,k} dt) \delta_{ij} + 2\mu \dot{u}_{(i,j)} \quad (\text{IVC.7})$$

A time-discrete form of the pressure part of the constitutive equation is

$$-\Delta p = \Delta t \rho \beta \dot{u}_{k,k} \quad (\text{IVC.8})$$

from which it follows that

$$\hat{D} = \begin{bmatrix} \Delta t \rho \beta + 2\mu & 0 & \Delta t \rho \beta & \Delta t \rho \beta & 0 & 0 \\ 0 & \mu & 0 & 0 & 0 & 0 \\ \Delta t \rho \beta & 0 & \Delta t \rho \beta + 2\mu & \Delta t \rho \beta & 0 & 0 \\ \Delta t \rho \beta & 0 & \Delta t \rho \beta & \Delta t \rho \beta + 2\mu & 0 & 0 \\ 0 & 0 & 0 & 0 & \mu & 0 \\ 0 & 0 & 0 & 0 & 0 & \mu \end{bmatrix} \quad (\text{IVC.9})$$

References

1. A. C. Eringen, Continuum Physics, Vols. I and II (Academic Press, New York and London, 1974).
2. K. S. Pister, "Continuum mechanics--a brief review," Lectures on Finite Element Method in Continuum Mechanics (J. T. Oden and E. R. de Arantes e Olivera, eds.) (University of Alabama, Huntsville, 1973).
3. Y. C. Fung, Foundations of Solid Mechanics (Prentice-Hall, Englewood Cliffs, New Jersey, 1965).
4. J. T. Oden, Finite Element of Nonlinear Continua (McGraw-Hill, New York, 1972).
5. J. K. Knowles, E. Sternberg, "Notes on mathematical theory of elasticity, Applied Mechanics (AM) 135 and 136", California Institute of Technology.
6. L. E. Malvern, Introduction to the Mechanics of a Continuous Medium, (Prentice Hall, 1969).
7. A. A. Amsden and C. W. Hirt, "YAQUI: An arbitrary Lagrangian-Eulerian computer program for fluid flow at all speeds," Report LA-5100, Los Alamos Scientific Laboratory, Los Alamos, New Mexico, March 1973.
8. J. Donea, P. Fasoli-Stella, and S. Giuliani, "Lagrangian and Eulerian finite element techniques for transient fluid-structure interaction problems," Trans. Fourth Internat. Conf. on Structural Mechanics in Reactor Technology, San Francisco, August 1977.
9. T. Belytschko and J. M. Kennedy, "Computer models for subassembly simulation," preprint.
10. T.J.R. Hughes, W. K. Liu, and T. K. Zimmermann, "Lagrangian, Eulerian finite element formulation for incompressible viscous flows," Presented at the U.S.-Japan Conf. on Interdisciplinary Finite-Element Analysis, Cornell University, Aug. 7-11, 1978.

11. J.E.A. John and W. Haberman, Introduction to Fluid Mechanics, (Prentice-Hall, Inc., 1971).
12. J. Chow, "Notes on Continuum Mechanics (Mate 316)," University of Illinois at Chicago Circle.
13. T.J.R. Hughes and J. M. Winget, "Finite rotation effects in numerical integration of rate constitutive equations arising in large-deformation analysis." *Internat. J. Numerical Math. in Eng.*, in press
14. J. O. Hallquist, "NIKE2D: An implicit, finite-deformation, finite-element code for analyzing the static and dynamic response of two-dimensional solids," Lawrence Livermore Laboratory, Report UCRL-52678, University of California, Livermore, March 3, 1979.
15. T.J.R. Hughes, W. K. Liu, and A. Brooks, "Review of finite element analysis of incompressible viscous flows by the penalty function formulation," *J. Computational Phys.* 30, 1-60 (1979).
16. T.J.R. Hughes and W. K. Liu, "Nonlinear finite element analysis of shells: Part I - Three-dimensional shells; Part II - Two-dimensional shells." *Computer Meth. in Appl. Mech. and Eng.*, in press.
17. T.J.R. Hughes, "On consistently derived tangent stiffness matrices," in preparation.
18. T.J.R. Hughes, "AE/AM108: Finite element method, class notes," California Institute of Technology.
19. R. M. McMeeking and J. R. Rice, "Finite element formulations for problems of large elastic-plastic deformation," *Internat. J. Solids and Structures* 11, 601-616 (1975).
20. T.J.R. Hughes and K. S. Pister, "Consistent linearization in mechanics of solids," *Computers and Structures* 8, 391-397 (1978).
21. R. D. Krieg and S. W. Key, "Implementation of a time independent plasticity theory into structural computer programs," Constitutive Equations in Viscoplasticity: Computational and Engineering Aspects, AMD 20 (ASME, New York, 1976).

22. C. Truesdell and W. Noll, The Nonlinear Field Theories of Mechanics, Vol. III/3 in Encyclopedia of Physics (S. Flügge, ed.), (Springer-Verlag, Berlin-Heidelberg-New York, 1965).
23. M. A. Biot, Mechanics of Incremental Deformation (John Wiley and Sons, Inc., 1965).
24. T.J.R. Hughes and J. E. Marsden, The Mathematical Foundations of Continuum Mechanics; in preparation.
25. O. C. Zienkiewicz, The Finite Element Method, 3d edition (McGraw-Hill, New York, 1977).
26. R. H. Gallagher, Finite Element Analysis Fundamentals (Prentice-Hall, Inc, 1975).
27. G. Horrigmoe, Nonlinear Finite Element Models in Solid Mechanics (The Norwegian Institute of Technology, University of Trondheim, Norway, 1976).
28. T.J.R. Hughes, "Current trends in finite element research," Feature article to appear in Applied Mechanics Reviews.
29. T.J.R. Hughes, "Recent developments in computer methods for structural analysis," Nucl. Eng. and Design 57, No. 2, May 1980.

Chapter 3

NUMERICAL SOLUTION TECHNIQUES

I. Numerical Integration of the Variational Equations

The exact integration of the expressions appearing in the variational equation (IVB.7 of Chapter 2) is, for all practical purposes, impossible, especially for complex, distorted elements. So instead, we employ numerical integration formulas to carry it out. For purposes of finite element analysis it is only necessary to use "sufficiently accurate" rules. With numerical integration we replace the integrals by a weighted sum of values of the integrand. However, the cost of numerical integration (i.e., computer time) can be quite significant. It is therefore of interest to determine the minimum integration requirement permitting "convergence", and yet to preserve the "rate of convergence" which would result if "exact integration" were used.

There are many numerical integration rules which may be used. In finite element work, the Gauss numerical integration or Gauss-Legendre quadrature, as it is now frequently called [1,2,3], is well suited for Cartesian produce subdomains (e.g., quadrilaterals and bricks).

I-A. Selective Integration

Historically, kinematical constraints have proven difficult to deal with by the standard "displacement" finite element method.

Examples of these kinematical constraints are:

- 1) "Nearly-incompressible" solids, in which the volumetric deformation is much much less than the deviatoric deformations.
- 2) "Incompressible" fluids, in which the divergence of the velocity

field is zero.

- 3) Beams, plates, and shells based upon theories which account for transverse shear deformations in which the transverse shear deformations approach zero in the thin beam (plate, shell, respectively) limit.

Simple, low-order elements have behaved particularly poorly. "Mixed" and "hybrid" [2,4-7,11] elements have been proposed as alternatives. The whole subject was poorly understood throughout the 1960's. In the early 1970's reduced integration procedures began to be used. However, they were also poorly understood and not generally adopted. In 1974, Fried [8], Nagtegaal et al. [9], and Malkus [10] performed important investigations focusing on the rank condition, constraint counts, and equivalence theorems, respectively. These workers created renewed interest in reduced/selective integration techniques and allied topics and, as a result, successful methods for kinematically constrained media could be developed within the displacement method.

Within recent years, a greater understanding of this subject has been achieved. Two techniques have proved very popular. They are the reduced/selective integration procedure as advocated by Malkus and Hughes [7], and the mean-dilatation formulation proposed by Nagtegaal et al. [9]. Both techniques have proven successful, but both have their limitations.

The reduced/selective integration technique is a fairly general concept and has been applied to a wide variety of finite elements. For details see [2,7,12-17]. In [12], Hughes and coworkers applied this technique to finite element analysis of plates, employing the basic

isoparametric elements [2]: the four-node bilinear quadrilateral and the nine-node biquadratic quadrilateral. In [13], Hughes and Cohen proposed the "heterosis" finite element for plate bending in which they used nine-node biquadratic shape functions for rotation fields and eight-node "serendipity" shape functions for displacement field, together with the reduced/selective integration technique. In [14] Hughes and Liu successfully extended the technique to nonlinear finite element analysis of shells as will be discussed in more detail in the next chapter. In [15,16] Hughes and coworkers applied the technique, together with the penalty function formulation, to finite element analysis of incompressible viscous flows and Lagrangian-Eulerian descriptions for incompressible fluids. They will be discussed in detail in Chapter 5. In [17] Hughes and Prevost employed the same ideas in nonlinear quasi-static finite element analysis of soil via the computer program DIRT II.

The mean-dilatation formulation is a more special technique which has been used mostly in the context of basic isoparametric elements. The two approaches are identical for the four-node quadrilateral in two-dimensional plane strain and the eight-node brick in three-dimensional analysis. However, the mean-dilatation formulation appears to behave somewhat better in axisymmetric analysis than does the corresponding reduced/selective integration procedure [9].

The rationale behind these two techniques has been discussed at length in [2,7-10,12-17], so we only provide a brief summary here.

The reduced/selective integration procedure for the continuum elements case goes as follows: The "stiff" term (dilatation term) may be segregated from the remainder (deviatoric term). A reduced quadrature rule is then used on the stiff term to lessen the constraint

("locking") and a normal, quadrature is used on the remainder such that correct rank is maintained. If the segregated terms are tensor invariants, that is, the resulting matrices transform properly with respect to rotation of the global reference frame [12], then the resulting arrays are similarly invariant. An example of selective Gauss-Legendre integration rules for two-dimensional isoparametric Lagrange elements is presented in Figure IA-1. Extension to three-dimensional isoparametric Lagrange elements is straightforward. One drawback of the reduced/selective integration procedure is that triangular elements and "serendipity" quadrilaterals generally exhibit inferior behavior [18].

In the context of the general material laws, such as equation (IVB.23) of Chapter 2, explicit segregation of the contributions to the matrix equations into dilatation, deviatoric, and coupling terms proves very inconvenient. In principle, a decomposition of this kind is possible, however, it is not at all clear how to treat the coupling terms. Also the element implementation is awkward. Clearly an alternative general scheme is called for.

Hughes proposed a generalization of selective integration procedures to anisotropic and nonlinear media [19]. Instead of separating the d_{ijkl} (in eq. (IIIB.5) of Chapter 2) into dilatation, deviatoric, and coupling terms, the matrix B_a^Y appearing in equation (IVB.7) of Chapter 2 is modified. A summary of the procedure is as follows; for details the reader is urged to consult [19]. The original B_a^Y is divided into B_a^{dil} and B_a^{dev} which are defined as:

$$B_a^Y = B_a^{dil} + B_a^{dev} \quad (IA.1)$$

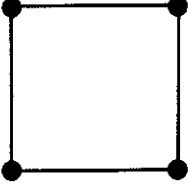
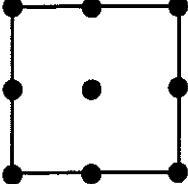
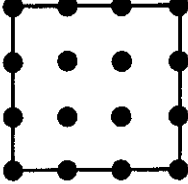
			
<p>shape functions</p>	<p>bilinear</p>	<p>biquadratic</p>	<p>bicubic</p>
<p>λ-term</p>	<p>1 point</p>	<p>2 x 2</p>	<p>3 x 3</p>
<p>μ-term</p>	<p>2 x 2</p>	<p>3 x 3</p>	<p>4 x 4</p>

Fig. IA-1. Selective Gauss-Legendre integration rules for 2-dimensional isoparametric Lagrange elements.

where

$$\tilde{B}_a^{dil} = \frac{1}{3} \begin{bmatrix} B_1 & B_2 & B_3 \\ 0 & 0 & 0 \\ B_1 & B_2 & B_3 \\ \hline B_1 & B_2 & B_3 \\ 0 & 0 & 0 \\ 0 & 0 & 0 \end{bmatrix} \quad (IA.2)$$

The deviatoric part is then given by:

$$\tilde{B}_a^{dev} = \begin{bmatrix} B_1 & 0 & 0 \\ B_2 & B_1 & 0 \\ 0 & B_2 & 0 \\ \hline 0 & 0 & B_3 \\ 0 & B_3 & B_2 \\ B_3 & 0 & B_1 \end{bmatrix} - \frac{1}{3} \begin{bmatrix} B_1 & B_2 & B_3 \\ 0 & 0 & 0 \\ B_1 & B_2 & B_3 \\ \hline B_1 & B_2 & B_3 \\ 0 & 0 & 0 \\ 0 & 0 & 0 \end{bmatrix} \quad (IA.3)$$

We construct a new \tilde{B}_a^Y called $\bar{\tilde{B}}_a^Y$ (which replaces \tilde{B}_a^Y) by:

$$\bar{\tilde{B}}_a^Y = \tilde{B}_a^{dev} + \bar{\tilde{B}}_a^{dil} \quad (IA.4)$$

in which $\bar{\tilde{B}}_a^{dil}$ is the "improved" dilatational contribution and is defined

by:

$$\bar{\tilde{B}}_a^{dil} = \frac{1}{3} \begin{bmatrix} \bar{B}_1 & \bar{B}_2 & \bar{B}_3 \\ 0 & 0 & 0 \\ \bar{B}_1 & \bar{B}_2 & \bar{B}_3 \\ \hline \bar{B}_1 & \bar{B}_2 & \bar{B}_3 \\ 0 & 0 & 0 \\ 0 & 0 & 0 \end{bmatrix} \quad (IA.5)$$

The resulting $\bar{B}_{\sim a}^Y$ is

$$\bar{B}_{\sim a}^Y = \left[\begin{array}{ccc|ccc} B_5 & B_6 & B_8 & & & \\ B_2 & B_1 & 0 & & & \\ B_4 & B_7 & B_8 & & & \\ \hline B_4 & B_6 & B_9 & & & \\ 0 & B_3 & B_2 & & & \\ B_3 & 0 & B_1 & & & \end{array} \right] \quad (\text{IA.6})$$

where

$$\left. \begin{array}{l} B_4 = (\bar{B}_1 - B_1) / 3 \\ B_5 = B_1 + B_4 \\ B_6 = (\bar{B}_2 - B_2) / 3 \\ B_7 = B_2 + B_6 \\ B_8 = (\bar{B}_3 - B_3) / 3 \\ B_9 = B_3 + B_8 \end{array} \right\} \quad (\text{IA.7})$$

With $\bar{B}_{\sim a}^Y$ defined, the stiffness matrix and internal force vector are integrated within one "DO LOOP" [20], using a single integration rule.

$\bar{B}_{\sim a}^{dil}$ can be constructed to be equivalent to: (1) selective integration of all orders; (2) mean-dilatation and higher-order generalizations. Similar procedures have been employed by Hughes and Liu [14] in nonlinear finite element analysis of plates and shells (see also Chapter 4).

As an example, let us pick $\bar{B}_{\sim a}^{dil}$ such that it is equivalent to selective integration. A quadrature rule is specified to integrate the element stiffness matrix and internal force vector. This rule is considered the "normal" one. Introduce a "reduced" rule; let \bar{N}_{int} and $\bar{\xi}_{\sim l}$ be the numbers of integration points and the corresponding locations

for the "reduced" rule. A specified set of shape functions, $\bar{N}_{\sim l}$'s, is defined with the nodal points equal to $\bar{\xi}_{\sim l}$'s (i.e., $\bar{N}_k(\bar{\xi}_{\sim l}) = \delta_{kl}$). The general form of \bar{B}_i is

$$\bar{B}_i(\bar{\xi}) = \sum_{\ell=1}^{\bar{N}_{int}} \bar{N}_{\ell}(\bar{\xi}) B_{i\ell} \quad (IA.8)$$

The equivalent of selective integration is achieved if $B_{i\ell} = B_i(\bar{\xi}_{\sim l})$.

The specialization of equation (IA.8) to mean-dilatation formulation and other generalizations has been discussed by Hughes [19], and will not be discussed here. A flow chart of the computer programming aspects is presented in Table IA-1.

Table IA-1. Flow Chart of Generalizations of Selective Integration Procedures

1. Loop over each element.
 2. Pick up position vector arrays.
 3. Define the shape functions $\bar{N}_i(\bar{\xi}_k)$ and derivatives $B_{i\ell}(\bar{\xi}_k)$ for $1 \leq k \leq \bar{N}_{int}$, and store.
 4. Loop on the "normal" integration points ($\bar{\xi}_{\sim l}$).
 5. Compute the "normal" shape functions, $N_i(\bar{\xi}_{\sim l})$, and corresponding derivatives $B_i(\bar{\xi}_{\sim l})$.
 6. Define $\bar{B}_i(\bar{\xi}_{\sim l})$ using equation (IA.8).
 7. Define $\bar{B}_a^Y(\bar{\xi}_{\sim l})$ using equations (IA.6) and (IA.7).
 8. Form stiffness matrix and internal forces.
 9. If $\ell < N_{int}$ GO TO 4
If $\ell \geq N_{int}$ GO TO 1
-

I-B. "Upwind" Finite Elements by Modifying the Standard Gauss-Legendre Rules

As can be seen from equation (IVB.7) of Chapter 2, the second and third terms constitute a nonsymmetric operator. The Galerkin finite element method has been successful in structural and solid mechanics in which the operator is a symmetric one. Until recently, nonself-adjoint cases (nonsymmetric operators) have not been well understood. If we use Gauss quadrature on the convective terms appearing in the above-mentioned equation, spurious spatial oscillations are exhibited for some high Reynolds number flows. These noisy results can only be corrected by mesh refinements. However, in most problems of engineering interest, convection is dominant and the geometry is so complex that severe mesh refinement is not economically feasible. To circumvent these problems, "upwind" finite elements [15,16,25-29] or Petrov-Galerkin methods [22-25] are used as alternatives to generate stable finite element approximations to highly convective flows.

As observed in the finite difference literature, "upwind" difference schemes [21] may be employed to preclude such oscillations, but due to excessive numerical diffusion, the accuracy of the solution may degrade considerably. Among the proposed upwind-type finite element procedures, some schemes are subject to the same criticisms. However, some have been shown to be superior (see e.g., [28,39,40]).

In fact, for some convection-dominated flows, the basic Galerkin/finite element method is adequate, and a great deal of success and progress has been reported in the finite element literature (see e.g., [30-36]). Nevertheless, based on the "Comments" and "Reply to the Comments" made by Gartling [37] and Zienkiewicz [38], respectively, and

also from the numerical example shown in [15], basic Galerkin/finite element methods exhibit spurious behavior wherever there is a downstream essential, or "hard" boundary condition, in convection dominated situations.

The first method used is based upon numerical integration rules which are simple, efficient, very easy to implement, and yet effective. Instead of using the standard Gauss-Legendre rules, a modified "upwind" integration rule was employed. The positions of the integration points are determined from the "element Reynolds number." Since it has been adequately documented elsewhere [see 16, and Sec. 4.3 of 15], this modified "upwind" integration rule will not be discussed here. However, we will show some numerical examples to demonstrate the effectiveness of the proposed theories in Chapter 5.

The performance of the "upwind" scheme used was found to be satisfactory for a wide class of slow problems, as will be discussed later. However, for some time-dependent convection-dominated flow problems it was found that the "spurious crosswind diffusion" produced by the upwind scheme degrades the accuracy of the solution [see 28,39]. A multidimensional upwind scheme with no "crosswind diffusion" was designed and shown to be superior to the quadrature scheme [28,39].

Computational fluid dynamics is still a relatively young science so it is still too early to evaluate the relative merits of the various proposed schemes. Although these schemes differ considerably in concept and implementation, they are "designed" to achieve similar ends. Therefore, it is beyond the scope of this thesis to design the "ultimate" scheme for computational fluid dynamics. The interested reader may profitably consult [25-39] and references cited therein for further information on this topic.

While the objective of this thesis is development of finite element procedures for fluid-structure interaction, it is worthwhile to implement new ideas and examine relative merits. Therefore, the upwind scheme with no "crosswind diffusion" proposed in [39] will be used for the examples shown in Chapter 6. However, for fluid-structure interaction problems in which the mixed Lagrangian-Eulerian formulation is employed, the scheme in [39], which is restricted to the Eulerian case, has to be modified. Following [39], we modify the equation of motion in the mixed Lagrangian-Eulerian description (equation IB.10) of Chapter 2) to:

$$\rho(\dot{u}_i) + \rho \dot{c}_j (\dot{u}_i)_{,j} = (\tau_{ij} + D_{ij})_{,j} \quad (\text{IB.1})$$

where D_{ij} is an artificial viscous force and is determined by:

$$D_{ij} = \dot{u}_{i,k} \tilde{\mu}_{jk} \quad (\text{IB.2})$$

in which

$$\tilde{\mu}_{jk} = \tilde{\mu} \hat{c}_k \hat{c}_j \quad (\text{IB.3})$$

$$\hat{c}_k = c_k / \|c\| \quad (\text{IB.4})$$

and $\tilde{\mu}$ is defined as follows:

$$\tilde{\mu} = \rho \left(\sum_{i=1}^{N_{SD}} \bar{\xi}_i c_{\xi i} h_{\xi i} \right) / N_{SD} \quad (\text{IB.5})$$

where

$$\bar{\xi}_i = \coth \alpha_{\xi i} - 1/\alpha_{\xi i}$$

or approximately

$$\bar{\xi}_i = \begin{cases} \alpha_{\xi i}/3 & -3 \leq \alpha_{\xi i} \leq 3 \\ \text{sgn } \alpha_{\xi i} & |\alpha_{\xi i}| > 3 \end{cases} \quad (\text{IB.6})$$

in which

$$\alpha_{\xi i} = \rho c_{\xi i} h_{\xi i} / 2\mu \quad (\text{IB.7})$$

and

$$c_{\xi i} = \underline{e}_{\xi i} \cdot \underline{c} \quad (\text{IB.8})$$

The meaning of $h_{\xi i}$ and $\underline{e}_{\xi i}$ is illustrated in Fig. IB-1 for the four-node bilinear quadrilateral. The corresponding variational equation for (IB.1) can be written as follows:

$$\begin{aligned} & \int_{R_y} [\rho \bar{u}_i (\dot{u}_i) + \tau_{ij} \bar{u}_{i,j}] dR_y \\ & + \int_{R_y} \rho (\bar{u}_i + \tilde{u}_i) c_j u_{i,j} dR_y \\ & = \int_{R_y} b_i \bar{u}_i dR_y + \int_{\partial R_y^h} h_i \bar{u}_i dA_y \end{aligned} \quad (\text{IB.9})$$

in which

$$\bar{u}_i = 0 \quad \text{on} \quad \partial R_y^g \quad (\text{IB.10})$$

and

$$\tilde{u}_i = \frac{\tilde{\mu}}{\rho \|\underline{c}\|} \bar{u}_{i,k} \hat{c}_k \quad (\text{IB.11})$$

In [28], it is suggested to use "consistent weighting." For the intended applications it was thought to be sufficient at this stage of development to neglect consistent weighting. Nevertheless, it is anticipated that a consistent weighted formulation (Petrov-Galerkin scheme) would lead to improved results in transient analysis. (This is being

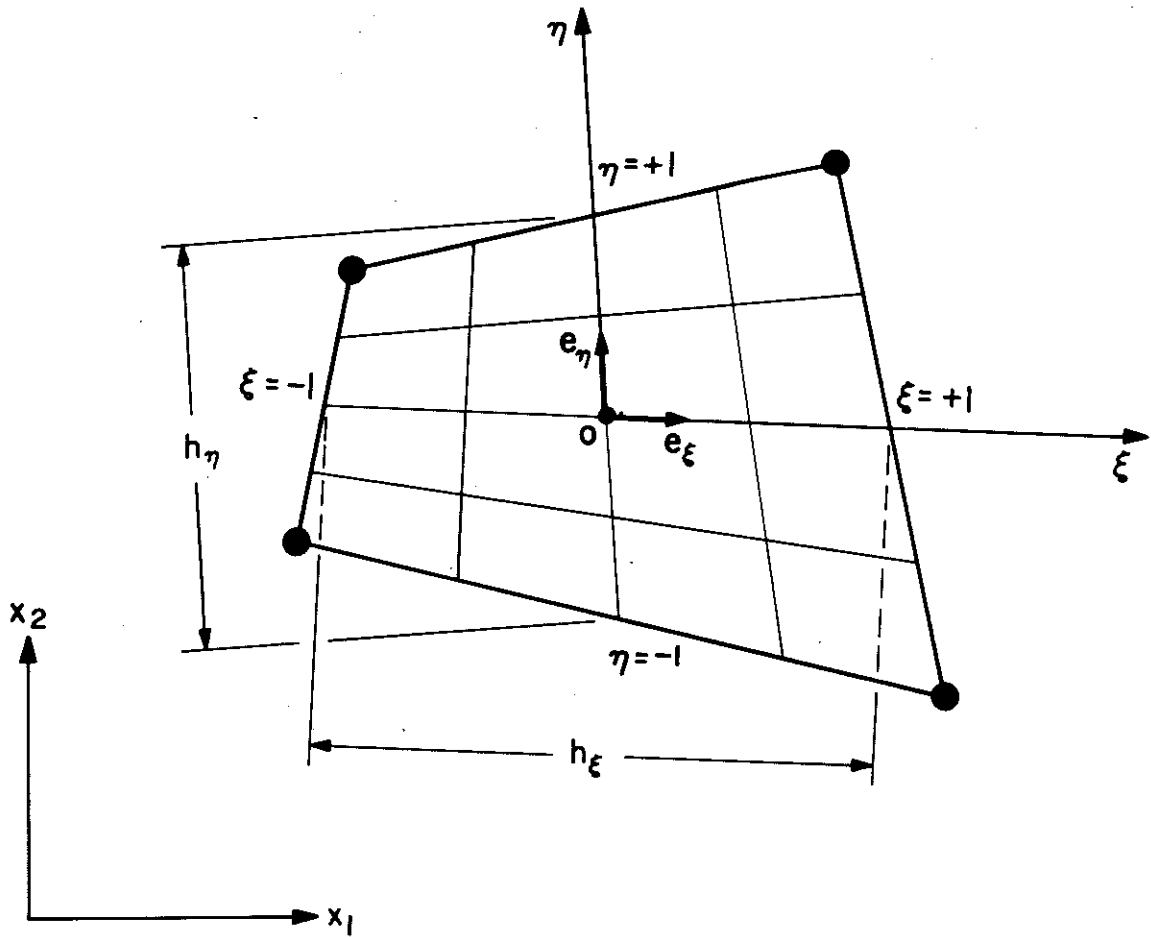


Fig. IB-1

undertaken in the thesis of Brooks [40].)

I-C. Mass Matrix

If we use the standard Gauss quadrature on the first term of equation (IVb.7) of Chapter 2, the resulting matrix is called the consistent mass matrix. It is symmetric and positive-definite. However, for several computational reasons, "lumped" mass matrices are desired. For two- and three-dimensional, rectilinear cases we employ product Lobatto integration rules [2] on Lagrange elements which gives rise to a diagonalized mass matrix. The first two Lobatto rules are the trapezoidal and Simpson's rules, whose products are appropriate for the 4- and 9-node elements, respectively, in the 2-dimensional case, and whose triple products are appropriate for the 8- and 27-node elements, respectively, for the 3-dimensional case.

In the axisymmetric case, zero masses along the z-axis, due to the factor r (radius) appearing in the volume element, would result if Lobatto integration rules were employed. This can cause difficulties in transient analysis. Thus a "row sum" technique is employed to circumvent the problem. The consistent mass matrix term is

$$m_{ab}^e = \int_{R_y^e} \rho N_a^T N_b dR_y \quad (IC.1)$$

The row sum matrix is defined to be

$$m_{aa}^e = \sum_{b=1}^{N_{en}} m_{ab}^e \quad \text{no sum on } a, \quad a = 1, \dots, N_{en} \quad (IC.2)$$

and thus we arrive at the row sum mass definition:

$$m_{ab}^e = \delta_{ab} \int_{R_y^e} \rho N_a dR_y \quad \text{no sum on } a, \quad a = 1, \dots, N_{en} \quad (\text{IC.3})$$

using the fact that $\sum_{a=1}^{N_{en}} N_a = 1$. We employ Gauss quadrature to evaluate the integral in (IC.3).

For direct integration procedures, the type of mass matrix that should be used depends on the method of temporal integration as will be discussed later in this chapter. It is interesting to point out that consistent mass matrices tend to overestimate the frequencies, whereas lumped masses underestimate the frequencies. However, mass lumping is still a controversial issue in fluid mechanics, due primarily to the results of Gresho et al. [41].

II. Implementation of Lagrangian-Eulerian Finite Elements

Since all the volume and surface integrals in the variational equations and thus the matrix equations are in terms of R_y and ∂R_y , respectively, it is important to specify what R_y is in our finite element discretization. We wish to think of the region R_x as our finite element mesh in the referential domain. R_y is the image of R_x at time $t \in [t_0, t_1]$. Hence, $\hat{\phi}$ is the "motion" of the mesh. In general $\hat{\phi}$ is arbitrary. The selection of $\hat{\phi}$ is generally made depending on the usefulness for the intended application. For our purpose, fluid-structure interaction, it is useful to specify \hat{u}' , or equivalently to specify \hat{u} and thus $\hat{\phi}$. So \hat{u} is the mesh displacement, \hat{u}' is the mesh velocity, and \hat{u}'' is the mesh acceleration.

If we select $\hat{u}' = 0$, we have the Eulerian description. If we select $\hat{u}' = \dot{\hat{u}}$, we have the Lagrangian description. If we select \hat{u}'

between $\underline{\hat{u}}$ and $\underline{\dot{u}}$, we have a mixed description which is employed in Chapter 6 for fluid-structure interaction problems.

We will employ the idea of split descriptions and relate $\underline{\hat{u}}'$ to $\underline{\hat{u}}$ and $\underline{\dot{u}}$, following classical ideas [42]. In this way the unknowns $\underline{\hat{u}}$, $\underline{\hat{u}}'$, and $\underline{\hat{\phi}}$ can be solved by temporal numerical integration [2,3,46], and $\underline{\hat{\phi}}$ is then uniquely specified. For further generalizations see [43-45].

II-A. Generalized Description Using Isoparametric Finite Elements

In this section it is assumed that unless otherwise indicated, there is no sum on repeated i indices. Let us introduce a "Lagrange-Euler parameter array" defined by:

$$\underline{\alpha} = [\alpha_{ij}] = [\alpha_{ii}\delta_{ij}] \quad (\text{IIA.1})$$

where $\alpha_{ii} \in [0,1]$, for $i = 1, \dots, N_{SD}$. We relate $\underline{\hat{u}}'$ to $\underline{\hat{u}}$ and $\underline{\dot{u}}$ by:

$$\hat{u}'_i = \sum_{j=1}^{N_{SD}} \sum_{\substack{k=1 \\ \neq j}}^{N_{SD}} \left(\alpha_{ij} \dot{u}_j - \alpha_{ij} c_k \frac{\partial(\hat{u}_j + \hat{x}_j)}{\partial x_k} \Big|_{\xi \text{ or } \eta \text{ fixed}} \right) \quad (\text{IIA.2})$$

where

$$c_k = \dot{u}_k - \hat{u}'_k = (\delta_{kj} - \alpha_{kj}) \dot{u}_j \quad (\text{IIA.3})$$

We assume that the α_{ij} 's are constants in the present developments.

As an example, consider a two-dimensional mesh, and let $\alpha_{11} = 0$, $\alpha_{22} = 1$, (IIA.2) becomes

$$\hat{u}'_1 = 0$$

and

$$\hat{u}'_2 = \dot{u}_2 - \dot{u}_1 \frac{\partial(\hat{u}_2 + x_2)}{\partial x_1} \Big|_{\xi \text{ or } \eta \text{ fixed}} \quad (\text{IIA.4})$$

If $\alpha_{ij} = 0$ we have $\hat{\underline{u}}' = \underline{0}$, the Eulerian description. If $\alpha_{ij} = \delta_{ij}$ we have $\hat{\underline{u}}' = \dot{\underline{u}}$, the Lagrangian description. We may have split or mixed Lagrangian-Eulerian descriptions as in IIA.4. If α_{ij} takes on values strictly between 0 and 1, we have a very general description which is suitable for bubble dynamics and other related applications. See [43-45,47,48] for further details. However, for our applications we restrict ourselves to the first three cases.

For finite element implementation, we assign a value of α to each nodal point. Further, we employ isoparametric interpolation and let

$$\alpha_{ij} = \sum_{a=1}^{N_{en}} N_a \alpha_{ia}^e \quad i = 1, \dots, N_{sd} \quad (\text{IIA.5})$$

However, in attempting to evaluate the derivatives in (IIA.2), by virtue of the fact that we are using C^0 -continuity shape functions, discontinuities will result across element interfaces. Consequently, a "weakened" interpretation of (IIA.2) is necessitated. To this end we may introduce Galerkin approximations of (IIA.2).

Let

$$\hat{\underline{v}} = \{v_{iA}\} \quad (\text{IIA.6})$$

$$\underline{v} = \{v_{iA}\} \quad (\text{IIA.7})$$

$$\underline{A} = [\alpha_{iA}] \quad (\text{IIA.8})$$

where $\hat{\underline{v}}$, \underline{v} , and \underline{A} are the generalized global vectors of nodal mesh velocities ($\hat{\underline{u}}'$), material velocities ($\dot{\underline{u}}$), and Lagrange-Euler parameters

(a diagonal matrix), respectively. The subscript A takes the values 1, 2, ..., Numnp. The subscript i takes the values 1, ..., N_{sd}. With these definitions, the Galerkin equations may be written as:

$$\hat{\underline{v}} = \underline{A}(\underline{v} - \underline{L}^{-1}\underline{S}) \quad (\text{IIA.9})$$

where

$$\underline{L} = \sum_{e=1}^{\text{Numel}} \int_{R_x^e} \underline{N}^T \underline{N} \, dR_x \quad (\text{IIA.10})$$

$$\underline{S} = \sum_{e=1}^{\text{Numel}} \int_{R_x^e} \sum_{a=1}^{N_{en}} N_{a\tilde{ka}}^e \left(\sum_{b=1}^{N_{en}} N_{b'k} \left(\hat{u}_b^e + \hat{x}_b^e \right) \right) dR_x \quad (\text{IIA.11})$$

Here R_x^e is the referential region of the eth element. We employ Lobatto rules to evaluate the integrals in (IIA.10) and (IIA.11). The resulting matrix \underline{L} is symmetric, positive definite, and diagonal. One drawback of using Lobatto rules is that only Lagrange elements can be used, since "zeroes" or "negative" weighting will result if other element types are employed. In the axisymmetric case, we employ area average instead of volume average to avoid zeroes along the z-axis. If Gauss quadrature rules are employed to evaluate (IIA.10) and (IIA.11), \underline{L} is non-diagonal though banded; also, a "diffusion" of the description (Lagrangian-Eulerian) may take place [16].

III. Numerical Integration of Rate Constitutive Equations

The incremental constitutive equations in Chapter 2 (IVB.23) is a linearized expression. In a numerical formulation, the stresses will be calculated at all Gauss quadrature points which correspond to a set of material particles. As we have noticed before, the first term on

the right-hand side of the mentioned equation represents the material response due to deformations, whereas the second term accounts for rotational effects, which are uniquely specified by "objectivity." However, standard time-discretization procedures [49,51,57,58,60] when applied to this incremental constitutive equation typically only achieve objectivity in the limit of vanishingly small time steps, which is not economical in practical computing.

If one employs the polar decomposition to separate deformation and rotation effects [59], much larger time steps can be accommodated. However, it is too time consuming to extract the eigenvalues and eigenvectors [52] at each Gauss point.

Hallquist [50] has shown, in the context of two-dimensional analysis, how to maintain objectivity for larger time steps. However, there are some awkward aspects of the implementation, and the generalization to three dimensions is not apparent. Hughes [54] proposed an improved algorithm for integrating rate constitutive equations in large-deformation analysis. The algorithm is fairly simple and is shown to be objective with respect to large rotation increments.

Therefore we employed the mentioned technique in [54] to account for the rotational term (i.e., $\underline{\underline{S}}\omega$) and the various standard numerical integration algorithms [53,55,56] to account for the material response part (i.e., $\overline{\underline{\underline{C}}}\gamma$).

III-A. Numerical Algorithm for Rotational Term

We represent the position vector of a particle at time $t_n \in [t_0, t_1]$ by \underline{y}^n . Let Δt be the time increment. The position vector at

$t_n + \Delta t$ is denoted by \underline{y}^{n+1} which may be written as a function of \underline{y}^n and the time step; hence,

$$\underline{y}^{n+1} = \underline{y}^{n+1}(\underline{y}^n, \Delta t) \quad (\text{IIIA.1})$$

The particle displacement increment over the step is

$$\underline{\delta} = \underline{u}^{n+1} - \underline{u}^n \quad (\text{IIIA.2})$$

Here \underline{u}^{n+1} and \underline{u}^n are the approximated values of \underline{u} at time $t_n + \Delta t$ and time t_n , respectively. Consider the following one-parameter family of configurations:

$$\underline{y}^{n+\alpha} = (1 - \alpha)\underline{y}^n + \alpha\underline{y}^{n+1} \quad (\text{IIIA.3})$$

in which $\alpha \in [0, 1]$. Let \underline{G} denote the gradient of $\underline{\delta}$ with respect to $\underline{y}^{n+\alpha}$. In component form

$$G_{ij} = \partial \delta_i / \partial y_j^{n+\alpha} \quad (\text{IIIA.4})$$

The incremental strain vector $\underline{\gamma}$, and the incremental rotation vector, $\underline{\omega}$, may be defined in terms of \underline{G} as follows:

$$\underline{\gamma} = (\underline{G} + \underline{G}^T) / 2 \quad (\text{IIIA.5})$$

$$\underline{\omega} = (\underline{G} - \underline{G}^T) / 2 \quad (\text{IIIA.6})$$

The numerical algorithm for integrating the constitutive equation is as follows:

$$\underline{\tau}^{n+1} = \underline{\tau}^{n+1} + \Delta \underline{\tau} \quad (\text{IIIA.7})$$

$$\underline{\tau}^{n+1} = \underline{Q} \underline{\tau}^n \underline{Q}^T \quad (\text{IIIA.8})$$

$$\underline{Q} = \underline{1} + (\underline{1} - \alpha \underline{\omega})^{-1} \underline{\omega} \quad (\text{IIIA.9})$$

$$\Delta \underline{\tau} = \underline{\bar{C}} \underline{\gamma} \quad (\text{IIIA.10})$$

The expression for \underline{Q} is obtained by applying the generalized midpoint rule (see e.g., [61]) to the generating equation $d\underline{Q}/dt = \underline{\omega} \underline{Q}$. If $\alpha = 1/2$ it is a second order accurate algorithm.

For further details of the properties of the algorithm, consult [54].

III-B. Numerical Algorithms for Integration of Eq. (IIIA.10)

As already emphasized, the incremental equations derived in Chapter 2 admit a wide variety of material constitutive models. However, the application of these equations to physically nonlinear problems requires detailed knowledge of the material characterization, that is, \underline{C} and $\underline{\bar{C}}$. The constitutive algorithms one should use then depend solely on the definition of \underline{C} . Therefore we will consider numerical algorithms for linear elasticity, the Saint-Venant-Kirchhoff nonlinear elastic model, the Krieg-Key combined isotropic-kinematic hardening plasticity model, incompressible viscous fluids via the penalty function formulation, and the slightly compressible fluid. These are sufficiently general for the developments herein.

1. Linear Elasticity

The \underline{C} matrix in this case is constant and is given by:

$$\tilde{C} = \begin{bmatrix} \lambda+2\mu & 0 & \lambda & \lambda & 0 & 0 \\ 0 & \mu & 0 & 0 & 0 & 0 \\ \lambda & 0 & \lambda+2\mu & \lambda & 0 & 0 \\ \lambda & 0 & \lambda & \lambda+2\mu & 0 & 0 \\ 0 & 0 & 0 & 0 & \mu & 0 \\ 0 & 0 & 0 & 0 & 0 & \mu \end{bmatrix} \quad (\text{III B.1})$$

If the Truesdell rate is neglected, $\Delta \underline{\tau}$ can be computed easily by taking advantage of sparseness. Otherwise, a general matrix multiplication "routine" is employed.

2. Saint-Venant-Kirchhoff Nonlinear Elastic Model

The \tilde{C} matrix is defined by the following algorithm:

- a) Compute the deformation gradient matrix \underline{F} ($F_{ij} = \partial(u_i + x_i) / \partial x_j$).
- b) Compute determinant of \underline{F} ; $J = \det(\underline{F})$.
- c) Calculate the Finger tensor $\underline{B} = \underline{F} \underline{F}^T$
- d) Define an array B(1-6) with: $B(1) = B(1,1)$, $B(2) = B(2,2)$, $B(3) = B(3,3)$,
 $B(4) = B(1,2)$, $B(5) = B(2,3)$, and $B(6) = B(3,1)$.
- e) Define an array A(1-21) using the following algorithms:

$$K = 1$$

e1. LOOP ON I = 1,6

$$BB = B(I)$$

e2. LOOP ON J = 1,6

$$A(K) = BB * B(J)$$

$$K = K+1$$

IF(J.LT.6) GO TO e2.

IF(I.LT.6) GO TO e1.

f) Define constants C1 to C5

$$C1 = \lambda/J$$

$$C2 = \mu/J$$

$$C3 = C2 + C2$$

$$C4 = C1 + C2$$

$$C5 = C1 + C3$$

g) With the shorthand notation $A_I = A(I)$, the \tilde{C} matrix is then defined as follows:

$$\tilde{C} = \begin{bmatrix} C5*A1 & C5*A4 & C1*A2 & C1*A3 & C1*A5 & C5*A6 \\ & & +C3*A16 & +C3*A21 & +C3*A18 & \\ & C4*A16 & C5*A9 & C1*A13 & C4*A17 & C4*A18 \\ & +C2*A2 & & +C3*A20 & +C2*A11 & +C2*A5 \\ & & C5*A7 & C1*A8 & C5*A10 & C1*A11 \\ & & & +C3*A19 & & +C3*A17 \\ & & & C5*A12 & C5*A14 & C5*A15 \\ & & & & C4*A19 & C4*A20 \\ & & & & +C2*A8 & +C2*A13 \\ & & & & & C4*A21 \\ & & & & & +C2*A3 \end{bmatrix}$$

SYMMETRIC

(IIIB.2)

$\Delta \tilde{\tau}$ can then be computed using a general matrix multiplication routine.

3. Krieg-Key Combined-Isotropic-Kinematic Hardening Plasticity Model

For this model the radial return method [60] is employed. The numerical algorithm is as follows:

- a) Compute the elastic "trial" stress increment as described in the linear elasticity section. Update the elastic trial stress and call it $\tilde{\tau}^t$, using (IIIA.7).

b) Obtain the deviatoric part of $(\underline{\tau}^t - \underline{\alpha}^n)$:

$$\underline{\xi}_{rs}^t = \text{deviatoric part of } (\tau_{rs}^t - \alpha_{rs}^n) \quad (\text{IIIB.3})$$

c) Compute the second invariant, J_2 ,

$$J_2 = \frac{1}{6} [(\xi_{11}^t - \xi_{22}^t)^2 + (\xi_{22}^t - \xi_{33}^t)^2 + (\xi_{33}^t - \xi_{11}^t)^2] + \xi_{12}^{t2} + \xi_{13}^{t2} + \xi_{23}^{t2} \quad (\text{IIIB.4})$$

d) If $(3J_2 - (k^n)^2)$ is less than or equal to zero, $\underline{\tau}^{n+1} = \underline{\tau}^t$; go to h.

e) Compute plastic strain increment Δd^P ,

$$\Delta d^P = (Z - k^n)/(3\mu + B) \quad (\text{IIIB.5})$$

$$\text{where } Z = \sqrt{3J_2} \quad .$$

f) Compute the following quantities:

$$\Delta S = 3\mu \Delta d^P/Z \quad (\text{IIIB.6})$$

$$\Delta \alpha = (1 - \beta)B \Delta d^P/Z \quad (\text{IIIB.7})$$

g) Radial return for stresses, $\underline{\tau}^{n+1}$; position of yield centers, $\underline{\alpha}^{n+1}$; and yield stress k^{n+1} :

$$\underline{\tau}^{n+1} = \underline{\tau}^t - \Delta S \underline{\xi}^t \quad (\text{IIIB.8})$$

$$\underline{\alpha}^{n+1} = \underline{\alpha}^n + \Delta \alpha \underline{\xi}^t \quad (\text{IIIB.9})$$

$$k^{n+1} = k^n + \beta B \Delta d^P \quad (\text{IIIB.10})$$

h) If the tangent stiffness matrix is not required, exit.

i) Compute the $\underline{\zeta}$ matrix for tangent stiffness calculation as follows:

$$\underline{\zeta}^t \leftarrow \underline{\xi}^t * \sqrt{\frac{6\mu^2}{\|\underline{\xi}^t\|^2 (3\mu+B)}} \quad \dagger \quad (\text{IIIB.11})$$

$\dagger \leftarrow$ means "is replaced by."

$$\tilde{C} = \begin{bmatrix}
 \lambda+2\mu & & & & & \\
 -\xi_1^2 & -\xi_1\xi_2 & \lambda - \xi_1\xi_3 & \lambda - \xi_1\xi_4 & -\xi_1\xi_5 & -\xi_1\xi_6 \\
 & \mu & & & & \\
 & -\xi_2^2 & -\xi_2\xi_3 & -\xi_2\xi_4 & -\xi_2\xi_5 & -\xi_2\xi_6 \\
 & & \lambda+2\mu & & & \\
 & & -\xi_3^2 & \lambda - \xi_3\xi_4 & -\xi_3\xi_5 & -\xi_3\xi_6 \\
 & & & \lambda+2\mu & & \\
 & & & -\xi_4^2 & -\xi_4\xi_5 & -\xi_4\xi_6 \\
 & & & & \mu - \xi_5^2 & -\xi_5\xi_6 \\
 & & & & & \mu - \xi_6^2
 \end{bmatrix}$$

SYMMETRIC

(IIIB.12)

In (IIIB.12) the shorthand notation $\xi_I = \xi_{ij}$ is employed (as described by (IVB.18) in Chapter 2.

4. Incompressible Viscous Fluid via Penalty Function Formulation

By virtue of the fact that the incompressible viscous fluid used is isotropic, equations (IIIA.7) through (IIIA.10) are replaced by:

$$\tilde{\tau}^{n+1} = \tilde{\tau}^n + \Delta\tilde{\tau} \tag{IIIA.13}$$

$$\Delta\tilde{\tau} = \tilde{C} \tilde{\gamma} \tag{IIIA.14}$$

where \tilde{C} is defined by (IIIB.1) and $\tilde{\gamma}$ is defined by (IIIA.1) through (IIIA.5) in which (IIIA.2) is replaced by:

$$\delta = \dot{\underline{u}}^{n+1} - \dot{\underline{u}}^n$$

The Lamé constant λ appearing in (IIIB.1) is interpreted as the "penalty parameter", which has been described in detail in [15]. Of course, due to the sparseness of \underline{C} in (IIIB.1), $\Delta \underline{\tau}$ can easily be computed without employing a matrix multiplication routine.

5. Slightly Compressible Viscous Fluid

We assume the fluid is slightly compressible. Equations (IIIA.13) and (IIIA.14) are employed. However, we divide the $\Delta \underline{\tau}$ computation into two parts, the viscous part and the pressure part. The viscous part can be computed using the procedures described above for the incompressible viscous fluid with λ set equal to zero. The pressure part is computed as follows. We assume the pressure at step n , p^n , is known and stored at each Gauss point. The divergence of the material velocity field, θ , is computed at the $n+\alpha$ geometry, that is:

$$\theta = \partial(\dot{u}_i^{n+\alpha}) / \partial(y_i^{n+\alpha}) \quad \text{sum on } i=1, \dots, N_{SD} \quad (\text{IIIA.15})$$

in which

$$\dot{\underline{u}}^{n+\alpha} = (1 - \alpha)\dot{\underline{u}}^n + \alpha\dot{\underline{u}}^{n+1}, \quad \text{etc.} \quad (\text{IIIA.16})$$

Then the new pressure p^{n+1} is:

$$p^{n+1} = p^n - \Delta t \rho \beta \theta \quad (\text{IIIA.17})$$

Since we approximate $\dot{\underline{u}}(t_n)$ by $\dot{\underline{u}}^n$, the divergence part of the linearized expression $\Delta \text{div } \dot{\underline{u}}$ (appearing in the 5th term of eq. (IVB.7) in Chapter 2) is approximated by $\Delta \text{div } \dot{\underline{u}}^{n+\alpha} = \alpha \text{div } \Delta \dot{\underline{u}}$ which is consistent with the pressure computation in which we evaluate θ at the $n+\alpha$

geometry. For implementational purposes, we include α in the tangent matrix \hat{D} (eq. (IVC.9) in Chapter 2) and

$$\hat{D} = \begin{bmatrix} \bar{\lambda}+2\mu & 0 & \bar{\lambda} & \bar{\lambda} & 0 & 0 \\ 0 & \mu & 0 & 0 & 0 & 0 \\ \bar{\lambda} & 0 & \bar{\lambda}+2\mu & \bar{\lambda} & 0 & 0 \\ \bar{\lambda} & 0 & \bar{\lambda} & \bar{\lambda}+2\mu & 0 & 0 \\ 0 & 0 & 0 & 0 & \mu & 0 \\ 0 & 0 & 0 & 0 & 0 & \mu \end{bmatrix} \quad (\text{IIIA.18})$$

in which $\bar{\lambda} = \Delta t \rho \beta \alpha$.

IV. Transient Analysis Techniques for the Variational Equations

There are two strategies used in dealing with the transient problem: (1) modal superposition, and (2) direct integration [2,3]. In modal superposition methods, the variational equations or matrix equations are diagonalized by finding the eigenvalues and eigenvectors. These eigenvalues and eigenvectors correspond to the natural frequencies and modes. In direct integration the matrix equations are integrated using a numerical step-by-step procedure without transformation of the equations into a different form like modal superposition. In linear analysis, the choice of method depends on the frequency content of the load and on which portion of the frequency response is of interest. For some particular cases, a combination of both methods is very effective [62].

In modal superposition procedures, the most critical and time-consuming aspect of the computation is the determination of the eigenvalues. There are a number of eigenvalue methods used in practice [1,3,46]; each one of them has its own merits. Modal superposition is

used very little in nonlinear analysis. It appears that it is not suitable for path-dependent material and finite deformation problems.

For most nonlinear problems, direct integration is the only effective method in transient analysis. Since we are dealing mostly with nonlinear problems, only direct integration techniques will be discussed.

Basically, there are two general classes of direct integration methods: (1) implicit integration, and (2) explicit integration [2,3,46]. Both methods are developed from difference formulas that relate the accelerations, velocities, and displacements. Implicit algorithms, some of which are unconditionally stable, permit large time steps, but the cost per step is high and storage requirements tend to increase dramatically with the size of the mesh. On the other hand, explicit algorithms, which are conditionally stable, tend to be inexpensive per step and require less storage than implicit algorithms; but numerical stability requires the size of the time step to be inversely proportional to the highest frequency of the mesh.

Belytschko and Mullen [63,64], Hughes and Liu [65,66], and Park et al. [67-69] proposed implicit-explicit nodal partition, implicit-explicit mesh partition, and staggered solution procedures, respectively, to circumvent these difficulties. Other procedures in transient analysis algorithms have also been proven to be successful [70-83]. Nevertheless, a generalization of all these ideas in one package, though desirable, requires further research in theoretical and implementation aspects.

IV-A. Temporal Integration of the Variational Equations

In this section we are going to employ the new family of implicit-explicit algorithms developed in [65,66] for the temporal discretization of the variational equations. Although there are many difference formulas that can be used in time discretization [2,3], based on previous studies, the Newmark family of methods [84] appears most suitable for fluid-structure interaction problems.

For discussion purposes, let $\hat{\underline{d}}_n$, $\hat{\underline{v}}_n$, and $\hat{\underline{a}}_n$ be the nodal vectors of mesh displacements, mesh velocities, and mesh accelerations (i.e., $\hat{\underline{u}}_n$, $\hat{\underline{u}}'_n$, $\hat{\underline{u}}''_n$) respectively; likewise, \underline{d}_n , \underline{v}_n , and \underline{a}_n are the material displacements, material velocities and material referential accelerations (i.e., \underline{u}_n , \underline{u}'_n , \underline{u}''_n), respectively. The solution at time step $n+1$ is determined by the following equations (in order):

$$i = 0 \quad (i \text{ is the iteration counter}) \quad (\text{IVA.1})$$

$$\underline{d}_{n+1}^{(i)} = \tilde{\underline{d}}_{n+1} \quad (\text{IVA.2})$$

$$\underline{v}_{n+1}^{(i)} = \tilde{\underline{v}}_{n+1} \quad (\text{IVA.3})$$

$$\underline{a}_{n+1}^{(i)} = \underline{0} \quad (\text{IVA.4})$$

$$\tilde{\underline{d}}_{n+1} = \underline{d}_n + \Delta t \underline{v}_n + \left(\frac{1}{2} - \beta\right) \Delta t^2 \underline{a}_n \quad (\text{IVA.5})$$

$$\tilde{\underline{v}}_{n+1} = \underline{v}_n + (1 - \gamma) \Delta t \underline{a}_n \quad (\text{IVA.6})$$

$$\hat{\underline{d}}_{n+1}^{(i)} = \tilde{\underline{d}}_{n+1} \quad (\text{IVA.7})$$

$$\hat{\underline{v}}_{n+1}^{(i)} = \tilde{\underline{v}}_{n+1} \quad (\text{IVA.8})$$

$$\tilde{\underline{d}}_{n+1} = \hat{\underline{d}}_n + \Delta t \hat{\underline{v}}_n + \left(\frac{1}{2} - \beta\right) \Delta t^2 \hat{\underline{a}}_n \quad (\text{IVA.9})$$

$$\tilde{\underline{v}}_{n+1} = \hat{\underline{v}}_n + (1 - \gamma) \Delta t \hat{\underline{a}}_n \quad (\text{IVA.10})$$

} predictor phase for material displacements, velocities, and accelerations

} predictor phase for mesh displacements, and velocities

$$\tilde{M}^* \Delta \tilde{a} = \Delta \tilde{F}^* \quad \text{momentum equations} \quad (\text{IVA.11})$$

$$\begin{aligned} \tilde{M}^* &= \tilde{M} + \gamma \Delta t D \cdot \tilde{N}_c(\hat{v}_{n+1}^{(i)}, v_{n+1}^{(i)}, \hat{d}_{n+1}^{(i)}) \\ &\quad + \gamma \Delta t K_v(d_{n+1}^{(i)}) \\ &\quad + \beta \Delta t^2 K_d(v_{n+1}^{(i)}, \hat{d}_{n+1}^{(i)}, d_{n+1}^{(i)}) \end{aligned} \quad (\text{IVA.12})$$

$$\begin{aligned} \Delta \tilde{F}^* &= F_{n+1}^{\text{ext}} + F_B(\hat{d}_{n+1}^{(i)}) + F_S(\hat{d}_{n+1}^{(i)}) \\ &\quad - I(\hat{d}_{n+1}^{(i)}, a_{n+1}^{(i)}) - N_c(\hat{v}_{n+1}^{(i)}, v_{n+1}^{(i)}, \hat{d}_{n+1}^{(i)}) \\ &\quad - F_{n+1}^{\text{int}}(v_{n+1}^{(i)}, \hat{d}_{n+1}^{(i)}, d_{n+1}^{(i)}) \end{aligned} \quad (\text{IVA.13})$$

$$\tilde{M} = \sum_{e=1}^{\text{Nume}\ell} \int_{R_y^e} \rho N^T N \, dR_y \quad \text{mass matrix} \quad (\text{IVA.14})$$

$$D \cdot \tilde{N}_c = \underbrace{\sum_{e=1}^{\text{Nume}\ell} \int_{R_y^e} (B^1)^T [E^1(B^1) + E^2(B^2)] \, dR_y}_{\text{tangential convective matrix}} \quad (\text{IVA.15})$$

$$K_v = \sum_{e=1}^{\text{Nume}\ell} \int_{R_y^e} B^{\gamma T} \hat{D} B^{\gamma} \, dR_y \quad \text{pressure and viscous tangent matrix} \quad (\text{IVA.16})$$

$$K_d = \sum_{e=1}^{\text{Nume}\ell} \int_{R_y^e} B^T D B \, dR_y \quad \text{tangent stiffness matrix} \quad (\text{IVA.17})$$

$$F_{n+1}^{\text{ext}} = \text{discrete nodal applied forces} \quad (\text{IVA.18})$$

$$F_B = \sum_{e=1}^{\text{Nume}\ell} \int_{R_y^e} N^T b \, dR_y \quad \text{body forces} \quad (\text{IVA.19})$$

$$\tilde{F}_S = \sum_{e=1}^{Nume\ell} \int_{\partial R_y^e} \tilde{N}^T h \tilde{d}A_y \quad \text{surface forces} \quad (IVA.20)$$

$$\tilde{I} = \sum_{e=1}^{Nume\ell} \int_{R_y^e} \rho N^T \tilde{a}_{n+1}^{(i)} dR_y \quad \text{inertia forces} \quad (IVA.21)$$

$$\tilde{N}_c = \sum_{e=1}^{Nume\ell} \int_{R_y^e} \rho N^T \tilde{\eta} dR_y \quad \text{convective forces} \quad (IVA.22)$$

$$\tilde{F}_{n+1}^{int} = \sum_{e=1}^{Nume\ell} \int_{R_y^e} B^Y T \tilde{\tau}_{n+1}^{(i)} dR_y \quad \text{internal forces} \quad (IVA.23)$$

$$\tilde{a}_{n+1}^{(i+1)} = \tilde{a}_{n+1}^{(i)} + \Delta \tilde{a} \quad (IVA.24)$$

$$\tilde{v}_{n+1}^{(i+1)} = \tilde{v}_{n+1} + \gamma \Delta t \tilde{a}_{n+1}^{(i+1)} \quad (IVA.25)$$

$$\tilde{d}_{n+1}^{(i+1)} = \tilde{d}_{n+1} + \beta \Delta t^2 \tilde{a}_{n+1}^{(i+1)} \quad (IVA.26)$$

corrector phase
for material
displacements,
velocities, and
accelerations

$$\hat{v}_{n+1}^{(i+1)} = A(\tilde{v}_{n+1}^{(i+1)} - \tilde{v}_{n+1}) - L^{-1} S \quad \text{mesh velocity representation} \quad (IVA.27)$$

$$\hat{a}_{n+1}^{(i+1)} = (\hat{v}_{n+1}^{(i+1)} - \tilde{v}_{n+1}) / \gamma \Delta t \quad (IVA.28)$$

$$\hat{d}_{n+1}^{(i+1)} = \tilde{d}_{n+1} + \beta \Delta t^2 \hat{a}_{n+1}^{(i+1)} \quad \text{corrector phase for mesh accelerations and displacements} \quad (IVA.29)$$

corrector phase
for mesh
accelerations and
displacements

The notations used in equations (IVA.14) through (IVA.23) have been defined in Chapter 2 (equation IVB.7). The numerical integration for $\tilde{\tau}_{n+1}^{(i)}$ that appears in equation (IVA.23) has been discussed in the previous section. The mesh velocity update formula, equation (IVA.27), has been discussed in Section II of this chapter.

Let I be the total number of iterations. If $I = 0$, the algorithm is a predictor-corrector algorithm. If more iterations are required (i.e., $I > 0$), it is a predictor-multicorrector algorithm. The generalizations of (IVA.1) through (IVA.29) to implicit, explicit, implicit-explicit mesh partitions, implicit-explicit operator splitting, dynamic relaxation, and quasi-Newton updates for symmetric and nonsymmetric equation systems have been discussed in detail in [66,72,79]. The stability, accuracy, and convergence have been discussed in [65,72,73]. For detailed analyses of the above algorithms, the reader should consult [75,66,72,73,79] and references cited therein.

IV-B. Computer Implementation of Equations (IVA.1) through (IVA.29)

We assume the initial data $\underline{d}_0, \underline{v}_0, \underline{a}_0, \hat{\underline{d}}_0, \hat{\underline{v}}_0, \hat{\underline{a}}_0$ are all given. If the mixed description is used, the global array \underline{L} is computed according to equation (IIA.10) and stored. For computer implementation purposes, let "I" and "E" denote "implicit" and "explicit" element groups. If the entire mesh is treated explicitly,

$$\underline{\underline{M}}^* = \underline{\underline{M}}^E \quad \text{which is a diagonal matrix} \quad (\text{IVB.1})$$

$$\underline{\underline{\Delta F}}^* = (\underline{\underline{F}}^{\text{ext}})^E + \underline{\underline{F}}_B^E + \underline{\underline{F}}_S^E - \underline{\underline{I}}^E - \underline{\underline{N}}^E - (\underline{\underline{F}}^{\text{int}})^E \quad (\text{IVB.2})$$

The terms on the right-hand side of equation (IVB.2) are defined by equation (IVA.18) to (IVA.23) with i set to zero. If the entire mesh is treated implicitly, $\underline{\underline{M}}^*$ is defined as in equation (IVA.12) and equations (IVA.13) through (IVA.17). $\underline{\underline{M}}^*$ can be reformed and factorized whenever necessary. However, $(\underline{\underline{\Delta F}}^*)^I$ is recomputed for every iteration. If a linear implicit/nonlinear explicit splitting is desired, $\underline{\underline{M}}^*$ is

defined as

$$\tilde{M}^* = \tilde{M} + \gamma \Delta t \tilde{K}_v^I + \beta \Delta t^2 \tilde{K}_d^I \quad (\text{IVB.3})$$

where \tilde{M}^* is constant and is computed once and stored. The corresponding $\Delta \tilde{F}^*$ is recomputed according to equation (IVA.13) for every iteration. We notice that $\tilde{M}^I + \tilde{M}^E = \tilde{M}$, and $(\tilde{F}^{\text{ext}})^I + (\tilde{F}^{\text{ext}})^E = \tilde{F}^{\text{ext}}$. With these definitions in mind, the solution procedures are as follows:

- a) Loop on number of time steps, N.
- b) Define predictor "material" values according to equations (IVA.1) through (IVA.6).
- c) Define predictor "mesh" values according to equations (IVA.7) through (IVA.10), if required.
- d) Form $\tilde{F}_{n+1}^{\text{ext}}$ and $(\Delta \tilde{F}^*)^E$ as described previously and store.
- e) Loop on number of iterations, $i = 1, \dots, I$.
- f) Reform and factorize \tilde{M}^* if required, where $\tilde{M}^* = (\tilde{M}^*)^I + (\tilde{M}^*)^E$.
- g) Form $(\Delta \tilde{F}^*)^i$ and $\Delta \tilde{F}^* = (\Delta \tilde{F}^*)^I + (\Delta \tilde{F}^*)^E$.
- h) Solve for $\Delta \tilde{a}$ according to equation (IVA.11).
- i) Update material displacements, velocities, and accelerations according to equations (IVA.24) through (IVA.27).
- j) Form \tilde{S} according to equation (IIA.11) if required.
- k) Update mesh velocities according to equation (IVA.27), if required.
- l) Update mesh accelerations and mesh displacements according to equations (IVA.28) and (IVA.29), if required.
- m) Check convergence, if required. If convergence check is required then for $\|\Delta \tilde{a}\| \leq \epsilon$ go to o.
- n) If convergence check is required and $i = I$ stop. If $i < I$, go to e.
- o) $\tilde{\tau}_n$ is replaced by $\tilde{\tau}_{n+1}^{(i+1)}$.

- p) $\tilde{d}_n, \tilde{v}_n, \tilde{a}_n$ are replaced by $\tilde{d}_{n+1}^{(i+1)}, \tilde{v}_{n+1}^{(i+1)}$, and $\tilde{a}_{n+1}^{(i+1)}$, respectively.
- q) $\hat{d}_n, \hat{v}_n, \hat{a}_n$ are replaced by $\hat{d}_{n+1}^{(i+1)}, \hat{v}_{n+1}^{(i+1)}$, and $\hat{a}_{n+1}^{(i+1)}$, respectively.
- r) If $N < \text{maximum number of time steps}$, go to a.

References

1. C-E. Fröberg, Introduction to Numerical Analysis, 2nd edition. (Addison-Wesley Publishing Co., 1969).
2. O. C. Zienkiewicz, The Finite Element Method, 3rd edition. (McGraw-Hill, 1977).
3. K-J. Bathe and E. L. Wilson, Numerical Methods in Finite Element Analysis. (Prentice-Hall, Inc., 1976).
4. G. Horrigmoe, "Nonlinear Finite Element Models in Solid Mechanics" Report No. 76-2, The University of Trondheim, Norway, 1976.
5. G. Horrigmoe, "Finite Element Instability Analysis of Free-Form Shells," Report No. 77-2, The University of Trondheim, Norway, 1977.
6. T.H.H. Pian, "Derivation of element stiffness matrices by assumed stress distributions," AIAA Jour. 2, 1333-1336 (1964).
7. D. S. Malkus and T.J.R. Hughes, "Mixed-finite element methods-- reduced and selective integration techniques: A unification of concepts," Computer Meth. in Appl. Mech. and Eng. 15, 63-81 (1978).
8. I. Fried, "Finite element analysis of incompressible material by residual energy balancing," Internat. J. Solids and Structures 10, 993-1002 (1974).
9. J. C. Nagtegaal, D. M. Parks, and J. R. Rice, "On numerically accurate finite element solutions in the fully plastic range," Computer Meth. in Appl. Mech. and Eng. 4, 153-178 (1974).
10. D. S. Malkus, "Finite element analysis of incompressible solids," Ph.D. thesis, Boston University, Boston, 1975.
11. T.H.H. Pian, "Hybrid models," in Numerical and Computer Methods for Solid Continua, S. J. Fenves et al. (eds.) (Academic Press, New York, 1973).
12. T.J.R. Hughes, M. Cohen, and M. Haroun, "Reduced and selective integration techniques in the finite element analysis of plates," Nucl. Eng. and Design 46, 203-222 (1978).

13. T.J.R. Hughes and M. Cohen, "The 'heterosis' finite element for plate bending," *Computers and Structures* 9, 445-450 (1978).
14. T.J.R. Hughes and W. K. Liu, "Nonlinear finite element analysis of shells: Part I - Three-dimensional shells; Part II - Two-dimensional shells", *Computer Meth. in Appl. Mech. and Eng.*, in press.
15. T.J.R. Hughes, W. K. Liu, and A. Brooks, "Review of finite element analysis of incompressible viscous flows by the penalty function formulation," *J. Computational Phys.* 30, 1-60 (1979).
16. T.J.R. Hughes, W. K. Liu, and T. Zimmermann, "Lagrangian-Eulerian finite element formulation for incompressible viscous flows," U.S.-Japan Seminar on Interdisciplinary Finite Element Analysis, Cornell University, Ithaca, New York, August 7-11, 1979.
17. T.J.R. Hughes and J. H. Prevost, "DIRT II - A nonlinear quasistatic finite element analysis program," California Institute of Technology, 1979.
18. D. S. Malkus, "A finite element displacement model valid for any value of the compressibility," *Internat. J. Solids and Structures* 12, 731-738 (1976).
19. T.J.R. Hughes, "Generalization of selective integration procedures to anisotropic and nonlinear media," *Internat. J. Numerical Meth. in Eng.*, to appear.
20. P. Cress, P. Dirksen, and J. Graham, Fortran IV with WATFOR and WATFIV, (Prentice-Hall, Inc., 1970).
21. P. J. Roache, Computational Fluid Dynamics (Hermosa Publishers, Albuquerque, New Mexico, 1976).
22. I. Christie, D. F. Griffiths, A. R. Mitchell, and O. C. Zienkiewicz, "Finite element methods for second order differential equations with significant first derivatives," *Internat. J. Numerical Meth. in Eng.* 10, 1389-1396 (1976).
23. D. F. Griffiths, "On the approximation of convection problems in fluid dynamics," Research paper No. 317, University of Calgary, Calgary, Alberta, Canada, Sept. 1976.

24. J. C. Heinrich, P. S. Huyakorn, O. C. Zienkiewicz, and A. R. Mitchell, "An 'upwind' finite element scheme for two-dimensional convective transport equations," *Internat. J. Numerical Meth. in Eng.* 11, 131-143 (1977).
25. T.J.R. Hughes (ed.), Finite element methods for convection dominated flows, AMD Vol. 34, ASME, New York, Dec. 1979.
26. T.J.R. Hughes, "A simple scheme for developing 'upwind' finite elements," *Internat. J. Numerical Meth. in Eng.* 12, 1359-1365 (1978).
27. T.J.R. Hughes and J. Atkinson, "A variational basis for 'upwind' finite elements," *IUTAM Symp. on Variational Methods in the Mechanics of Solids*, Northwestern University, Evanston, Ill., Sept. 1978.
28. A. Brooks and T.J.R. Hughes, "Streamline-upwind/Petrov-Galerkin methods for advection dominated flows," *Third Internat. Conf. on Finite Element Methods in Fluid Flow*, Banff, Canada, 1980.
29. T. Belytschko, J. M. Kennedy, and D. F. Schoeberle, "Quasi-Eulerian finite element formulation for fluid-structure interaction," *J. Pressure Vessel Technol.* 102, 62-69 (1980).
30. R. H. Gallagher, J. T. Oden, C. Taylor, and O. C. Zienkiewicz (eds.), Finite Elements in Fluids 1: Viscous Flow and Hydrodynamics (John Wiley, London, 1975).
31. R. H. Gallagher, J. T. Oden, C. Taylor, and O. C. Zienkiewicz (eds.), Finite Elements in Fluids 2: Mathematical Foundations, Aerodynamics, and Lubrication (John Wiley, London, 1975).
32. R. H. Gallagher, O. C. Zienkiewicz, J. T. Oden, M. Morandi-Gechi, and C. Taylor (eds), Finite Elements in Fluids 3 (John Wiley, London, 1978).
33. D. K. Gartling, "Finite element analysis of viscous incompressible flow," *TICOM Report 74-8*, University of Texas, Austin, December 1974.

34. D. K. Gartling, "Recent developments in the use of finite element methods in fluid dynamics" in Computing in Applied Mechanics, AMD Vol. 18 (ASME, New York, 1976), pp. 65-92.
35. P. Gresho, R. Lee, and R. Sani, "On the time-dependent solution of the incompressible Navier-Stokes equations in two and three dimensions," in Recent Advances in Numerical Methods in Fluids (Pineridge Press, Swansea, to appear).
36. C. Taylor, K. Morgan, and C. A. Brebbia (eds), Numerical Methods in Laminar and Turbulent Flow (John Wiley, New York, 1978).
37. D. K. Gartling, "Some comments on the paper by Heinrich, Huyakorn, Zienkiewicz, and Mitchell," Internat. J. Numerical Meth. in Eng. 12, 187-190 (1978).
38. O. C. Zienkiewicz, "Reply to comments by Gartling," Internat. J. Numerical Meth. in Eng. 12, 191 (1978).
39. T.J.R. Hughes and A. Brooks, "A multi-dimensional upwind scheme with no crosswind diffusion," AMD 34 (ASME, New York, 1979), pp. 19-35.
40. A. Brooks, "Finite element solution to Navier-Stokes equation," Ph.D. thesis, California Institute of Technology. In preparation.
41. P. M. Gresho, R. L. Lee, and R. L. Sani, "Advection-dominated flows with emphasis on the consequence of mass lumping," in Preprints of Second Internat. Symp. on Finite Element Methods in Flow Problems, S. Margherita, Italy, June 14-18, 1976.
42. G. B. Whitham, Linear and Nonlinear Waves, Pure and Applied Mathematics (Wiley-Interscience, New York, 1974).
43. J. Donea, P. Fasoli-Stella, S. Giuliani, J. P. Halleux, and A. V. Jones, "The computer code EURDYN-1M for transient dynamic fluid-structure interaction," EUR 6751 EN, Commission of the European Communities Joint Research Center, Ispra Establishment, Italy. Preprint, 1980.
44. T. Belytschko and U. Schumann, "Fluid-structure interaction in light water reactor systems." Preprint.

45. T. Belytschko (ed.), Fluid-Structure Interaction in LWR Systems, Internat. Congress Center, Berlin (west), Germany, Aug. 20-21, 1979.
46. T.J.R. Hughes, "Finite element method class notes, AE/AM 108", California Institute of Technology
47. T.J.R. Hughes, "Current trends in finite element research," Feature article to appear in Applied Mechanics Reviews.
48. T.J.R. Hughes, "Recent developments in computer methods for structural analysis," Nucl. Eng. and Design 57, No. 2, May 1980.
49. R. D. Krieg, "An efficient numerical method for time independent plasticity," SAND 77-0943, Sandia Laboratories, Albuquerque, New Mexico, 1977.
50. J. O. Hallquist, "NIKE 2D: An implicit, finite-deformation, finite-element code for analyzing the static and dynamic response of two-dimensional solids," Lawrence-Livermore Laboratory Report UCRL-52678, University of California, Livermore, Ca., March 3, 1979.
51. R. M. McMeeking and J. R. Rice, "Finite element formulation for problems of large elastic-plastic reformation," Internat. J. Solids and Structures 11, 601-616 (1975).
52. B. Noble, Applied Linear Algebra (Prentice-Hall, Englewood Cliffs, N.J., 1969).
53. H. L. Schreyer, R. T. Kulak, and J. M. Kramer, "Accurate numerical solutions for elastic-plastic models," J. Pressure Vessel Technol. 101, 226-234, August 1979.
54. T.J.R. Hughes and J. Winget, "Finite rotation effects in numerical integration of rate constitutive equations arising in large-deformation analysis," Internat. J. Numerical Meth. in Eng., in press.
55. H. Armen, "Assumptions, models, and computational methods for plasticity," Computers and Structures 10, 161-174 (1979).
56. R. D. Krieg and D. B. Krieg, "Accuracies of numerical solution method for the elastic-perfectly plastic model," ASME J. Pressure Vessel Technol. 99, 510-515 (1977).

57. S. W. Key, "Hondo, a finite element computer program for large deformation dynamic response of axisymmetric solids," Sandia Laboratories, Albuquerque, N.M., SLA-74-0039, April 1974.
58. D. P. Mondkar and G. H. Powell, "Static and dynamic analysis of nonlinear structures," ANSR-I, Report EERC-75-10, University of California, Berkeley, 1975.
59. J. K. Knowles, E. Sternberg, "Notes on mathematical theory of elasticity, AM135 and 136," California Institute of Technology.
60. R. D. Krieg and S. W. Key, "Implementation of a time independent plasticity theory into structural computer programs," Constitutive Equations in Viscoplasticity: Computational and Engineering Aspects," AMD 20 (ASME, New York, 1976).
61. T.J.R. Hughes, "Stability of one-step methods in transient nonlinear heat conduction," Trans. 4th Internat. Conf. on Structural Mechanics in Reactor Technology, San Francisco, CA, August 1977.
62. M. A. Haroun, Dynamic analysis of liquid storage tanks, Ph.D. thesis, California Institute of Technology, December 1979.
63. T. Belytschko and R. Mullen, "Mesh partitions of explicit-implicit time integration," in Formulations and Computational Algorithms in Finite Element Analysis, K. J. Bathe, J. T. Oden, and W. Wunderlich (eds.) (M.I.T. Press, Cambridge, Mass., 1977).
64. T. Belytschko and R. Mullen, "Stability of explicit-implicit mesh partitions in time integration," Internat. J. Numerical Meth. in Eng. 12, 1575-1586 (1978).
65. T.J.R. Hughes and W. K. Liu, "Implicit-explicit finite elements in transient analysis: stability theory," J. Appl. Mech. 45, 371-374 (1978).
66. T.J.R. Hughes and W. K. Liu, "Implicit-explicit finite elements in transient analysis: implementation and numerical examples," J. Appl. Mech. 45, 375-378 (1978).
67. C. A. Felippa, K. C. Park, and H. C. Yee, "Synthesis of staggered solution procedures for coupled field analysis," 2nd Internat. Conf.

- Appl. Numerical Modeling, Polytechnical University of Madrid, Madrid, Sept. 11-15, 1978.
68. K. C. Park, C. A. Felippa, and J. A. DeRuntz, "Stabilization of staggered solution procedures for fluid-structure interaction analysis," in Computational Methods for Fluid-Structure Interaction Problems T. Belytschko and T. L. Geero (eds), Applied Mechanics Symposia Series (ASME, New York, 1977).
 69. K. C. Park, "Partitioned transient analysis procedure for coupled-field problems," presented at Second Conf. on Numerical Methods in Nonlinear Mechanics, TICOM, University of Texas, Austin, March, 1979.
 70. K. C. Park and C. A. Felippa, "Direct time integration methods in nonlinear structural dynamics," Computer Meth. in Appl. Mech. and Eng. 17/18, 277-313 (1979).
 71. K. C. Park and P. G. Underwood, "A variable-step central difference method for structural dynamics analysis - Part I: Theoretical aspects," ASME Paper No. 79-PVP-120, presented at the Pressure Vessels and Piping Conf., San Francisco, CA, June 25-29, 1979.
 72. T.J.R. Hughes, K. S. Pister, and R. L. Taylor, "Implicit-explicit finite elements in nonlinear transient analysis," Computer Meth. in Appl. Mech. and Eng. 17/18, 159-182 (1979).
 73. T.J.R. Hughes and R. A. Stephenson, "Convergence of implicit-explicit algorithms in nonlinear transient analysis," to appear in Internat. J. Eng. Science.
 74. T. Belytschko, R. L. Chiapatta, and H. D. Bartel, "Efficient large scale nonlinear-transient analysis by finite elements," Internat. J. Numerical Meth. in Eng. 10, 579-596 (1976).
 75. T. Belytschko, J. R. Osias, P. V. Marcal (eds.), Finite element analysis of transient nonlinear structural behavior, AMD 14 (ASME, New York, August 1975).
 76. T. Belytschko, "Transient analysis," in Structural Mechanics Computer Programs (University Press of Virginia, Charlottesville, VA, 1974),

pp. 255-276.

77. H. M. Hilber, T.J.R. Hughes, "Collocation, dissipation, and 'overshoot' for time integration schemes in structural dynamics," Earthquake Eng. Struct. Dynamics 6, 99-118 (1978).
78. T.J.R. Hughes, T. K. Caughey, and W. K. Liu, "Finite element methods for nonlinear elastodynamics which conserve energy, J. Appl. Mech. 45, 366-370 (1978).
79. T.J.R. Hughes, "Implicit-explicit finite element techniques for symmetric and nonsymmetric systems," Proc. Conf. on Nonlinear Problems in Mechanics, University of Swansea, Swansea, U.K., Sept. 2-5, 1980.
80. T. Belytschko, H. J. Yen, and R. Mullen, "Mixed methods for time integration," Computer Meth. in Appl. Mech. and Eng. 17/18, 259-275 (1979).
81. P. G. Underwood and K. C. Park, "A variable-step central difference method for structural dynamics analysis - Part II. Implementation and performance evaluation," ASME Paper No. 79-PVP-121, presented at the Pressure Vessels and Piping Conf., San Francisco, CA, June 25-29, 1979.
82. J. P. Wright, "Mixed time integration schemes," Computers and Structures 10, 235-238 (1979).
83. J. Isenberg, D. K. Vaughan, I., and I. Sandler, "Nonlinear soil-structure interaction," EPRI NP-945, Project 810-2, Final Report, Dec. 1978.
84. N. M. Newmark, "A method of computation for structural dynamics," J. Eng. Mech. Div. ASCE, 67-94 (1959).

Chapter 4

NONLINEAR FINITE ELEMENT ANALYSIS OF SHELLS

I. Introduction

Within recent years, shell structures have assumed increased importance due to new developments in industry; in particular in offshore structures, nuclear reactors, cooling towers, and oil tanks. The demand for "better" design of a shell structure requires improved shell analysis procedures, and in many cases the safety of shell structures cannot be estimated unless a nonlinear analysis is undertaken.

As a result of the increased speed and storage capacity of present computers, many nonlinear numerical analyses of shells have been attempted. Finite element procedures for plate and shell analysis now span over 20 years. A history of finite element shell analysis is traced in [1,2]. Descriptions and references to many important works may be obtained by consulting standard texts [3,4], the review articles [5], and thesis [6]. The innumerable proposed shell and plate elements demonstrate the wide dissatisfaction with available methodology.

There are two classical approaches in finite element analysis of shells: (1) the direct approach which is deduced from a classical shell theory [7]; (2) the degeneration approach [4,8] which is deduced from the field equations of the three-dimensional theory with various assumptions. The associated shell differential equations derived from the direct approach, often higher than second order, may require a higher-order interpolation function by the finite element process. Another disadvantage of this approach is the unavailability of a convenient,

general enough nonlinear shell theory. It is concluded that to develop a general enough nonlinear shell theory which can accommodate finite strains and finite rotations, and permits use of arbitrary, three-dimensional nonlinear constitutive equations, one must adopt the "degeneration" approach. Mindlin theory [9] is the most widely adopted basis of the degeneration approach, since generalization to the fully-general nonlinear case is straightforward, and an analogous two-dimensional formulation which includes several special cases of practical interest, namely the axisymmetric case for shells of revolution, the plane strain case for long tubes, and the plane stress case for rings and two-dimensional beam/frame structures, can be deduced from the three-dimensional formulation. This theory was originally employed in the linear case by Ahmad et al. [10], later by Hughes and coworkers [11-14]. Recent works in the nonlinear area which may be mentioned are [8,15-20, 39]. However, there are still certain numerical difficulties remaining in the development of a fully-general nonlinear shell theory. As has been mentioned by Hughes and Liu [20], they are (1) selective integration techniques, (2) numerical integration of constitutive equations, and (3) rank-deficiency problems associated with the in-plane rotational mode.

Of course, there are other approaches to develop nonlinear shell theory. The interested reader may consult [6,21-23] and references therein.

The equations of motion derived in Chapter 2 can be used directly in shell analysis. The Lagrangian formulation will be adopted (i.e., $R_x = R_z$). For discussion purposes we will denote \tilde{x} as an undeformed

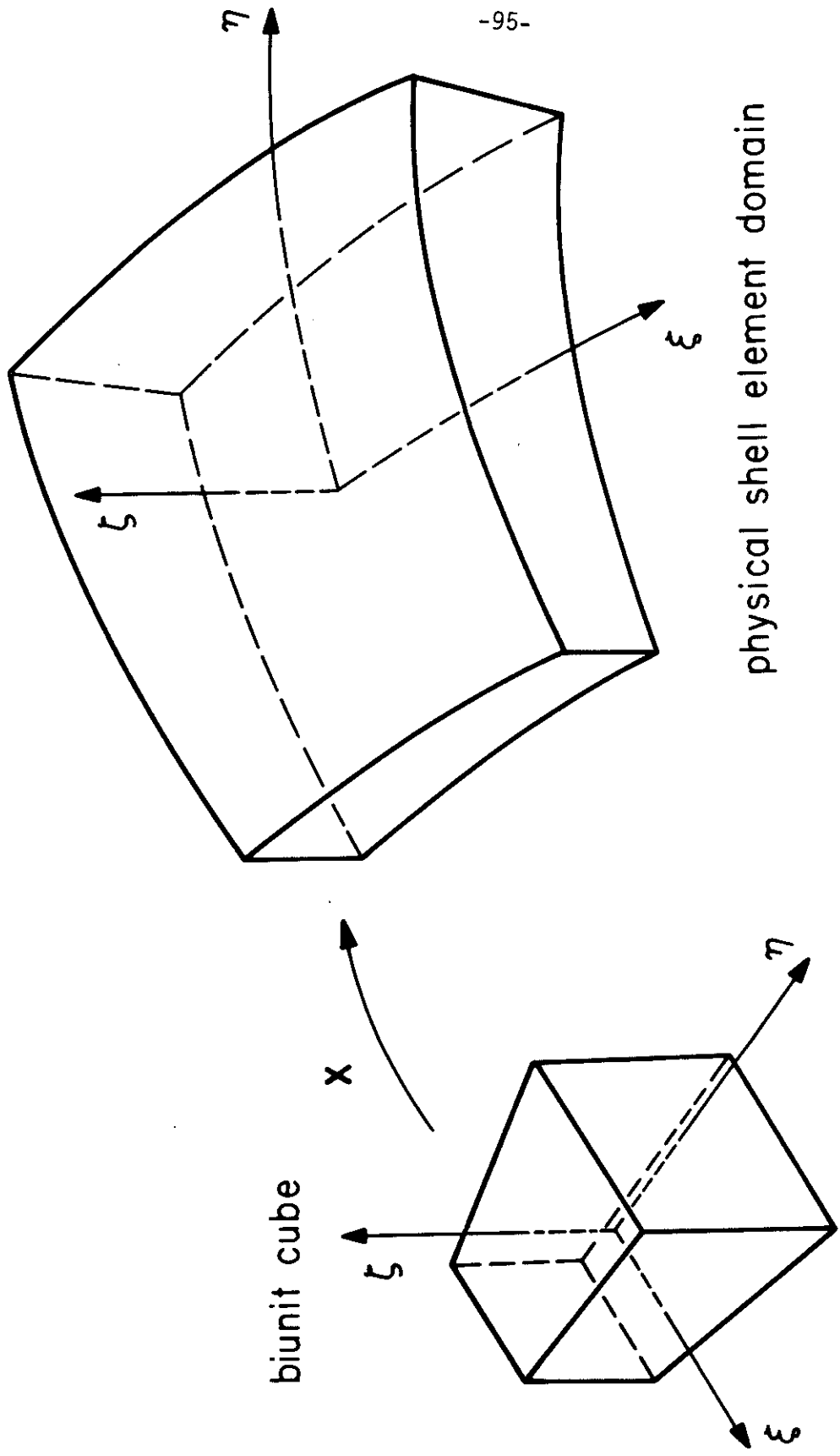
position vector and \tilde{y} as the deformed position vector.

In Section II, the geometrical and kinematical behavior of a typical shell element will be described. The construction of "lamina" and "fiber" coordinate systems is derived along with the corresponding transformation arrays which relate these systems to the global frame. In Section III, numerical integration of the constitutive equations and the "corotational approximation" [22,24,25] are discussed. The definitions of element arrays, selective/reduced integration techniques, numerical integration of the lumped mass matrix and shear correction factors are discussed in Section IV. In Section V, we discuss the reduced integration Lagrange elements and the heterosis element. Sample problems involving a number of the elements are contained in Section VI.

II. Geometric and Kinematic Descriptions

II-A. Geometry

We denote the position vector of a generic point of the shell in the undeformed configuration, which is also the reference configuration, by \tilde{x} . It is equal to the sum of the position vector of a point in the reference surface $\bar{\tilde{x}}$ and a position vector based at a point in the reference surface which defines the "fiber direction" through the point \tilde{x} . Following the finite element discretization procedures described in Section IV-A of Chapter 3, a smooth mapping of the biunit cube into the physical shell domain (see Figure IIA-1) is defined by the follow-



physical shell element domain

Fig. II A-1

ing equations:

$$\tilde{x}(\xi, \eta, \zeta) = \bar{\tilde{x}}(\xi, \eta) + \tilde{\chi}(\xi, \eta, \zeta) \quad (\text{IIA.1})$$

$$\bar{\tilde{x}}(\xi, \eta) = \sum_{a=1}^{n_{en}} N_a(\xi, \eta) \bar{\tilde{x}}_a \quad (\text{IIA.2})$$

$$\tilde{\chi}(\xi, \eta, \zeta) = \sum_{a=1}^{n_{en}} N_a(\xi, \eta) \tilde{\chi}_a(\zeta) \quad (\text{IIA.3})$$

$$\tilde{\chi}_a(\zeta) = z_a(\zeta) \hat{\tilde{\chi}}_a \quad (\text{no sum}) \quad (\text{IIA.4})$$

$$z_a(\zeta) = N_+(\zeta) z_a^+ + N_-(\zeta) z_a^- \quad (\text{IIA.5})$$

$$N_+(\zeta) = \frac{1}{2} (1 + \zeta), \quad N_-(\zeta) = \frac{1}{2} (1 - \zeta) \quad (\text{IIA.6})$$

In equations (IIA.2) - (IIA-6), $\bar{\tilde{x}}_a$ is the position vector of nodal point a ; N_a denotes a two-dimensional shape function associated with node a ; n_{en} is the number of element nodes; $\hat{\tilde{\chi}}_a$ is a unit vector emanating from node a in the fiber direction; and z_a is a "thickness function," associated with node a , which is defined by the location of the reference surface. A lamina surface is defined by equation (IIA.1) for ζ fixed; and a fiber line is defined by the same equation for ξ, η fixed. In general, the fibers are not perpendicular to the laminae. It has been found convenient to take as input the coordinates of the top and bottom surfaces of the shell along each nodal fiber (\tilde{x}_a^+ and \tilde{x}_a^- , respectively) and a parameter $\bar{\zeta} \in [-1, +1]$ which defines the location of the reference surface. For example, if $\bar{\zeta} = -1, 0, +1$ (respectively), then the reference surface is taken to be the bottom, middle, top (respectively) of the shell. From these input data, we may calculate $\bar{\tilde{x}}_a$, $\hat{\tilde{\chi}}_a$, z_a^+ , and z_a^- ($a = 1, 2, \dots, n_{en}$) from:

$$\bar{x}_{\sim a} = \frac{1}{2} (1 - \bar{\zeta}) x_{\sim a}^- + \frac{1}{2} (1 + \bar{\zeta}) x_{\sim a}^+ \quad (\text{IIA.7})$$

$$\hat{x}_{\sim} = (x_{\sim a}^+ - x_{\sim a}^-) / \|x_{\sim a}^+ - x_{\sim a}^-\| \quad (\text{IIA.8})$$

$$z_{\sim a}^+ = \frac{1}{2} (1 - \bar{\zeta}) \|x_{\sim a}^+ - x_{\sim a}^-\| \quad (\text{IIA.9})$$

$$z_{\sim a}^- = -\frac{1}{2} (1 + \bar{\zeta}) \|x_{\sim a}^+ - x_{\sim a}^-\| \quad (\text{IIA.10})$$

$\|\cdot\|$ denotes the Euclidean norm (i.e., $\|x_{\sim}\| = (x_1^2 + x_2^2 + x_3^2)^{1/2}$).

An illustration of these ideas is presented in Figure IIA-2. By virtue of the fact that the top- and bottom-surface coordinates are uniquely defined at element interfaces, there are no gaps or overlaps along element boundaries.

Similarly, the position vector \underline{y} of the same generic point of the shell in the deformed configuration is defined by:

$$\underline{y}(\xi, \eta, \zeta) = \bar{y}(\xi, \eta) + \underline{Y}(\xi, \eta, \zeta) \quad (\text{IIA.11})$$

$$\bar{y}(\xi, \eta) = \sum_{a=1}^{n_{en}} N_a(\xi, \eta) \bar{y}_{\sim a} \quad (\text{IIA.12})$$

$$\underline{Y}(\xi, \eta, \zeta) = \sum_{a=1}^{n_{en}} N_a(\xi, \eta) \underline{Y}_{\sim a}(\zeta) \quad (\text{IIA.13})$$

$$\underline{Y}_{\sim a}(\zeta) = z_{\sim a}(\zeta) \hat{y}_{\sim a} \quad (\text{no sum}) \quad (\text{IIA.14})$$

where $z_{\sim a}(\zeta)$ and N_+, N_- are defined by (IIA.5) and (IIA.6), respectively. We observe from equations (IIA.4) and (IIA.14) that the nodal fibers are assumed to be inextensible, i.e., they may rotate, but cannot stretch or contract. Therefore $\hat{y}_{\sim a}$ is a unit vector.

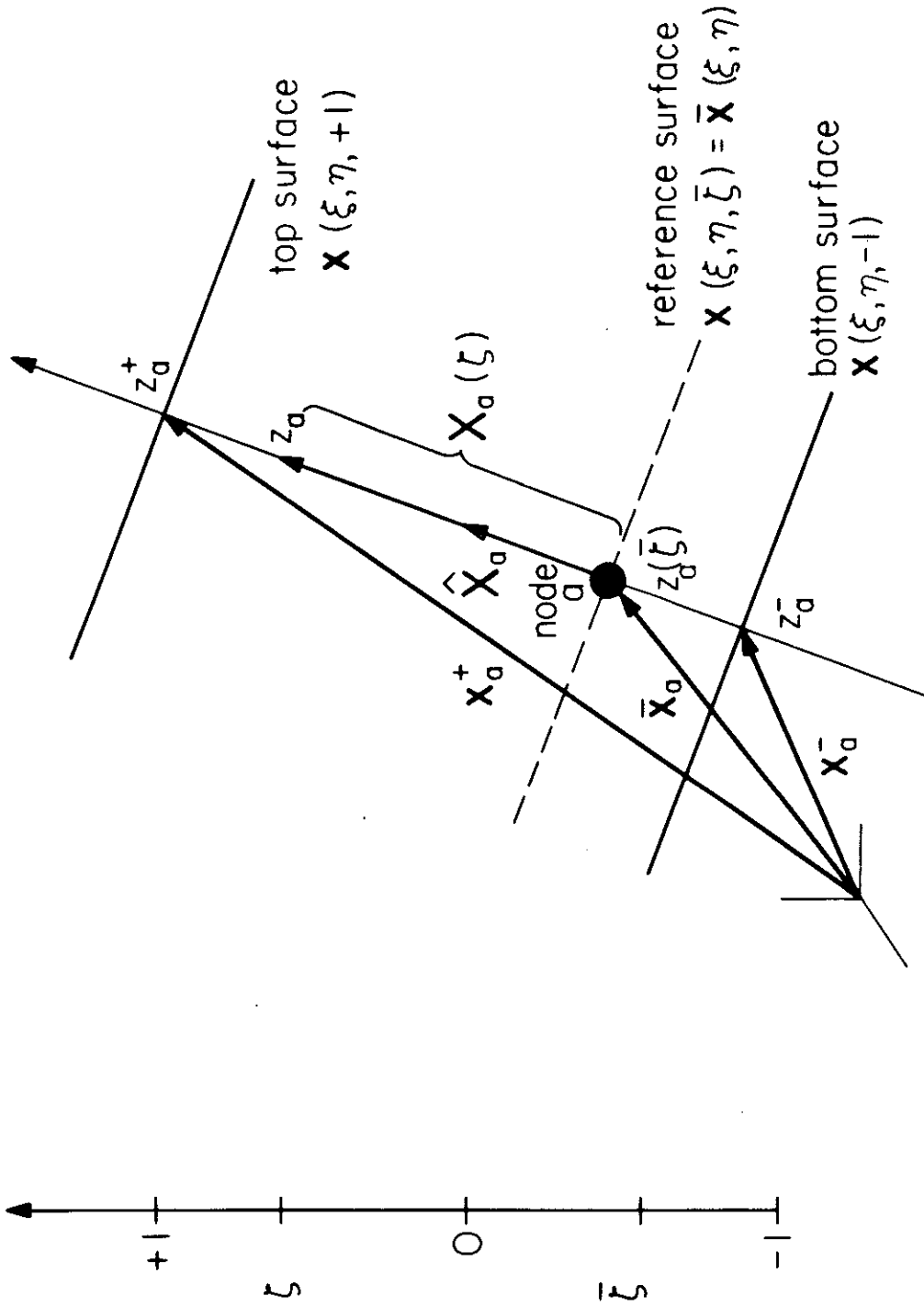


Fig. II A-2

II-B. Kinematics

We define the displacement \underline{u} of a generic point to be the difference between the deformed and the reference configurations of the same point. It can be written in terms of the sum of the displacement of that point on the reference surface $\bar{\underline{u}}$, and the "fiber displacement" \underline{U} . Therefore (see Figure IIB-1),

$$\underline{u} = \underline{y} - \underline{x} = \bar{\underline{u}} + \underline{U} \quad (\text{IIB.1})$$

$$\bar{\underline{u}} = \bar{\underline{y}} - \bar{\underline{x}} \quad (\text{IIB.2})$$

$$\bar{\underline{u}}_{\sim a} = \bar{\underline{y}}_{\sim a} - \bar{\underline{x}}_{\sim a} \quad (\text{IIB.3})$$

$$\underline{U} = \underline{Y} - \underline{X} \quad (\text{IIB.4})$$

$$\underline{U}_{\sim a} = \underline{Y}_{\sim a} - \underline{X}_{\sim a} = z_{a\sim a} \hat{\underline{U}}_{\sim a} \quad (\text{no sum}) \quad (\text{IIB.5})$$

$$\hat{\underline{U}}_{\sim a} = \hat{\underline{Y}}_{\sim a} - \hat{\underline{X}}_{\sim a} \quad (\text{IIB.6})$$

By virtue of the definition of \underline{u} , the kinematics of the shell element are defined by invoking the isoparametric hypothesis that the same expressions are used for kinematics as for geometry with displacement variables in place of coordinate variables. In order to define \underline{y} , a trial value of $\hat{\underline{U}}_{\sim a}$ is calculated (i.e., $\hat{\underline{U}}_{\sim a}^{\text{trial}}$) and projected radially to maintain inextensibility. The steps in the procedure are as follows (see Figure IIB-2):

$$\hat{\underline{Y}}_{\sim a} = (\hat{\underline{X}}_{\sim a} + \hat{\underline{U}}_{\sim a}^{\text{trial}}) / \|\hat{\underline{X}}_{\sim a} + \hat{\underline{U}}_{\sim a}^{\text{trial}}\| \quad (\text{IB.7})$$

$$\hat{\underline{U}}_{\sim a} = \hat{\underline{Y}}_{\sim a} - \hat{\underline{X}}_{\sim a} \quad (\text{IB.8})$$

We have found the present scheme to be both economical and effective

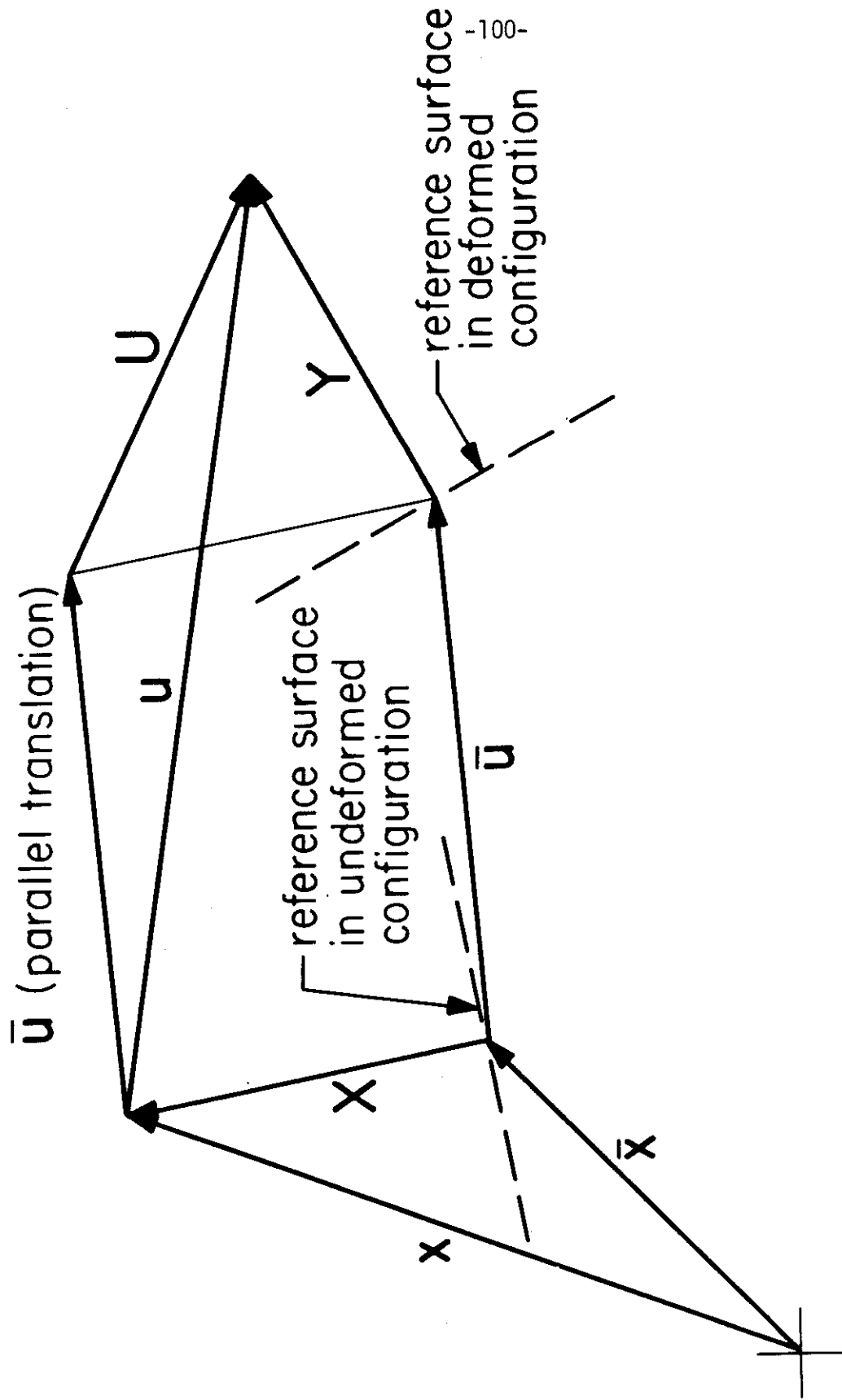


Fig. II B-1

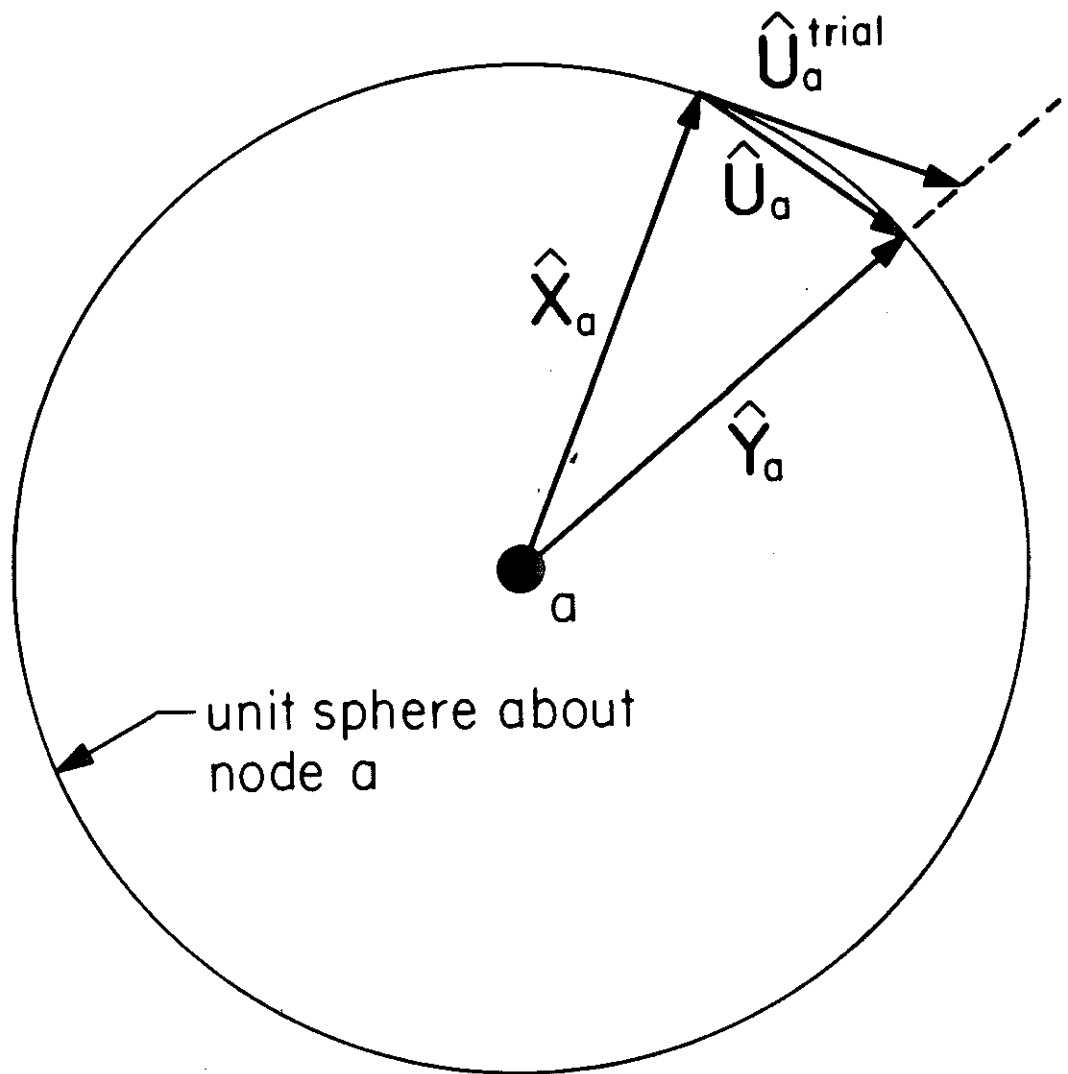


Fig. II B-2 Nodal fiber inextensibility condition maintained by radial return normalization

in practice.

II-C. Lamina Coordinate Systems

In order to invoke the plane stress hypothesis, at each integration point in the element a coordinate system is defined as follows:

$$\tilde{e}_1^l = \tilde{y}_{,\xi} / \|\tilde{y}_{,\xi}\| \quad (\text{IIC.1})$$

$$\tilde{e}_3^l = \tilde{e}_1^l \times \tilde{y}_{,\eta} / \|\tilde{e}_1^l \times \tilde{y}_{,\eta}\| \quad (\text{IIC.2})$$

$$\tilde{e}_2^l = \tilde{e}_3^l \times \tilde{e}_1^l \quad (\text{IIC.3})$$

where a comma is used to denote partial differentiation (e.g., $\tilde{y}_{,\xi} = \partial \tilde{y} / \partial \xi$) and "x" denotes the cross product. We call this coordinate system the lamina coordinate system (see Fig. IIC-1). The \tilde{e}_3^l direction is used for the purpose of invoking the zero normal stress hypothesis. We should note that \tilde{e}_3^l in general is not parallel to the ζ axis (see Figure IIC-2), that is, the fiber direction. In order to have a global finite element formulation, an orthogonal transformation matrix \tilde{q} is defined:

$$\tilde{q} = [\tilde{e}_1^l \ \tilde{e}_2^l \ \tilde{e}_3^l]^T: \text{ global} \rightarrow \text{ lamina} \quad (\text{IIC.4})$$

II-D. Fiber Coordinate Systems

Due to the plane stress hypothesis, the rank of the material response matrix \tilde{C} is five, even though it is a 6×6 matrix in the general three-dimensional constitutive theory. In order to remove

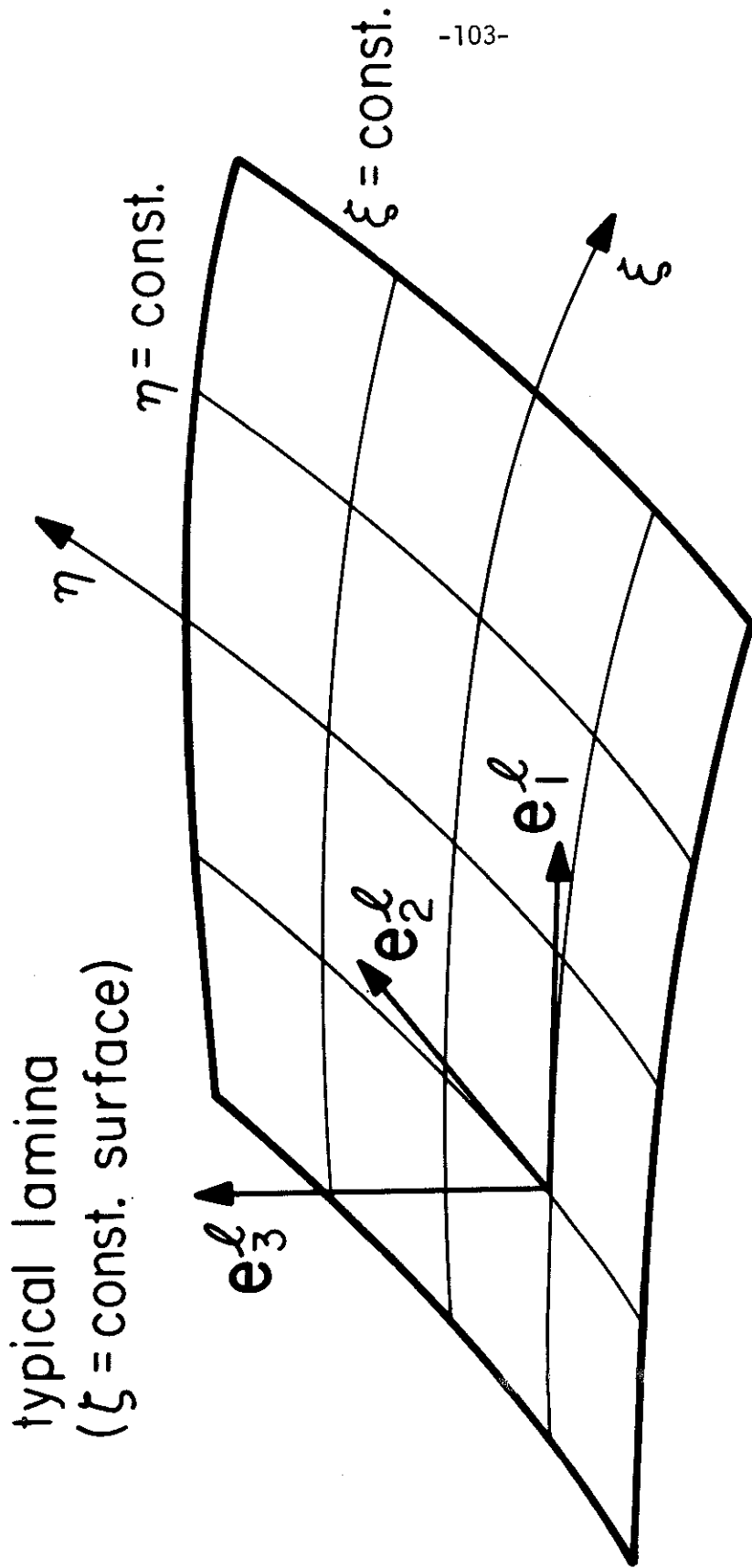


Fig. II C-1 Typical lamina coordinate system

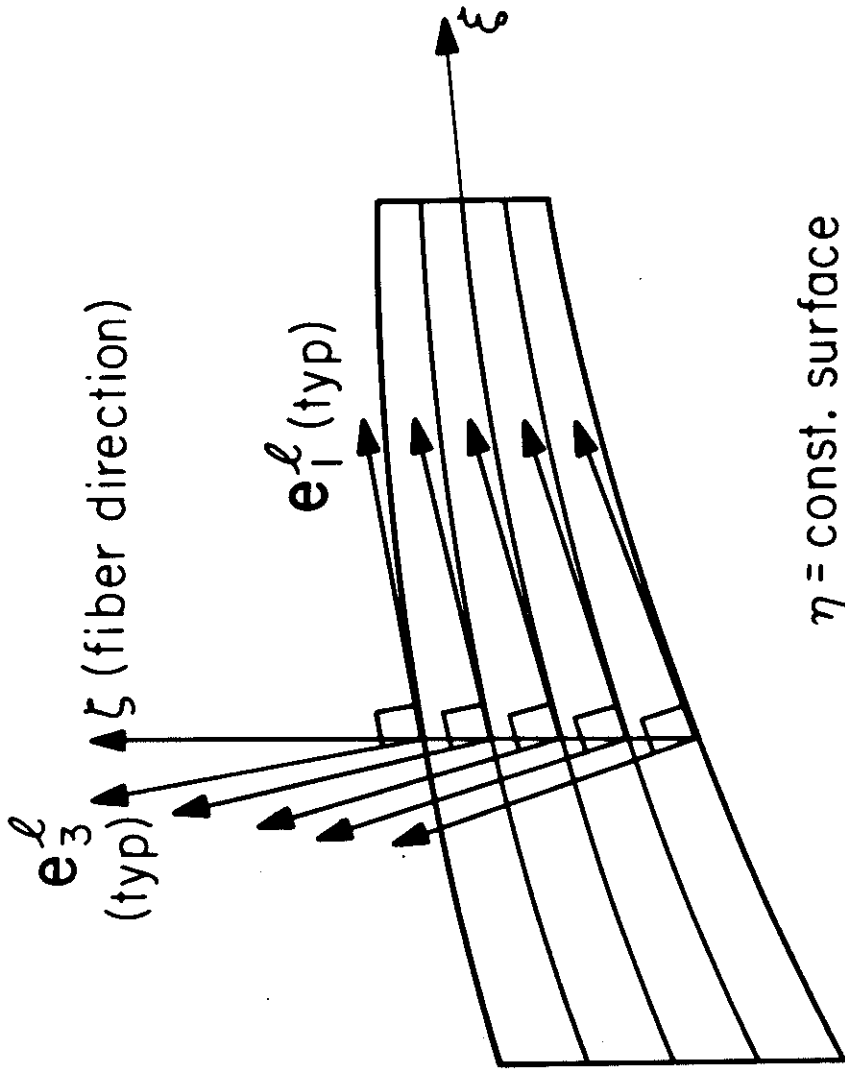


Fig. II C-2 Lamina coordinate systems along a fiber

the in-plane twist mode, we define a unique local Cartesian coordinate system at each node which is used as a reference frame for rotation increments. The algorithm is as follows:

$$1. \text{ Let } a_i = |\hat{Y}_{\sim i}|, \quad i = 1, 2, 3 \quad (\text{IID.1})$$

$$2. \quad j = 1 \quad (\text{IID.2})$$

$$3. \text{ If } a_1 > a_3, \text{ then } a_3 = a_1, \text{ and } j = 2. \quad (\text{IID.3})$$

$$4. \text{ If } a_2 > a_3, \quad j = 3. \quad (\text{IID.4})$$

$$5. \quad \underline{e}_3^f = \hat{Y}_{\sim j} \quad (\text{IID.5})$$

$$6. \quad \underline{e}_2^f = (\hat{Y}_{\sim j} \times \underline{e}_j) / \|\hat{Y}_{\sim j} \times \underline{e}_j\| \quad (\text{IID.6})$$

$$7. \quad \underline{e}_1^f = \underline{e}_2^f \times \hat{Y}_{\sim j} \quad (\text{IID.7})$$

This orthonormal fiber basis is chosen in such a way that if $\hat{Y}_{\sim j}$ is "close" to the third axis of the global system, then $\underline{e}_1^f, \underline{e}_2^f, \underline{e}_3^f$ will be "close" to the global axes (see Figure IID-1). With these definitions, an orthogonal transformation matrix \underline{r} is defined such that for each time step the three incremental fiber displacements in the global coordinate system can be contracted to two incremental rotations.

Let $\Delta\hat{U}_1, \Delta\hat{U}_2, \Delta\hat{U}_3$ be the global incremental vector components of $\Delta\hat{U}$, also let $\Delta\theta_1$ and $\Delta\theta_2$ be the rotation increments about the basis vectors \underline{e}_2^f and \underline{e}_1^f , respectively. The sign convention is defined in Figure IID-1. The relationship between $\Delta\hat{U}$ and $\Delta\theta$ is:

$$\Delta\hat{U} = \underline{r}^T \Delta\theta \quad (\text{IID.8})$$

where $\underline{r}: \text{ fiber} \rightarrow \text{global} \quad (\text{IID.9})$

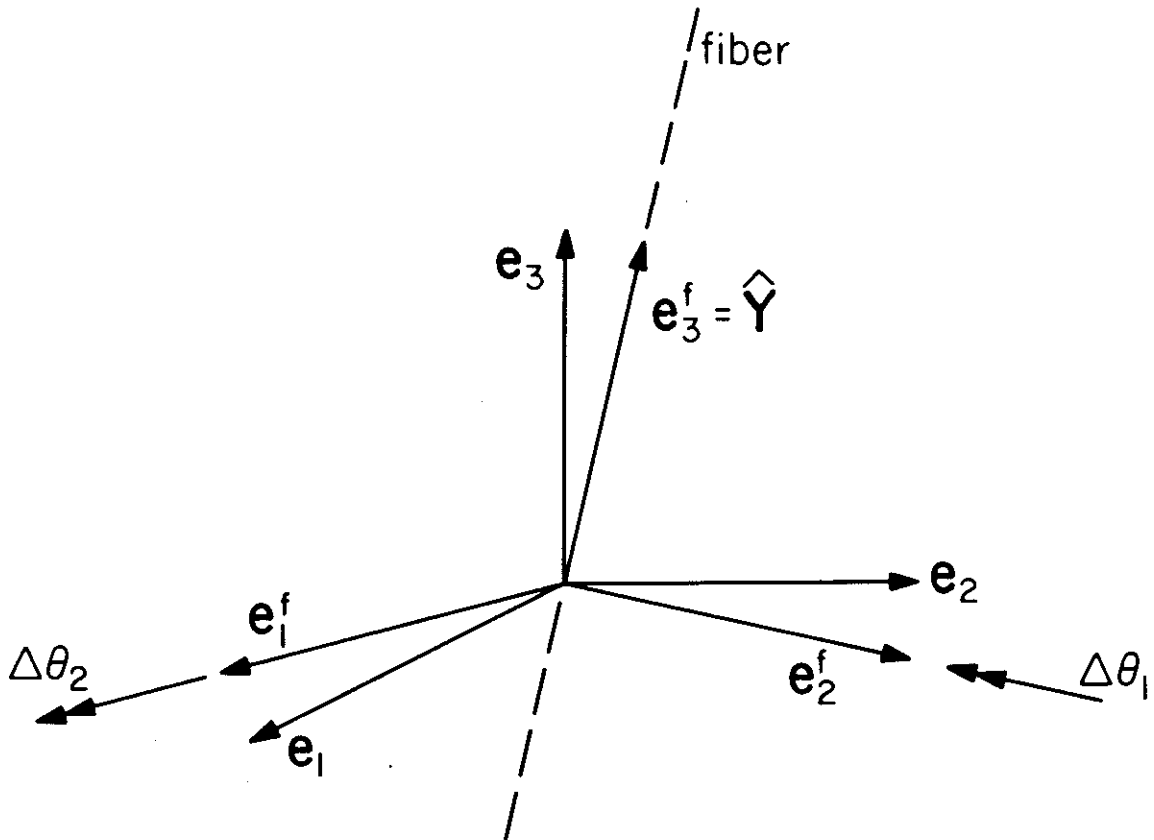


Fig. II D-1 Nodal fiber basis

and

$$\tilde{\mathbb{T}} = \begin{bmatrix} -1 & 0 \\ 0 & -1 \\ 0 & 0 \end{bmatrix} \quad (\text{IID.10})$$

$$\tilde{\Delta\hat{U}} = \left\{ \begin{array}{c} \Delta\hat{U}_1 \\ \Delta\hat{U}_2 \\ \Delta\hat{U}_3 \end{array} \right\} \quad (\text{IID.11})$$

$$\tilde{\Delta\theta} = \left\{ \begin{array}{c} \Delta\theta_1 \\ \Delta\theta_2 \end{array} \right\} \quad (\text{IID.12})$$

Equations (IID.8) through (IID.12) enable the reduction of the nodal degrees-of-freedom from six to five in the matrix incremental equilibrium equations. This obviates the need to develop artificial in-plane torsional stiffnesses to numerically stabilize rotation about the fiber direction [17].

When beam-type stiffeners are assembled with shell elements, the bending stiffness of the beam naturally provides the in-plane torsional stiffness of the composite structure, equations (IID.8) through (IID.12) can be ignored, and six degrees-of-freedom are retained in the global incremental equilibrium equations.

III. Integration of Constitutive Equations

III-A. Numerical Algorithms

The numerical algorithms described in Section III of the last chapter cannot be used directly, due to the stress components being referred to a rotating basis. Also, the zero normal-stress constraint needs to be enforced with respect to the third direction of the lamina

basis. So the integration of the rate type constitutive equations requires special considerations.

We define $\underline{\gamma}$ and $\underline{\omega}$ according to equations (IIA.1) through (IIIA.6) of Chapter 3. The orientations of the lamina bases at time t_n and t_{n+1} are defined, respectively by:

$$\underline{q}^n: \text{global} \rightarrow \text{lamina at } t_n \quad (\text{IIIA.1})$$

$$\underline{q}^{n+1}: \text{global} \rightarrow \text{lamina at } t_{n+1} \quad (\text{IIIA.2})$$

Consequently, the incremental transformation between lamina bases is given by:

$$\underline{\Delta q} = \underline{q}^{n+1}(\underline{q}^n)^T: \text{lamina at } t_n \rightarrow \text{lamina at } t_{n+1} \quad (\text{IIIA.3})$$

With these definitions, the numerical algorithms are:

$$\underline{\tau}^{n+1} = \underline{R} \underline{\tau}^n \underline{R}^T \quad (\text{IIIA.4})$$

$$\underline{\tau}^{n+1} = \underline{\tau}^{n+1} + \underline{\Delta \tau} \quad (\text{IIIA.5})$$

where

$$\underline{R} = (\underline{I} + (\underline{I} - \frac{1}{2} \underline{\omega})^{-1} \underline{\omega}) \underline{\Delta q} \quad (\text{IIIA.6})$$

$$\underline{\Delta \tau}_{ij} = \bar{C}_{ijkl} \gamma_{kl} \quad (\text{IIIA.7})$$

and

$$\gamma_{33} = -(\bar{\tau}_{33}^{n+1} - \sum_{ij \neq 33} \bar{C}_{33ij} \gamma_{ij}) / \bar{C}_{3333} \quad (\text{IIIA.8})$$

The matrix \underline{R} is in general an approximation to the rotation of the material particle relative to the lamina basis; (IIIA.8) is used to insure satisfaction of the zero normal-stress condition in the lamina basis at t_{n+1} (i.e., $\tau_{33}^{n+1} = 0$). In many situations of practical interest, the particle rotation will be closed to the rotation of the

lamina basis and thus $\underline{\underline{R}} \approx \underline{\underline{I}}$. This is the case for what is classically known as the "small strain-finite rotation approximation. In this case, the calculation of $\underline{\underline{R}}$ may be omitted. This philosophy has been exploited in the works of Argyris [21,23,26,27] and Belytschko [22,24, 25].

IV. Element Arrays

IV-A. Material Tangent Matrix

The element tangent matrix $\underline{\underline{D}}$ is defined by equations (IVB.13) of Chapter 2. For application to shell analysis, the $\underline{\underline{D}}$ matrix needs to be modified to account for the zero normal-stress condition. We define a zero normal-stress projection operator $\underline{\underline{P}}$ such that the row and column of $\underline{\underline{D}}$ corresponding to γ_{33} are removed, i.e.,

$$\underline{\underline{\tilde{D}}} = \underline{\underline{P}}^T \underline{\underline{D}} \underline{\underline{P}} \quad (\text{IVA.1})$$

where

$$\underline{\underline{P}} = \begin{bmatrix} \underline{\underline{P}} & \underline{\underline{0}}_{63} \\ \underline{\underline{0}}_{36} & \underline{\underline{I}}_3 \end{bmatrix} \quad (\text{IVA.2})$$

$$\underline{\underline{P}} = \begin{bmatrix} 1 & 0 & 0 & 0 & 0 \\ 0 & 1 & 0 & 0 & 0 \\ 0 & 0 & 1 & 0 & 0 \\ P_1 & P_2 & P_3 & P_5 & P_6 \\ 0 & 0 & 0 & 1 & 0 \\ 0 & 0 & 0 & 0 & 1 \end{bmatrix} \quad (\text{IVA.3})$$

and

$$P_I = - \bar{C}_{33ij} / \bar{C}_{3333} \quad (\text{IVA.4})$$

IV-B. Strain-Displacement Matrix

In order to prevent "mesh-locking" phenomena [11-14, 17-20], special treatment needs to be given to transverse shear terms. We will employ the same idea, namely reduced/selective integration techniques, which have been discussed in Chapter 3. We implement the selective integration procedure by a simple modification of the strain-displacement matrix. The definition of the strain-displacement matrix adopted is given as follows:

$$\tilde{B} = [B_1, B_2, \dots, B_{n_{en}}] \quad (\text{IVB.1})$$

$$\tilde{B}_a = \begin{bmatrix} B_a^Y \\ \tilde{B}_a \\ B_a^\omega \end{bmatrix}, \quad a = 1, 2, \dots, n_{en} \quad (\text{IVB.2})$$

$$B_a^Y = \left[\begin{array}{ccc|ccc} B_1 & 0 & 0 & B_4 & 0 & 0 \\ B_2 & B_1 & 0 & B_5 & B_4 & 0 \\ 0 & B_2 & 0 & 0 & B_5 & 0 \\ \hline 0 & \bar{B}_3 & \bar{B}_2 & 0 & \bar{B}_6 & \bar{B}_5 \\ \bar{B}_3 & 0 & \bar{B}_1 & \bar{B}_6 & 0 & \bar{B}_4 \end{array} \right] \quad (\text{IVB.3})$$

$$B_a^\omega = \left[\begin{array}{ccc|ccc} B_2 & -B_1 & 0 & B_5 & -B_4 & 0 \\ 0 & B_3 & -B_2 & 0 & B_6 & -B_5 \\ -B_3 & 0 & B_1 & -B_6 & 0 & B_4 \end{array} \right] \quad (\text{IVB.4})$$

$$B_i = \begin{cases} N_{a,i} & , \quad i = 1, 2, 3 \\ (N_{a,z_a})_{(i-3)} & , \quad i = 4, 5, 6 \end{cases} \quad (\text{IVB.5})$$

Note that $N_{a,i} = \partial N_a / \partial y_i^{\ell}$ where y_i^{ℓ} are the components of the coordinates in lamina systems. The definition of the \bar{B}_i 's is found in equation (IA.8) of Chapter 3. For details consult [20,28]. For the two-dimensional case, uniform reduced-integration Lagrange elements are employed. In this case, B_i 's are taken to be equal to \bar{B}_i 's.

There appears to be no general nonlinear theory which includes shear correction effects. An ad hoc procedure, which amounts to replacing each \bar{B}_i in (IVB.3) by $\kappa^{1/2} \bar{B}_i$ where κ is the shear correction factor, is employed herein. (For the example problems in Section VI we have employed $\kappa = 5/6$.) The strain increments may be computed as follows:

$$\underline{\gamma}_{vec} = \sum_{a=1}^{n_{en}} B_a^Y \left\{ \begin{array}{c} \Delta \bar{u}_a \\ \Delta \hat{u}_a^{\ell} \end{array} \right\} \quad (IVB.6)$$

where

$$\underline{\gamma}_{vec} = \left\{ \begin{array}{c} \gamma_1 \\ \gamma_2 \\ \gamma_3 \\ \gamma_5 \\ \gamma_6 \end{array} \right\} = \left\{ \begin{array}{c} \gamma_{11} \\ 2\gamma_{12} \\ \gamma_{22} \\ 2\gamma_{23} \\ 2\gamma_{31} \end{array} \right\} \quad (IVB.7)$$

IV-C. Transformation Matrices

Since we employ a global finite element formulation, all the arrays have to be transformed to the global system before they can be assembled by the standard finite element procedures. The stiffness matrices and internal force vectors are defined with respect to the lamina coordinate systems. Two transformation matrices are required;

$$\tilde{Q}_a = \begin{cases} \begin{bmatrix} \tilde{q} & 0_{33} \\ 0_{33} & \tilde{q} \end{bmatrix} & 6 \text{ dof} \\ \begin{bmatrix} \tilde{q} & 0_{32} \\ 0_{33} & \tilde{r}_a \end{bmatrix} & 5 \text{ dof} \end{cases} \quad (\text{IVC.1})$$

$$\tilde{r}_a = r_a \begin{bmatrix} -1 & 0 \\ 0 & -1 \\ 0 & 0 \end{bmatrix} \quad (\text{IVC.2})$$

$$\tilde{S}_a = \begin{cases} I_6 & 6 \text{ dof} \\ \begin{bmatrix} I_3 & 0_{32} \\ 0_{33} & \tilde{s}_a \end{bmatrix} & 5 \text{ dof} \end{cases} \quad (\text{IVC.3})$$

$$\tilde{s}_a = s_a \begin{bmatrix} -1 & 0 \\ 0 & -1 \\ 0 & 0 \end{bmatrix} \quad (\text{IVC.4})$$

IV-D. Tangent Stiffness Matrix and Internal Force Vector

The element stiffness and internal force are defined as follows:

$$\tilde{k} = [k_{\tilde{a}\tilde{b}}] \quad , \quad \tilde{f}^{\text{int}} = \{f_{\tilde{a}}^{\text{int}}\} \quad (\text{IVD.1})$$

$$k_{\tilde{a}\tilde{b}} = \int_{\square} \int_{-1}^{+1} Q_a^T B_a^T \tilde{D} B_b Q_b^j d\zeta d\square \quad (\text{IVD.2})$$

$$f_{\tilde{a}}^{\text{int}} = \int_{\square} \int_{-1}^{+1} Q_a^T (B_a^Y)^T \tilde{\tau}_{\text{vec}}^j d\zeta d\square \quad (\text{IVD.3})$$

where

$$\int_{\square} \dots d\square = \int_{-1}^{+1} \int_{-1}^{+1} \dots d\xi d\eta \quad (\text{laminar integral}) \quad (\text{IVD.4})$$

$$j = \det \begin{bmatrix} y_{1,\xi} & y_{1,\eta} & y_{1,\zeta} \\ y_{2,\xi} & y_{2,\eta} & y_{2,\zeta} \\ y_{3,\xi} & y_{3,\eta} & y_{3,\zeta} \end{bmatrix} \quad (\text{IVD.5})$$

$$\underline{\tau}_{\text{vec}} = \begin{Bmatrix} \tau_1 \\ \tau_2 \\ \tau_3 \\ \tau_5 \\ \tau_6 \end{Bmatrix} = \begin{Bmatrix} \tau_{11} \\ \tau_{12} \\ \tau_{22} \\ \tau_{23} \\ \tau_{31} \end{Bmatrix}$$

In most situations the variation of Q_a with ζ will be insignificant. For this reason we can take Q_a outside the fiber integral, viz,

$$\underline{k}_{ab} = \int_{\square} Q_a^T \left[\int_{-1}^{+1} \underline{B}_a^T \underline{\tilde{D}} \underline{B}_b j d\zeta \right] Q_b d\square \quad (\text{IVD.7})$$

$$\underline{f}_a^{\text{int}} = \int_{\square} Q_a^T \left[\int_{-1}^{+1} (\underline{B}_a^Y)^T \underline{\tau}_{\text{vec}} j d\zeta \right] d\square \quad (\text{IVD.8})$$

IV-E. External Force Vector

We allow for both body and surface force vectors.

Body force

The element body force vector is given by:

$$\underline{f}^{\text{body}} = \{ \underline{f}_a^{\text{body}} \} \quad (\text{IVE.1})$$

$$\tilde{f}_a^{\text{body}} = S_a^T \int_{\square} \int_{-1}^{+1} \tilde{N}_a^T \tilde{b} \rho_0 j_0 d\zeta d\square \quad (\text{IVE.2})$$

where ρ_0 is the mass density in the initial configuration, \tilde{b} is the prescribed body force vector (per unit mass),

$$j_0 = \begin{bmatrix} x_{1,\xi} & x_{1,\eta} & x_{1,\zeta} \\ x_{2,\xi} & x_{2,\eta} & x_{2,\zeta} \\ x_{3,\xi} & x_{3,\eta} & x_{3,\zeta} \end{bmatrix} \quad (\text{IVE.3})$$

and

$$\tilde{N}_a = \begin{bmatrix} N_a & 0 & 0 & \vdots & N_a z_a & 0 & 0 \\ 0 & N_a & 0 & \vdots & 0 & N_a z_a & 0 \\ 0 & 0 & N_a & \vdots & 0 & 0 & N_a z_a \end{bmatrix} \quad (\text{IVE.4})$$

Surface force

The element surface vector is defined by

$$\tilde{f}_a^{\text{surf}} = \{ \tilde{f}_a^{\text{surf}} \} \quad (\text{IVE.5})$$

$$\tilde{f}_a^{\text{surf}} = S_a^T \int_{\square} \tilde{N}_a^T \tilde{h} j_s d\square, \quad \zeta = \begin{cases} +1 & \text{top} \\ -1 & \text{bottom} \end{cases} \quad (\text{IVE.6})$$

$$j_s = \| \tilde{y}_{,\xi} \times \tilde{y}_{,\eta} \| \quad \text{surface Jacobian} \quad (\text{IVE.7})$$

where \tilde{h} is the surface force vector per unit surface area.

Since we consider rather general nonlinear behavior, the fiber integrals need to be evaluated by a numerical integration technique instead of analytically. When the shell consists of one homogeneous layer, Gaussian quadrature is most efficient. If it is desired to include the outermost fiber points (i.e., $\zeta = \pm 1$) then

Lobatto rules are most accurate. If the shell is built up from a series of layers of different materials, then Gaussian rules may be effectively used over each layer. If there are a large number of approximately equal-sized layers, then midpoint rule on each layer should suffice.

IV-F. Stress Resultants

Bending moments, membrane forces, and transverse shear resultants may be computed at the lamina quadrature points of the "normal" rule at which stresses are stored. Let $\bar{\xi}_l = (\xi_l, \xi_l)$ be the quadrature points, $1 \leq l \leq n_{int}$; the resultants are:

moments

$$m_{\alpha\beta}(\bar{\xi}_l) = \int_{-1}^{+1} \tau_{\alpha\beta}(\bar{\xi}_l, \zeta) z(\bar{\xi}_l, \zeta) d\zeta z_{,\zeta}(\bar{\xi}_l), \quad 1 \leq \alpha, \beta \leq 2 \quad (IVF.1)$$

$$z(\bar{\xi}_l, \zeta) = N_+(\zeta) z^+(\bar{\xi}_l) + N_-(\zeta) z^-(\bar{\xi}_l) \quad (IVF.2)$$

$$z^\pm(\bar{\xi}_l) = \sum_{a=1}^{n_{en}} N_a(\bar{\xi}_l) z_a^\pm \quad (IVF.3)$$

$$z_{,\zeta}(\bar{\xi}_l) = [z^+(\bar{\xi}_l) - z^-(\bar{\xi}_l)] / 2 \quad (IVF.4)$$

membrane forces

$$n_{\alpha\beta}(\bar{\xi}_l) = \int_{-1}^{+1} \tau_{\alpha\beta}(\bar{\xi}_l, \zeta) d\zeta z_{,\zeta}(\bar{\xi}_l), \quad 1 \leq \alpha, \beta \leq 2 \quad (IVF.5)$$

shears

$$q_\alpha(\bar{\xi}_l) = \kappa^{1/2} \int_{-1}^{+1} \tau_{\alpha 3}(\bar{\xi}_l, \zeta) d\zeta z_{,\zeta}(\bar{\xi}_l) \quad (IVF.6)$$

The sign conventions for the stress resultants are illustrated in

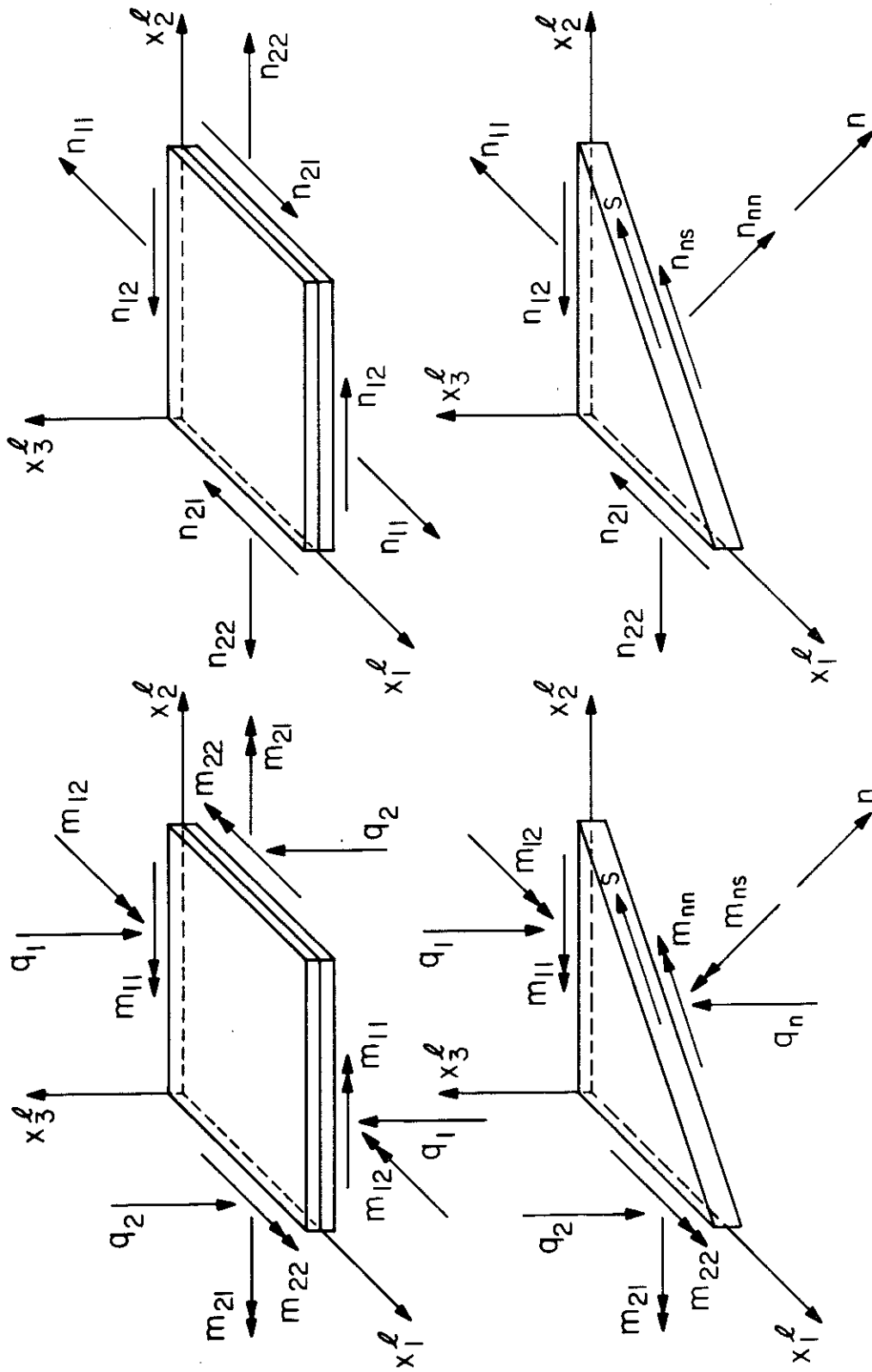


Fig. IV F-1 Sign conventions for stress resultants

Figure IVF-1.

IV-G. Mass Matrix

If the consistent mass matrix is desired, Gaussian integration rules are used. The consistent mass matrix is:

$$m_{ab} = \int_{\square} \int_{-1}^{+1} \rho_0 N_a N_b j_0 d\zeta d\xi \quad (\text{IVG.1})$$

where j_0 and N_a are defined by (IVE.3) and (IVE.4), respectively.

If lumped mass is required, Lobatto rules are employed. However, the Δt restriction is stringent for explicit transient calculations [13,38]. Therefore, the following algorithm is used to obtain a lumped mass matrix for shells such that a much larger time step can be employed with no convergence rate loss.

Algorithm

- a) Define variables; M_a^{rot} = rotational mass, M_a^{disp} = translational mass
 1. Clear necessary variables and arrays.
 2. Loop on lamina integration points.
 3. Loop on fiber integration points.
 4. $M_a^{\text{rot}} = M_a^{\text{rot}} + \rho_0 N_a^2 j_0(\tilde{\xi}_\ell, \tilde{\eta}_\ell, \tilde{\zeta}_\ell) W_\ell$, where W_ℓ is the weight of the ℓ^{th} integration point.
 5. $M_a^{\text{disp}} = M_a^{\text{rot}}$ if not heterosis.
 6. $M_a^{\text{disp}} = M_a^{\text{disp}} + \rho_0 (N_a + P_a(0)N_9)^2 j_0(\tilde{\xi}_\ell, \tilde{\eta}_\ell, \tilde{\zeta}_\ell) W_\ell$ if heterosis.
 7. If heterosis and $a = 9$, $M_a^{\text{disp}} = 0$. (Here P_a 's are the serendipity shape functions.)
- b) Normalization
 1. $\tilde{M}^{\text{rot}} = \sum_{a=1}^{n_{\text{en}}} M_a^{\text{rot}}$

$$2. \tilde{M}^{\text{disp}} = \sum_{a=1}^{n_{\text{en}}} M_a^{\text{disp}}$$

$$3. M_a^{\text{rot}} \leftarrow M_a^{\text{rot}} \left\{ \frac{XM}{\tilde{M}^{\text{rot}}} \right\}$$

$$4. M_a^{\text{disp}} \leftarrow M_a^{\text{disp}} \left\{ \frac{XM}{\tilde{M}^{\text{disp}}} \right\}$$

where XM is the total mass.

c) Adjustment to rotational mass:

$$1. \alpha_a = \frac{1}{4} (z_a^+ + z_a^-)^2 + \frac{1}{12} (z_a^+ - z_a^-)^2$$

$$2. \bar{z}_{\text{effective}} = \sum_{a=1}^{n_{\text{en}}} (z_a^+ - z_a^-) / n_{\text{en}}$$

$$3. A = \text{effective area} = \text{volume} / \bar{z}_{\text{effective}}$$

$$4. \alpha_a = \max\{\alpha_a; A/8\}$$

$$5. M_a^{\text{rot}} \leftarrow M_a^{\text{rot}} \alpha_a$$

For further details of mass lumping for shells and the critical time step calculation, see [13,38].

V. Shell Elements

The elements employed in this work are generalizations of ones that have been proposed by Hughes [11-14].

IV-A. Reduced Integration Lagrange Elements and Heterosis Elements

The lamina shape functions and quadrature rules for the Lagrange elements are shown in Figure VA-1. In each case the appropriate reduced rule is one order lower than the normal rule. The corresponding lamina shape functions and quadrature rules for the two-dimensional cases are shown in Figure VA-2. For this case uniform reduced integration is optimal. As has been discussed in detail by Hughes and

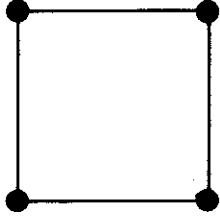
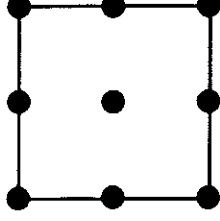
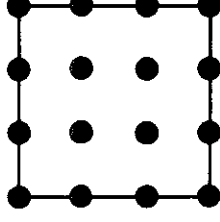
			
lamina shape functions	bilinear	biquadratic	bicubic
normal Gaussian rule	2×2	3×3	4×4
reduced Gaussian rule	1×1	2×2	3×3

Fig. V A-1 Lagrange shell elements

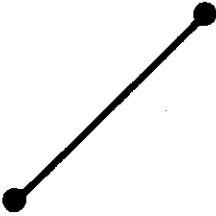
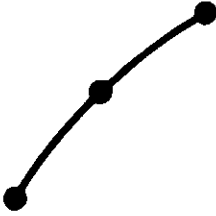
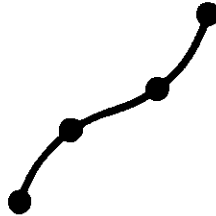
			
shape functions	linear	quadratic	cubic
quadrature rule	1-point	2-point	3-point

Fig. V A-2 Uniform reduced integration two-dimensional shell elements

coworkers [11-13,20], selective reduced integration elements behave well in thin shell applications, but may occasionally engender rank deficiency [11-13]. Research has been undertaken to efficiently remove the mechanisms. Hughes and Cohen [11,12] proposed the heterosis concept in which the 9-node Lagrange shape functions are used for rotation fields and the 8-node serendipity shape functions are used for the displacement fields. The resulting element possesses correct rank and behaves well in the thin shell limit. The heterosis element is implemented by first constructing the arrays for the selectively integrated Lagrange element (say, e.g., \tilde{k}_{lag} , $\tilde{\Delta f}_{lag}$, etc.), then a projection matrix, \tilde{H} , is constructed from the serendipity shape functions associated with the element-boundary nodes. For details of \tilde{H} see [11,12]. The heterosis arrays are then defined by

$$\begin{aligned}\tilde{k}_{het} &= \tilde{H}^T \tilde{k}_{lag} \tilde{H} \\ \tilde{\Delta f}_{het} &= \tilde{H}^T \tilde{\Delta f}_{lag}\end{aligned}\tag{VA.1}$$

VI. Sample Problems

All computations were performed on an IBM 3032 computer at the California Institute of Technology Computing Center in double precision (64 bits per floating-point word). If linear elastic properties were used, two-point Gaussian fiber integration was employed. If plasticity theory was used, four-point Gaussian fiber integration was employed. The following notations will be used for identifying the types of elements in three dimensions:

- U1 - 4-node, uniform reduced integration
- S1 - 4-node, selective reduced integration
- S2 - 9-node, selective reduced integration
- HS2 - 9-node, selective reduced integration heterosis elements

The full definition of the rotation matrix \underline{R} and the corotational approximation $\underline{R} \approx \underline{I}$ were both employed. In no case were the differences discernible. The material model is considered to be homogeneous and linearly elastic unless otherwise specified. The shear correction factor, κ , was taken to be 5/6 throughout, and for three-dimensional case, the five-degree-of-freedom nodal system was employed; for the two-dimensional case the three-degree-of-freedom nodal system was employed.

For dynamic analysis, the Newmark parameters were taken to be $\beta = 1/4$ and $\gamma = 1/2$ throughout, unless otherwise indicated.

VI-A. The Elastica

The post-buckling behavior of a clamped beam column was analyzed with a mesh of twenty 2-node elements. The analytical solution is available in Timoshenko and Gere [29]. The beam column is tilted initially off center with a slope of 1:500. This imperfection is introduced to initiate a non-trivial solution after bifurcation (buckling). Data employed in the calculations are given as follows: Young's modulus = 4.8×10^9 ; Poisson's ratio = 0, length (L) = 10, and thickness (h) = 0.01. Load-deflection results and deformed profiles are shown in Figure VI-A.

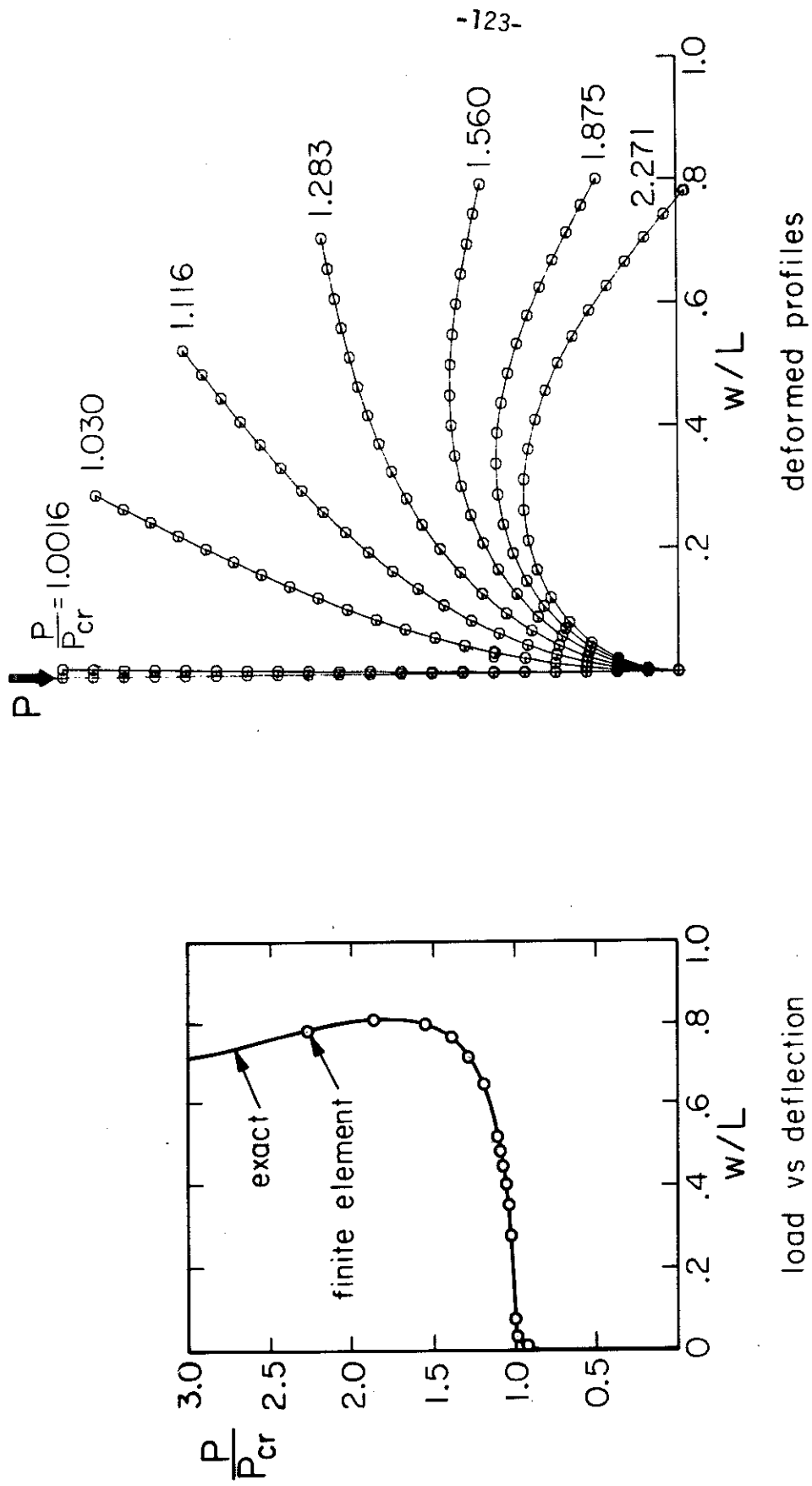


Fig. VI A The elastica

VI-B. Pure Bending of a Cantilevered Beam

A thin cantilevered beam was subjected to an end moment. The analytical solution for this problem is given by the deformed midsurface curvature = ML/EI , where M is the applied bending tip moment, L is the length of the beam, I is the moment of inertia about the axis of bending and E is Young's modulus. The end moment was increased linearly up to a final value of 2π . Two-hundred load steps were employed and approximately two iterations per step were needed for convergence. The parameters of the beam were chosen such that the exact final diameter to length ratio (D/L) equaled $\pi^{-1} = 0.3183$. Both twenty 2-node elements and ten 3-node elements were employed to model this beam and the results were found to be virtually indistinguishable. Deformed profiles are shown in Figure VI-B. The approximate D/L equaled 0.3182.

VI-C. Large Deflection of a Diamond-Shaped Frame

A pinned-hinged diamond shaped frame was analyzed, and results were compared with analytical and experimental data from [30] (see Figure VI-C). Thirty 2-node elements were employed to model one-quarter of the frame structure due to the double symmetries. Seventy-six equal load steps were employed. The average number of iterations per step over the first forty steps was less than three. Subsequently the number of iterations necessary for convergence increased. During the last six steps between sixteen and thirty iterations per step were required.

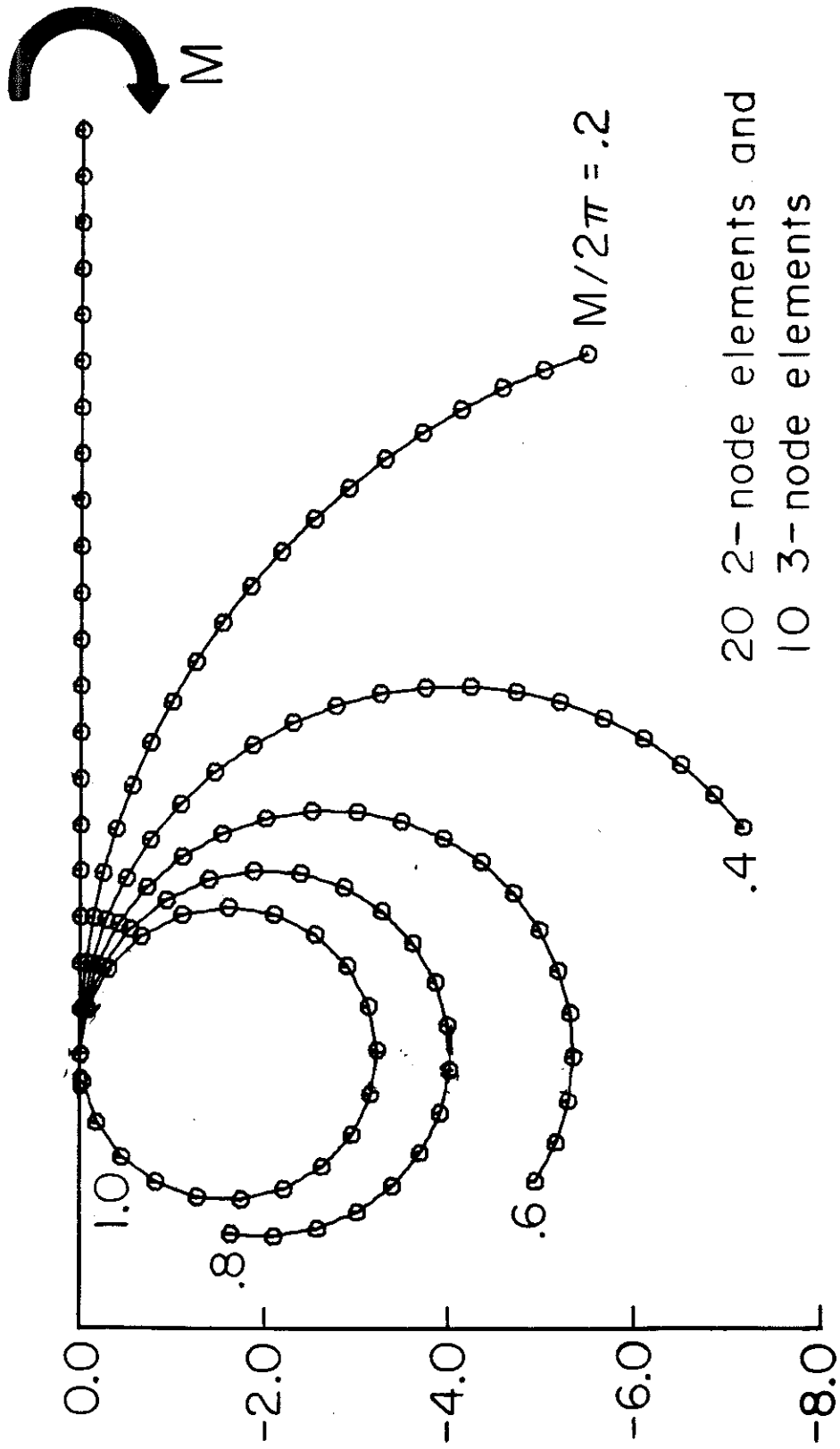
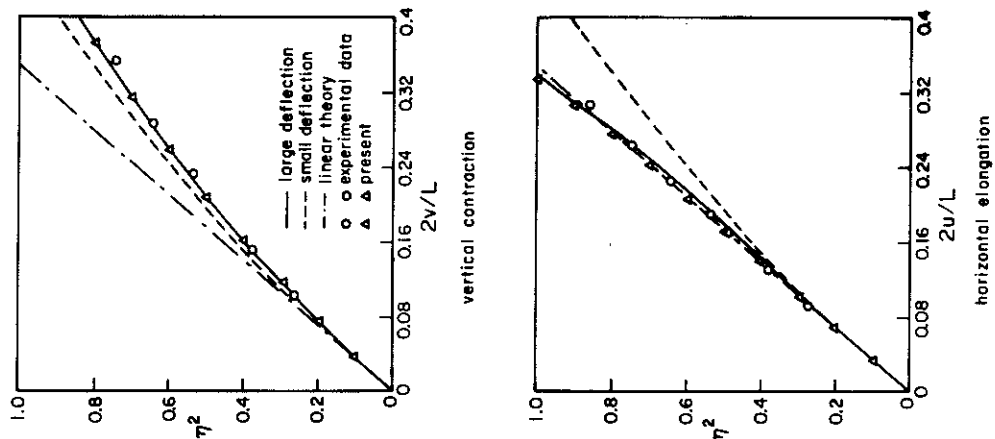
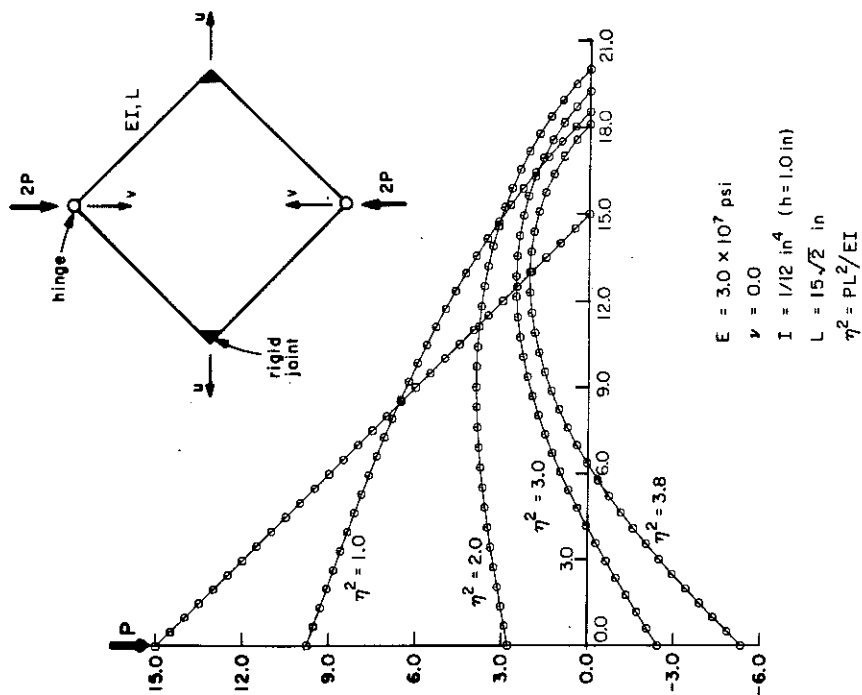


Fig. VI B Pure bending of a cantilever beam



experiment data and analytical results are from
J. A. Jenkins et al.



deflected shapes for thirty
2-node elements

Fig. VI C Large deflection of a diamond-shaped frame

VI-D. Clamped Spherical Cap Subjected to a Concentrated Load

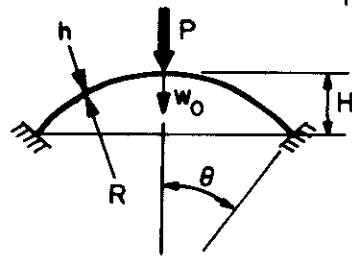
A thin spherical cap which is clamped around the circumferential edge is subjected to a concentrated force at the vertex. Twenty and thirty 2-node elements and ten and fifteen 3-node elements were employed for the spatial discretizations. Deformed profiles and load-deflection results are shown in Figure VI-D. The different spatial discretizations did not produce discernible difference in results. However, refining the load discretization from fifty to one-hundred did bring the results in closer agreement with results of other investigators [31-33].

VI-E. Clamped Circular Plate Subjected to Uniform Pressure

A clamped circular plate subjected to uniform pressure (nonconservative) was analyzed using thirty-two and sixty-four 2-node elements. The displacement versus load results and bending moment versus displacement results are compared with analytical results [34] in Figure VI-E. Twenty-four equal load steps were used. Both meshes gave virtually identical results.

VI-F. Plate Strip under Uniform Load

This problem is actually one-dimensional and an analytical solution is available in Timoshenko and Woinowsky-Krieger [34]. We applied the plane strain assumption to a mesh of five 4-node elements for half of the plate. The plate is simply supported. Pertinent data and results are shown in Figure VI-F. The load was treated as nonconservative. Comparison is made with the analytical solution and results of Horrigmoe [6] who employed hybrid elements. As expected, both S1 and



$R = 4.76$ in
 $h = 0.01576$ in
 $H = 0.0859$ in
 $\theta = 10.9^\circ$
 $E = 10 \times 10^6$ lb/in²
 $\nu = 0.3$

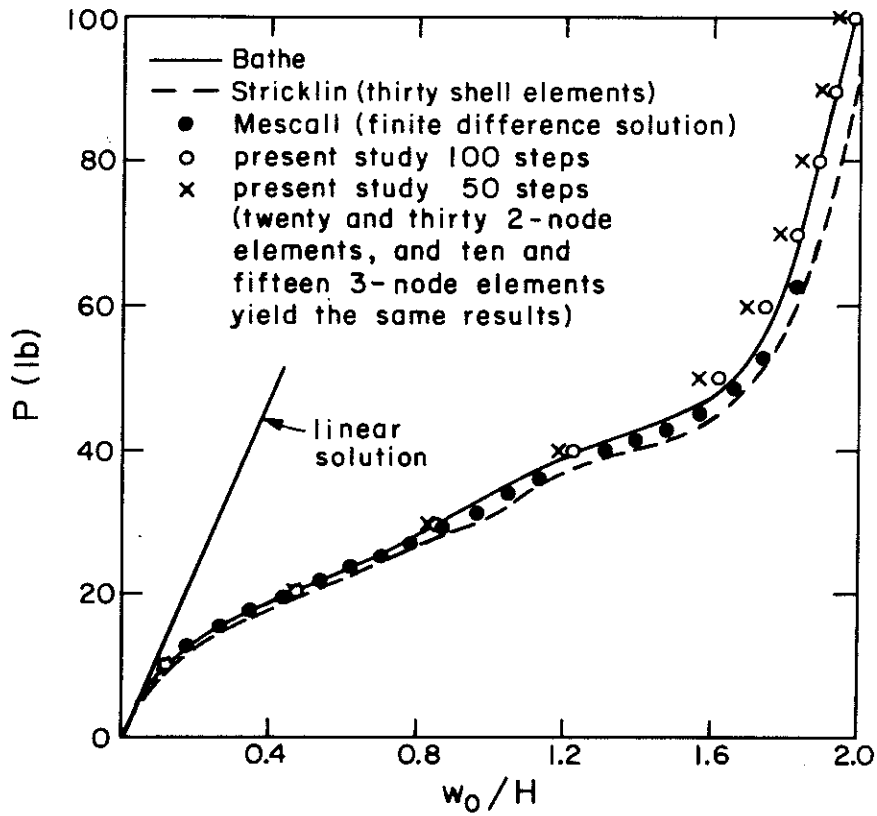
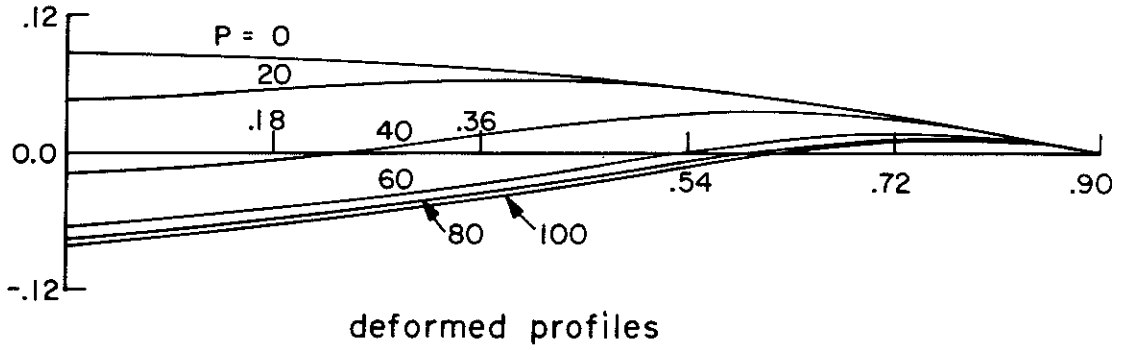
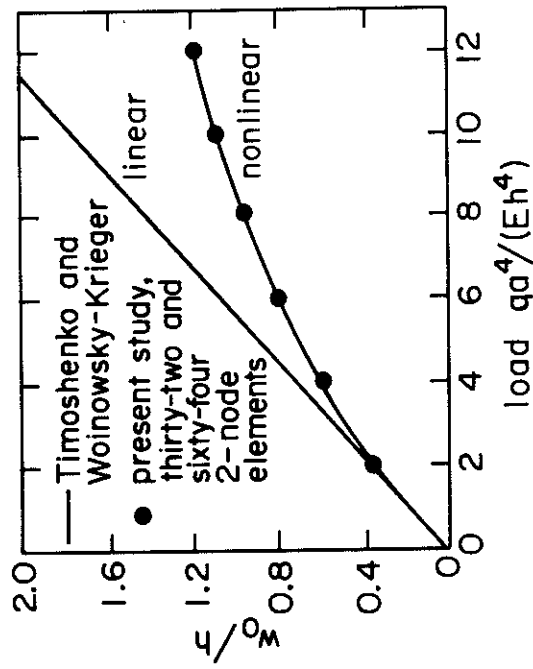
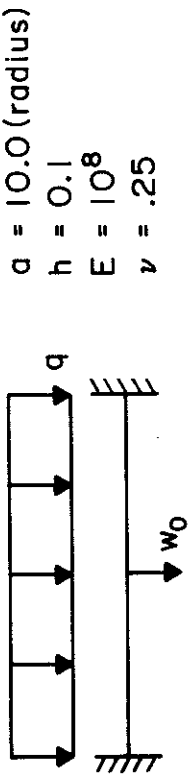
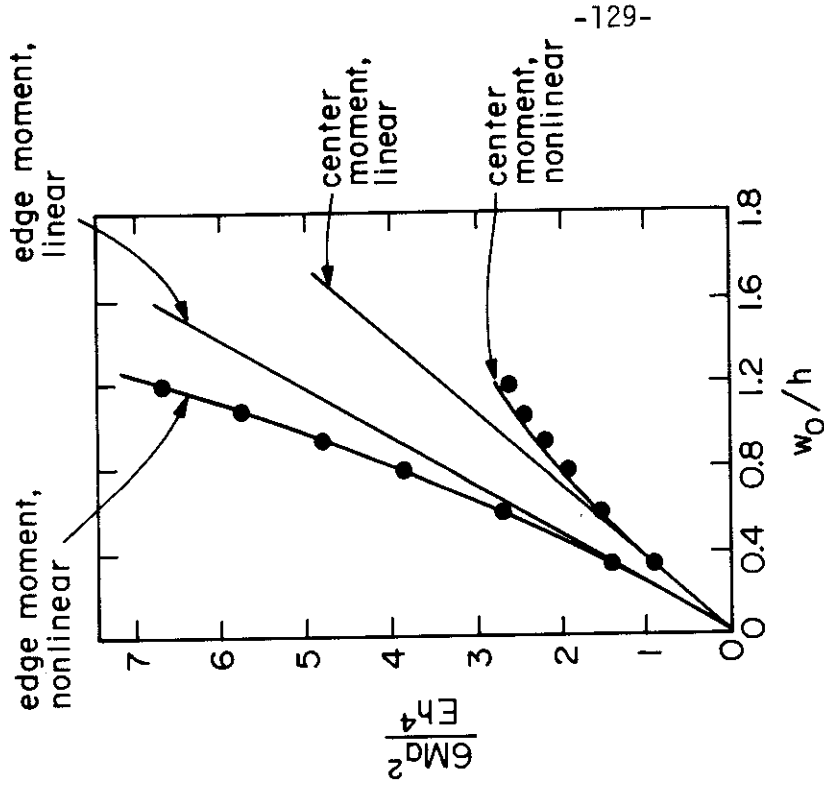


Fig. VI D Clamped spherical cap subjected to concentrated load



displacement vs load



bending moment vs displacement

Fig. VI E Clamped circular plate subjected to uniform pressure

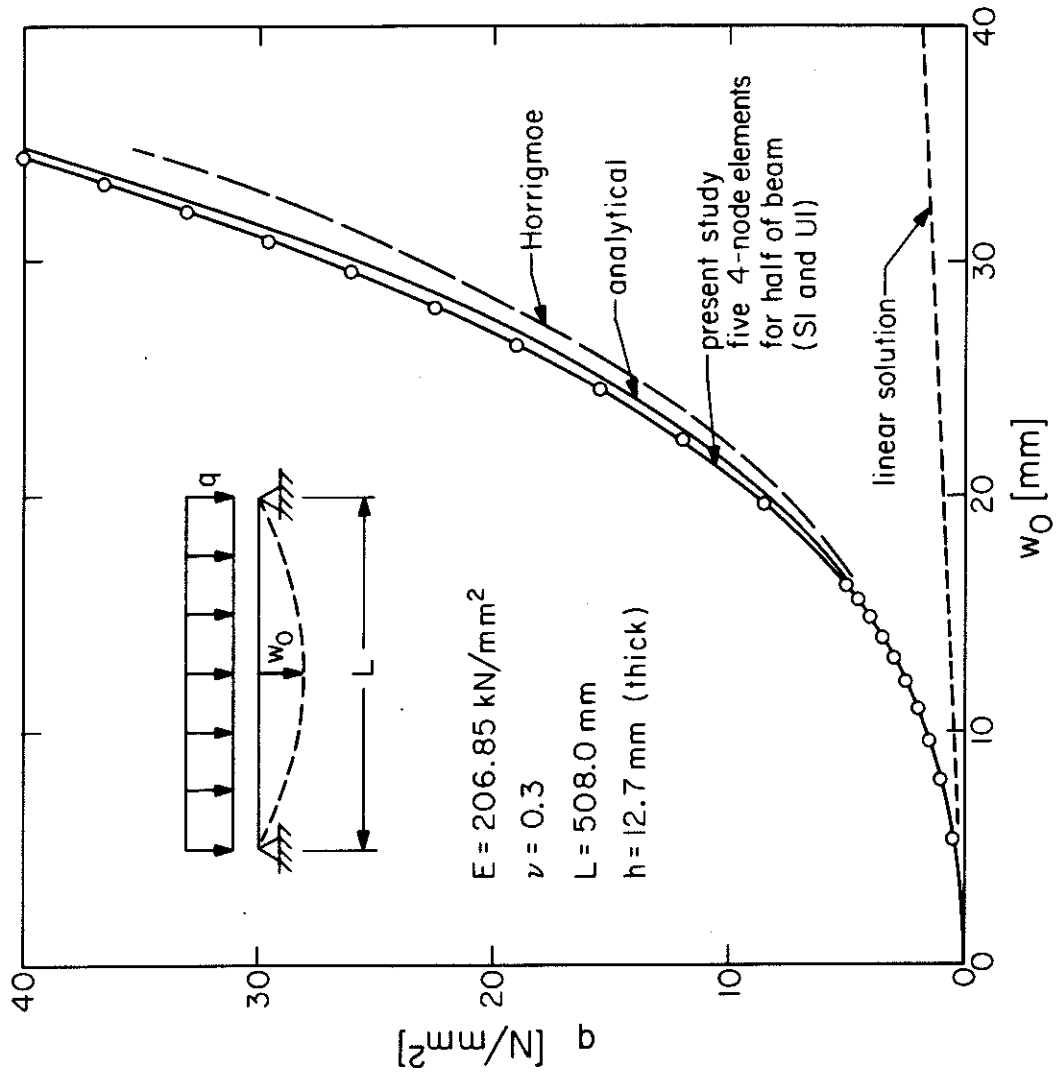


Fig. VI F Plate strip under uniform load

U1 elements yielded virtually identical results for this case, even though the S1 elements took approximately two iterations per load step, whereas the U1 elements took 4 to 5. Nevertheless, CPU time for the S1 elements was more than double that for the U1 elements. For small problems of this type, all other things being equal, the CPU time is dominated by the number of numerical integration points.

VI-G. Shallow Circular Arch under Concentrated Load

The problem statement of this one-dimensional problem is depicted in Figure VI-G. This problem has been solved by Bathe et al. [35] using 8-node continuum elements. We employed sixteen 4-node elements for half of the arch. A plane strain assumption in the out-of-plane direction was used. As in the previous analysis, the results for S1 and U1 elements were virtually identical. In each case snap-through occurred at $P = 35.8$ lb. The number of iterations per step was 1 to 2 for the S1 elements and averaged slightly over 4 per step for the U1 elements. Again, however, the S1 analysis required more than double the CPU time of the U1 analysis. The load-deflection curve was compared with the results due to Bathe et al. [35] and was shown in Figure VI-G.

VI-H. Clamped Square Plate under Uniform Load

The problem configuration is defined in Figure VI-H. Plotted results are for four HS2 elements and sixteen U1 elements. We also used meshes of four S2 elements, and sixteen and sixty-four S1 elements. In the latter three cases, the results fell pointwise between the former two plotted cases. For clarity, the latter three cases were omitted from the plotted results. Our finite element results were

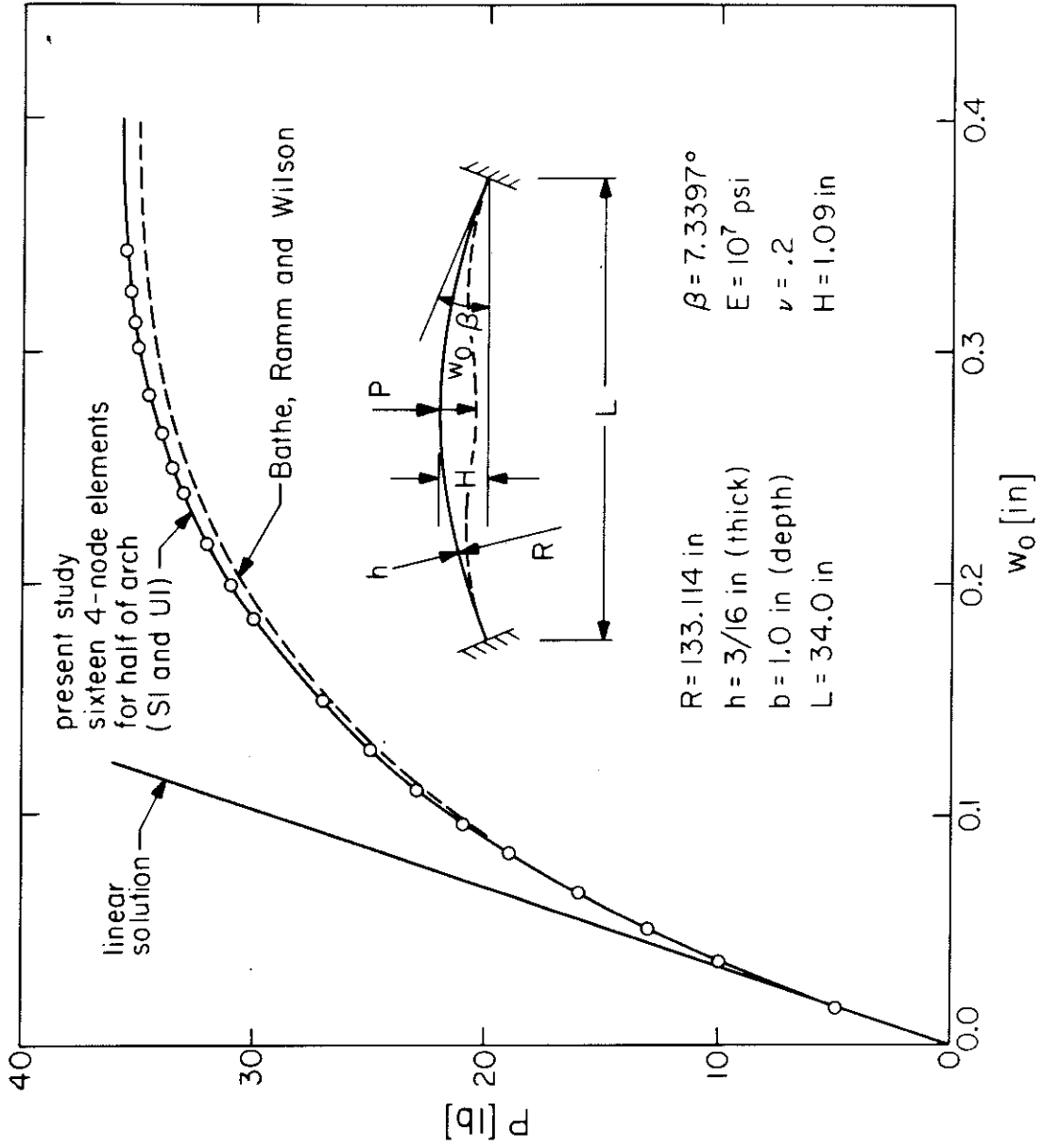


Fig. VI G Shallow circular arch under concentrated load

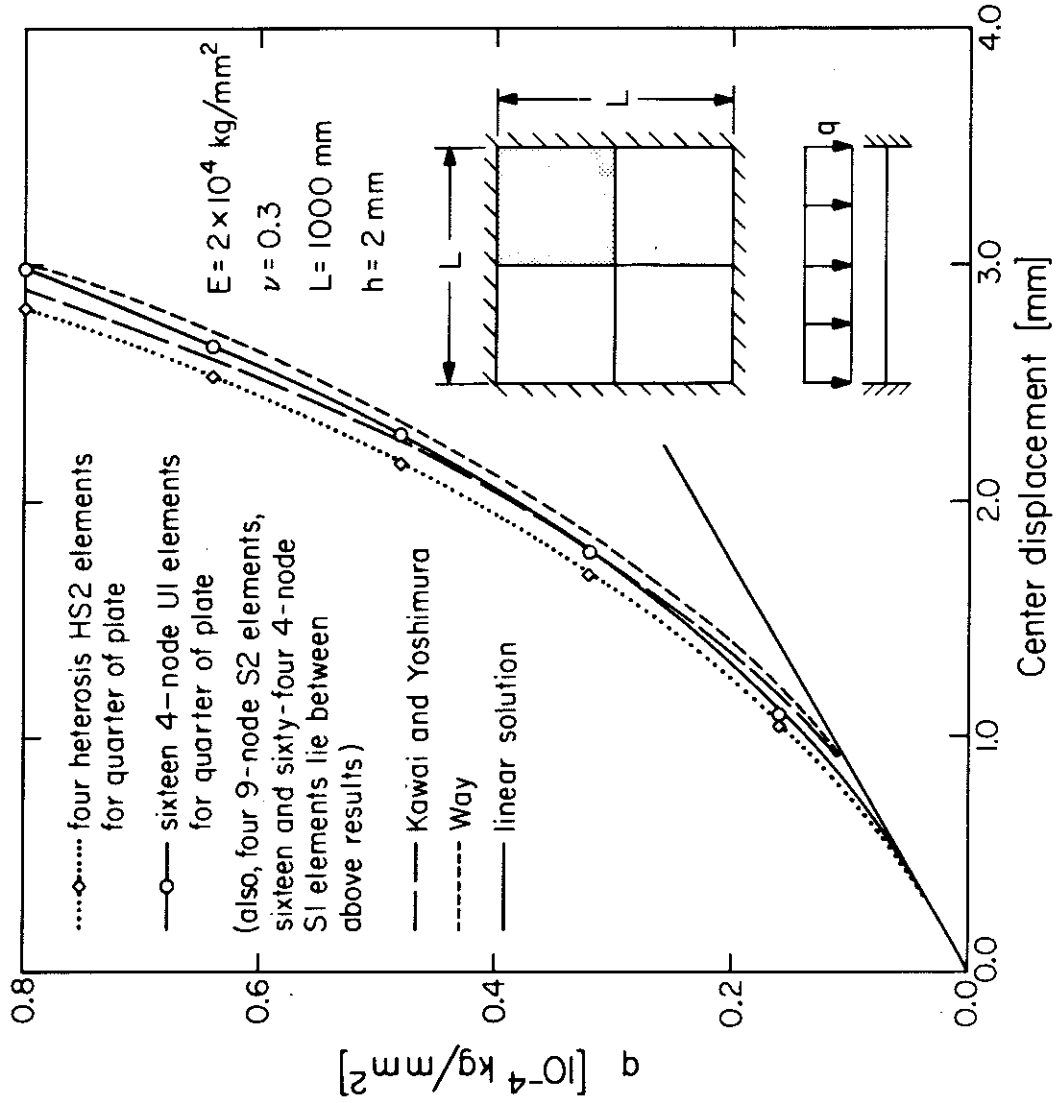


Fig. VI H Clamped square plate under uniform load

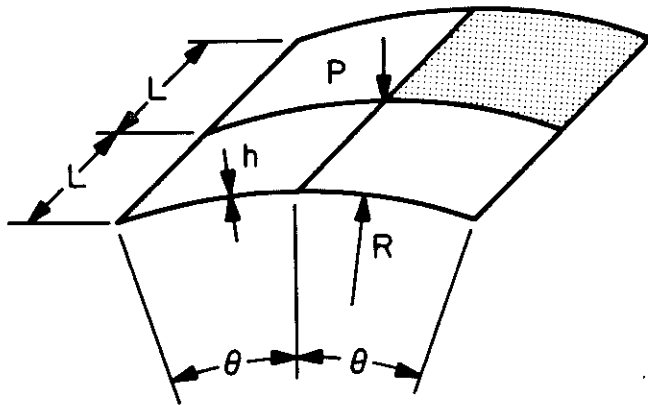
compared to the classical Rayleigh-Ritz solution obtained by Way [36] and the finite element results of Kawai and Yoshimura [37]. For this problem we experimented with treating the load as conservative and non-conservative. This produced no discernible differences. We also experimented with omitting the \underline{T} and \hat{C} matrices in the calculations. The results were almost identical, even though the number of iterations per load step was increased from an average of 3 when we included both \underline{T} and \hat{C} , to about 7 or 8.

VI-I. Hinged Cylindrical Shell under Concentrated Load

Figure VI-I shows a circular cylindrical shell with a concentrated central load applied on the convex side. The straight edges are hinged, whereas the curved edges are completely free. Due to symmetry, four-element meshes of S2 and HS2 elements and sixteen 4-node elements (both S1 and U1) are used to model one-quarter of the shell. All of our results were in close agreement and could not be distinguished on the scale of the plot. Comparison is made with the results obtained by Horrigmoe [6] and Bathe and Bolourchi [15].

VI-J. Transient Elastic-Plastic Response of a Simply-Supported Plate

This problem was solved previously by Liu and Lin [40] who used small deflection theory, ignoring membrane effects. In our calculations we assumed full geometric as well as material nonlinearity. One would anticipate some stiffening in this case due to the tensile stresses developed as the plate deforms. Since the center displacement is of the order of half the plate thickness, one would expect small, but not insignificant differences. As may be seen from the results of



$R = 2540 \text{ mm}$
 $L = 254 \text{ mm}$
 $h = 12.7 \text{ mm}$
 $\theta = 0.1 \text{ rad}$
 $E = 3102.75 \text{ N/mm}^2$
 $\nu = 0.3$

straight edges are hinged and immovable,
curved edges are free

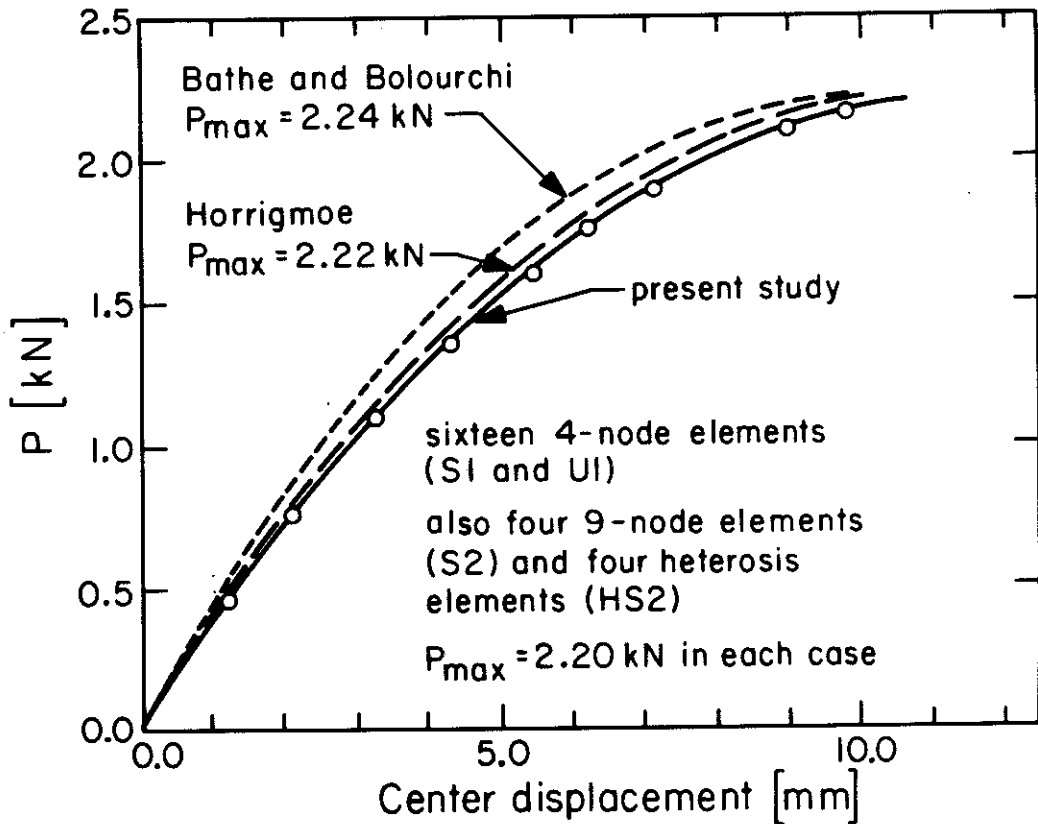


Fig. VI | Hinged cylindrical shell under concentrated load

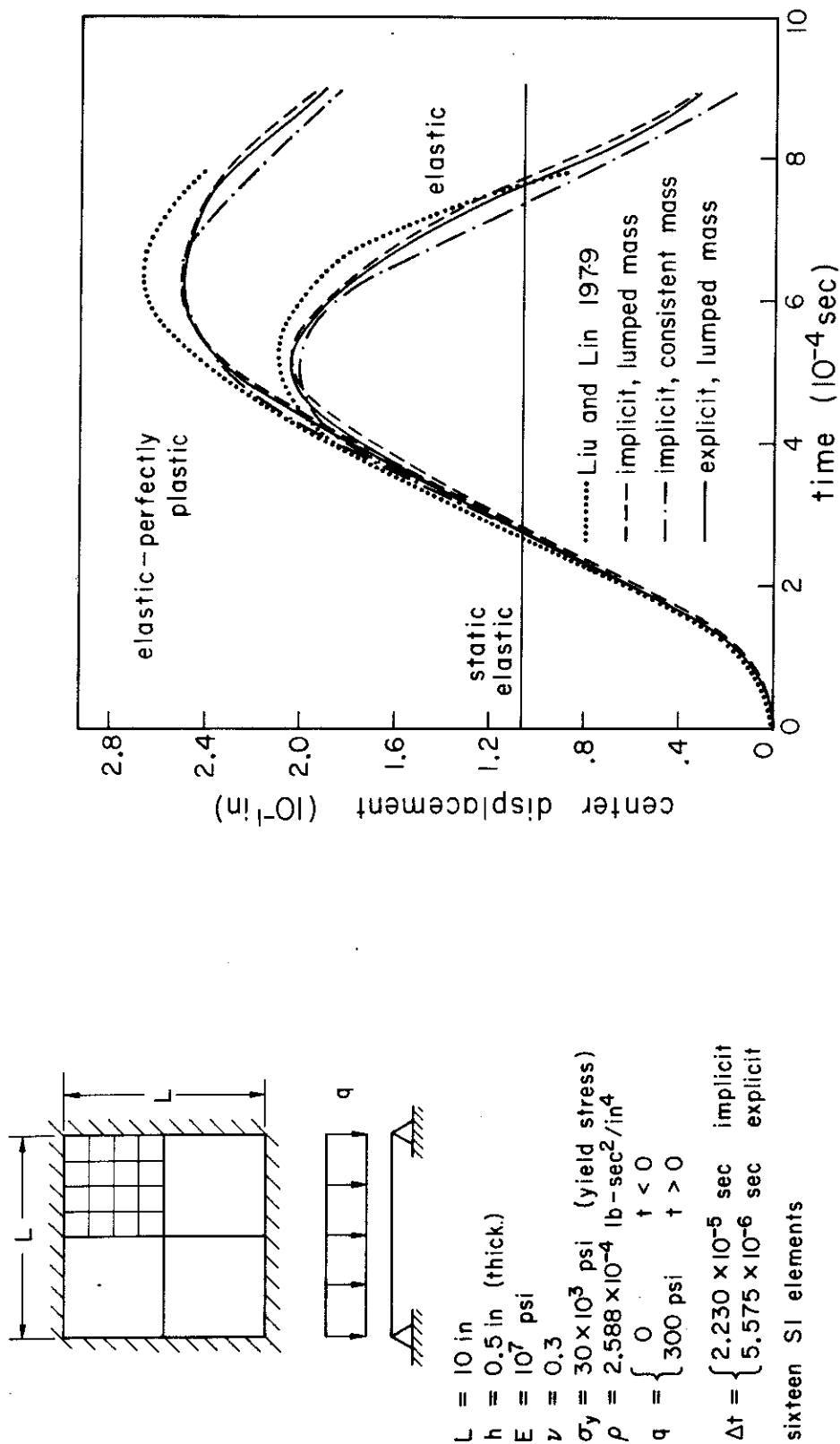


Fig.VI.J. Transient response of a simply-supported plate.

Figure VI-J, the expected behavior is produced by our calculations which tend to be slightly stiffer than Liu and Lin's with respect to peak response. This is more pronounced in the elastic perfectly plastic case than in the purely elastic case as may be seen. This is also reasonable, since larger membrane effects would tend to develop due to the smaller bending resistance in plasticity.

Comparisons between lumped and consistent mass matrices, and implicit and explicit algorithms tend to be quite good. Despite the fact that the explicit time step was taken to be one-fourth the implicit, an economy of approximately a factor of seven was noted for the explicit calculations in the elastic-plastic case. In the purely elastic case this was reduced to a factor of four favoring the explicit technique.

VI-K. Impulsively Loaded Elastic-Plastic Strip

Experimental results for this problem were given by Balmer and Witmer [41] and results of a finite element calculation were presented by Belytschko and Marchertas [42] who used an elastic, perfectly plastic model with artificial viscosity. In our calculations, we experimented with different types of hardening, but did not include any viscous effects. Another difference between the Belytschko-Marchertas calculation and ours was transverse shear effects which were not included in theirs, but were included in both the kinematics and constitution of ours. A comparison of results is presented in Figure VI-K. The displacement is quite large, being approximately six times the strip thickness. Our peak responses tend to be in good agreement with the experimental value, although they tend to occur at somewhat earlier times. The closest agreement we are able to get is attained with

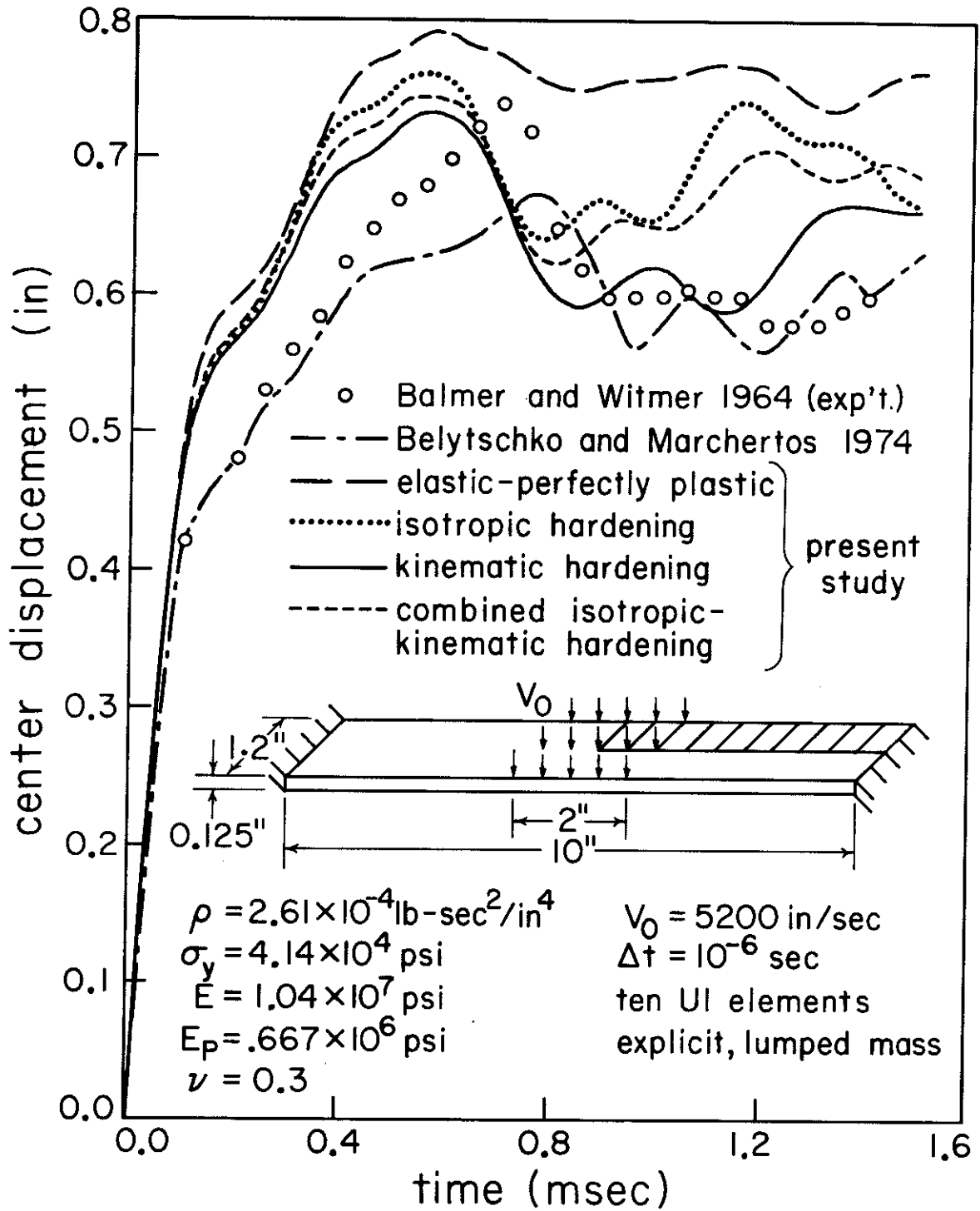


Fig. VI-K. Impulsively loaded elastic-plastic strip.

purely kinematic hardening, as may be seen. Considering the ambiguities in material modeling, the calculation is felt to be quite reasonable.

References

1. S. F. Pawsey, "The analysis of moderately thick to thin shells by the finite element method," SESM Report No. 70-12, Dept. of Civil Engineering, U.C. Berkeley, August 1970.
2. H. H. Dovey, "Extension of three-dimensional analysis to shell structures using the finite-element idealization," SESM Report No. 74-2, Dept. of Civil Engineering, U.C. Berkeley, January 1974.
3. R. H. Gallagher, Finite-Element Analysis Fundamentals (Prentice-Hall, 1975).
4. O. C. Zienkiewicz, The Finite-Element Method, Third edition (McGraw-Hill, London, 1977).
5. R. H. Gallagher, "Shell elements," Proc. First World Congress on Finite-Element Methods in Structural Mechanics, Bournemouth, England, 1975.
6. G. Horrigmoe, "Finite-element instability analysis of free-form shells," Report 77-2, Div. Structural Mechanics, Norwegian Institute of Technology, University of Trondheim, Norway, May 1977.
7. P. M. Naghdi, "The theory of shells and plates," Report AM-71-1/2 Div. Applied Mechanics, U.C. Berkeley, 1971.
8. E. Ramm, "A plate/shell element for large deflections and rotations," in Formulation and Computational Algorithms in Finite Element Analysis (K. J. Bathe, J. T. Oden, W. Wunderlich, eds.) (M.I.T. Press, 1977).
9. R. D. Mindlin, "Influences of rotatory inertia and shear on flexural motions of isotropic, elastic plates," J. Appl. Mech. 18, 31-38 (1951).
10. S. Ahmed, B. M. Irons, and O. C. Zienkiewicz, "Analysis of thick and thin shell structures by curved finite elements," Internat. J. Numerical Meth. in Eng. 2, 419-451 (1970).
11. T.J.R. Hughes and M. Cohen, "The 'heterosis' finite element for plate bending," Computers and Structures 9, 445-450 (1978).

12. T.J.R. Hughes and M. Cohen, "The 'heterosis' family of plate finite elements," Proc. ASCE Electronic Computations Conf., St. Louis, Mo., August 6-8, 1979.
13. T.J.R. Hughes, M. Cohen, and M. Haroun, "Reduced and selective integration techniques in the finite element analysis of plates," Nucl. Eng. and Design 46, 203-222 (1978).
14. T.J.R. Hughes, R. L. Taylor, and W. Kanoknukulchai, "A simple and efficient element for plate bending," Internat. J. Numerical Meth. in Eng. 11, 1529-1543 (1977).
15. K. J. Bathe and S. Bolourchi, "A geometric and material nonlinear plate and shell element," J. Computers and Structures, to appear.
16. B. Brendel and E. Ramm, "Linear and nonlinear stability analysis of cylindrical shells," Internat. Conf. on Eng. Applications of the Finite Element Method, Høvik, Norway, May 9-11, 1979.
17. W. Kanoknukulchai, "A large deformation formulation for shell analysis by the finite element method," Ph.D. Thesis, University of California, Berkeley, November 1978.
18. H. Parisch, "Geometrical nonlinear analysis of shells," Computer Meth. in Appl. Mech. and Eng. 14, 159-178 (1978).
19. H. Parisch, "A critical survey of the 9-node degenerate shell element with special emphasis on thin shell applications and reduced integration," Computer Meth. in Appl. Mech. and Eng. 20, 323-350 (1979).
20. T.J.R. Hughes and W. K. Liu, "Nonlinear finite element analysis of shells. Part I - Three-dimensional shells; Part II - Two-dimensional shells," to appear in Computer Meth. in Appl. Mech. and Eng.
21. J. H. Argyris, H. Balmer, J. St. Doltsinis, P. C. Dunne, M. Haase, M. Kleiber, G. A. Malejannakis, H-P. Mlejnek, M. Muller, and D. W. Scharpf, "Finite-element method--the natural approach," Computer Meth. in Appl. Mech. and Eng. 17/18, 1-106 (1979).
22. T. Belytschko, L. Schwer, and M. J. Klein, "Large displacement transient analysis of space frames," Internat. J. Numerical Meth.

- in Eng. 11, 64-84 (1977).
23. J. H. Argyris, P. C. Dunne, G. A. Malejannekis, and D. W. Scharpf, "On large displacement--small strain analysis of structures with rotational degrees of freedom," Computer Meth. in Appl. Mech. and Eng. 14, 401-451 (1978).
 24. T. Belytschko and L. Glaum, "Application of higher-order corotational formulation for nonlinear finite element analysis," Computers and Structures 10, 175-182 (1979).
 25. T. Belytschko and B. J. Hsieh, "Nonlinear transient finite element analysis with convected coordinates," Internat. J. Numerical Meth. in Eng. 7, 255-271 (1973).
 26. J. H. Argyris, "Recent advances in matrix methods of structural analysis," Progress in Aeronautical Sciences, Vol. 4 (Pergamon Press, Oxford, 1964).
 27. J. H. Argyris, "Continua and discontinua," Proc. Conf. on Matrix Methods in Structural Mechanics, Wright-Patterson A. F. Base, Ohio, October 1965.
 28. T.J.R. Hughes, "Generalization of selective integration procedures to anisotropic and nonlinear media," Internat. J. Numerical Meth. in Eng., to appear.
 29. S. P. Timoshenko and J. M. Gere, Theory of Elastic Stability (McGraw-Hill, New York, 1961).
 30. J. A. Jenkins, T. B. Seitz, and J. S. Przemieniecki, "Large deflections of diamond-shaped frames," Internat. J. Solids and Structures 2, 591-603 (1966).
 31. K. J. Bathe, E. L. Wilson, and R. H. Iding, NONSAP--A structural analysis program for static and dynamic response of nonlinear systems, UC SESM 74-3, Dept. of Civil Eng., University of California, Berkeley, 1974.
 32. J. F. Mescall, "Large deflection of spherical shells under concentrated loads," J. Appl. Mech. 32, 936-938 (1965).

33. J. A. Stricklin, "Geometrically nonlinear static and dynamic analysis of shells of revolution," High Speed Computing of Elastic Structures, Proc. IUTAM Symp., University of Liege, 1970.
34. S. P. Timoshenko and S. Woinowsky-Krieger, Theory of Plates and Shells, 2nd edition (McGraw-Hill, New York, 1959).
35. K. J. Bathe, E. Ramm, and E. L. Wilson, "Finite element formulations for large displacement and large strain analysis," Report UC-SESM-73-14, Dept. Civil Eng., University of California, Berkeley, Sept. 1973.
36. S. Way, "Uniformly loaded, clamped, rectangular plates with large deformation," Proc. 5th Internat. Congress Appl. Mech., Cambridge, Mass., 1938.
37. T. Kawai and N. Yoshimura, "Analysis of large deflection of plates by the finite-element method," Internat. J. Numerical Meth. in Eng. 1, 123-133 (1969).
38. R. D. Krieg and S. W. Key, "Transient shell response by numerical time integration," Internat. J. Numerical Meth. in Eng. 7, 273-286 (1973).
39. E.D.L. Pugh, E. Hinton, and O. C. Zienkiewicz, "A study of quadrilateral plate bending elements with 'reduced' integration," Internat. J. Numerical Meth. in Eng. 12, 1059-1079 (1978).
40. S. C. Liu and T. H. Lin, "Elastic-Plastic dynamic analysis of structures using known elastic solutions," Earthquake Eng. and Structural Dynamics 7, 147-159 (1979).
41. H. A. Balmer and E. A. Witmer, "Theoretical-experimental correlation of large dynamic and permanent deformations of impulsively loaded simple structures," FDL-TDR-64-108, A. F. Flight Dynamics Laboratory, Wright-Patterson A. F. Base, Ohio, July 1964.
42. T. Belytschko and A. H. Marchertas, "Nonlinear finite element method for plates and its application to dynamic response of reactor fuel subassemblies," J. Pressure Vessel Technol. 96, 251-257 (1974).

Chapter 5

NUMERICAL EXAMPLES OF FINITE ELEMENT ANALYSIS OF INCOMPRESSIBLE
VISCIOUS FLOWS BY THE PENALTY FUNCTION FORMULATION

I. Introduction

In this chapter, sample numerical examples are presented and compared with available data to illustrate the accuracy and versatility of this technique, namely, finite element analysis of incompressible viscous flows by the penalty function formulation. As has been mentioned in Chapters 2 and 3, the selection of the penalty parameter λ is not trivial. Clearly, λ must be large enough so that the compressibility and pressure errors are negligible, yet not so large that numerical ill-conditioning ensues. Dimensional analysis reveals that, for Stokes flow, λ should be picked according to the relation

$$\lambda = c\mu \quad (I.1)$$

where c is a constant which is computer word length dependent only. Numerical studies reveal that for floating-point word lengths of 60 to 64 bits an appropriate choice of c is 10^7 . However, in the presence of the convective momentum which generally dominates the viscous term, the criterion for the Navier-Stokes equation is empirically defined as:

$$\lambda = c \max\{\mu, \mu Re\} \quad (I.2)$$

where μ is the dynamic viscosity and Re is the Reynolds number as given by

$$Re = UL/\nu \quad (I.3)$$

Here U and L are "characteristic" velocity and length, respectively, $\nu = \mu/\rho$ is the "kinematic viscosity," and ρ is the density. Usually U was taken to be the maximum expected velocity and L the maximum dimension.

The solution strategy used for the steady Navier-Stokes equations is an incremental Newton-Raphson scheme in which density is used as a "load parameter," see [1-4] for details. The solution of the Stokes problem is the initial guess. Within each load level, iterations are performed until convergence is achieved, and the converged solution is used as the initial guess for the next load level. It should be noted that the matrix to be inverted [equation (IVA.12) of Chapter 3] is nonsymmetric, but possesses a symmetric band-profile structure [4]. Even though it is well known that, under appropriate hypothesis, the Newton-Raphson scheme exhibits second-order convergence of the iterates, the reforms and factorizations of the nonsymmetric stiffness are very expensive. Furthermore, the storage requirement is extremely demanding. Research in developing more effective solution algorithms has been a very active area of late (see, e.g., [5-7]).

The solution strategy we used for the transient Navier-Stokes equations in this chapter is a one-step linear implicit/nonlinear explicit operator splitting algorithm. The advantages of this linear-implicit predictor-corrector method are that the matrix is symmetric and need be formed and factorized only once; also the critical time step is independent of the Reynolds number. The computer program developed may be run at a constant (input) time step, or at a step redefined adaptively, for each t_n , according to the formula below:

$$\Delta t \leq 1 / \left(\sum_{i=1}^{N_{sd}} \frac{|u_{\xi_i}|}{h_{\xi_i}} \right) \quad (I.4)$$

where u_{ξ_i} is the velocity component in the ξ_i direction and h_{ξ_i} is the element length in the ξ_i direction.

It is important to cut down on reform and factorization costs when Δt is being selected adaptively. We have employed a scheme such that, instead of refactorization, γ is redefined to compensate for the step-size change. Specifically, we proceed as follows. Let Δt_{fact} and γ_{fact} denote the values of Δt and γ respectively, used during the last factorization, and let

$$c = \gamma_{\text{fact}} \Delta t_{\text{fact}} \quad (I.5)$$

Based on the velocity field at step n , Δt_{crit} is calculated according to (I.4). Define

$$\gamma_{n+1} = c / \Delta t_{\text{crit}} \quad (I.6)$$

For stability, γ_{n+1} must be between 1/2 and 1. If $\gamma_{n+1} \in [\frac{1}{2}, 1]$, do not refactorize, but set $\gamma = \gamma_{n+1}$ and $\Delta t = \Delta t_{\text{crit}}$ in ΔF^* . If, on the other hand, $\gamma_{n+1} \notin [\frac{1}{2}, 1]$, set $\Delta t = \Delta t_{\text{crit}}$, $\gamma = 3/4$ and refactorize. This value of γ is picked to reduce the likelihood of refactorization in subsequent steps. There are other procedures along these lines under investigation [8-10].

There is a drawback to the present schemes due to the convection stability condition (I.4). For example, if we are interested in an essentially steady flow, and the length of time interval, T , required

to attain steady conditions engenders many steps (e.g., see cavity flows in the next section), a "fully implicit," unconditionally stable scheme is no doubt superior. Gresho et al. [11] and Smith and Brebbia [12] have described such fully implicit schemes. However, we believe that the storage (due to nonsymmetric matrix) and computational effort engendered by fully implicit algorithms are prohibitive in most cases, as often accuracy dictates taking as small a time step as the convective stability condition.

To solve large, implicit, three-dimensional problems, iterative or at least partially iterative methods seem to be a necessity. Although there is much interest in this topic, a generally reliable iterative scheme, competitive with direct schemes, does not yet seem to be available. Attempts have been made to overcome the mentioned difficulties; see [5-7,13-18] and references therein for details.

A least-squares type smoothing procedure [19] is used to perform the necessary filtering of the "checkerboard mode" [4] of the pressure field. A comprehensive study of such techniques has been performed by Lee et al. [20]. We employed the same ideas in [20] with slight modification for our purposes. As these have been documented in [4], the smoothing procedures are omitted here.

II. Sample Problems

All computations were performed on an IBM 3032 computer at the California Institute of Technology Computing Center in double precision (64 bits per floating-point word). The penalty parameter is picked according to (I.1) or (I.2). Variable time stepping and "upwinding" are employed throughout the transient analysis problems, according to

equations (I.4) to (I.6), unless otherwise specified. Lumped mass matrices are used for two-dimensional problems, and row sum mass matrices are used for axisymmetric problems.

II-A. Driven Cavity Flow

Several investigators have studied the problem (see [3,4,20-23]). A problem description is shown in Figure IIA-1. We observe that the boundary conditions are discontinuous at the upper corners. Two meshes of 4-node elements, employing different approximations of the boundary conditions, are shown in Figure IIA-2. The midplane velocity profiles employing the 20 x 20 and 20 x 21 meshes for $Re = 100$ and 400 are presented in Figure IIA-3. As can be clearly seen from Figure IIA-3, different treatments of the boundary conditions can result in significant quantitative differences, especially as the Reynolds number is increased. By virtue of the sensitivity of the result to the treatment of the boundary conditions, care must be taken in interpretation. For this problem, the fully implicit Newton-Raphson method without "upwind" technique is employed.

The boundary condition problem may also create discrepancies when different elements are compared. Consider a 10 x 10 mesh of square, 9-node elements. This mesh would have the same number of degrees-of-freedom as the 20 x 20 mesh of 4-node elements, and it may seem appropriate to compare results. However, one should keep in mind that the setting of the nodal boundary conditions in identical fashion actually implies different representations along the vertical edges of the corner elements (c.f., Figures IIA-2 and IIA-4) since a linear variation in velocity is employed for the 4-node element, whereas a quadratic

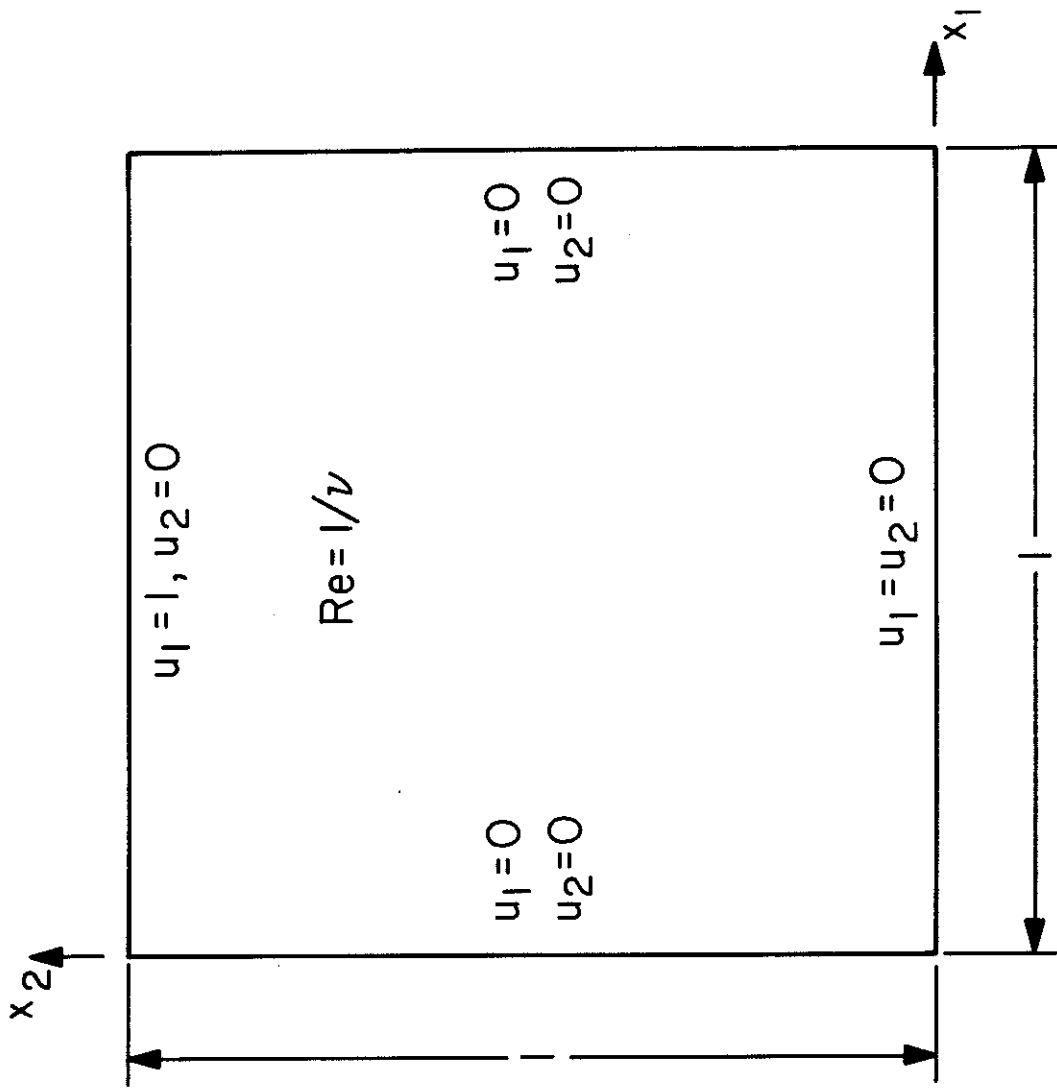


Fig. II A-1. Driven cavity flow: Problem description.

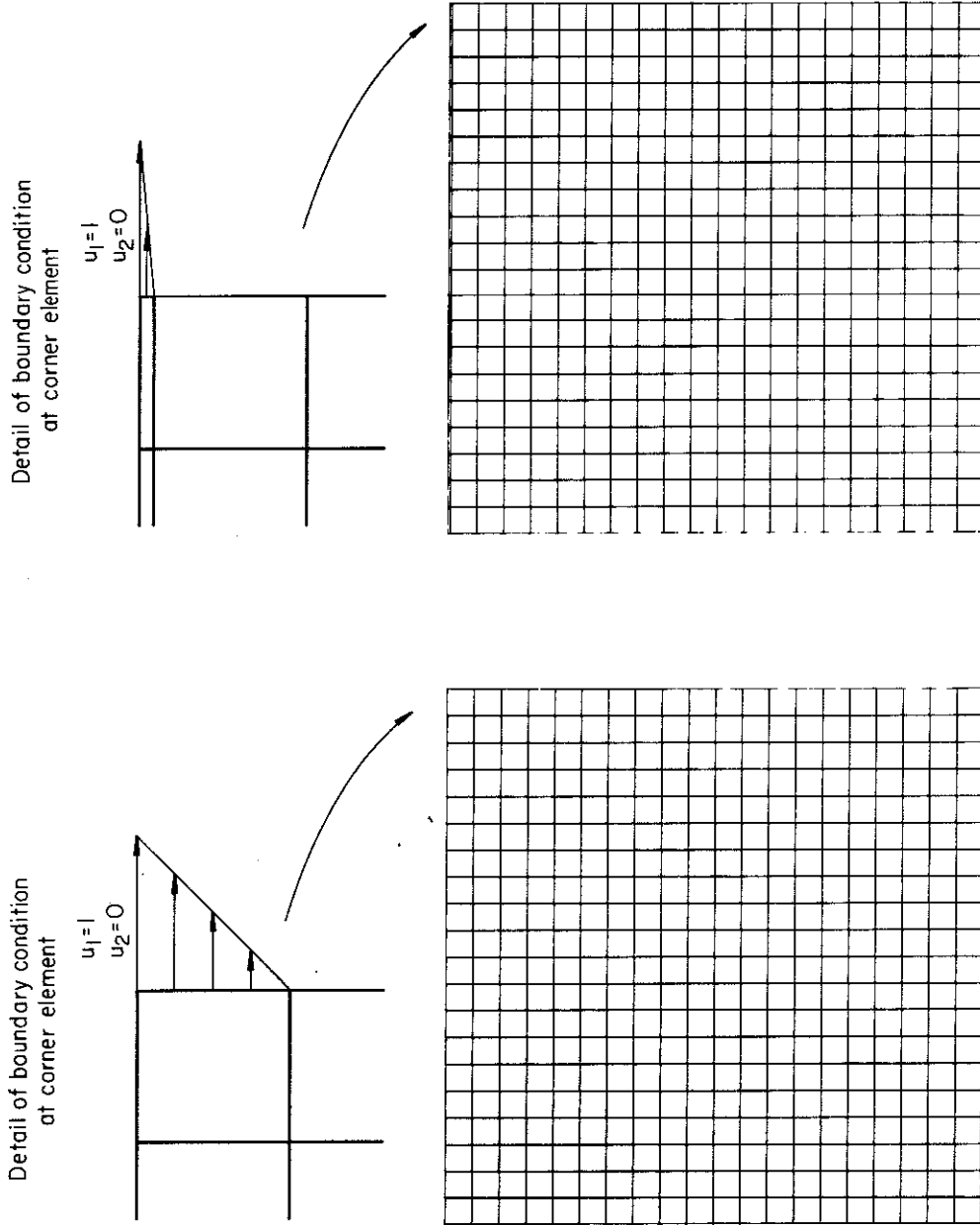


Fig. II A-2. Driven cavity flow: Finite element meshes employing different approximations of discontinuous corner boundary conditions.

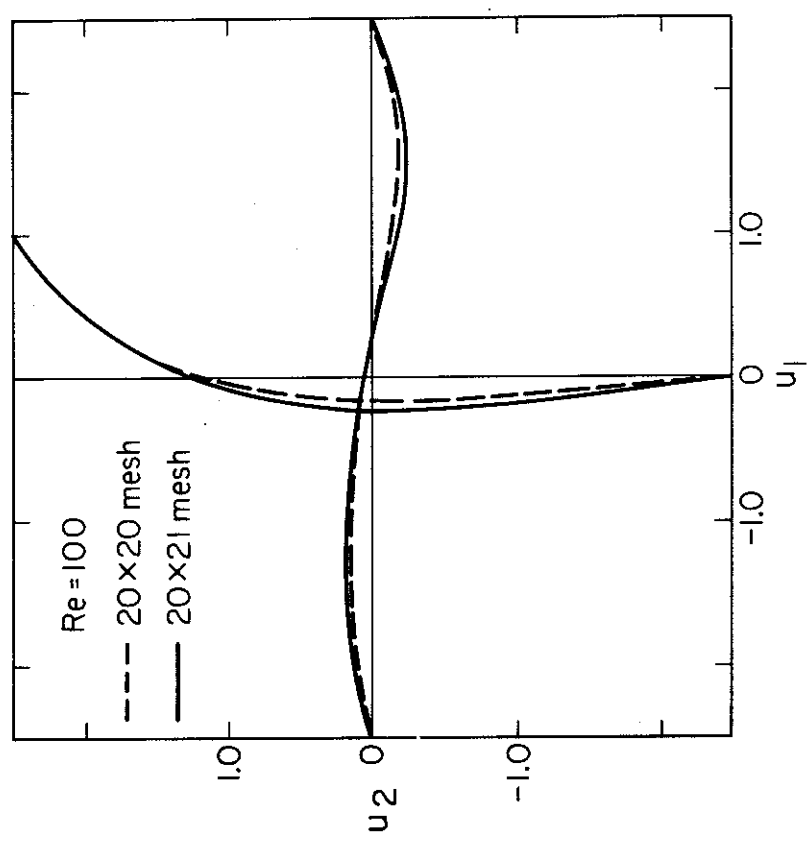
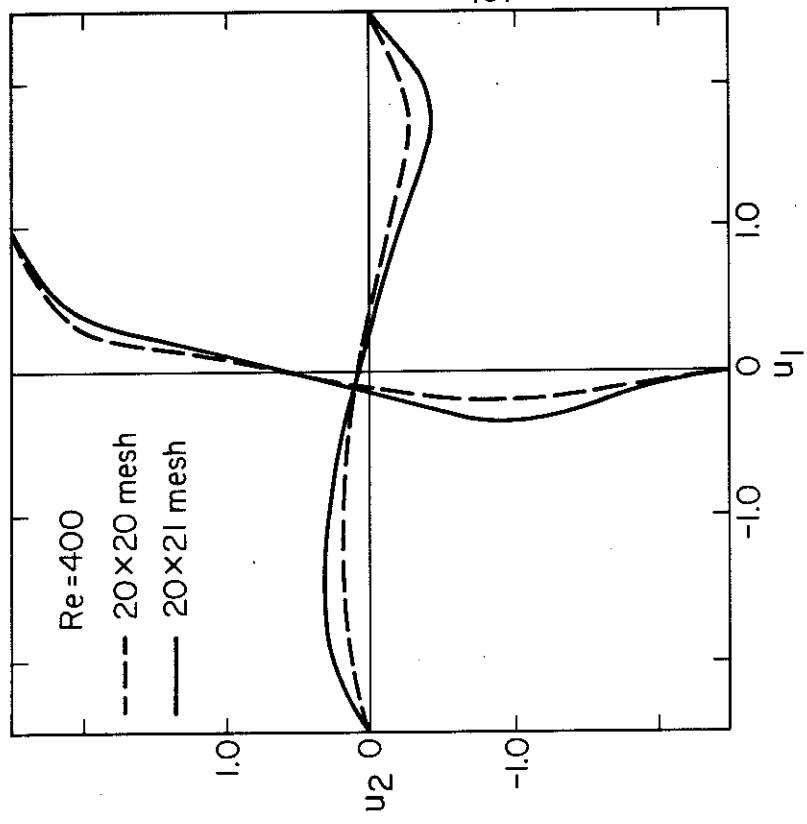


Fig. II A-3. Driven cavity flow: Midplane velocity profiles.

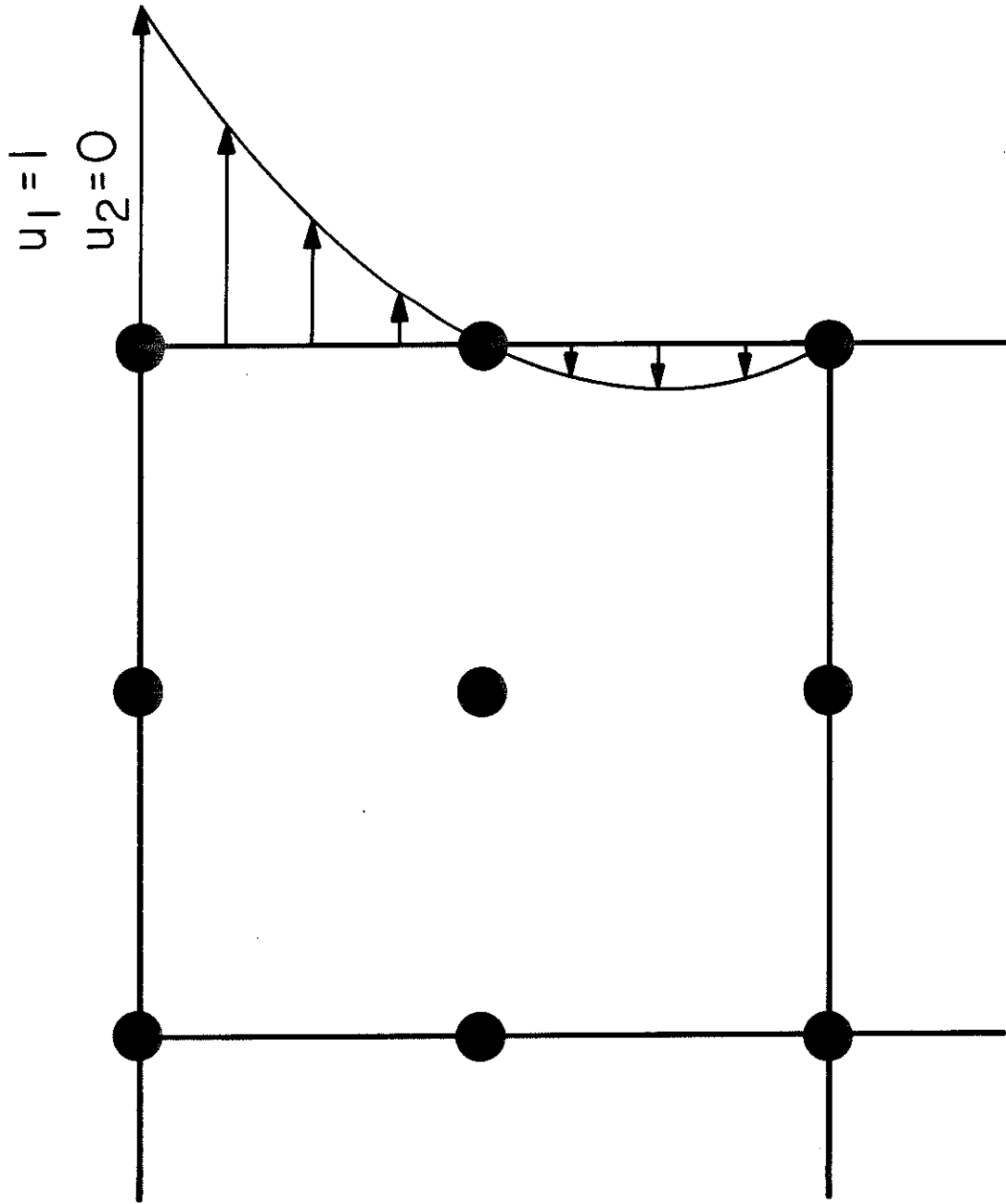
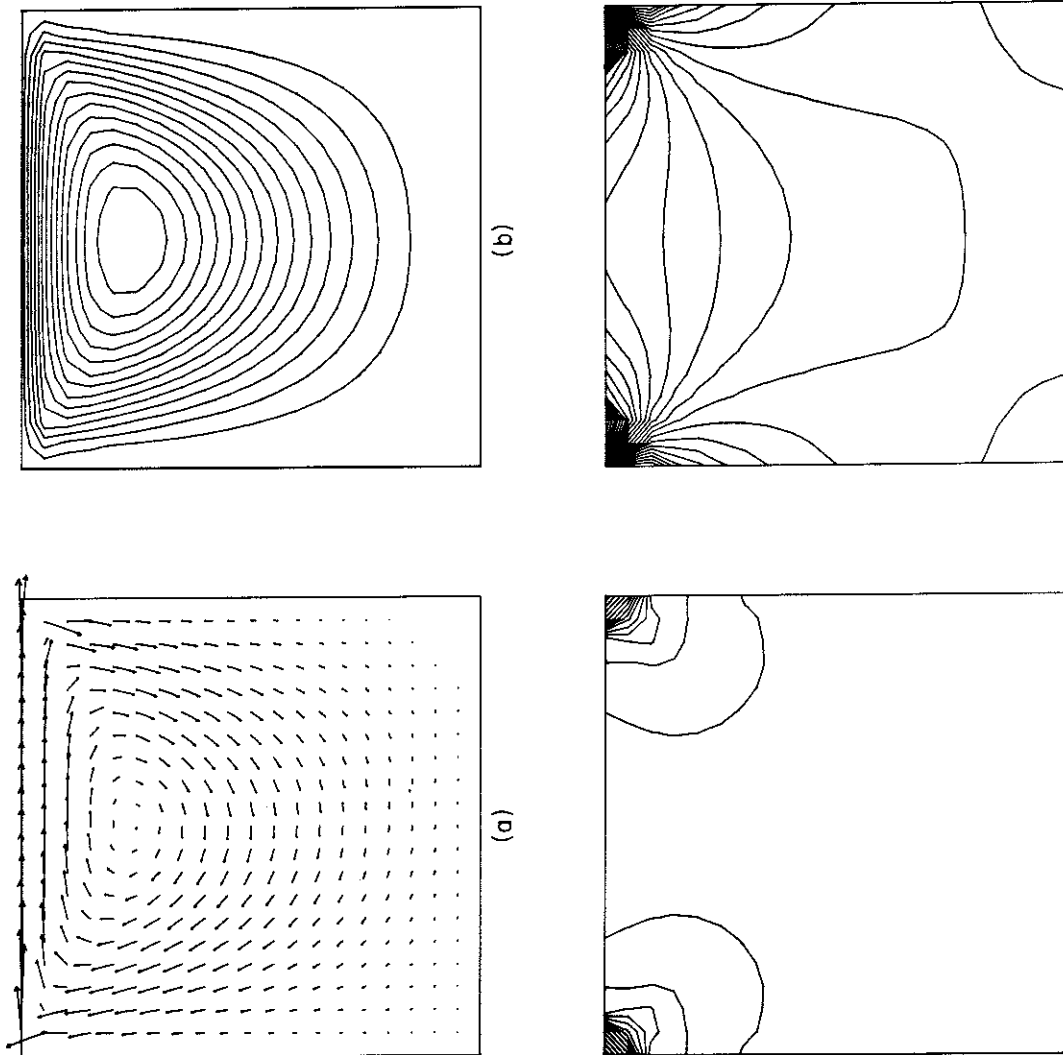
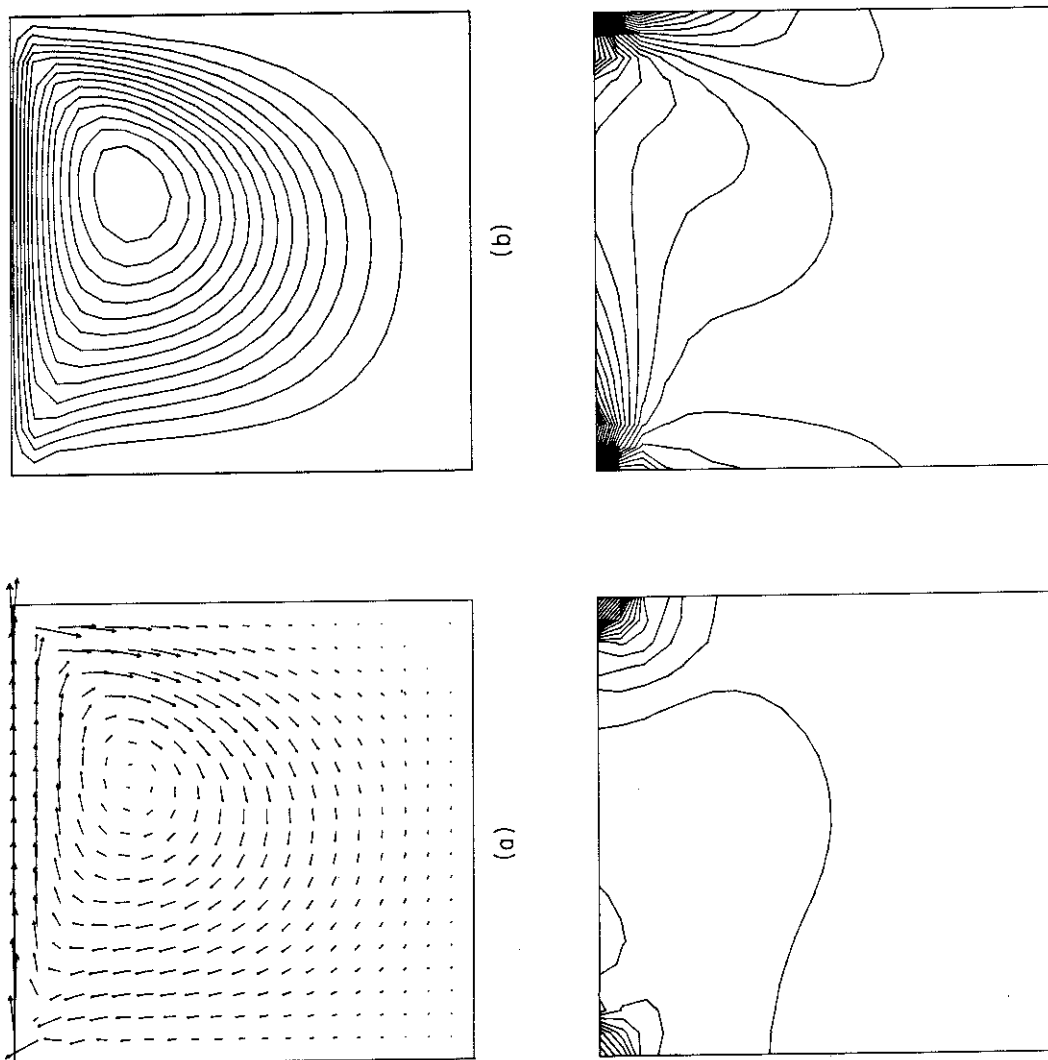


Fig. II A-4. Driven cavity flow: Approximation of discontinuous corner boundary condition for a 9-node element.



(a) (b) (c) (d)
Fig. IIA-5. Driven cavity flow ($Re = 0$, 20×21 mesh);
(a) velocity vectors; (b) streamlines; (c) pressure contours; and (d) vorticity contours.



(a) Velocity vectors; (b) streamlines; (c) pressure contours; and (d) vorticity contours.

(c)
Fig. IIA-6. Driven cavity flow ($Re = 100$; 20×21 mesh);
(d)

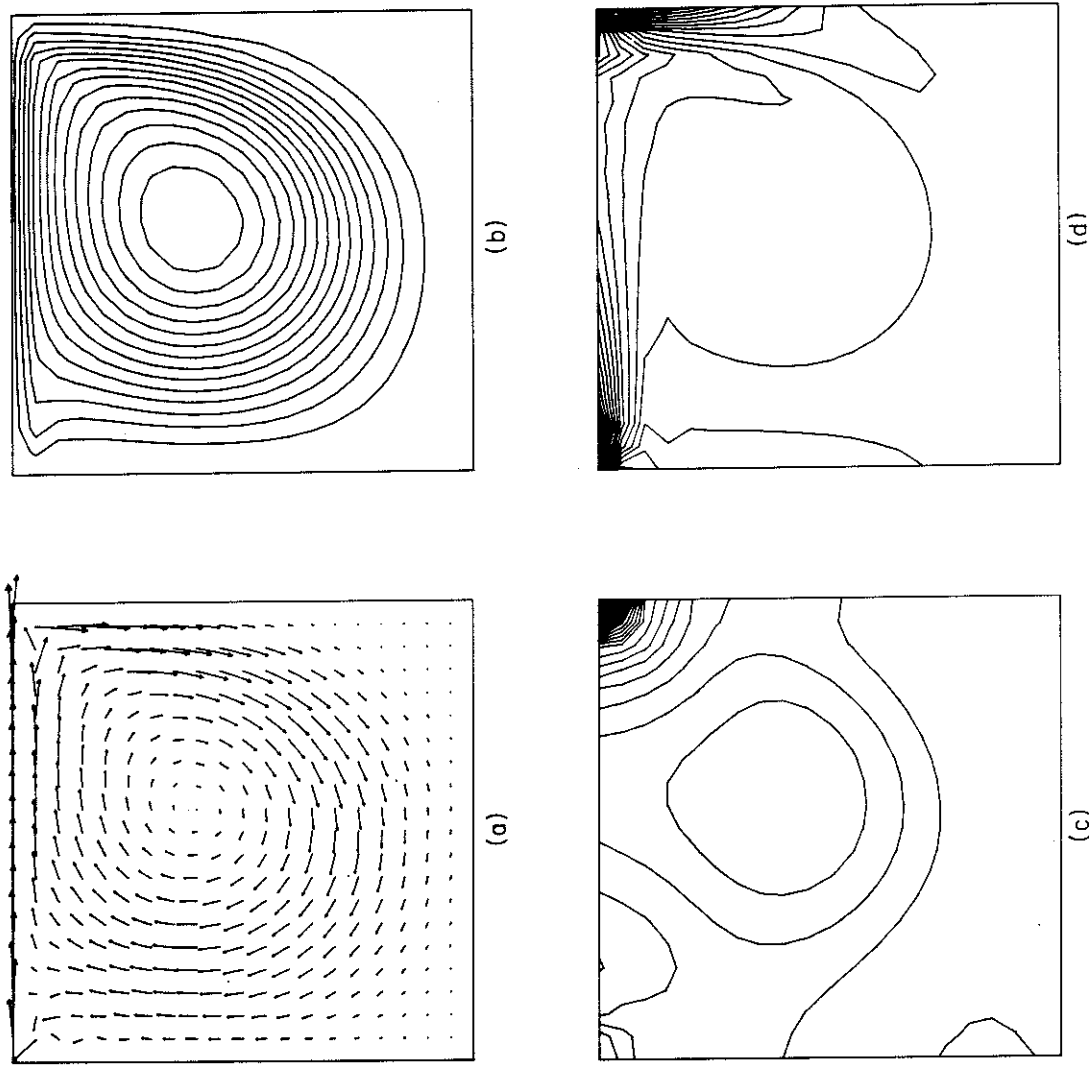


Fig. IIA-7. Driven cavity flow ($Re = 400$; 20×21 mesh):
(a) Velocity vectors; (b) vorticity contours; (c) streamlines; and (d) pressure contours.

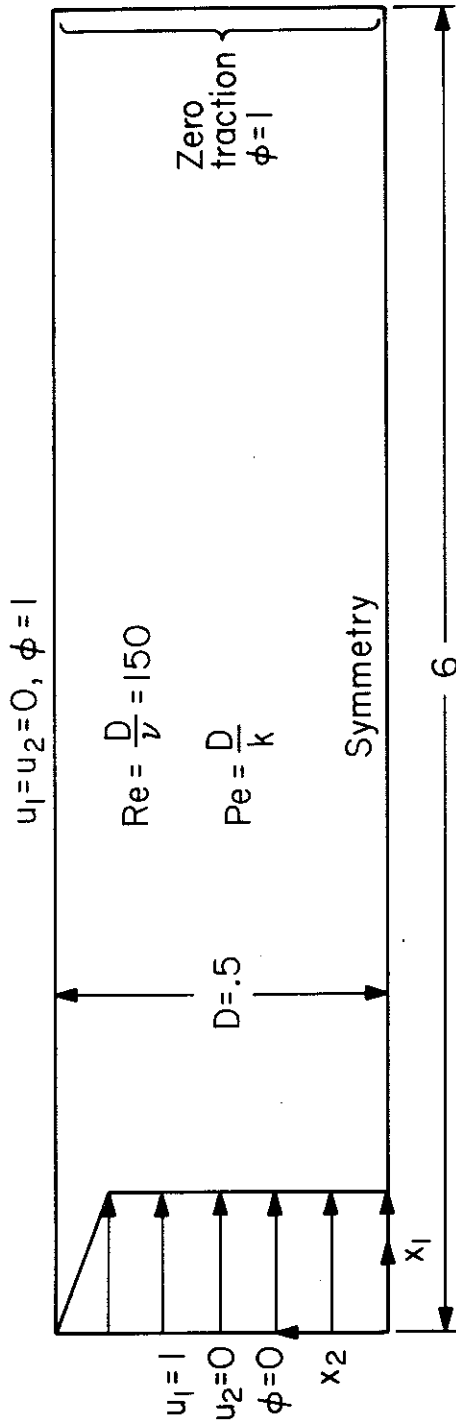
variation in velocity is employed for the 9-node element, and thus the amount of fluid "injected" into the cavity is different. Discrepancies noted between midplane velocity profiles (see [24]) may be attributed to the different boundary conditions, and are not indicative of the respective merits of the elements.

The velocity field, streamlines, pressure contours, and velocity contours for $Re = 0$ employing the 20×21 mesh are presented in Figure IIA-5. The corresponding plots for $Re = 100$ and $Re = 400$ using the same mesh are presented in Figure IIA-6 and Figure IIA-7, respectively.

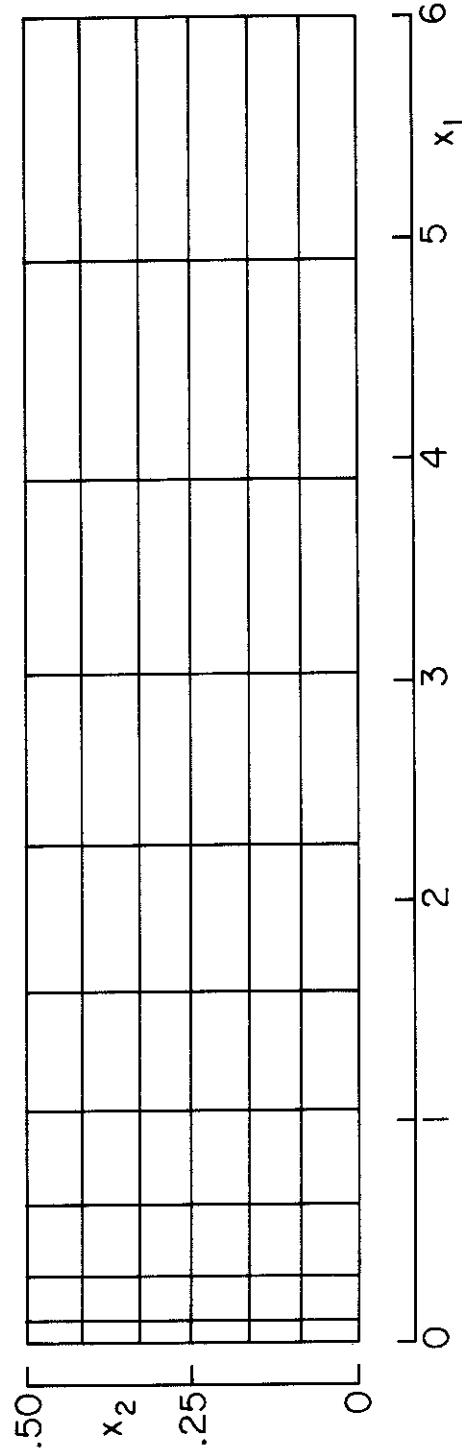
II-B. Entry Flow in a Channel

In order to demonstrate the necessity of the "upwind" scheme, entry flow in a channel is studied. The problem statement and the corresponding finite element mesh are shown in Figure IIB-1. We obtained the velocity field by employing the steady Navier-Stokes algorithm described above. Four different integration treatments of the advection terms are used and comparisons are presented in Figure IIB-2 for a Peclet number of 150. For details of the upwind scheme, consult Chapter 3 and Ref. [4]. As can be seen, the upwind schemes are superior to the Gauss schemes. For this high a Peclet number, there is little difference between the optimal and fully upwind schemes.

A much higher Peclet number (1.5×10^7) was studied. The optimal and full upwind schemes give identical results, whereas the Gauss schemes plot off scale (see Figure IIB-3).



(a) Problem statement



(b) Mesh

Fig. II B-1. Entry flow in a channel: Problem description and finite element mesh.

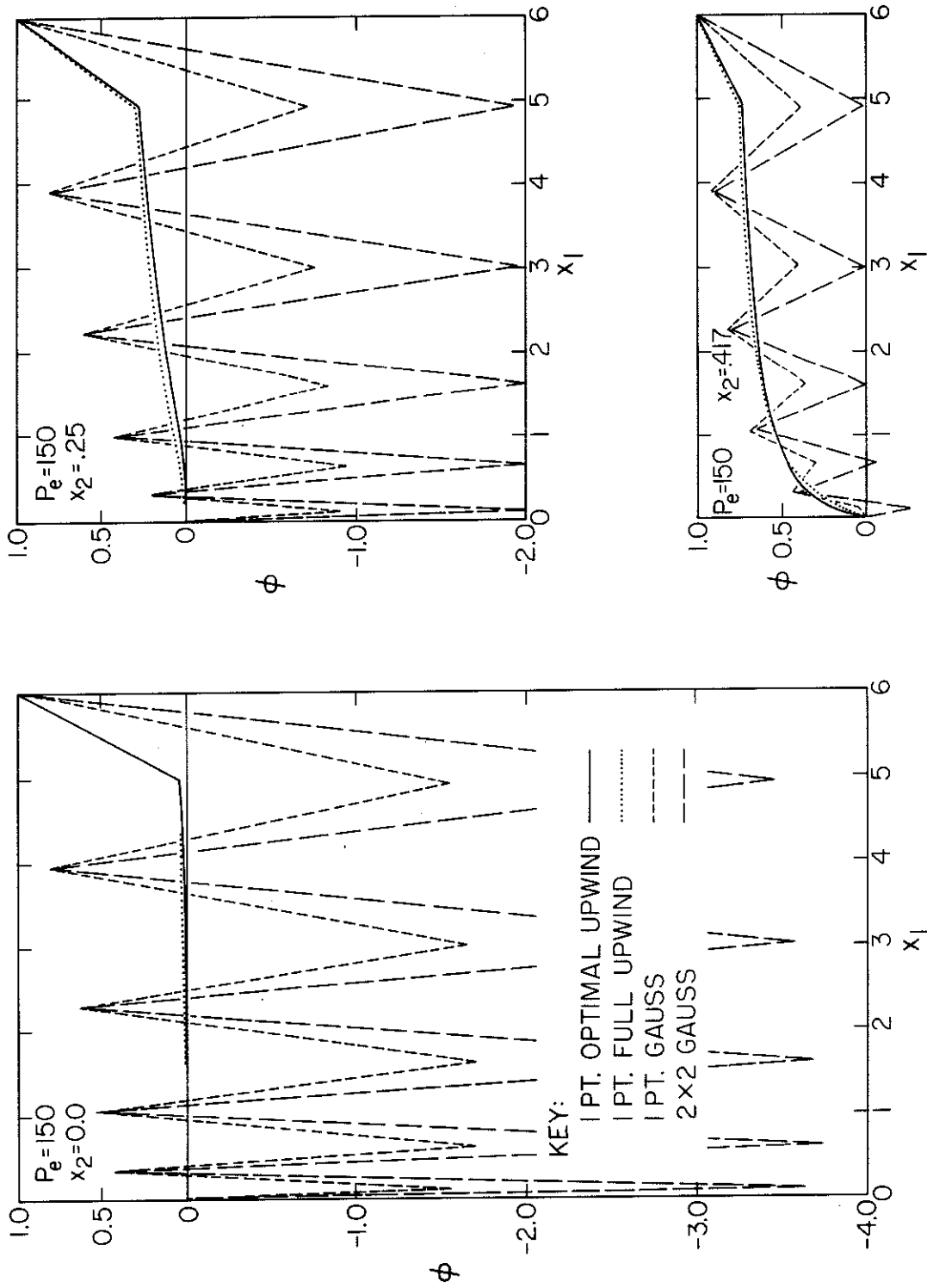


Fig.IIB-2. Entry flow in a channel: Comparison of results for four different integration treatments of the advection term.

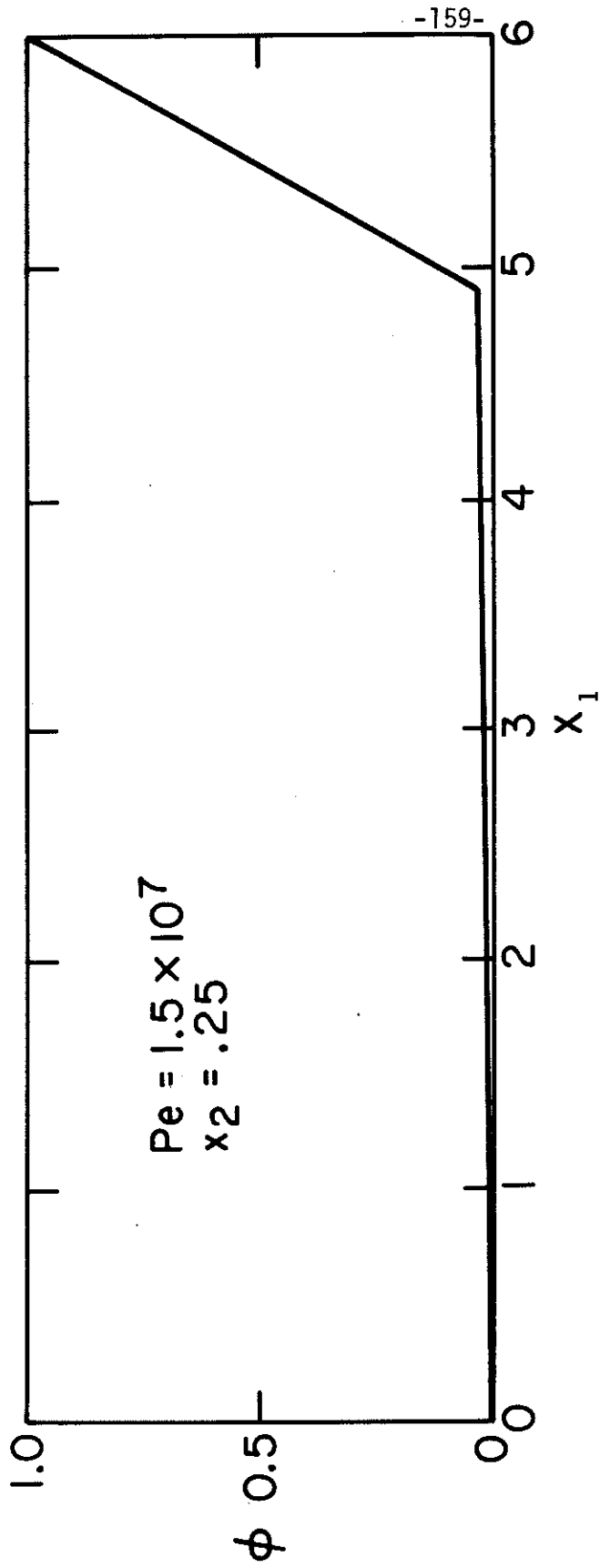


Fig. II B-3. Entry flow in a channel: Results for optimal and full upwind schemes at high Peclet number.

II-C. Couette Flow

This problem actually is one-dimensional. The exact solution can be found in standard texts [25,26]. The problem description and mesh are shown in Figure IIC-1 and results are shown in Figure IIC-2. This is a simple problem in which the convection term is identically zero. A boundary layer develops along the lower edge and diffuses upward, forming a steady, linear velocity profile as t increases.

II-D. Dam-Reservoir Problem

It is very important for engineers to know the hydrodynamic pressure along the inclined upstream face of a dam, due to earthquake motions. Explicit analytic formulas for calculating total horizontal, vertical, and normal loads are due to Chwang and Housner [27,28]. Approximate solutions and numerical solutions of the same problems have been given in [29,30]. The problem statement is shown in Figure IID-1. The dam is assumed rigid. The fluid is assumed to be incompressible and inviscid. The initial conditions are quiescent and at $t = 0^+$ the dam face is set in constantly accelerating motion toward the reservoir. Data for the problems are given as follows: $\mu = 0$; $\rho = 1$; $L = 2$; $H = 1$; $\lambda = 10^7$; $\gamma = 1$; $\Delta t = 0.025$; and $T = 0.1$ (4 time steps). Meshes and results for the 60° dam and 90° dam are shown in Figure IID-2. Pressures are compared in Figure IID-3 with the exact, potential flow solution due to Chwang [27]. As can be seen, the results are in good agreement. Also from Figure IID-2, the pressure contours are orthogonal to the streamline contours. It is expected from potential theory even though the full Navier-Stokes equation is

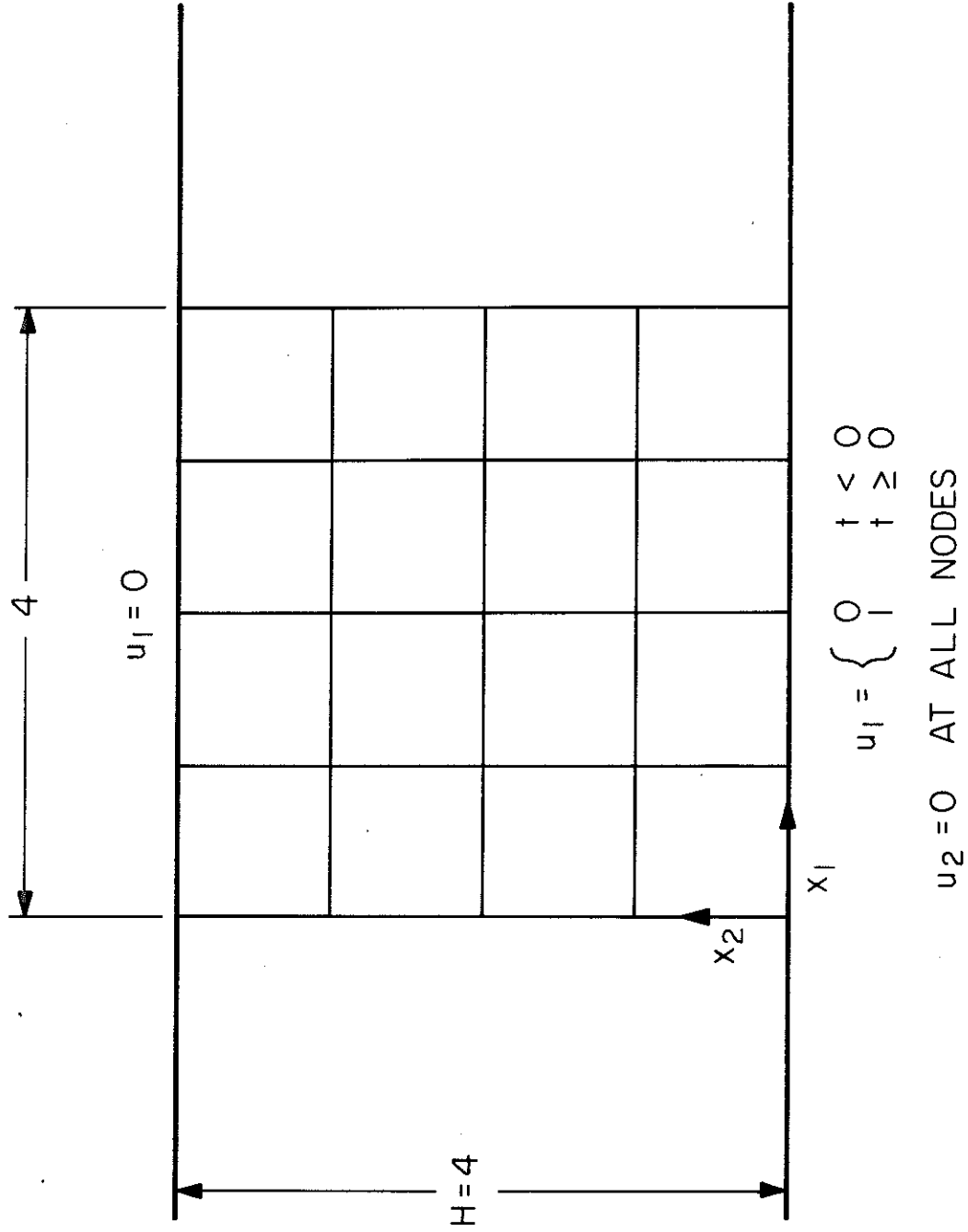


Fig. IIC-1. Couette flow: Finite element mesh and problem description.

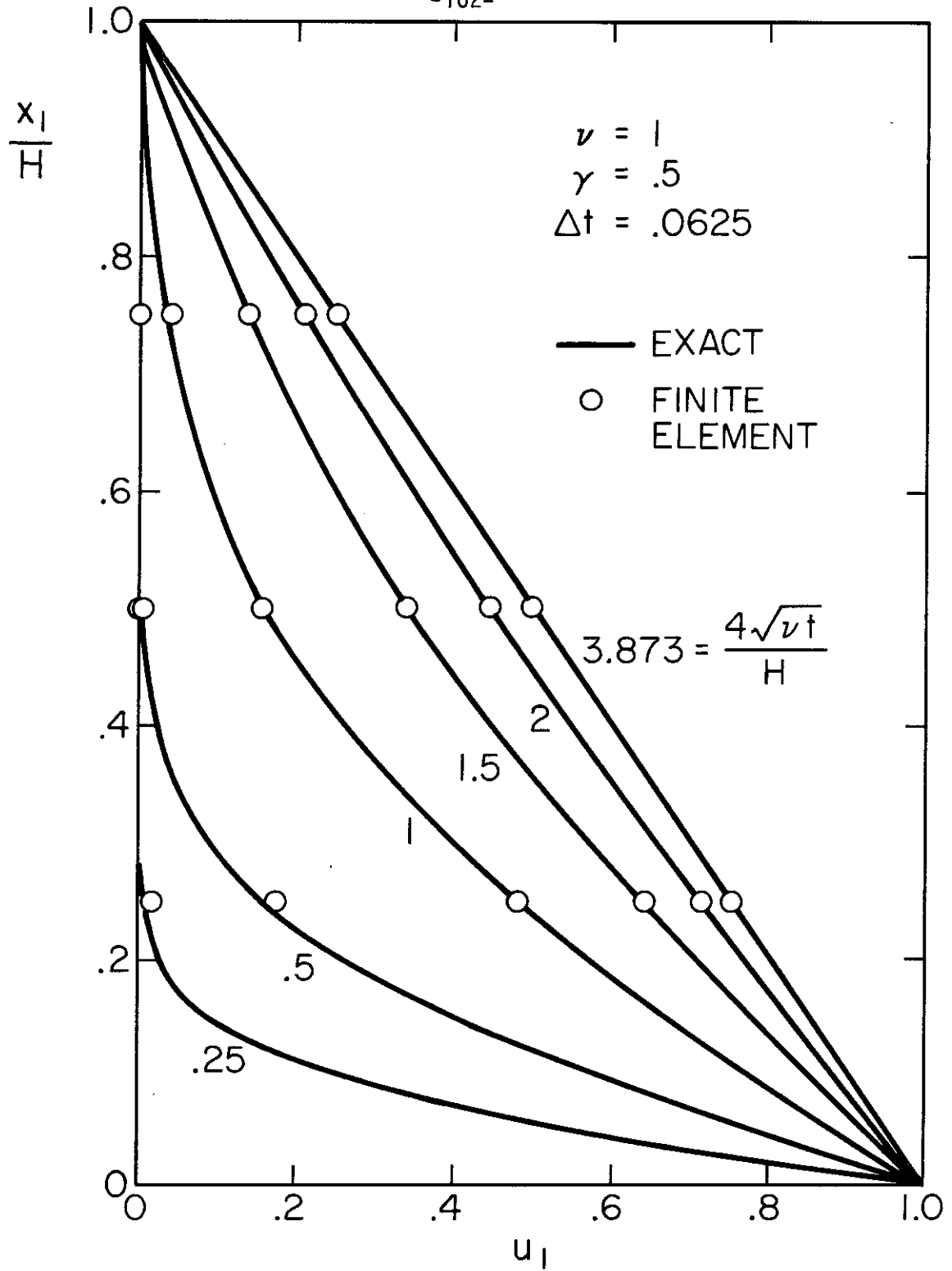


Fig.IIC-2. Couette flow: Comparison of finite element results with exact solution.

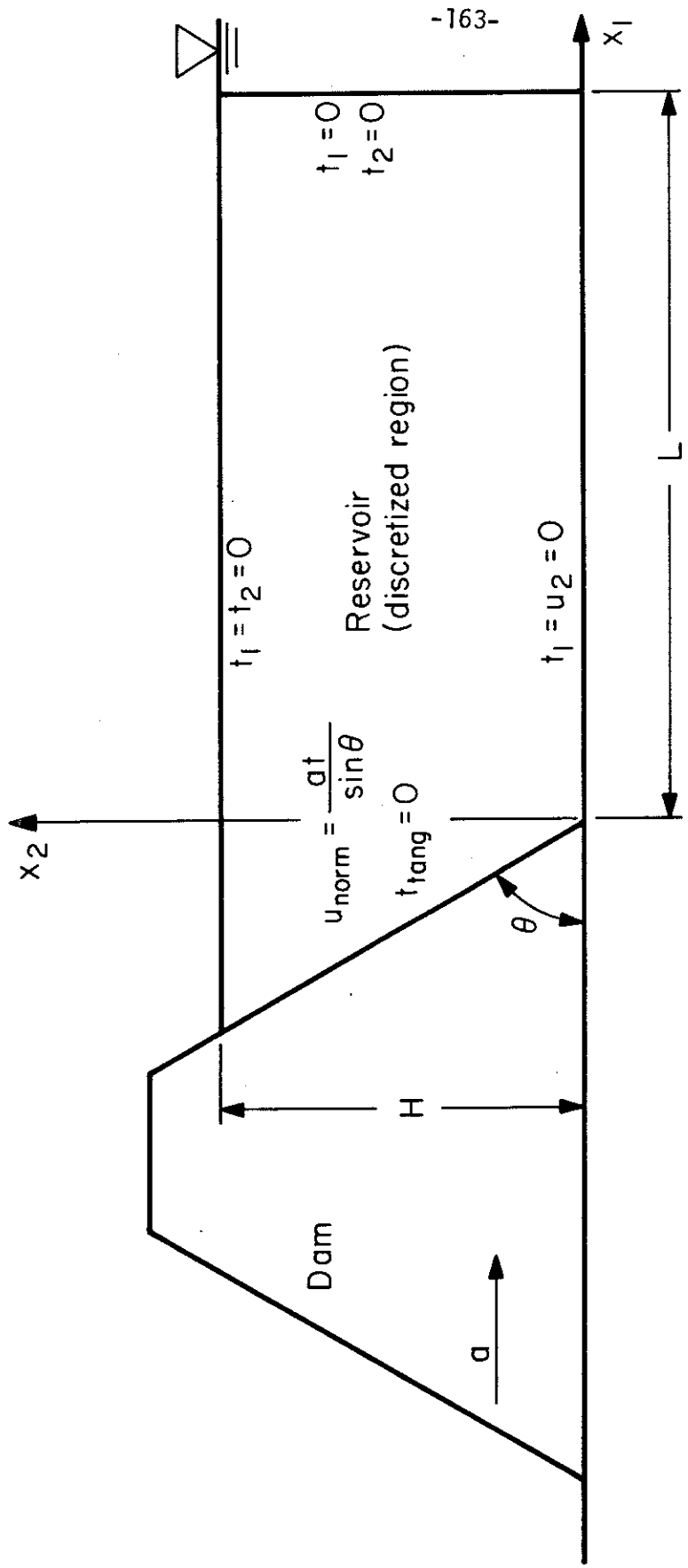


Fig.IID-1. Dam-reservoir problem: Description.

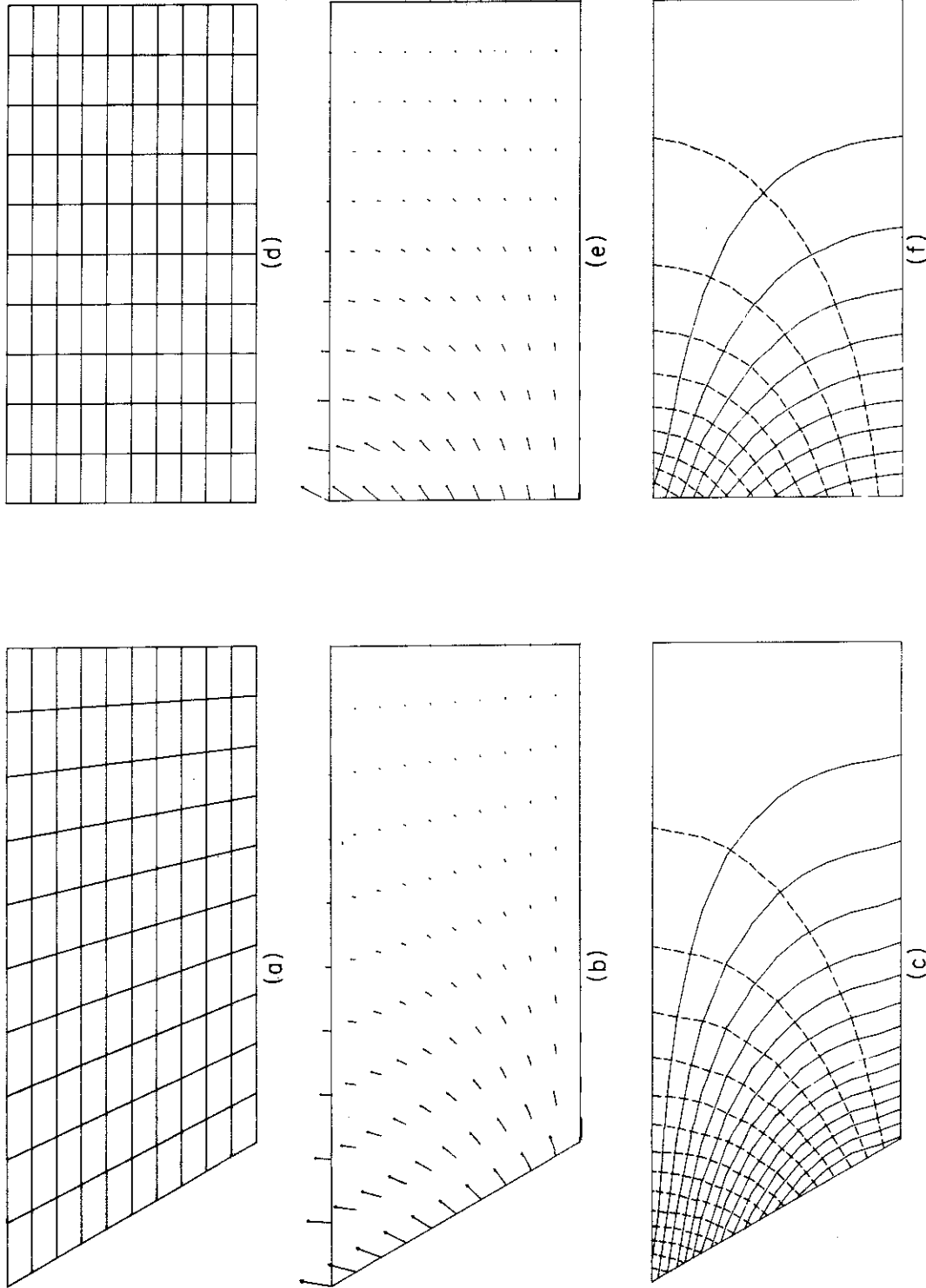


Fig.IID-2. Dam-reservoir problem. ($\theta = 60^\circ$): (a) Finite element mesh; (b) velocity vectors; and (c) pressure contours (—) and streamlines (- - -). ($\theta = 90^\circ$): (d) Finite element mesh; (e) velocity vectors; and (f) pressure contours (—) and streamlines (- - -).

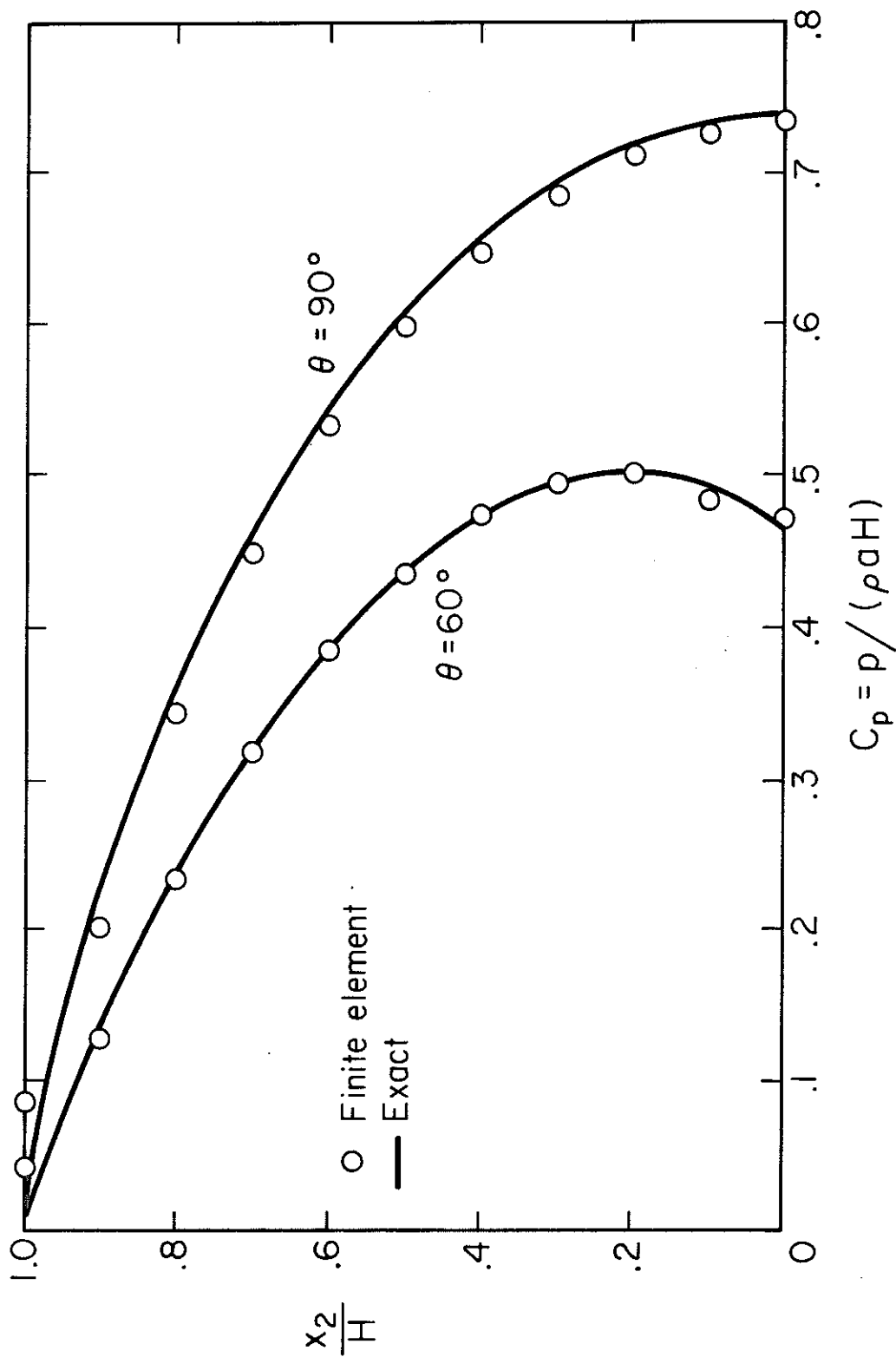


Fig. ID-3. Dam-reservoir problem: Comparison of finite element and exact results.

employed here.

II-E. Hamel Problem

A problem statement is depicted in Figure IIE-1. The Hamel problem of convergent flow in a channel ("inflow problem") has been considered recently by several investigators (see [3,4,24,31]). The exact solution can be found in [25]. For the particular mesh employed, a radial velocity profile, in accord with the high Reynolds number approximation to the exact solution, is set at the outer radius ($r=4$) having constant value of $1/4$. The Reynolds number thus may be taken as $Re = \pi/(6\nu)$. The circumferential velocity at $r=4$ is set to zero. The outflow boundary condition at $r=1/4$ is assumed traction free. At high Reynolds number this approximates the situation adequately. Results for $Re = 500$ and 5×10^7 are presented in Figures IIE-2 and IIE-3. As can be seen, the correlation with the exact solution is very good. (Pressures in Figure IIE-2 and IIE-3 are reported at the element centers and are "unsmoothed.")

II-F. Flow over a Step

A problem statement is depicted in Figure IIF-1. We used this problem to demonstrate the necessity of "upwinding" when there is a "hard" upwind-facing boundary condition (see upwind section of Chapter 3) and too coarse a mesh is used. In Figure IIF-1 we present results of a calculation performed with 9-node Lagrange elements. A (product) Simpson's rule was used to construct the mass matrix, whereas Gauss-Legendre rules of order 3×3 , 3×3 , and 2×2 were used on the convection, μ and λ terms, respectively. Data employed were: $\mu = 1$, $\rho = 200$;

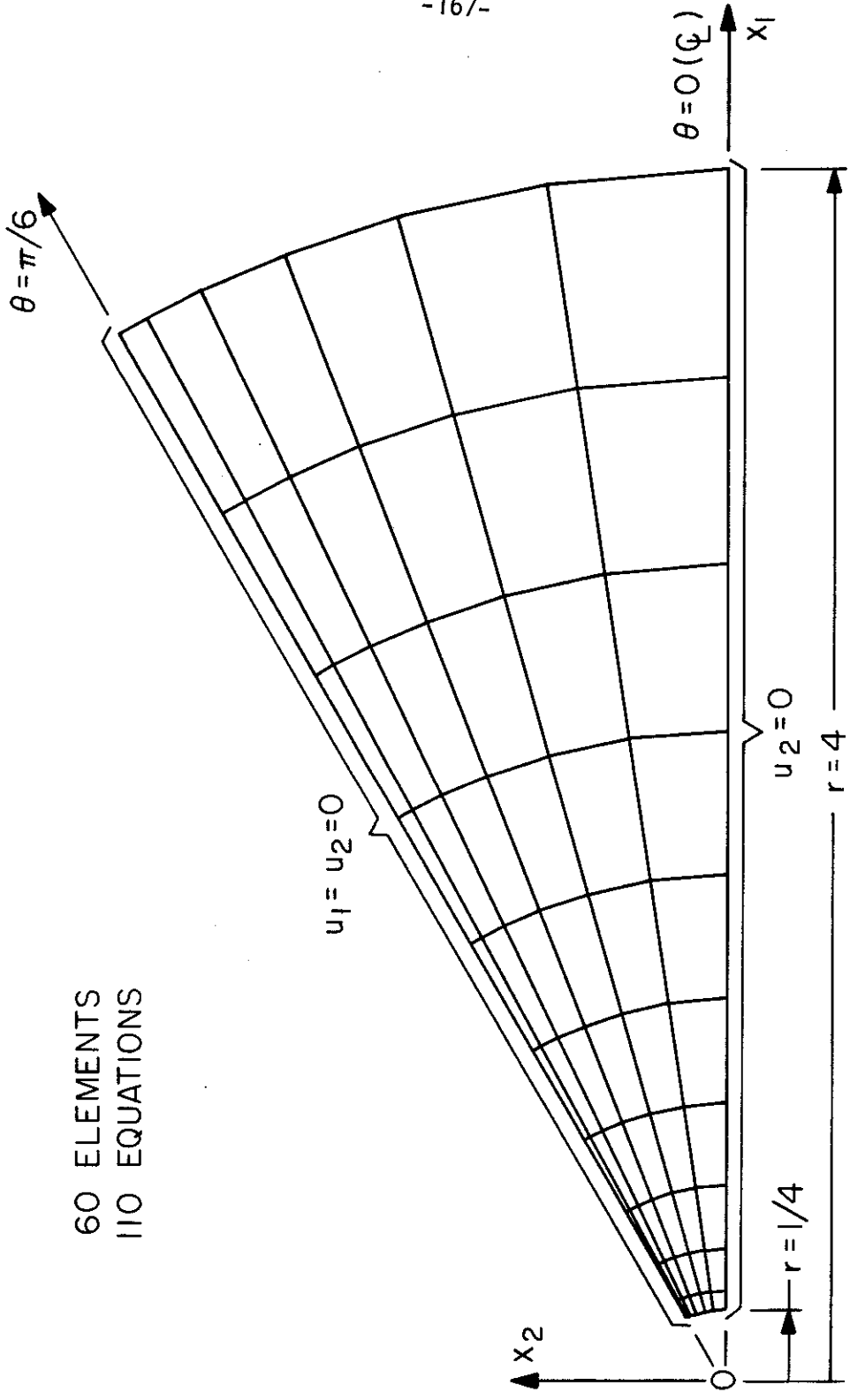
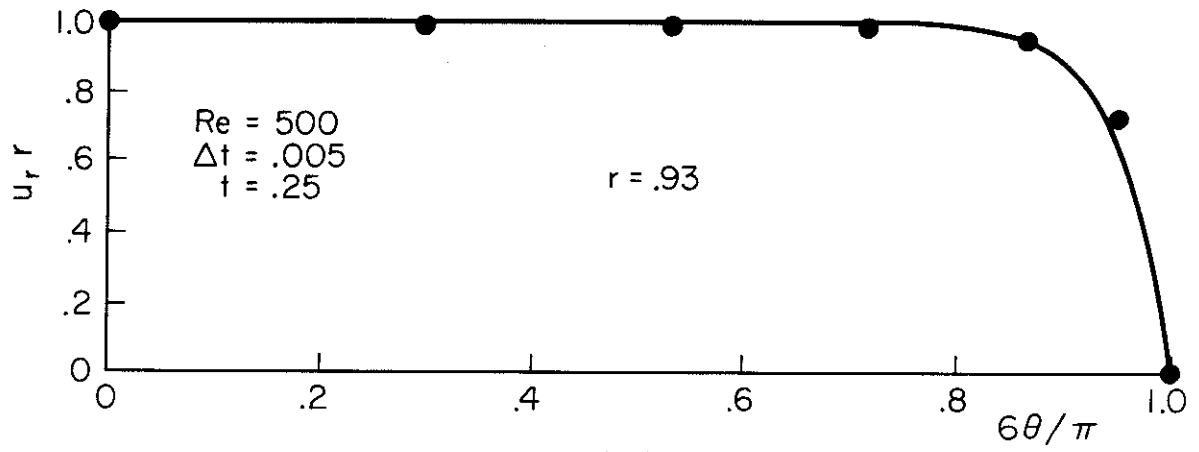
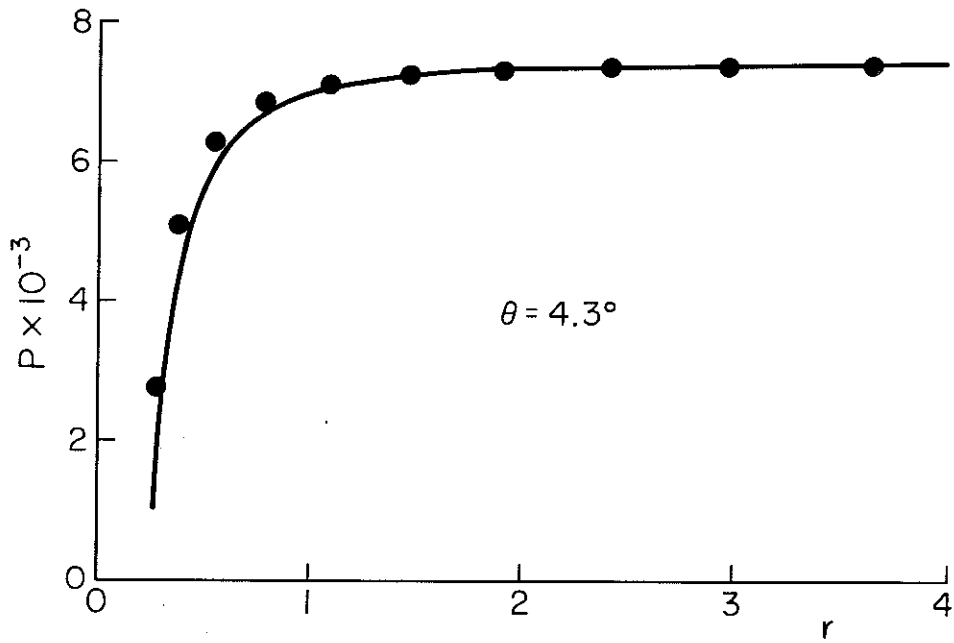


Fig. IIE-1. Hamel flow: Finite element mesh.



(a)



(b)

Fig.IIE-2. Hamel flow: Comparison of finite element (●) with exact (—) results at low Reynolds number. (a) Velocity; and (b) pressure.

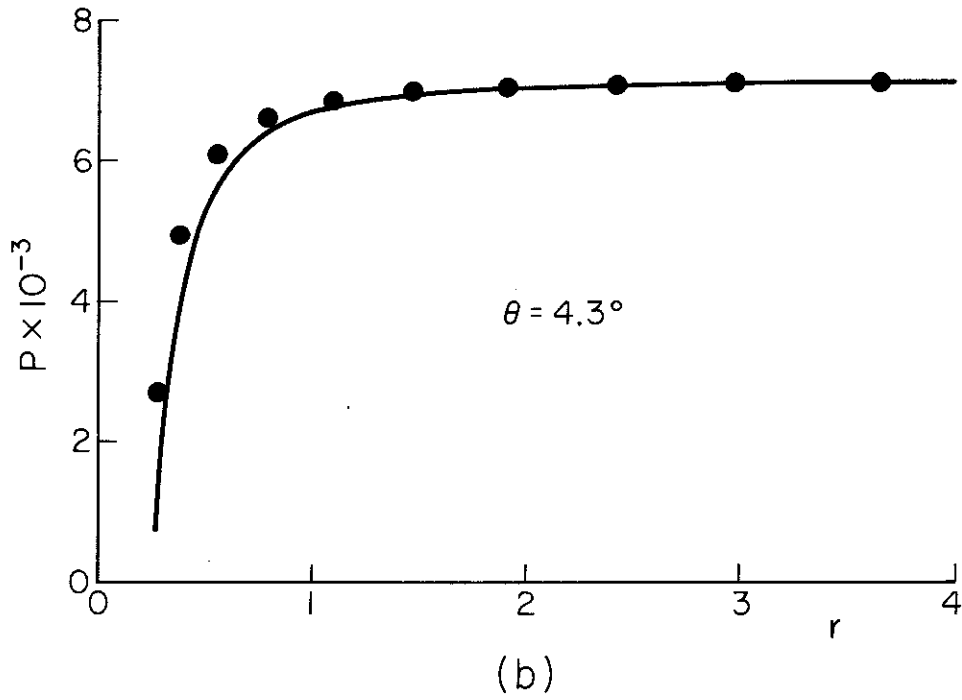
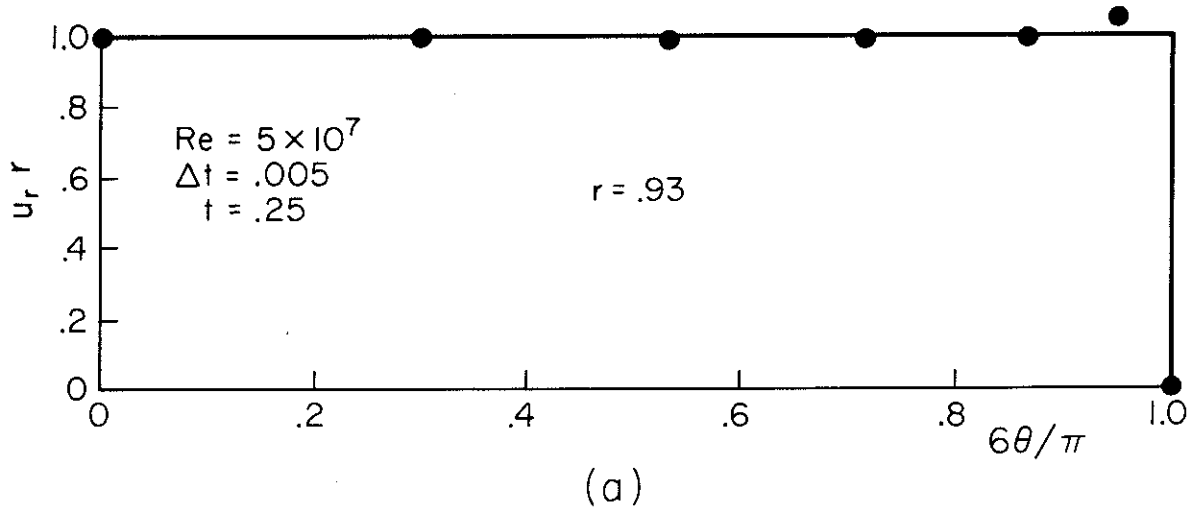


Fig.IIE-3. Hamel flow: Comparison of finite element (●) with exact (—) results at high Reynolds number. (a) Velocity; and (b) pressure.

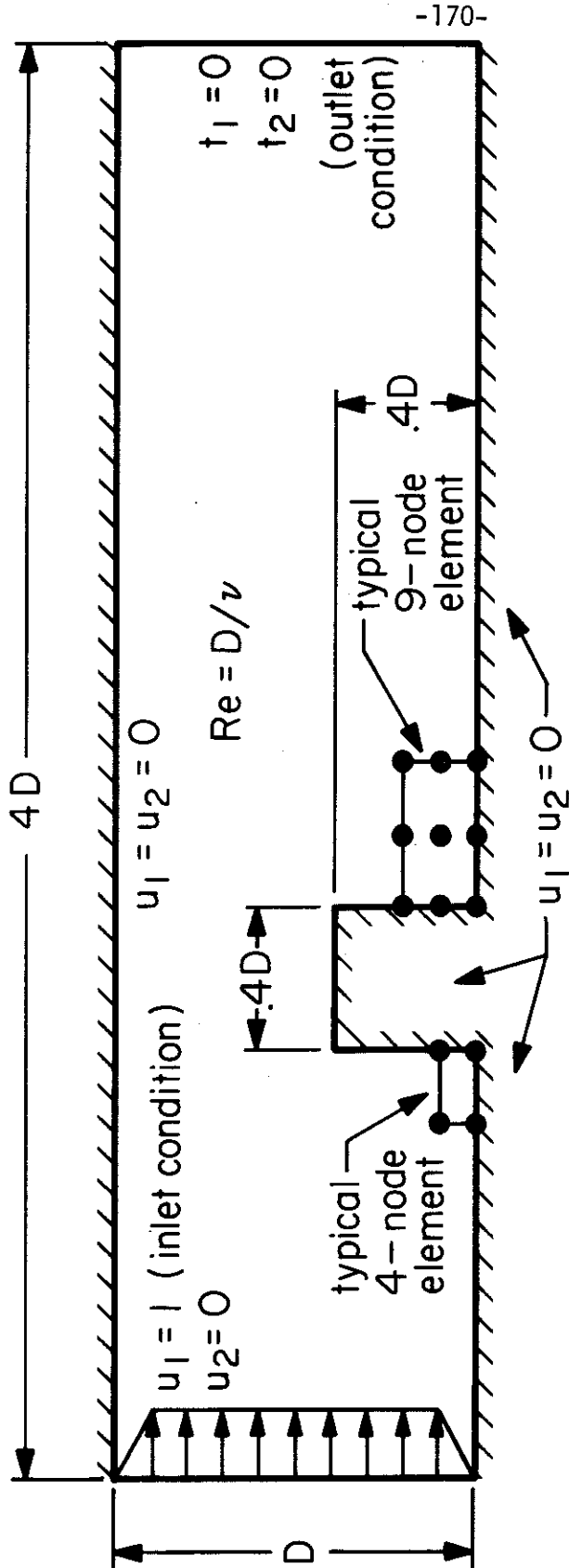
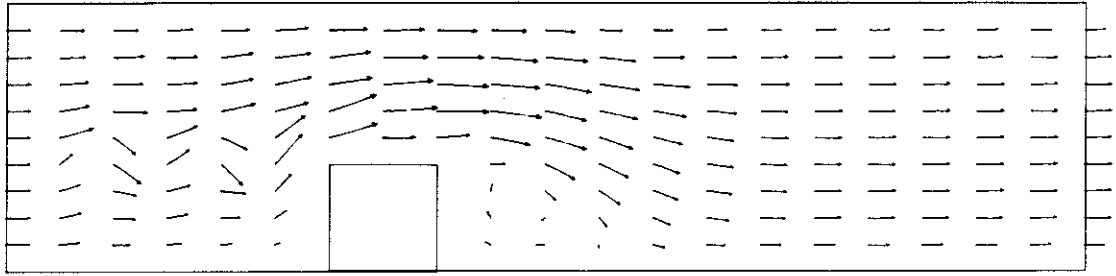
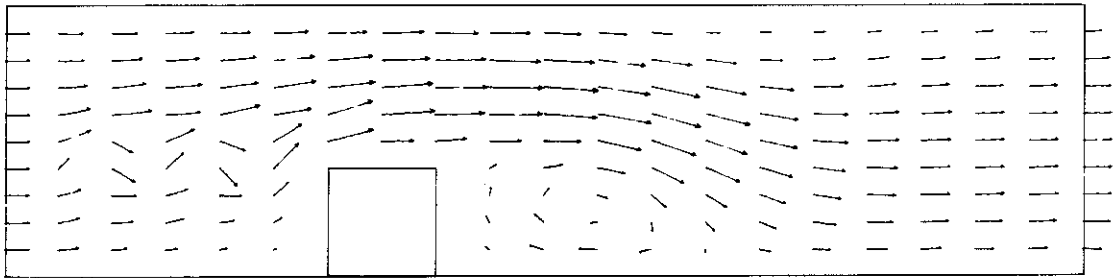


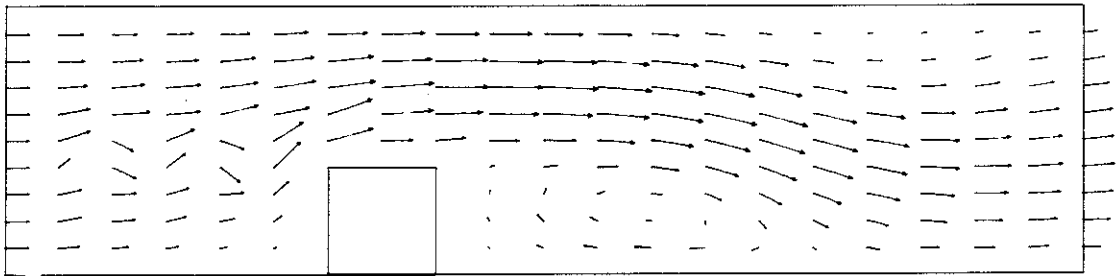
Fig.IIF-1.. Flow over a step: Problem description and finite element mesh information.



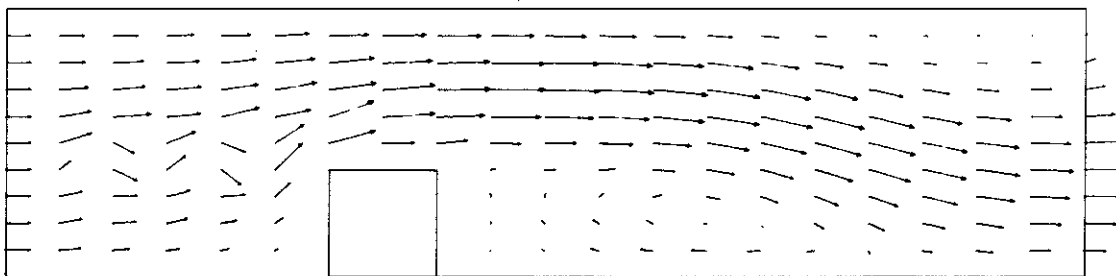
$t=0.7$ ($n=10$)



$t=1.4$ ($n=20$)

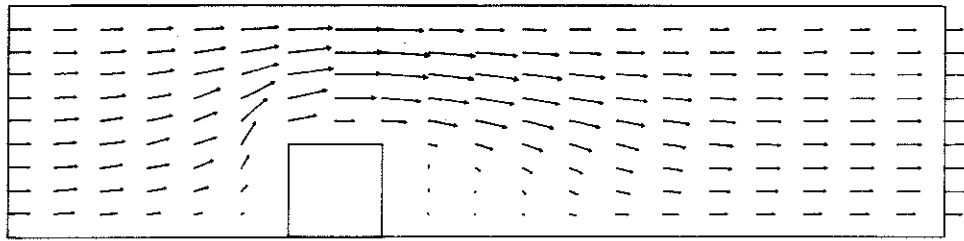


$t=2.1$ ($n=30$)

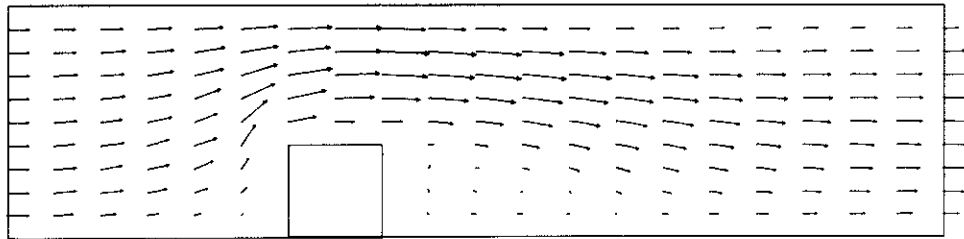


$t=2.8$ ($n=40$)

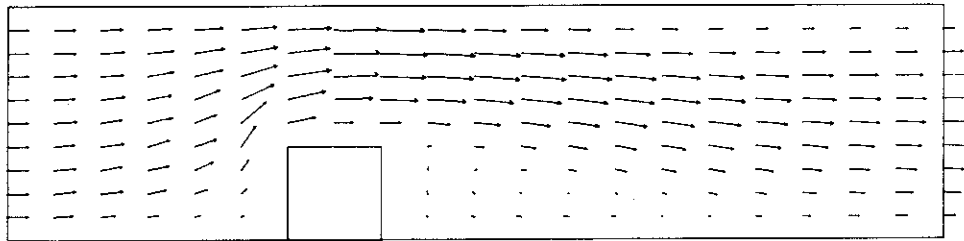
Fig. IIF-2. Flow over a step ($Re = 200$): Finite element results for 9-node elements with Gauss-Legendre integration of convection terms.



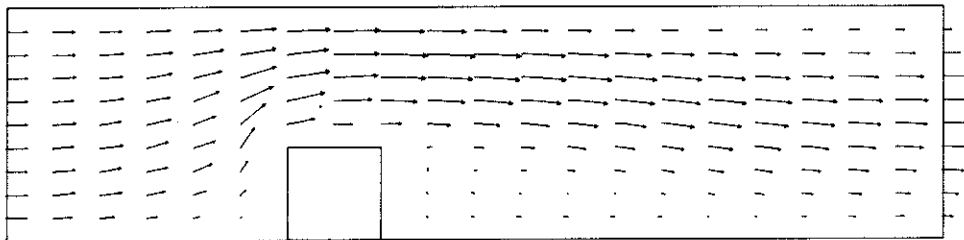
$t = 0.749$ ($n = 10$)



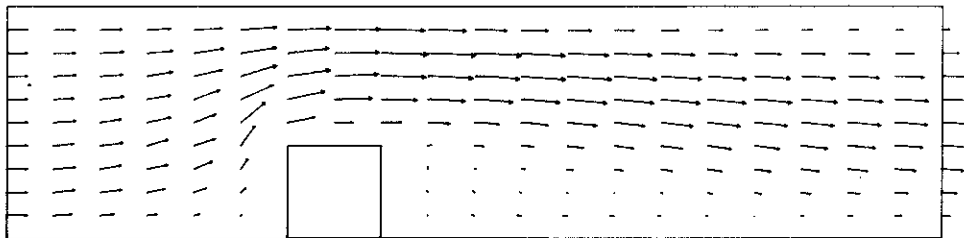
$t = 1.50$ ($n = 20$)



$t = 2.25$ ($n = 30$)

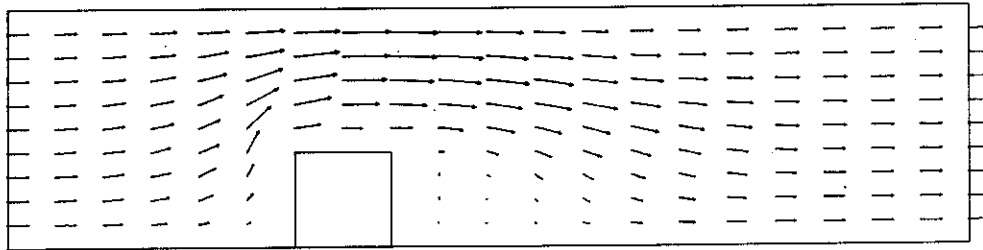


$t = 3.00$ ($n = 40$)

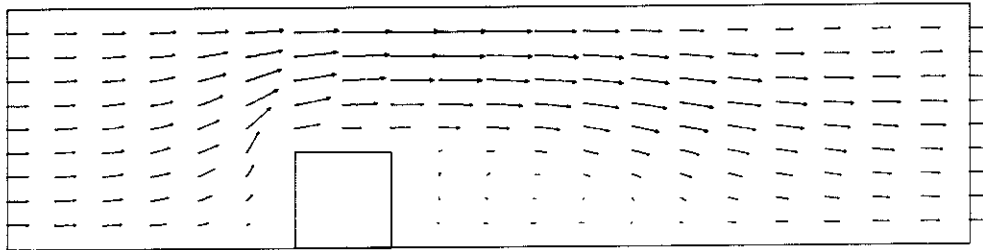


$t = 3.75$ ($n = 50$)

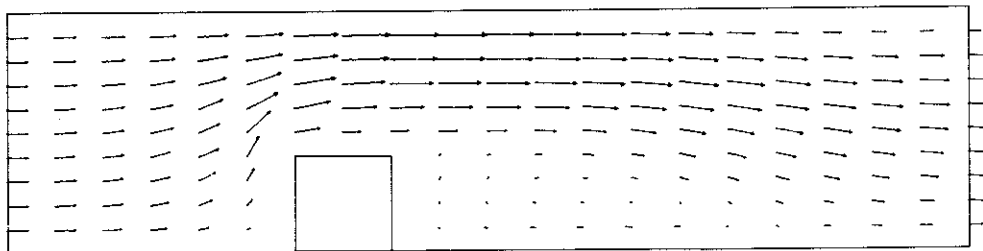
Fig. IIF-3. Flow over a step ($Re = 200$): Finite element results for 4-node elements with modified upwind treatment of convection terms.



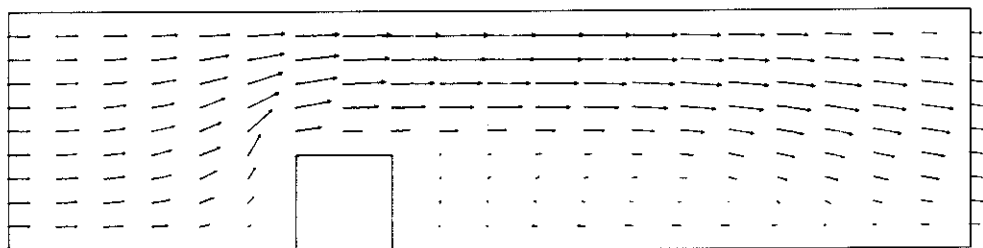
$t = 0.756$ ($n = 10$)



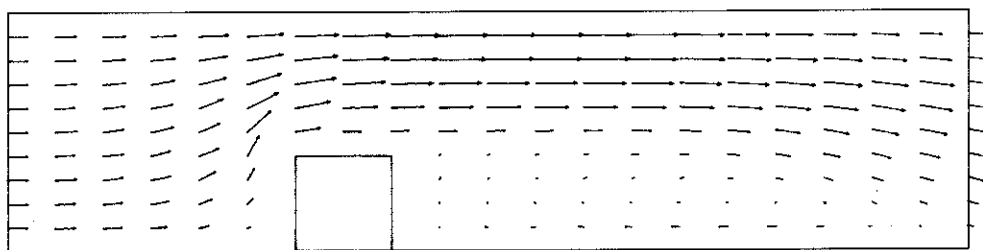
$t = 1.51$ ($n = 20$)



$t = 2.26$ ($n = 30$)



$t = 3.02$ ($n = 40$)



$t = 3.77$ ($n = 50$)

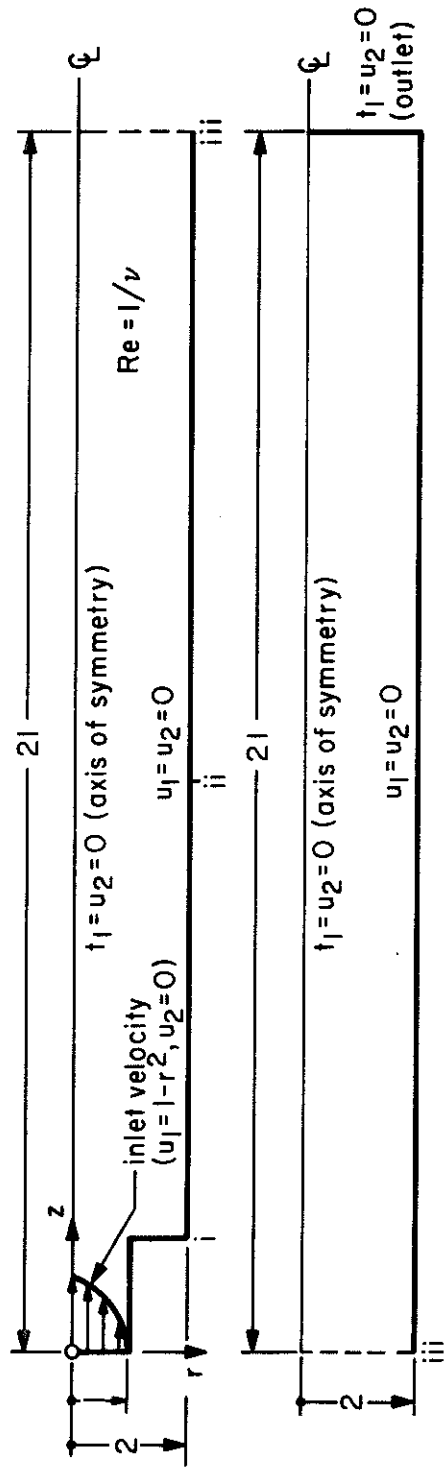
Fig.IIF-4. Flow over a step ($Re = 10^7$): Finite element results for 4-node elements with modified upwind treatment of convection terms,

$\lambda = 10^9$; $\gamma = 1$; and $\Delta t = 0.07$. As is clearly visible, "wiggles" appear upstream of the step. Similar results are obtained for the 4-node elements employing Gauss-Legendre integration of the convective term. It is felt that this problem demonstrates the inappropriateness of Gauss-Legendre integration of the convected terms under the circumstances described.

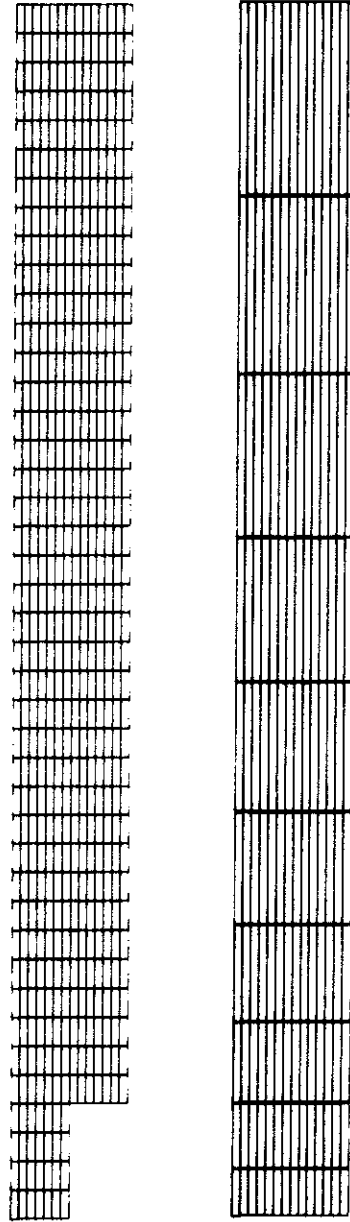
As can be seen from Figures IIF-3 and IIF-4, results for the 4-node elements which employ the modified upwind treatment of the convection term at $Re = 200$ and 10^7 , respectively, are smooth, and the upstream "wiggles" are removed in both cases. The data employed in these cases were: ($Re = 200$) $\mu = 1$; $\rho = 200$; $\lambda = 10^8$; $\gamma = 1$; ($Re = 10^7$) $\mu = 1$; $\rho = 10^{13}$; and $\gamma = 1$. Time steps were selected adaptively.

II-G. Axisymmetric Flow through a Sudden Enlargement

The problem description and finite element mesh used are depicted in Figure IIG-1. The domain and mesh are split at Section iii for pictorial purposes only. Macagno and Hung [32] have obtained both experimental and numerical results for this problem. A fixed time step of $\Delta t = 0.5$ was employed, and $\gamma = 0.75$ was used for the transient algorithm. The dynamic viscosity, μ , was set to 1 throughout. Thus $Re = \rho$ and the penalty parameter was taken to be $10^7 \rho$. One point integration of the λ term was employed. The calculations were performed in three sequences and were compared to experimental and numerical results due to Macagno and Hung. In the first sequence, the initial conditions were quiescent and $Re = 30$. The sequence consisted of 60 time steps and a steady flow was achieved after approximately 30 steps. The flow was used as the initial condition for the second sequence in which $Re = 60$. This sequence consisted of 40 steps and a steady condition was attained



(a) Problem statement



(b) Finite element mesh

Fig. II G-1. Axisymmetric flow through a sudden enlargement: Problem description.

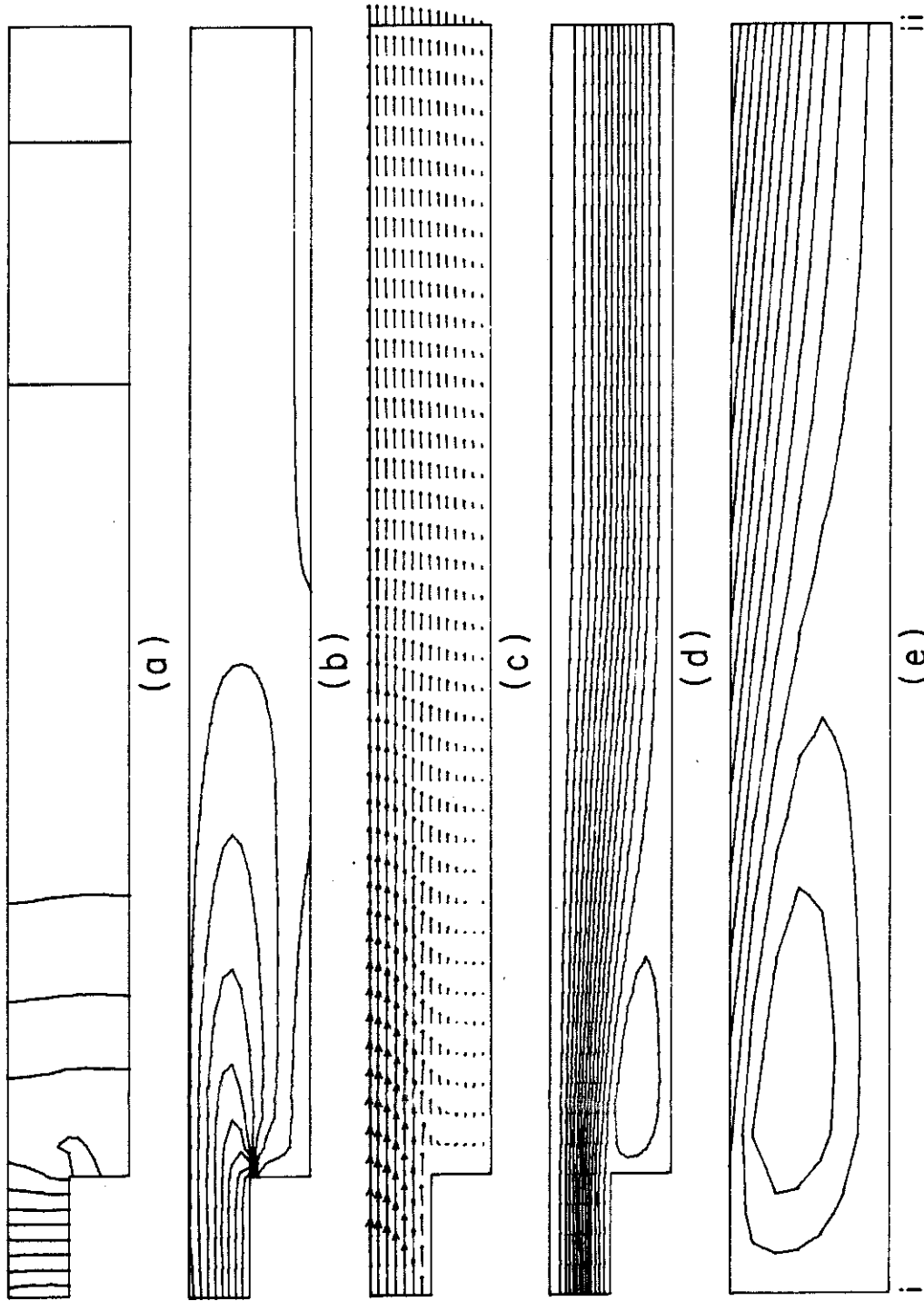


Fig. II G-2. Axisymmetric flow through a sudden enlargement (Re = 60): (a) Pressure contours; (b) vorticity contours; (c) velocity vectors; (d) streamlines; and (e) detail of streamlines in recirculation region.

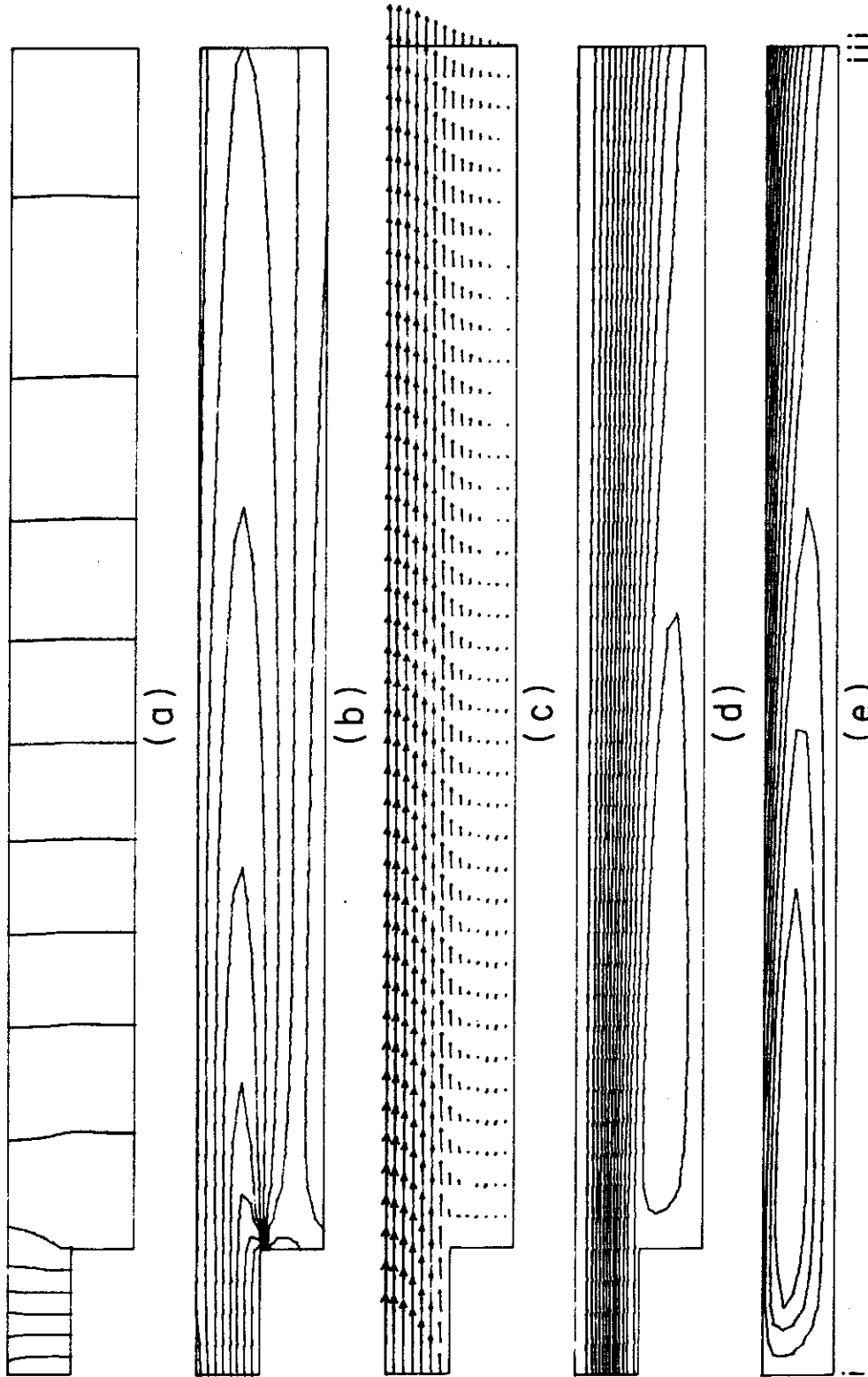


Fig. II G-3. Axisymmetric flow through a sudden enlargement (Re = 200): (a) Pressure contours; (b) vorticity contours; (c) velocity vectors; (d) streamlines; and (e) detail of streamlines in recirculation region.

after 20 steps. Results for this flow are presented in Figure IIG-2. With this flow as an initial condition, the final sequence in which $Re = 200$ was run for 90 steps. It took almost all this time for the region just upstream of section iii to become steady. Results are presented in Figure IIG-3.

The overall flow patterns and length scales of the trapped annular eddies are in good agreement with [32]. To study flows at higher Re would require refinement and extension of the mesh downstream of section iii, as the recirculation regime tends to stretch out considerably with increasing Re .

II-H. Viscous Flow about an Airfoil

Viscous flow about an NACA0018 airfoil geometry is studied. The problem statement is shown in Figure IIH-1. The finite element mesh is shown in Figure IIH-2. We employed unit chord length (i.e., L) throughout. The dynamic viscosity, μ , was set to 1. The input inlet velocity is 1, therefore $Re = \rho$.

Several runs were made with this mesh. The first, at low Reynolds number (i.e., 400) and quiescent initial conditions, shows well the diffusion of vorticity with the development of the boundary layer; see Figures IIH-3 and IIH-4. Accompanying pressure profiles are shown in Figure IIH-5.

Steady, high Reynolds number results with quiescent initial conditions are presented in Figures IIH-6 and IIH-7. Obviously, from the velocity vector plots, this mesh is not adequate for such a high Reynolds number. The infinite-domain, potential flow, pressure profiles are presented in Fig. IIH-7 for comparison purposes. It is conjectured

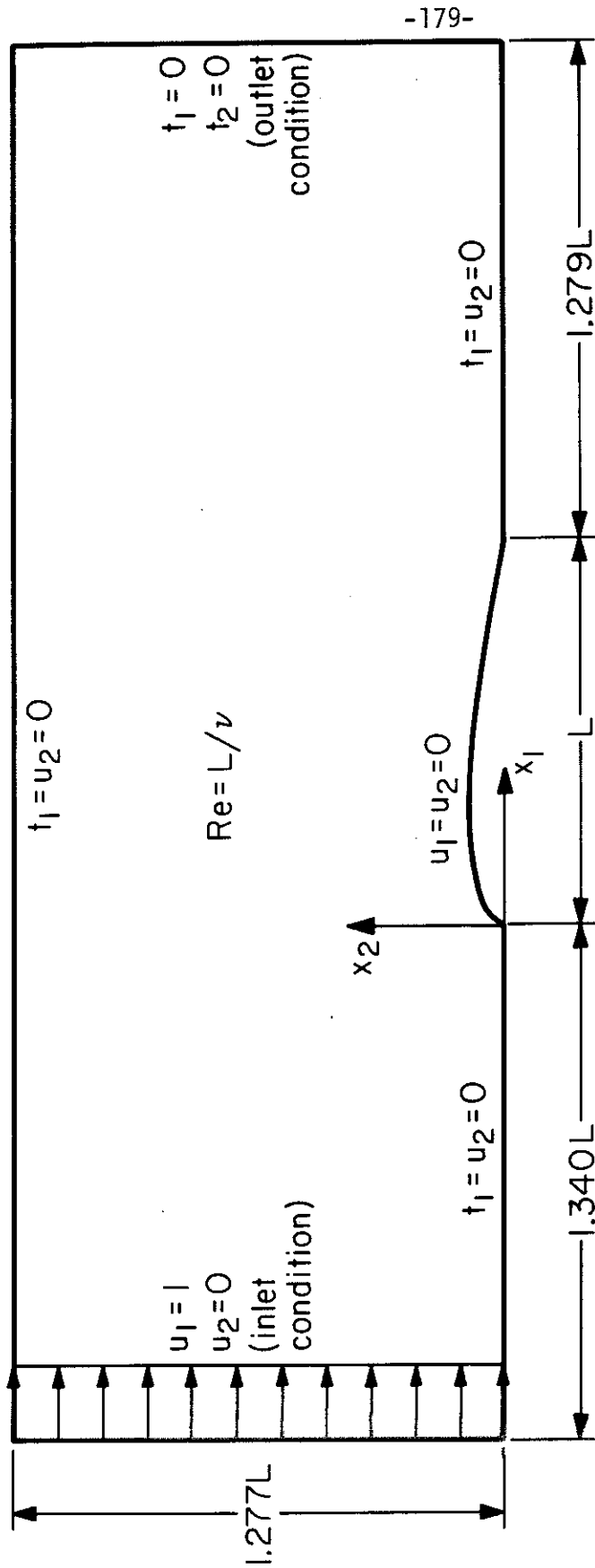


Fig.IH-1. Viscous flow about an airfoil: Problem statement.

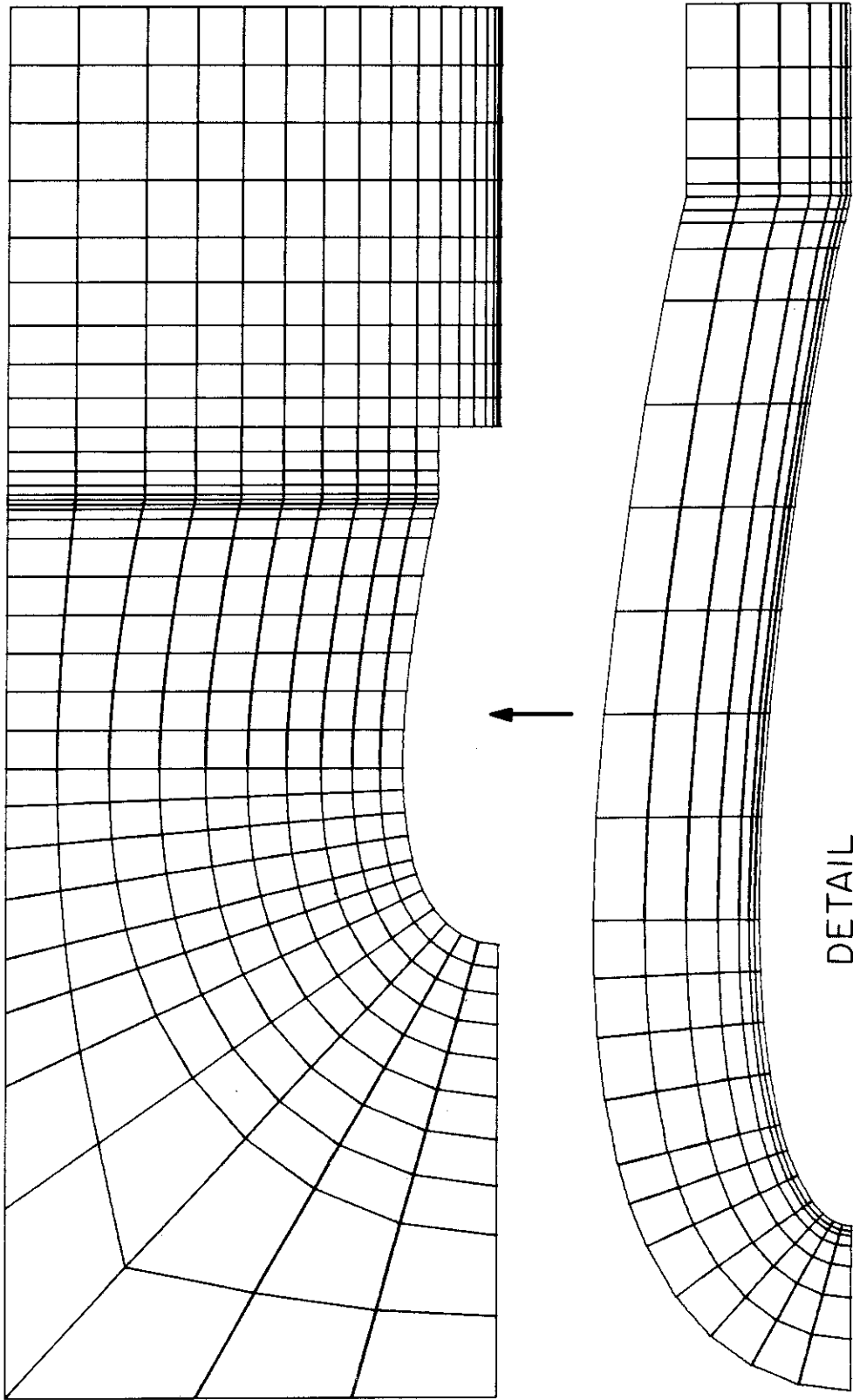


Fig.II-2. Viscous flow about an airfoil: Finite element mesh.

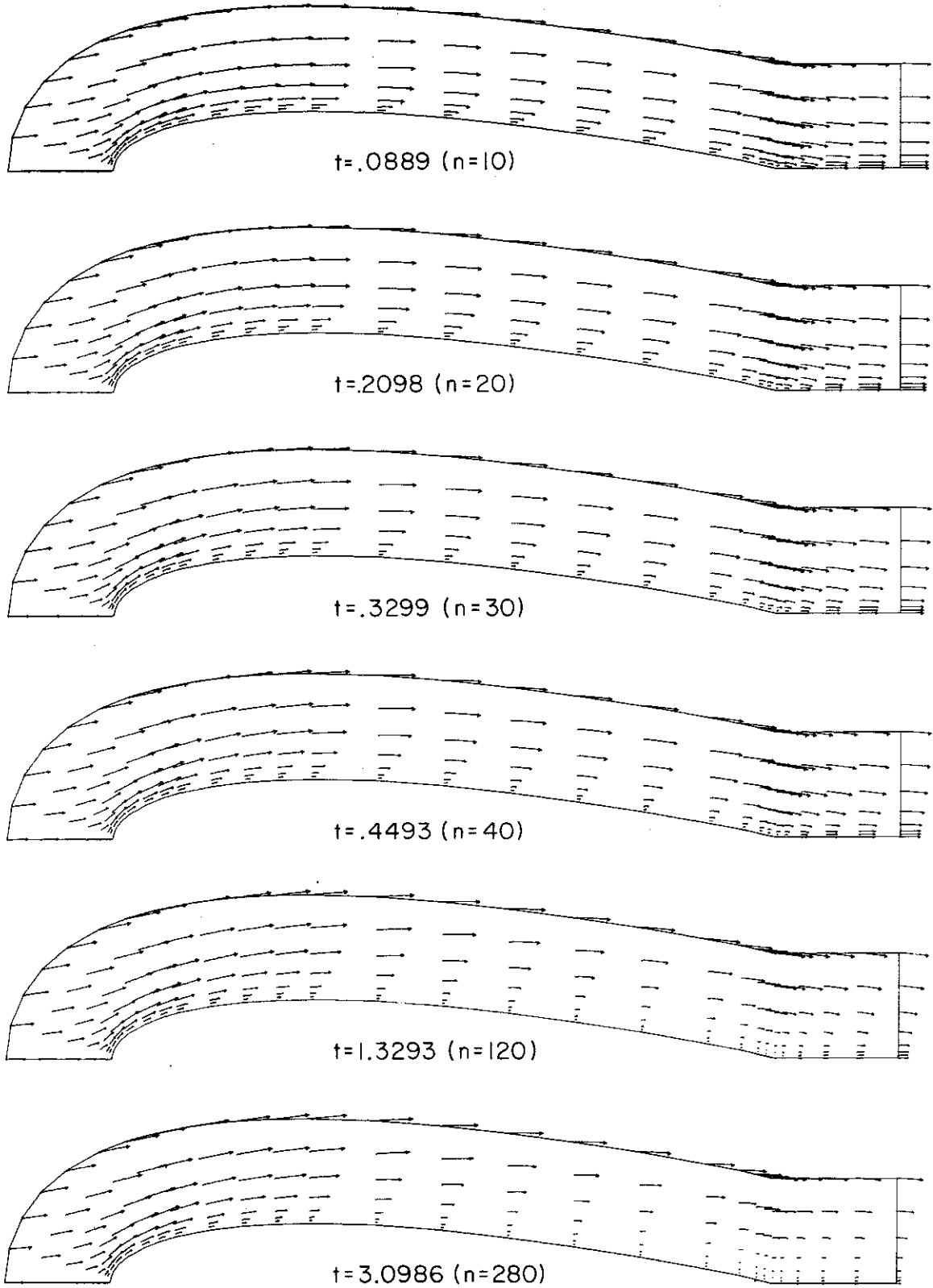


Fig.IH-3. Viscous flow about an airfoil ($Re = 400$): Velocity vectors.

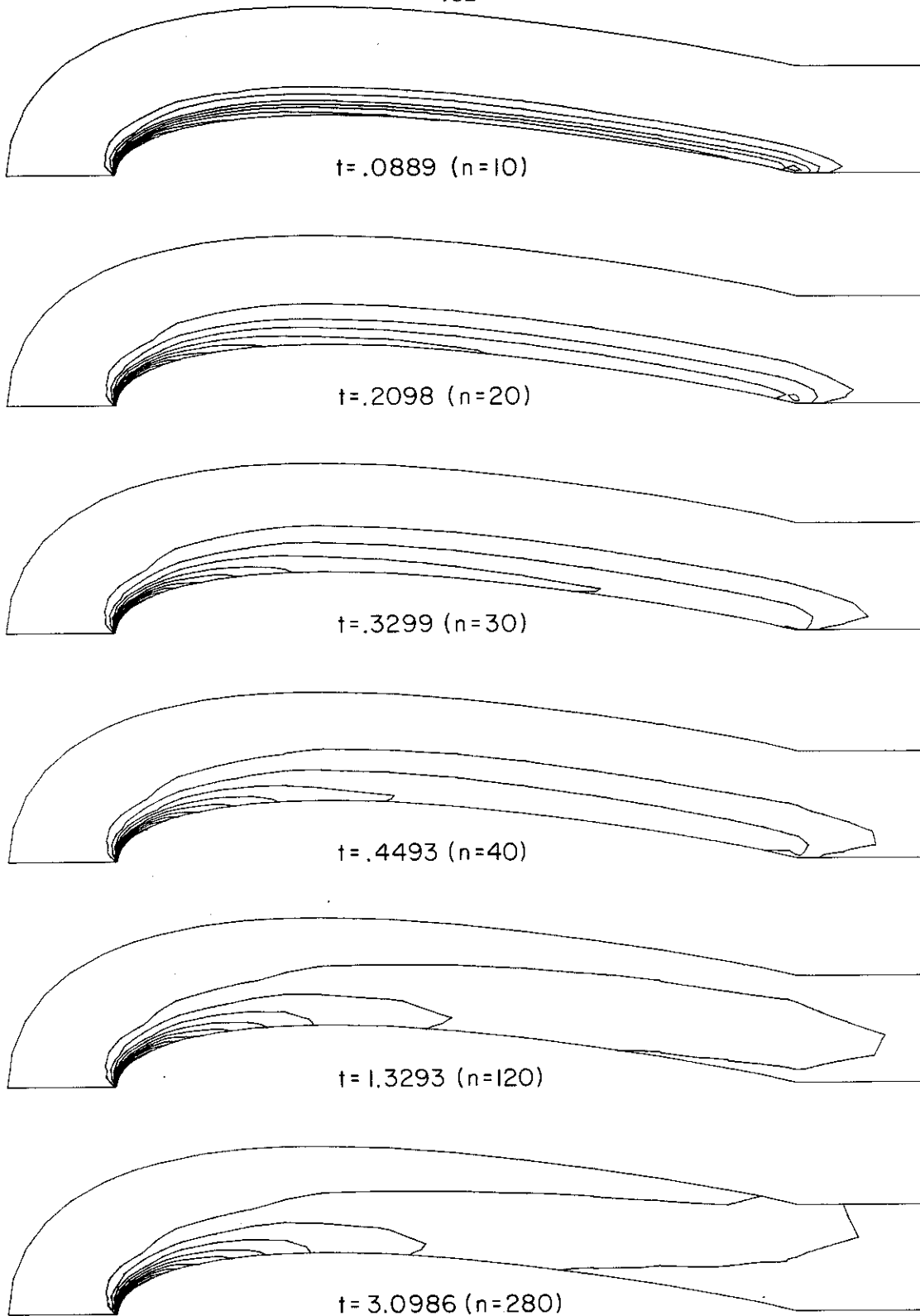


Fig.IIH-4. Viscous flow about an airfoil ($Re = 400$): Vorticity contours.

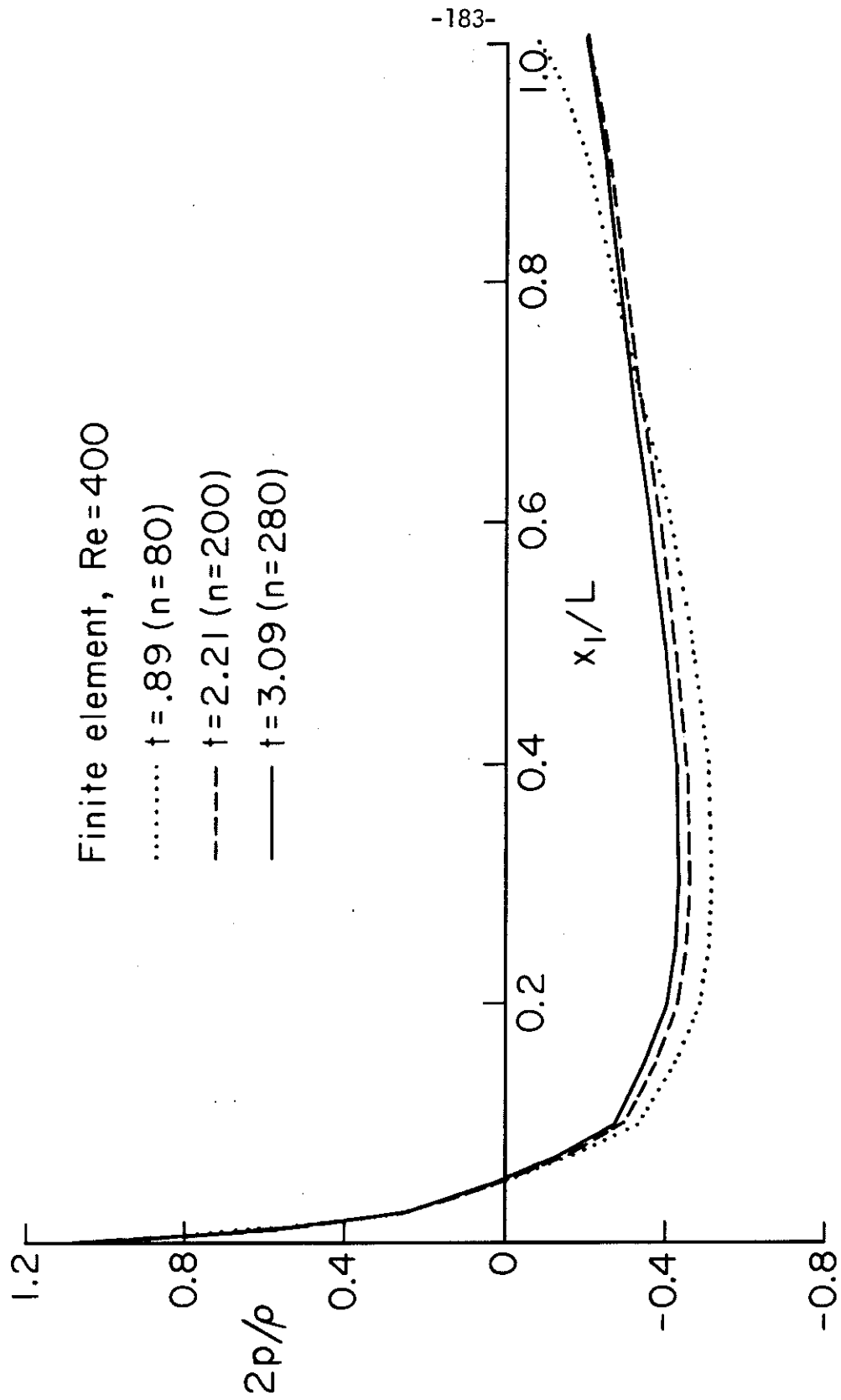


Fig. IIH-5. Viscous flow about an airfoil ($Re = 400$): Pressures.

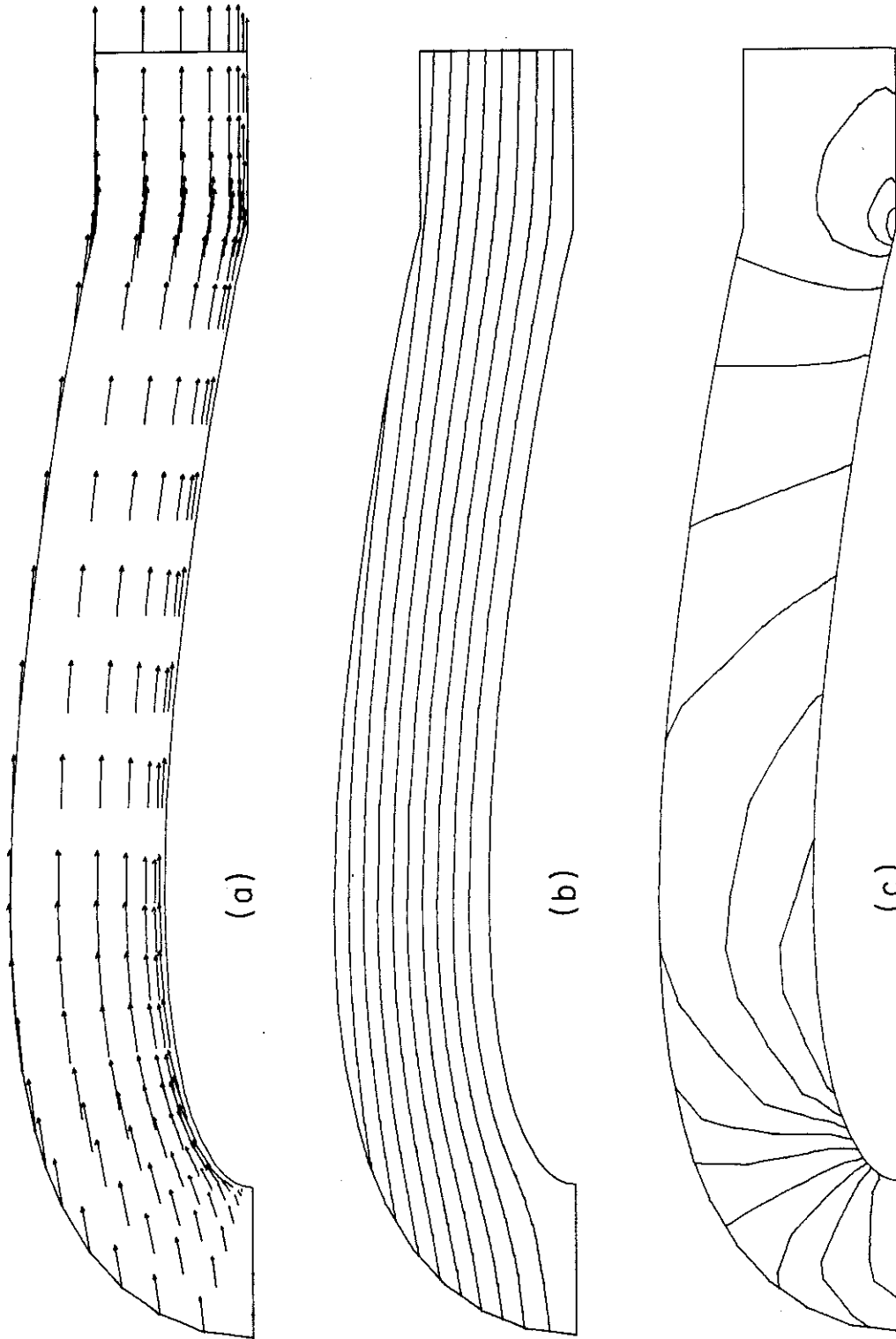


Fig. IIH-6. Viscous flow about an airfoil ($Re = 10^8$): (a) Velocity vectors; (b) streamlines; and (c) pressure contours.

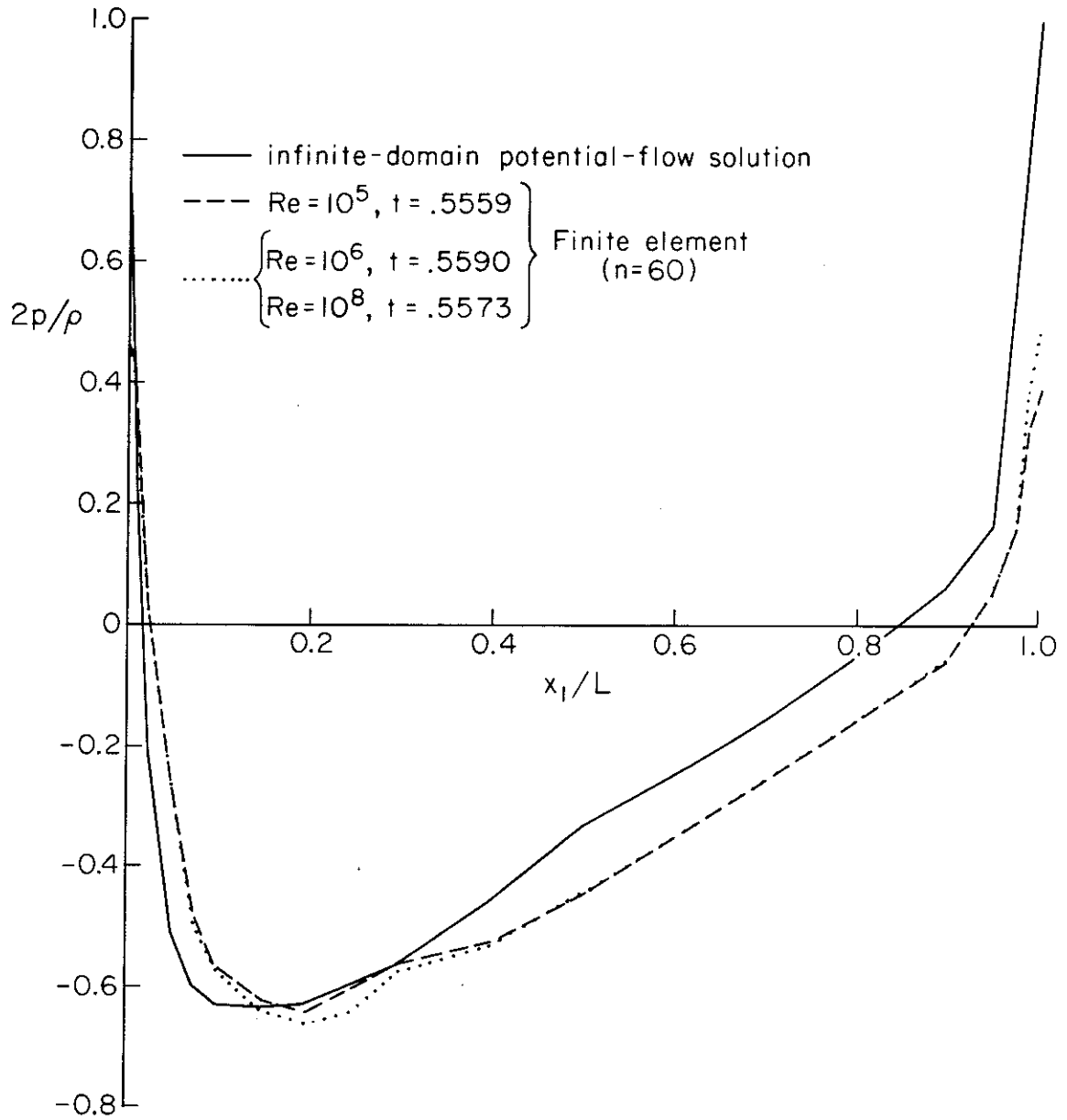


Fig. IIH-7. Viscous flow about an airfoil: Comparison of pressures at different Reynolds numbers.

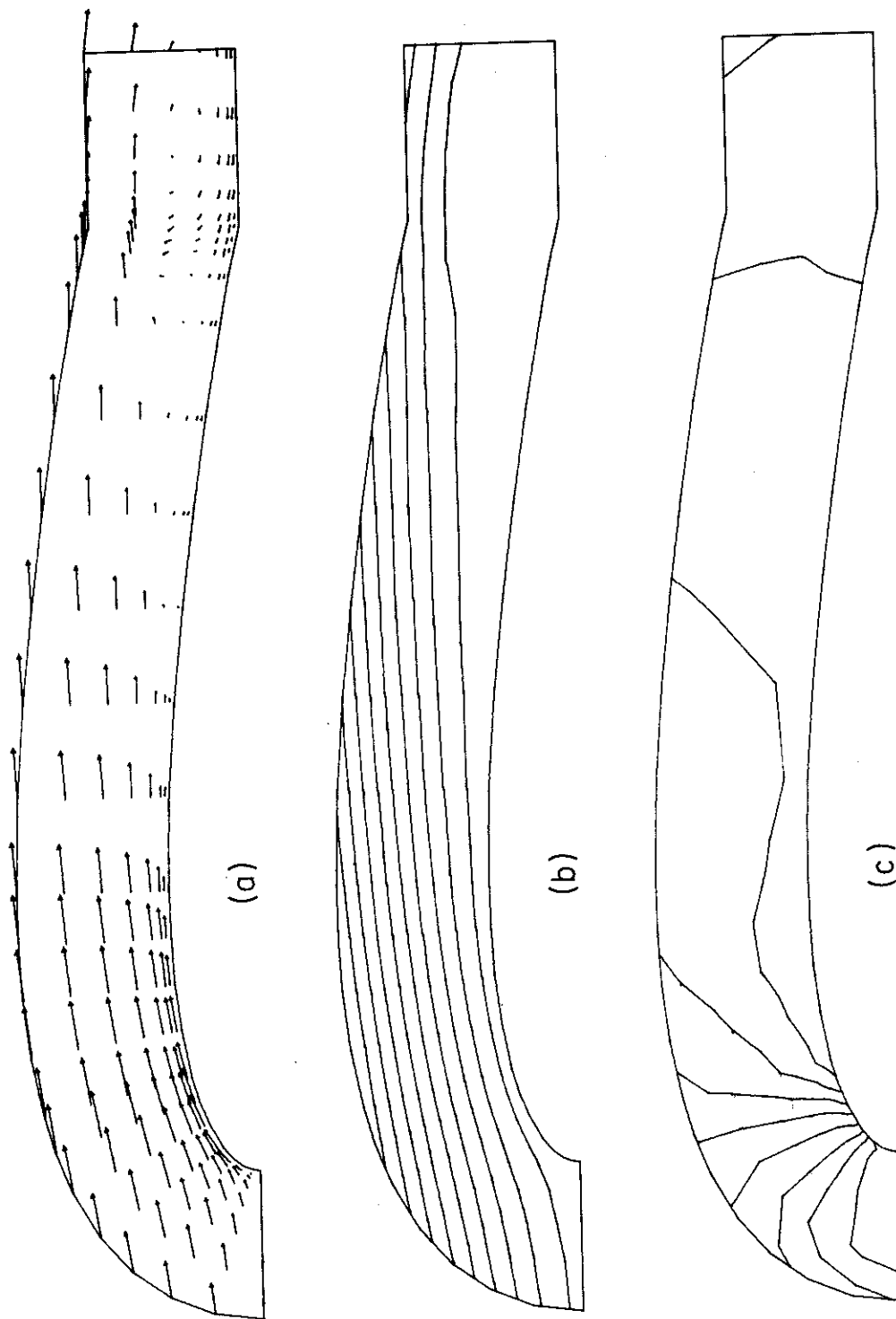


Fig.II-H-8. Viscous flow about an airfoil; Results obtained after changing Re from 400 to 10^6 at $t = 1.2$:
(a) Velocity vectors; (b) streamlines; and (c) pressure contours.

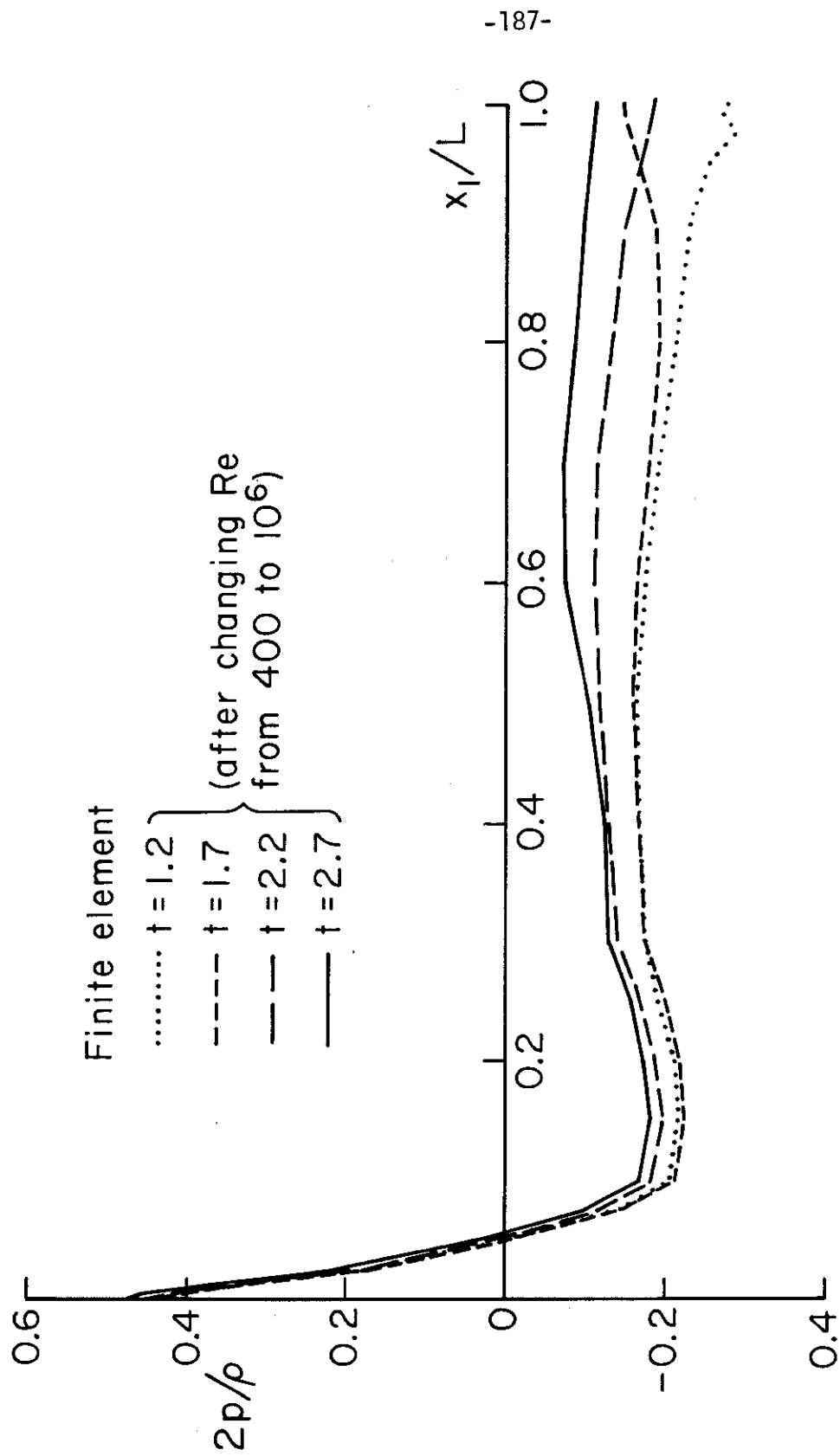


Fig.III-9. Viscous flow about an airfoil: Pressures obtained after changing Re from 400 to 10^6 .

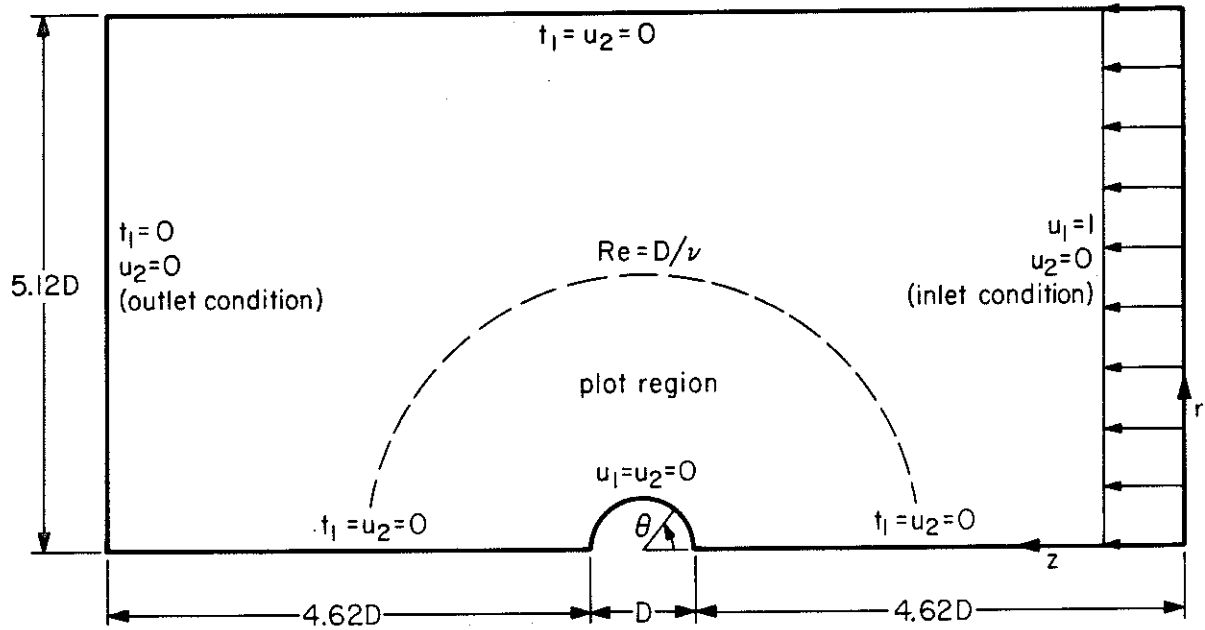
that enlarging the domain and refining the leading-edge region of the mesh would bring the results in closer agreement, although the pressure drop at the trailing edge is to be expected in a viscous computation.

An $Re = 10^6$ calculation was made using the $Re = 400$ solution at time 3.0986 as an initial condition. In this case the flow separated; sample results are shown in Figures IIH-8 and IIH-9. At later times (not shown) the separation point and recirculation regime moved downstream.

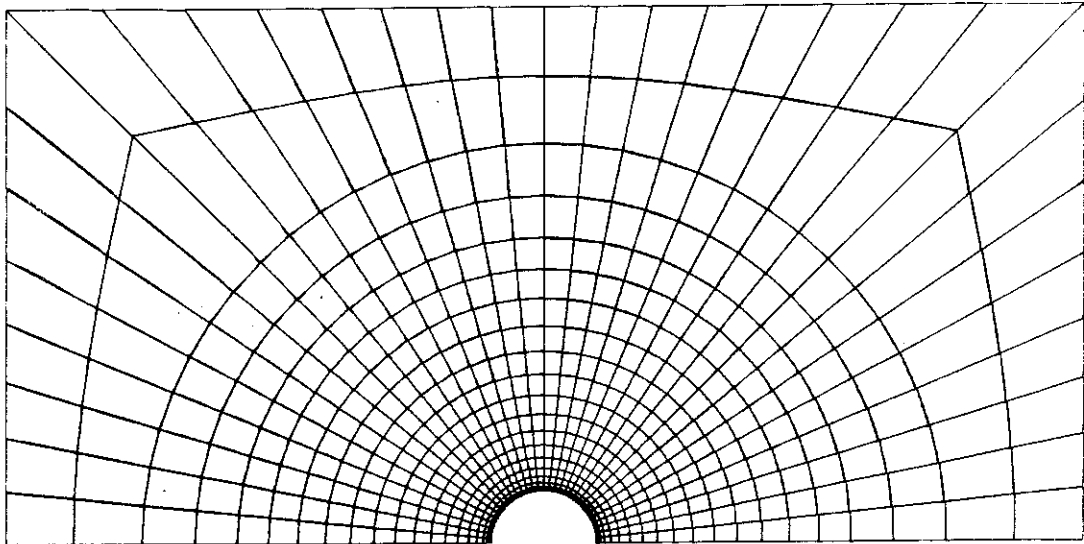
II-I. Axisymmetric Flow around a Sphere

The problem description and mesh are shown in Figure III-1. Initial conditions were assumed quiescent and the "mean-incompressible" treatment of the λ -term was employed.

Runs at $Re = 10$ and 40 were made; sample results are shown in Figures III-2 and III-3. After the flows became steady, comparisons were made with the infinite-domain, analytical results of Dennis and Walker [33]. As can be seen from Figure III-3, vorticity (ζ) and pressure are in good agreement. It is somewhat surprising that the results at $Re = 40$ are in such good agreement, as our finite-domain model seems hardly adequate for this high a Reynolds number. In Table II-I, pressure-drag (C_p), viscous-drag (C_v), and total drag (C_D) coefficients are compared with the results of Dennis and Walker. (The coefficients are normalized as follows: $drag/(\pi\rho(D/2)^2)$.) The agreement is quite good overall, but better at $Re = 10$ than at $Re = 40$, as may be expected.



(a) Problem statement



(b) Finite element mesh

Fig. II 1-1. Axisymmetric flow around a sphere: Problem description and finite element mesh.

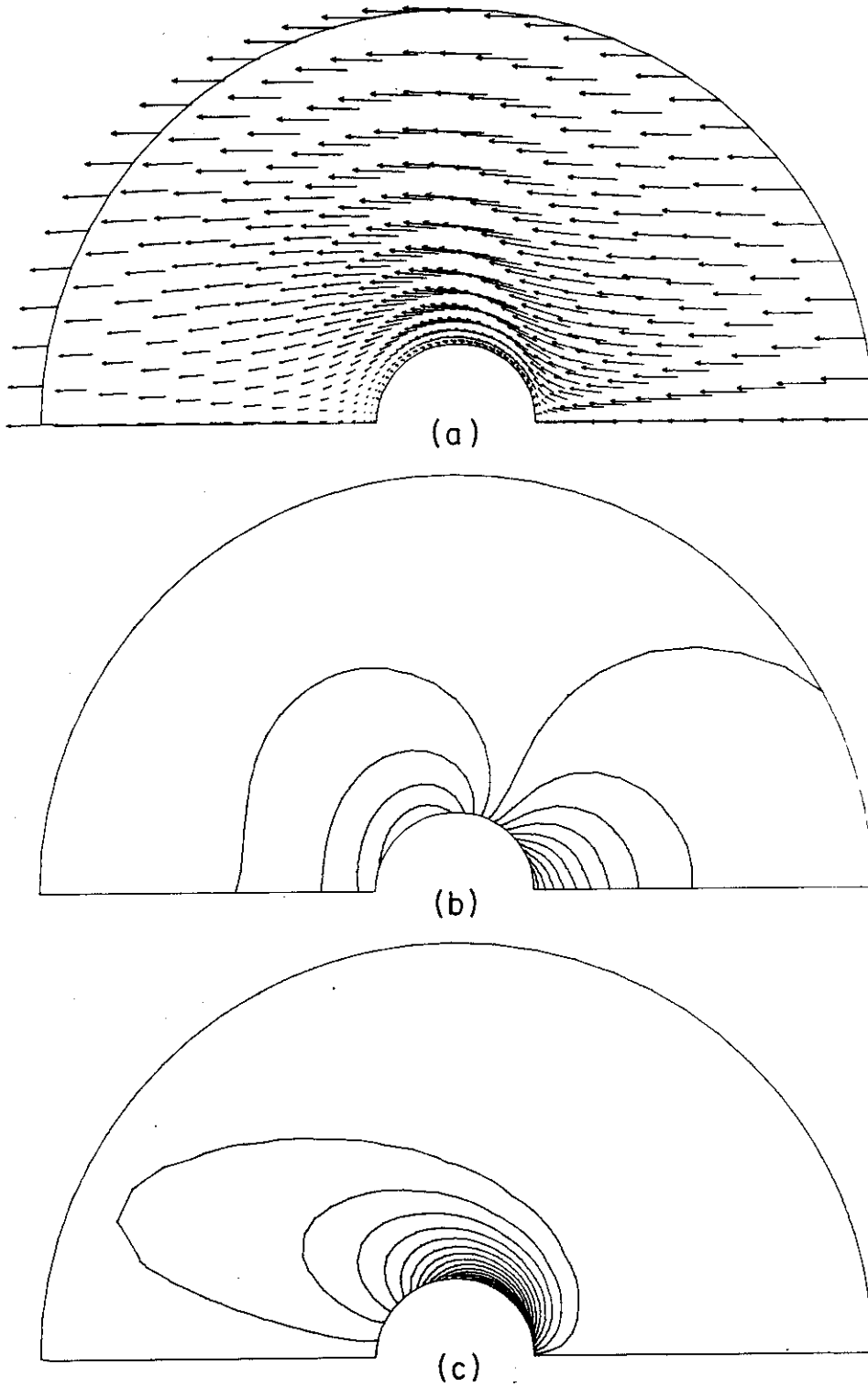


Fig. II 1-2. Axisymmetric flow around a sphere ($Re = 10$):
(a) Velocity vectors; (b) pressure contours; and
vorticity contours.

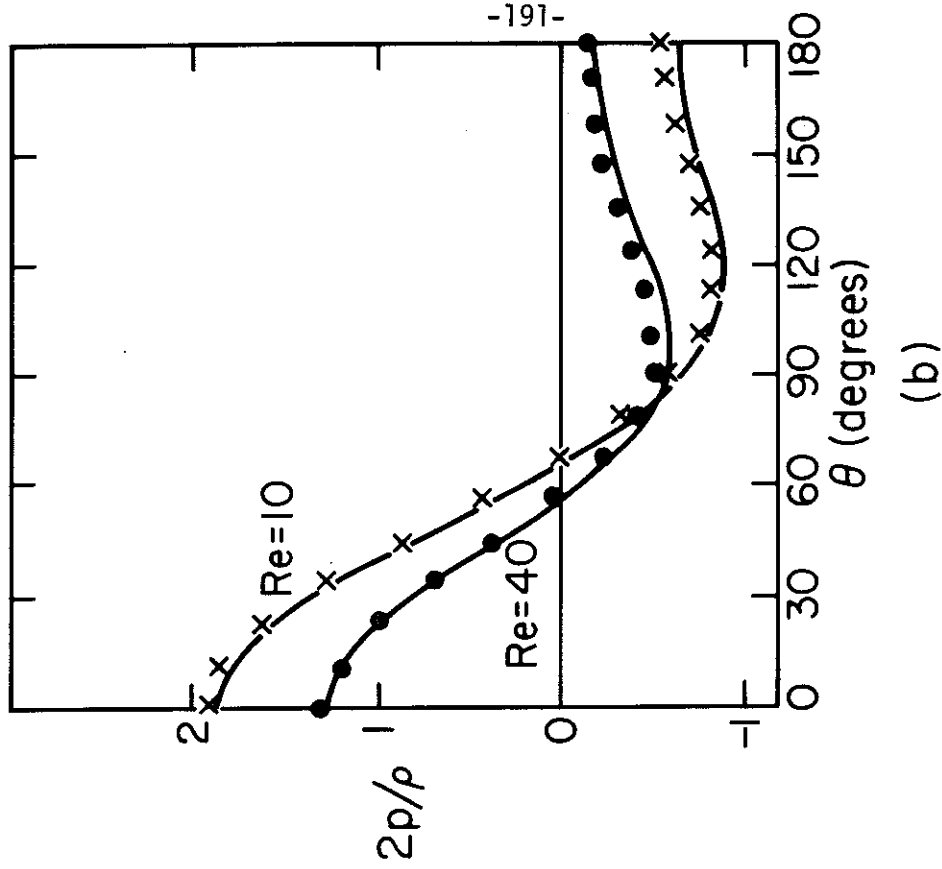
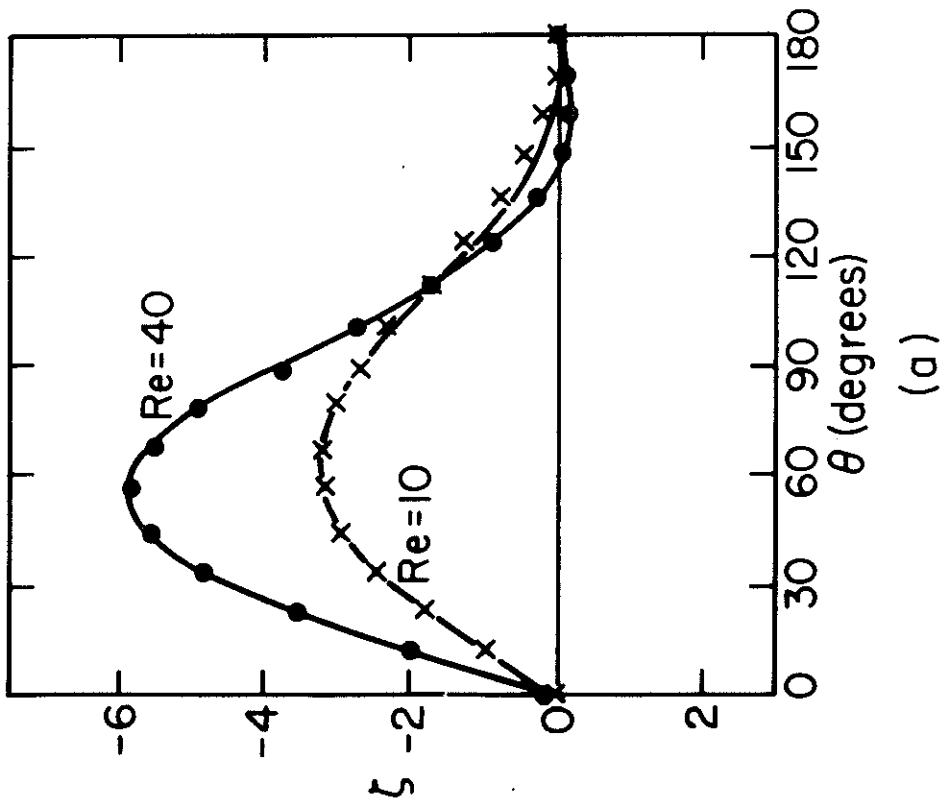


Fig. II 1-3. Axisymmetric flow around a sphere: Comparison of finite element (•, x) and analytical (—) results.
 (a) Vorticity; and (b) pressure.

Table II-I

Comparison of Drag Coefficients for Flow around a Sphere

Coefficients	Re = 10		Re = 40	
	Present Study	Dennis & Walker	Present Study	Dennis & Walker
C_p	0.774	0.785	0.347	0.368
C_v	1.419	1.427	0.520	0.536
C_D	2.194	2.212	0.868	0.904

III. Remark on Slightly Compressible Formulation for Viscous Fluid Flow

The slightly compressible formulation for viscous fluid flow (see Chapters 2 and 3) has been programmed and studied. The dam-reservoir (IID), Hamel flow (IIE), and the free-surface wave generation flow problem (see Chapter 6) have been solved. The results obtained using this formulation are virtually identical with the penalty function formulation described above. So the sample examples will not be presented here.

One of the main advantages of this formulation over the penalty function formulation is that when a static solution is reached, all accelerations and velocities will approach zero (due to the fact that it is a rate type constitutive equation, see Chapters 2 and 3). In the penalty formulation, a small nonzero velocity is produced to create a bulk viscous effect to support the loading (e.g., gravity). Hence, the slightly compressible approach is preferred and has been developed for the purpose of fluid-structure interaction problems which will be discussed in great detail in the next chapter.

References

1. T.J.R. Hughes, "Ae/Am 108 - Finite element method course notes," California Institute of Technology.
2. T.J.R. Hughes, R. L. Taylor, and J. R. Levy, "A finite element method for incompressible viscous flows," in 2d Internat. Symp. on Finite Element Meth. in Flow Problems, S. Margherita Ligure, Italy, June 14-18, 1976.
3. T.J.R. Hughes, R. L. Taylor, and J. F. Levy, "High Reynolds number, steady, incompressible flows by a finite element method," in Finite Elements in Fluids, vol. 3 (John Wiley, London, 1978).
4. T.J.R. Hughes, W. K. Liu, and A. Brooks, "Review of finite element analysis of incompressible viscous flows by the penalty function formulation," J. Computational Phys. 30, 1-60 (1979).
5. T.J.R. Hughes, "Implicit-explicit finite element techniques for symmetric and nonsymmetric systems," Proc. Conf. on Nonlinear Problems in Mechanics, University of Swansea, Swansea, U.K., Sept. 2-5, 1980.
6. M. A. Crisfield, "A faster modified Newton-Raphson iteration," Computer Meth. in Appl. Mech. and Eng. 20, 267-278 (1979).
7. M. A. Crisfield, "Iterative solution procedures for linear and nonlinear structural analysis," TRRL Laboratory Report 900, Dept. of the Environment, Dept. of Transport, 1979.
8. K. C. Park, "An implicit, variable-step technique for fluid dynamics problems," in Preprints of 2d Internat. Symp. on Finite Element Methods in Flow Problems, S. Margherita Ligure, Italy, June 14-18, 1976, pp. 33-39.
9. K. C. Park and P. G. Underwood, "A variable-step central difference method for structural dynamics analysis, Part I: Theoretical aspects," ASME Paper No. 79-PVP-120, presented at the Pressure Vessels and Piping Conference, San Francisco, CA, June 25-29, 1979.
10. P. G. Underwood and K. C. Park, "A variable-step central difference method for structural dynamic analysis, Part II: Implementation and

- performance evaluation," ASME Paper No. 79-PVP-121, presented at the Pressure Vessels and Piping Conference, San Francisco, CA, June 25-29, 1979.
11. P. M. Gresho, R. L. Lee, T. W. Stullich, and R. L. Sani, "Solution of the time-dependent Navier-Stokes equation via F.E.M.," 2nd Internat. Conf. on Finite Elements in Water Resources, London, England, July 10-14, 1978.
 12. S. L. Smith and C. A. Brebbia, *Applied Math. Mod.* 1, 234-266 (1977).
 13. T.J.R. Hughes, "Current trends in finite element research." Feature article to appear in *Applied Mechanics Reviews*.
 14. T.J.R. Hughes, "Recent developments in computer methods for structural analysis," *Nucl. Eng. and Design* 57, No. 2, May 1980.
 15. T.J.R. Hughes and W. K. Liu, "Implicit-explicit finite elements in transient analysis: Stability theory," *J. Appl. Mech.* 45, 371-374 (1978).
 16. T.J.R. Hughes and W. K. Liu, "Implicit-explicit finite elements in transient analysis: Implementation and numerical examples," *J. Appl. Mech.* 45, 375-378 (1978).
 17. T.J.R. Hughes, K. S. Pister, and R. L. Taylor, "Implicit-explicit finite elements in nonlinear transient analysis," *Computer Meth. in Appl. Mech. and Eng.* 17/18, 159-182 (1979).
 18. K. C. Park and C. A. Felippa, "Direct time integration methods in nonlinear structural dynamics," *Computer Meth. in Appl. Mech. and Eng.* 17/18, 277-313 (1979).
 19. E. Hinton, "Least squares analysis using finite elements," M.Sc. thesis, Civil Eng. Dept., University of Wales, Swansea, 1978.
 20. R. L. Lee, P. M. Gresho, and R. L. Sani, "Numerical smoothing techniques applied to some finite element solutions of the Navier-Stokes equation," 2d Internat. Conf. on Finite Elements in Water Resources, London, England, July 10-14, 1978.
 21. M. Bercovier and M. Engelman, *J. Computational Phys.*, in press.

22. O. R. Bruggraf, J. Fluid Mech. 24, 113-151 (1966).
23. D. K. Gartling, Finite element analysis of viscous incompressible flow, TICOM Report 74-8, University of Texas, Austin, December 1974.
24. J. C. Heinrich, R. S. Marshall, and O. C. Zienkiewicz, "Solution of Navier-Stokes equation by a penalty function finite element method," Report No. C/R/308-78, Dept. of Civil Eng., University of Wales, Swansea, 1978.
25. G. K. Batchelor, An Introduction to Fluid Mechanics (Cambridge University Press, Cambridge, England, 1970).
26. H. Schlichting, Boundary-Layer Theory (McGraw-Hill, 1968), 6th edition.
27. A. T. Chwang, "Hydrodynamic pressures on sloping dams during earthquakes. Part 2. Exact theory." J. Fluid Mech. 87, 343-348 (1978).
28. A. T. Chwang and G. W. Housner, "Hydrodynamic pressures on sloping dams during earthquakes. Part 1. Momentum method." J. Fluid Mech. 87, 335-342 (1978).
29. T. Von Karman, Trans. Amer. Soc. Civil Eng. 98, 418-433 (1933).
30. S. K. Sharan and G.M.L. Gladwell, "A method of analyzing dam-reservoir-foundation interaction problems," Proc. Symp. on Applications of Computer Methods in Engineering, Vol. II, pp. 1417-1487, University of Southern California, August 23-26, 1977.
31. D. K. Gartling, R. E. Nickell, and R. Z. Tanner, Internat. J. Numerical Meth. in Eng. 11, 1155-1174 (1977).
32. E. O. Macagno and T. K. Hung, J. Fluid Mech. 28, 43-67 (1967).
33. S.C.R. Dennis and J.D.A. Walker, J. Fluid Mech. 48, 771-789 (1971).

Chapter 6

APPLICATION TO FLUID-STRUCTURE INTERACTION

I. Introduction

In Chapter 4 a general three-dimensional finite element formulation was described for quasistatic and dynamic nonlinear shell analysis. This shell theory can easily be degenerated to an analogous two-dimensional formulation which includes several special cases of practical interest. Numerical examples indicate the good behavior of the elements studied.

In Chapter 3, the penalty function/finite element formulations of the Navier-Stokes equations was described. Numerical examples indicate the effectiveness of this scheme. The slightly compressible formulation for viscous fluid flow has been programmed and studied. As has been mentioned, one of the main advantages of this formulation over the penalty function formulation is that when a static solution is reached, all accelerations and velocities will approach zero. Hence, this slightly compressible approach will be used for the purpose of fluid-structure interactions.

As a practical application, the proposed finite element procedures are employed for the dynamic, three-dimensional, nonlinear, inelastic response of ground-supported, cylindrical liquid storage tanks which accounts for fluid-structure interaction and free-surface sloshing.

Early studies relevant to this topic were performed by Westergaard [1], Hoskins and Jacobsen [2], Jacobsen [3], Werner and

Sundquist [4], and Jacobsen and Ayre [5]. They assumed the tank to be rigid and the hydrodynamic wall pressures are then determined. Housner [6] developed an analytical method for determining hydrodynamic wall pressure under the same assumption that the tank is rigid. A mechanical equivalent model is developed and is widely used in current earthquake design practice [7].

Within recent years, studies performed by Veletsos [8], Yang [9], and Veletsos and Yang [10] have shown, however, that the rigid-tank assumption may lead to a significant under-estimation of the magnitude of the resulting forces. The first use of a digital computer in analyzing this problem with the aid of finite element methods was completed in 1969 by Edwards [11]. This investigation treated the coupled interaction between the elastic wall of the tank and the contained liquid. Recent developments along the same line were performed by Wu et al. [12] and Shaaban and Nash [13].

Haroun [14] recently conducted a theoretical and experimental investigation of the dynamic behavior of cylindrical liquid storage tanks to seek possible improvements in the design of such tanks to resist earthquakes. In this study, natural frequencies of vibration of the associated mode shapes are found through the use of a discretization scheme in which the elastic shell is modeled by finite elements and the fluid region is treated as a continuum by boundary solution techniques.

However, the methods cited are based on small motion linear response, and do not take satisfactory account of nonlinear effects observed in the field under the action of strong earthquakes,

such as lift-off of tanks from foundations, finite-amplitude sloshing, and nonlinear and inelastic tank response. Obviously a more advanced approach is called for. The whole subject is indeed very complicated and it is not the purpose of this thesis to perform a nonlinear tank study, yet the author hopes to have developed a tool which can be used eventually for that purpose and others.

Before we can perform a fluid-structure interaction calculation, a contact/sliding element is required to handle the sliding assumption of the fluid on the tank wall. We begin with the discussion of such a sliding element. A free-surface wave-propagation problem is then used to determine the effectiveness of the proposed mixed Lagrangian-Eulerian scheme. The classical static axisymmetrical buckling of elastic cylindrical shells subjected to three types of boundary conditions is then studied, followed by a buckling analysis of a tilted cylindrical liquid storage tank subjected to internal hydrostatic loading. Finally, a dynamic analysis of a liquid-filled cylindrical tank is performed to demonstrate the finite element fluid-structure interaction procedures.

II. Contact/Sliding Element

Contact elements may be used to impose inequality constraints between nodes. Either perfect friction (i.e., "stick") or frictionless (i.e., "slide") conditions may be achieved.

A contact element is defined by three nodes and a spring constant, or "penalty parameter," k , for our purposes. The connection from node A to node B defines the "slide line" direction; whereas, node C is the contact node (see Fig. II-1). The normalized projected distance of node C to node A is denoted by $\alpha \in [0,1]$ and is given by:

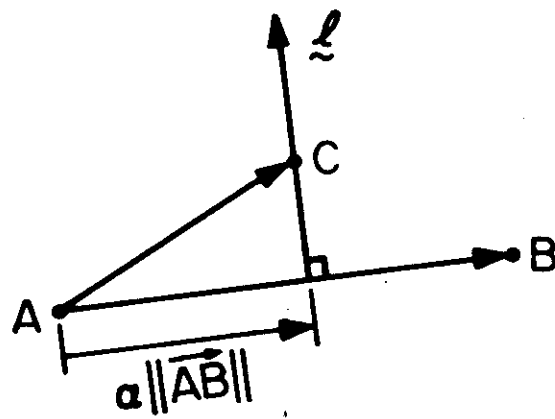


Fig. II-1 A contact element is defined by three nodes

$$\alpha = \vec{AC} \cdot \vec{AB} / \|\vec{AB}\|^2 \quad (II.1)$$

Here \vec{XY} denotes a vector connecting point X to point Y and " \cdot " is the dot product. The normal vector $\vec{\ell}$ from node C to \vec{AB} is defined by:

$$\vec{\ell} = (\vec{AB} \times \vec{AC}) \times \vec{AB} \quad (II.2)$$

$$\vec{\ell} \leftarrow \vec{\ell} / \|\vec{\ell}\| \quad (II.3)$$

where " \times " is the cross product and " \leftarrow " means "is replaced by." The local contact stiffness matrix \tilde{K}^{ℓ} is:

$$\tilde{K}^{\ell} = k \begin{bmatrix} (1-\alpha)^2 & \alpha(1-\alpha) & -(1-\alpha) \\ \text{sym} & \alpha^2 & -\alpha \\ & & 1 \end{bmatrix} \quad (II.4)$$

The rows and columns of the contact stiffness matrix are arranged in such a way that the first row or column corresponds to node A, while the 2nd row (or column) and 3rd row (or column) correspond to nodes B and C, respectively. Before the global assembly procedure, the local contact stiffness matrix is rotated to the global form \tilde{K}^G (for the sliding case) via:

$$\tilde{K}^G = \tilde{T}^T \tilde{K}^{\ell} \tilde{T} \quad (II.5)$$

$$\tilde{T} = \begin{bmatrix} \vec{\ell}^T & 0_{13} & 0_{13} \\ 0_{13} & \vec{\ell}^T & 0_{13} \\ 0_{13} & 0_{13} & \vec{\ell}^T \end{bmatrix} \quad (II.6)$$

$$\tilde{q}_{13} = [0 \quad 0 \quad 0] \quad (II.7)$$

For the sticking case \tilde{K}^G is

$$\tilde{K}^G = \begin{bmatrix} (1-\alpha)^2 & 0 & 0 & \alpha(1-\alpha) & 0 & 0 & -(1-\alpha) & 0 & 0 \\ & (1-\alpha)^2 & 0 & 0 & \alpha(1-\alpha) & 0 & 0 & -(1-\alpha) & 0 \\ & & (1-\alpha)^2 & 0 & 0 & \alpha(1-\alpha) & 0 & 0 & (1-\alpha) \\ & & & \alpha^2 & 0 & 0 & -\alpha & 0 & 0 \\ & & & & \alpha^2 & 0 & 0 & -\alpha & 0 \\ & & & & & \alpha^2 & 0 & 0 & -\alpha \\ & & & & & & 1 & 0 & 0 \\ & & & & & & & 1 & 0 \\ & & & & & & & & 1 \end{bmatrix} \quad (II.8)$$

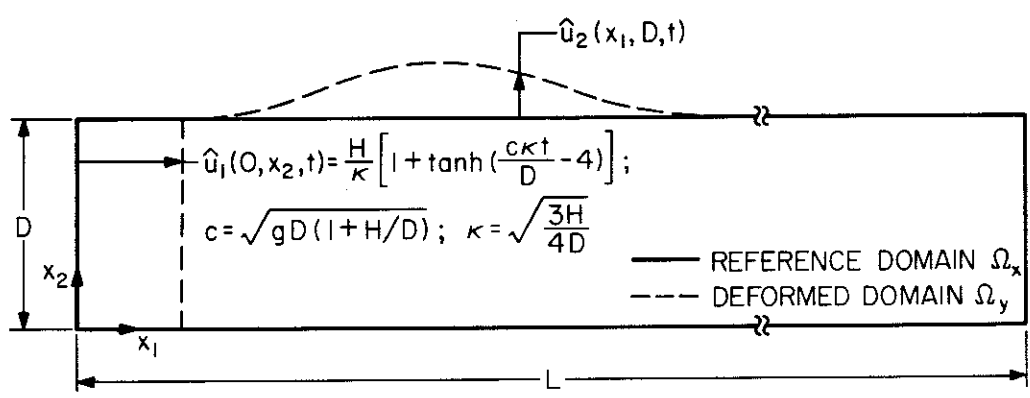
SYMMETRIC

III. Numerical Examples

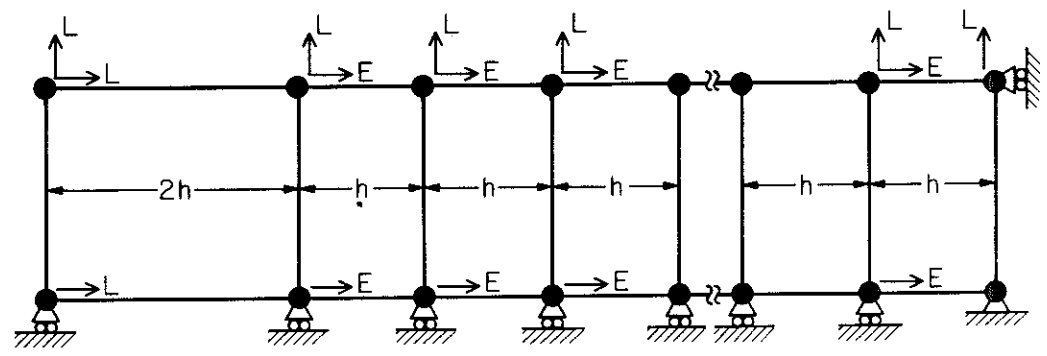
III-A. Free-Surface Wave-Propagation Problem

The problem statement and finite element meshes are shown in Figure IIA-1. We generate a wave numerically by prescribing a displacement-time history at the left-hand boundary of the domain. This prescribed function is designed in such a way that it is consistent with the experimental studies performed at Keck Laboratory of the California Institute of Technology. Its function is to produce a solitary wave--one in which the nonlinear and dispersive effects are balanced so that the wave propagates without distortion.

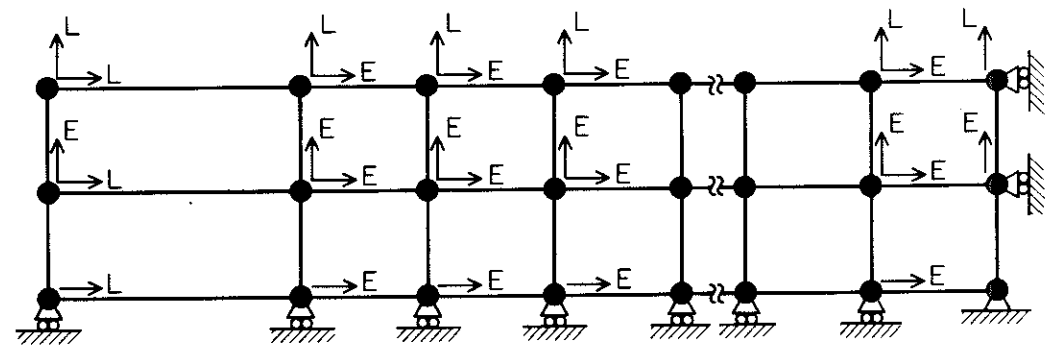
Data used in the analysis are given as follows: $g = 1$;
 $L = 949.095$; $D = 10$; $H = 0.86$, $h = 5.895$; and $\Delta t = h/c = 1.7888$.
 Meshes 1 and 2 consist of 160 and 320, 4-node elements, respectively.
 The flow was assumed inviscid, $\rho = 1$ and $\lambda = 2.6089 \times 10^7$.



(a) Problem statement and schematic of domains



(b) Finite element mesh 1



(c) Finite element mesh 2

Key { L - Lagrangian degree-of-freedom
 E - Eulerian degree-of-freedom

Fig. III A-1 Problem statement and finite-element meshes for free-surface flow

The finite element calculations employing a one-dimensional depth averaged theory [15] are compared with calculations for mesh 1, one element through the depth. The results are shown in Figure IIIA-2. The figure shows the results agree remarkably well, considering the two approaches are quite different. Notice that the rate of growth of the trough is a little greater with the present scheme than it is for the one-dimensional theory. Even though there is good agreement between the two theories, experimental results are not consistent with the previously obtained numerical results. The differences are: (1) the experimental waveform propagates somewhat faster and exhibits less amplitude decay; and (2) dispersion emanating from the back of the wave is not seen experimentally.

The reason for the discrepancy between the numerical and experimental results is the variation of the velocity through the depth is not linear. Both the one-dimensional depth average theory and one element through the depth, two-dimensional theory invoke this assumption. As can be seen in Figure IIIA-3, with two elements through the depth, the trough has been reduced and the relative wave height is essentially constant with propagation. The difference in having two instead of one element in depth is that the distribution of velocity is no longer constrained to be linear with depth.

It is also noted experimentally that "noise" superposed upon a solitary wave tends to propagate at a slower velocity than the main pulse. A numerical simulation of this phenomenon is shown in Figure IIIA-4. The noise is generated by setting a no-slip boundary condition

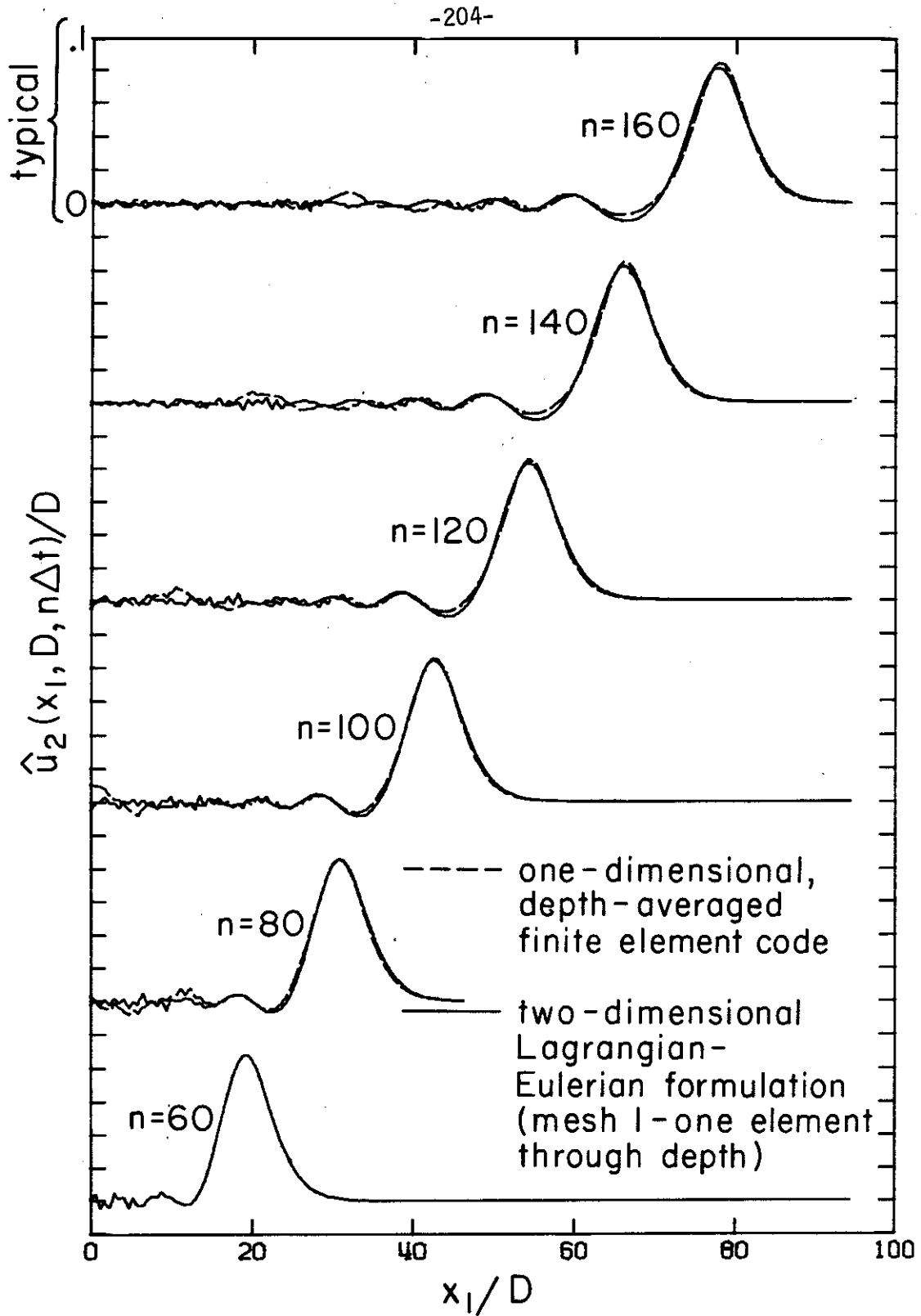


Fig. III A-2 Comparison of one-dimensional depth-averaged theory and two-dimensional Lagrangian-Eulerian formulation

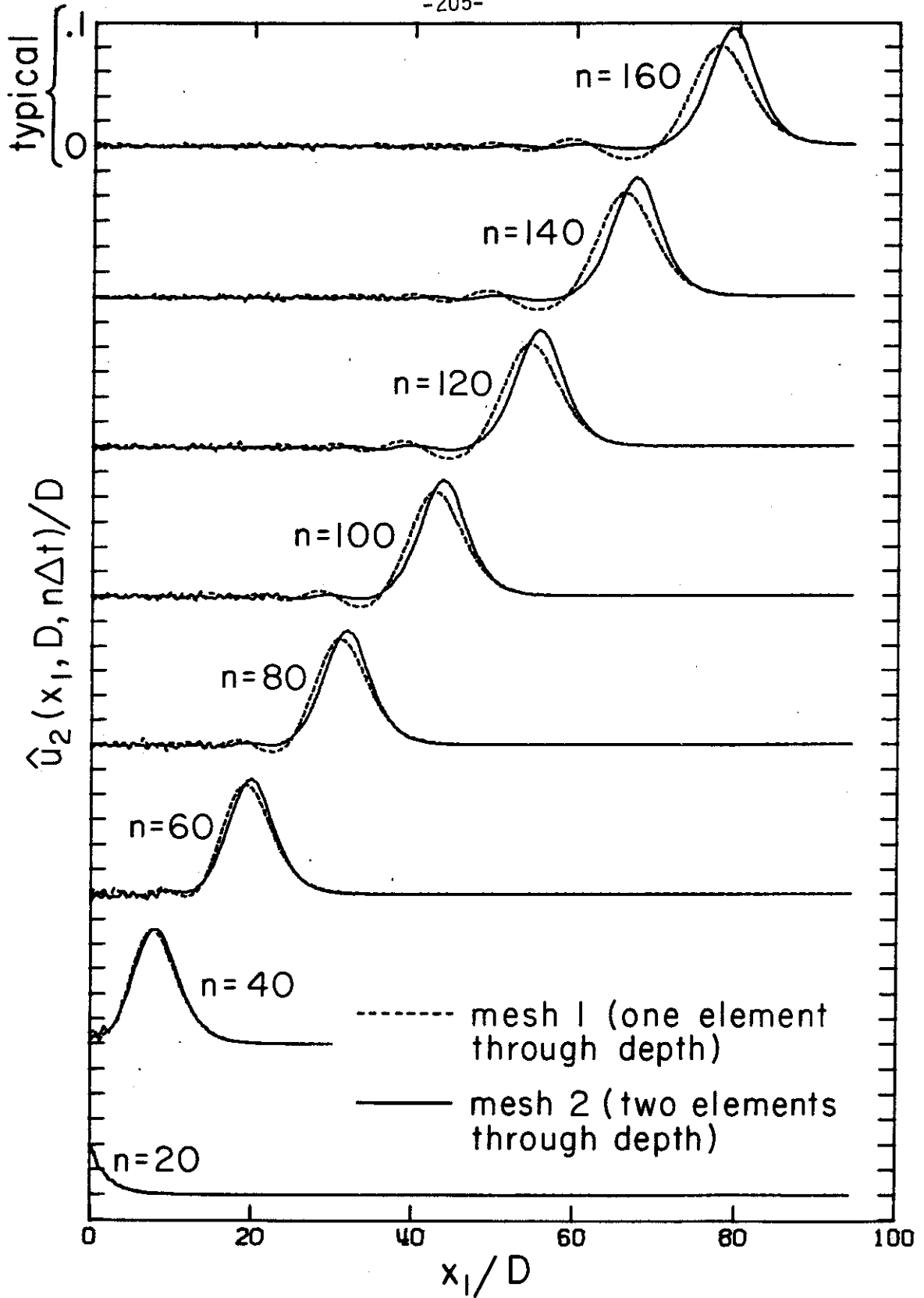


Fig. III A-3 Comparison of results for meshes 1 and 2

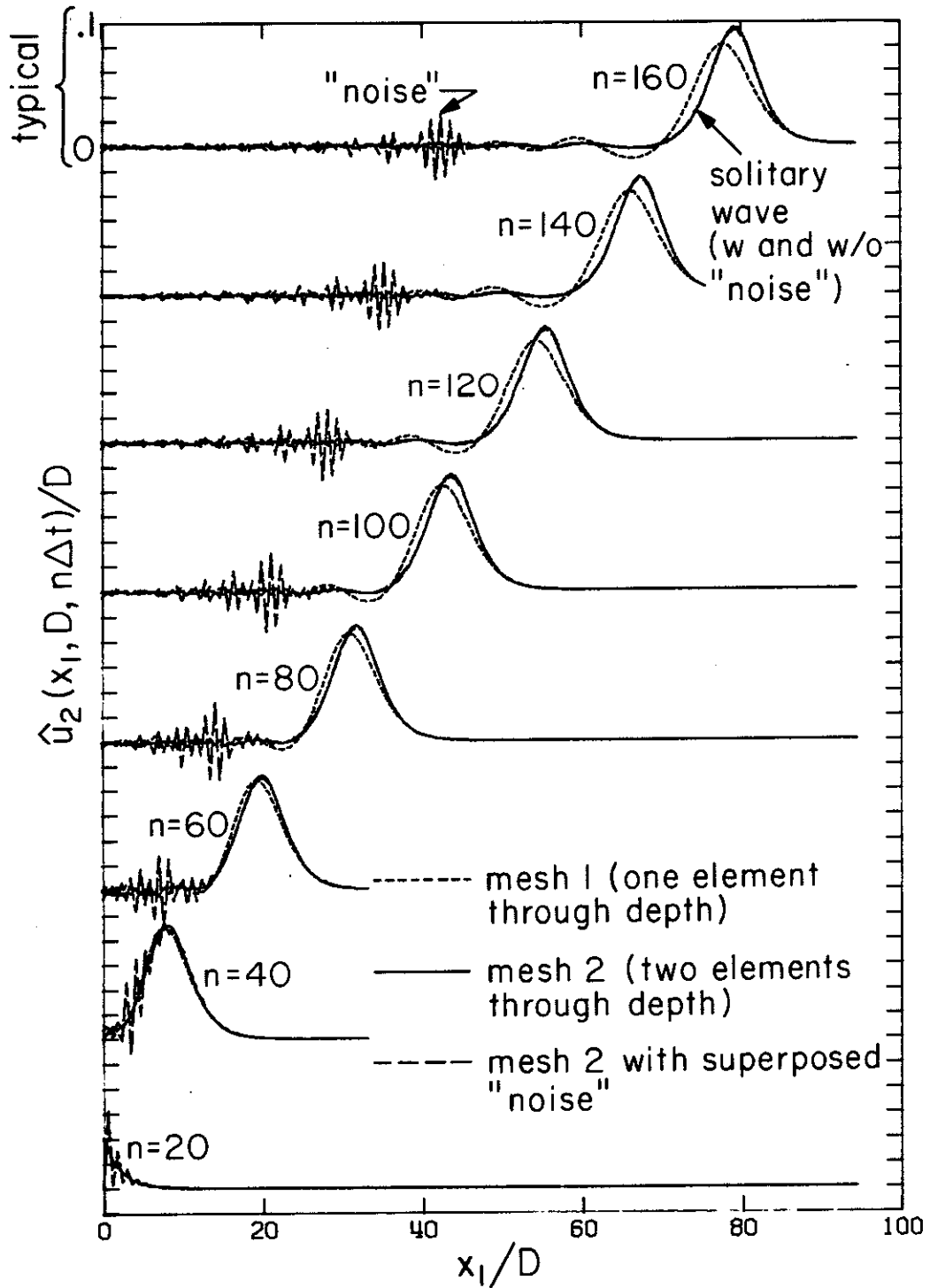


Fig. III A-4 Comparison of results with, and without, superposed "noise"

along the left-hand edge of the domain, in contrast to previous calculations in which a slip condition was employed. Note how the solitary wave emerges, unaffected by the initial perturbations.

III-B. Static Axisymmetric Buckling of Elastic Cylindrical Shells

Three types of boundary conditions were employed in this study:

- a) bottom fixed--top free;
- b) bottom fixed--top fixed with respect to horizontal displacement and rotation; and
- c) bottom simply supported--top fixed with respect to horizontal displacement.

Load versus displacement data and deformed profiles are shown in Figure IIIB-1 up to the buckling loads at which time the calculations were terminated. Comparison is made with analytical results based upon eigenvalue analysis (see e.g., [16]).

III-C. Cylindrical Shell Containing a Fluid

An analysis was performed of a tilted cylindrical shell subjected to internal hydrostatic loading. The problem statement is shown in Figure IIIC-1, along with the stress results prior to any significant nonlinear phenomena. Data employed in this analysis are given as follows:

$$E = 7.35 \times 10^5 \text{ lb/in}^2 \quad (\text{Young's modulus})$$

$$\nu = 0.3 \quad (\text{Poisson's ratio})$$

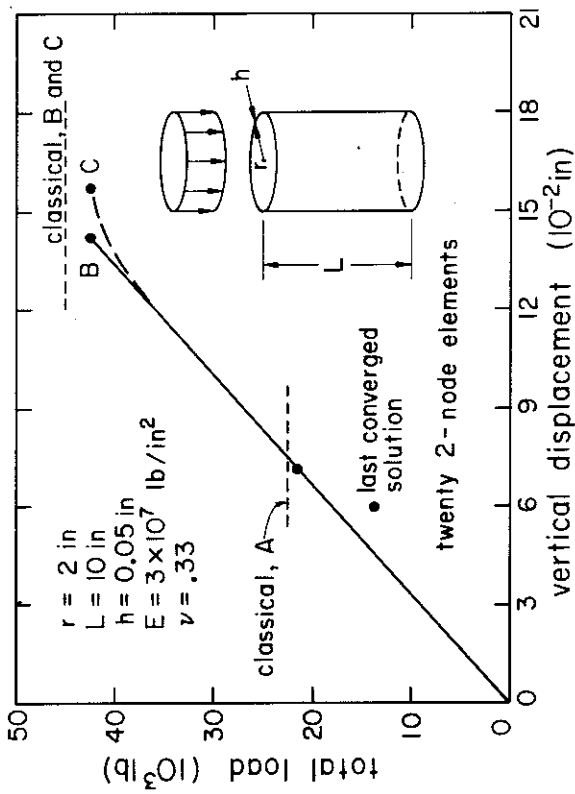
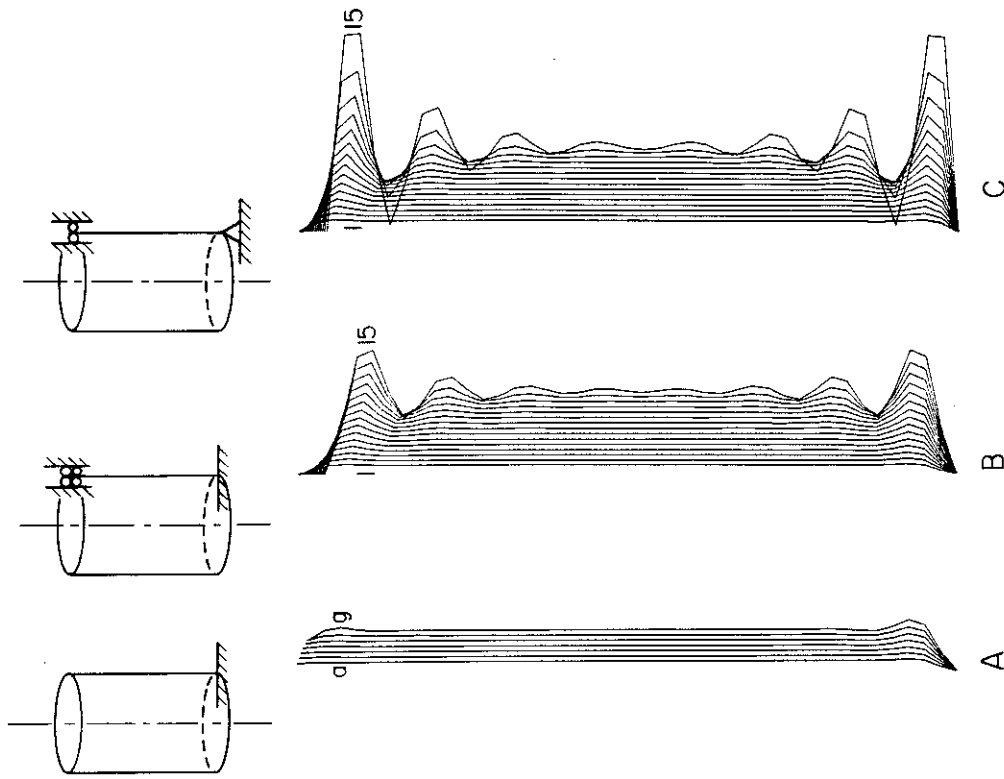
$$D = 16.0 \text{ in}$$

$$L = 20.0 \text{ in}$$

$$R = 4.0 \text{ in}$$

$$h = 0.01 \text{ in}$$

$$\alpha = 30.0^\circ$$



profile	load (10^3 lb)	profile	load (10^3 lb)
a	5.0	1	5.0
b	10.0	2	7.5
c	15.0	3	10.0
d	17.5	.	.
e	20.0	.	.
f	20.5	.	.
g	21.0	15	40.0

Fig. III B. Static axisymmetric buckling of elastic cylindrical shells.

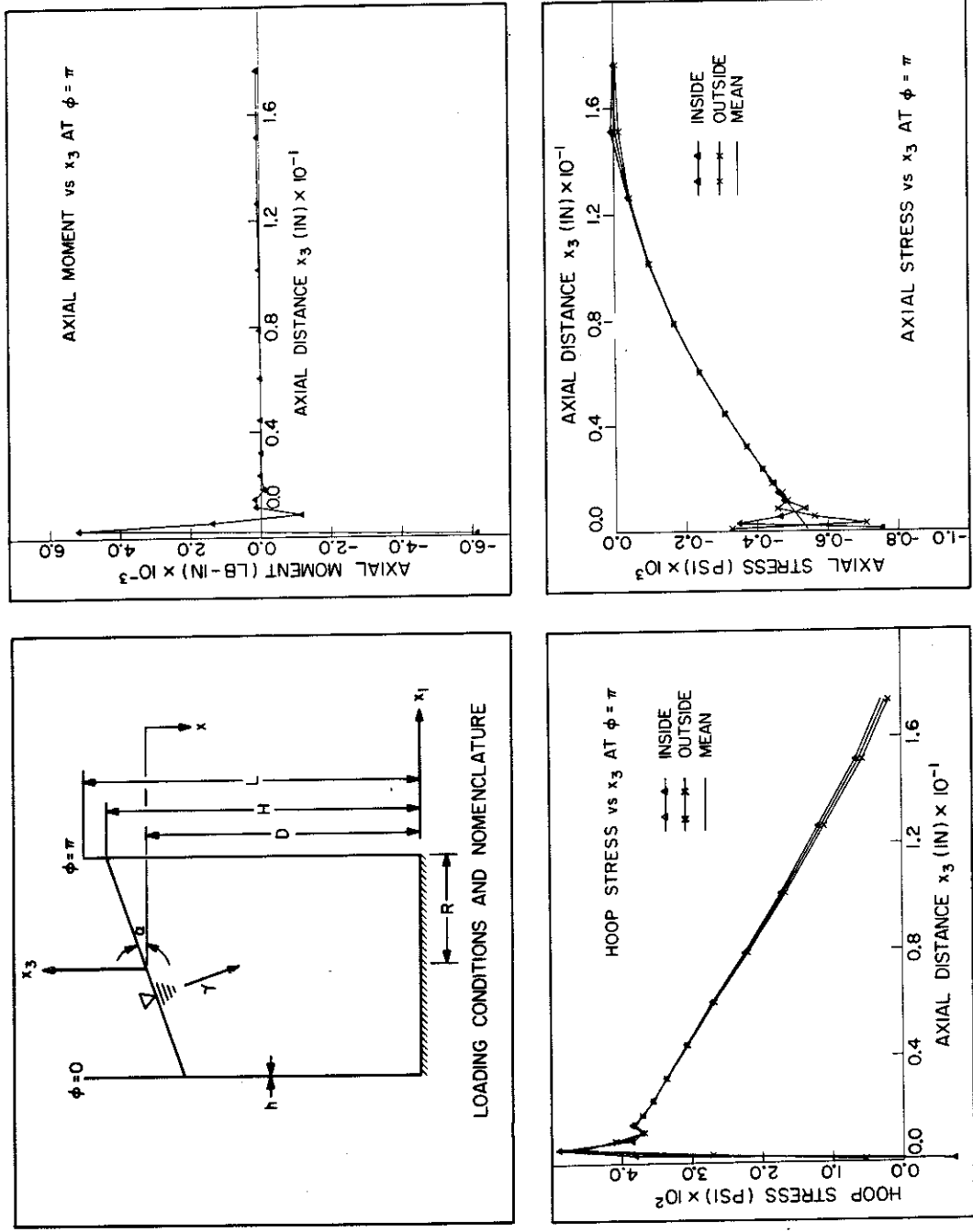


Fig.III-C-1. Tilted cylindrical shell subjected to internal hydrostatic loading. Stress results in the linear regime.

$$\gamma = 0.0361 \text{ lb/in}^3 \quad (\text{density of water})$$

The effective specific gravity, γ_{eff} , was defined to be $\gamma_{\text{eff}} = \gamma g$. The value of g used in obtaining the stresses shown in Figure IIIC-1 was 1.8. Comparison with a membrane theory solution [17] confirmed the correctness of the numerical results outside of the boundary layer at the fixed end. Buckling calculations were performed by incrementing g . Results are shown in Figures IIIC-2 and IIIC-3. As may be seen, the initial bifurcation occurred in attempting to increment g beyond 1.8. This corresponds to a maximum axial membrane stress of 547.53 psi at $x = L$, $\phi = \pi$, which is approximately half the classical value. Although this result was not anticipated, it bears a great deal of similarity to results obtained by Argyris and Dunne [18] in their penetrating study of a compressed cylindrical panel. They too found an initial bifurcation of approximately half classical. When they pursued the analysis into the post-buckled regime, a drop in load of only 3% was noted, at which time the load was able to be increased again to a value in the vicinity of classical. At this point a second, and more significant bifurcation ensued, and this was followed by several more bifurcations. An important point in considering the results of Argyris and Dunne was that a preliminary eigenvalue analysis, employing the same mesh used in the finite deformation case, yielded a buckling load approximating the classical value on the high side. This lends credence to the analysis, but a full understanding of the computed initial bifurcation in this case, and the present case, does not yet seem to exist. The results shown were obtained using S1 elements. Similar results were also obtained

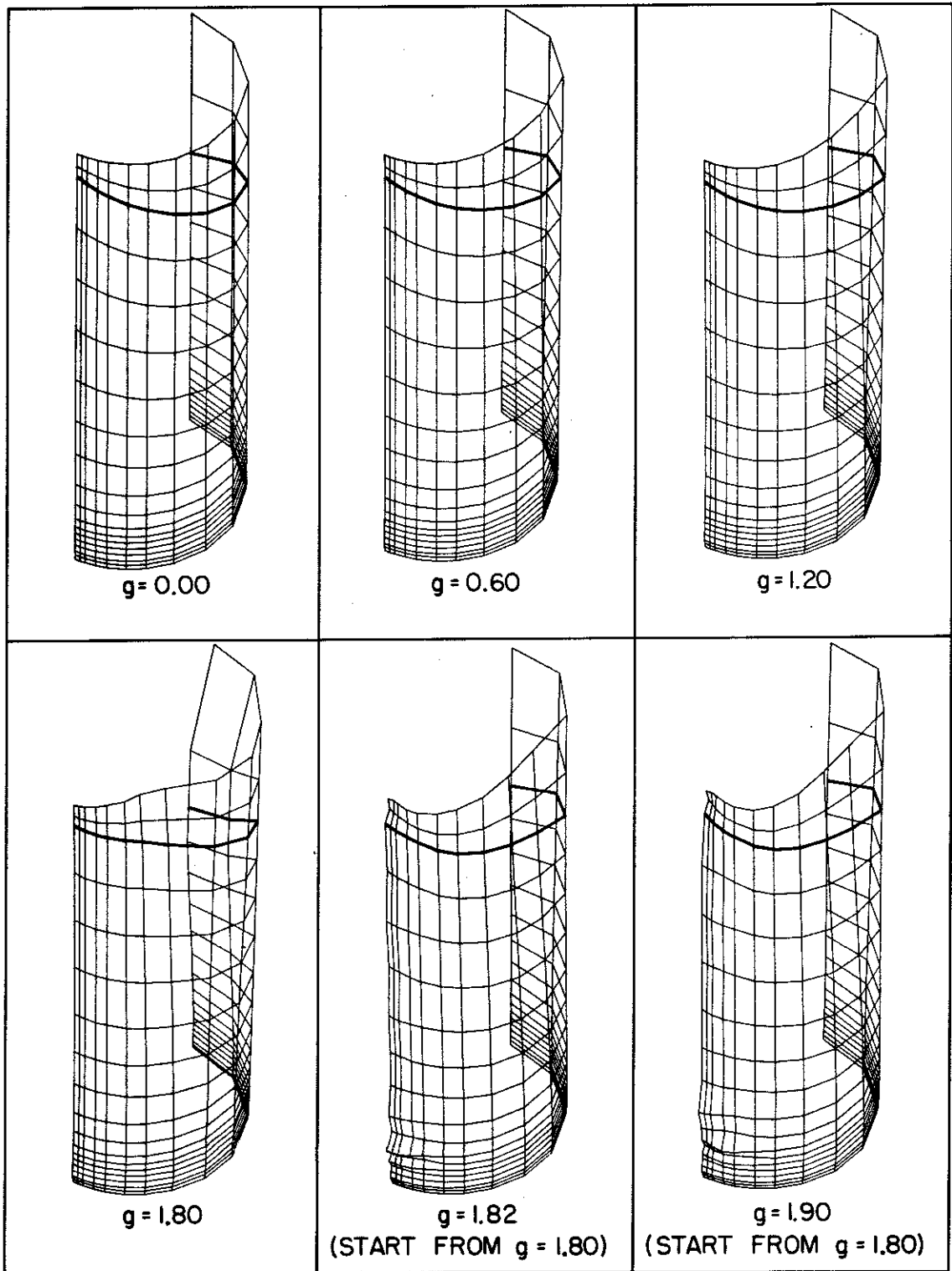


Fig.III C-2. Deformed configurations for the tilted cylindrical shell.

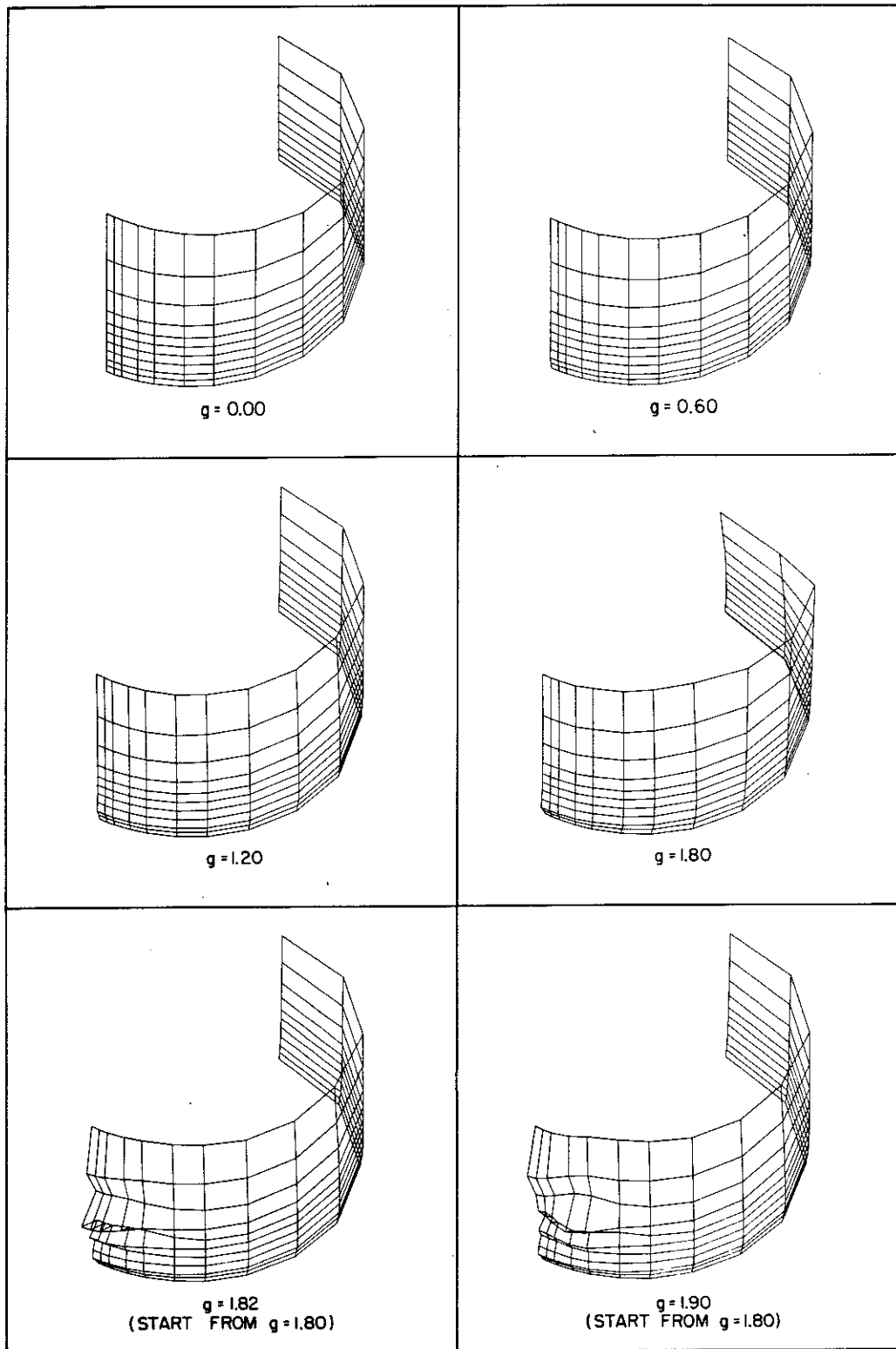


Fig.III C-3. Detail of lower regions for the tilted cylindrical shell.

with heterosis elements.

III-D. Dynamic Analysis of a Liquid Filled Cylindrical Tank

A dynamic analysis was performed of a liquid filled cylindrical tank subjected to a periodic saw-tooth ground acceleration excitation. The problem statement is shown in Figure IIID-1, along with displacement, velocity, and acceleration time histories at three different positions (node A, B, and C). The tank is subjected to the mentioned excitation in the x-direction only. Therefore all the bottom nodes of the tank are subjected to the same excitation with the other two directions (y and z) fixed. A typical input ground excitation (acceleration, velocity, and displacement) is given for node A. Due to symmetry, only half the tank is modeled by 36 S1 shell elements, 80 uniform-reduced integration 8-node fluid elements, and 30 sliding elements. The height of the tank is 864 ins (i.e., distance between A and C). The mean diameter of the tank is 577 in. (i.e., distance between B and C). The tank thickness is 1 inch. It is filled with water up to 720 in. The material properties of the tank and water are:

Tank (steel):

$$E = 3.0 \times 10^7 \text{ psi}$$

$$\nu = 0.3$$

$$\rho = 7.324 \times 10^{-4} \text{ lb sec}^2/\text{in}^4$$

$$\sigma_y = 3.0 \times 10^4 \text{ psi} \quad (\text{yield stress})$$

$$B = 0.0 \quad (\text{plastic modulus})$$

Water:

$$\beta = 6.991 \times 10^{12} \text{ psi} \quad (\text{bulk modulus})$$

$$\mu = 0.0 \quad (\text{dynamic viscosity})$$

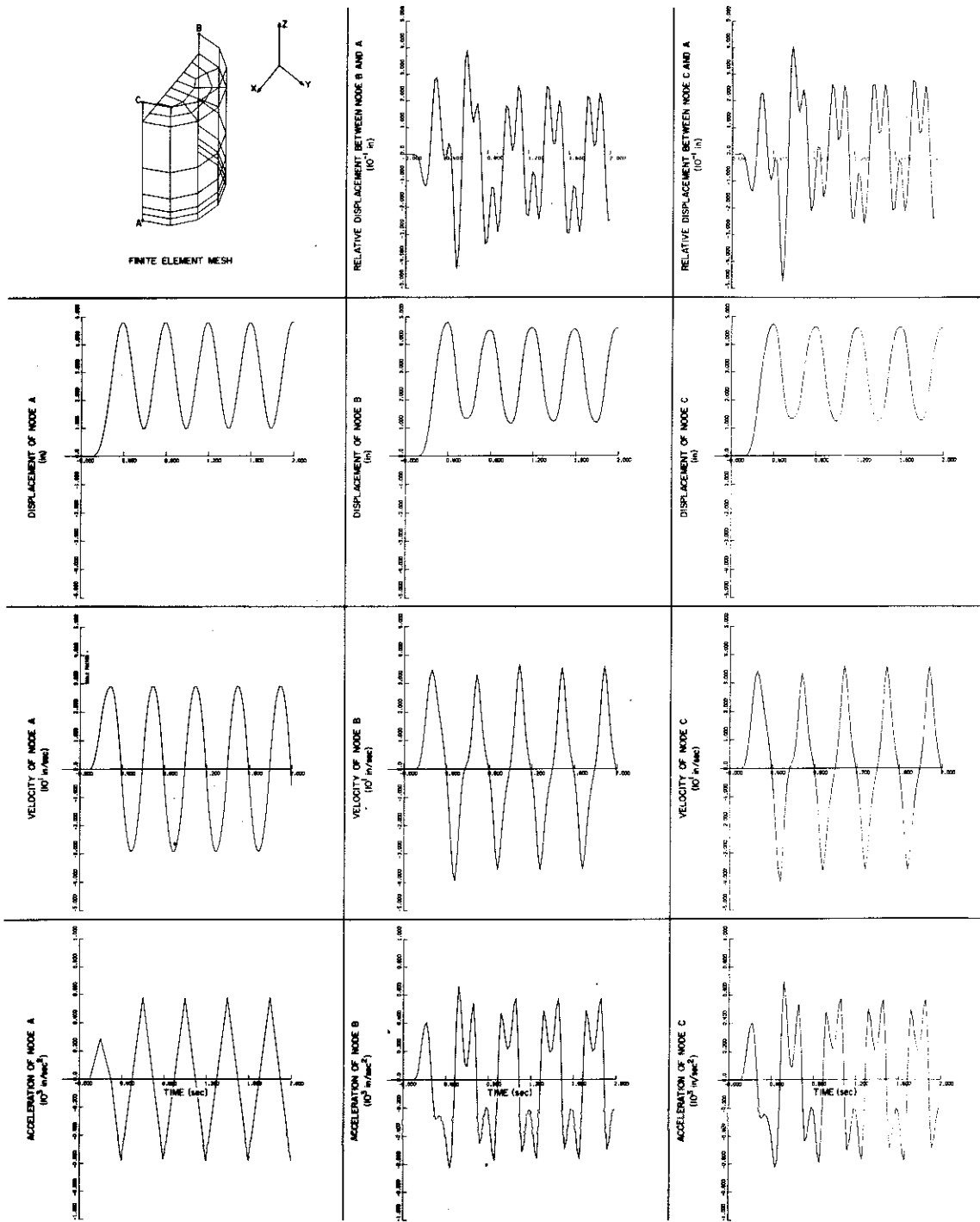


Fig. IIID-1.

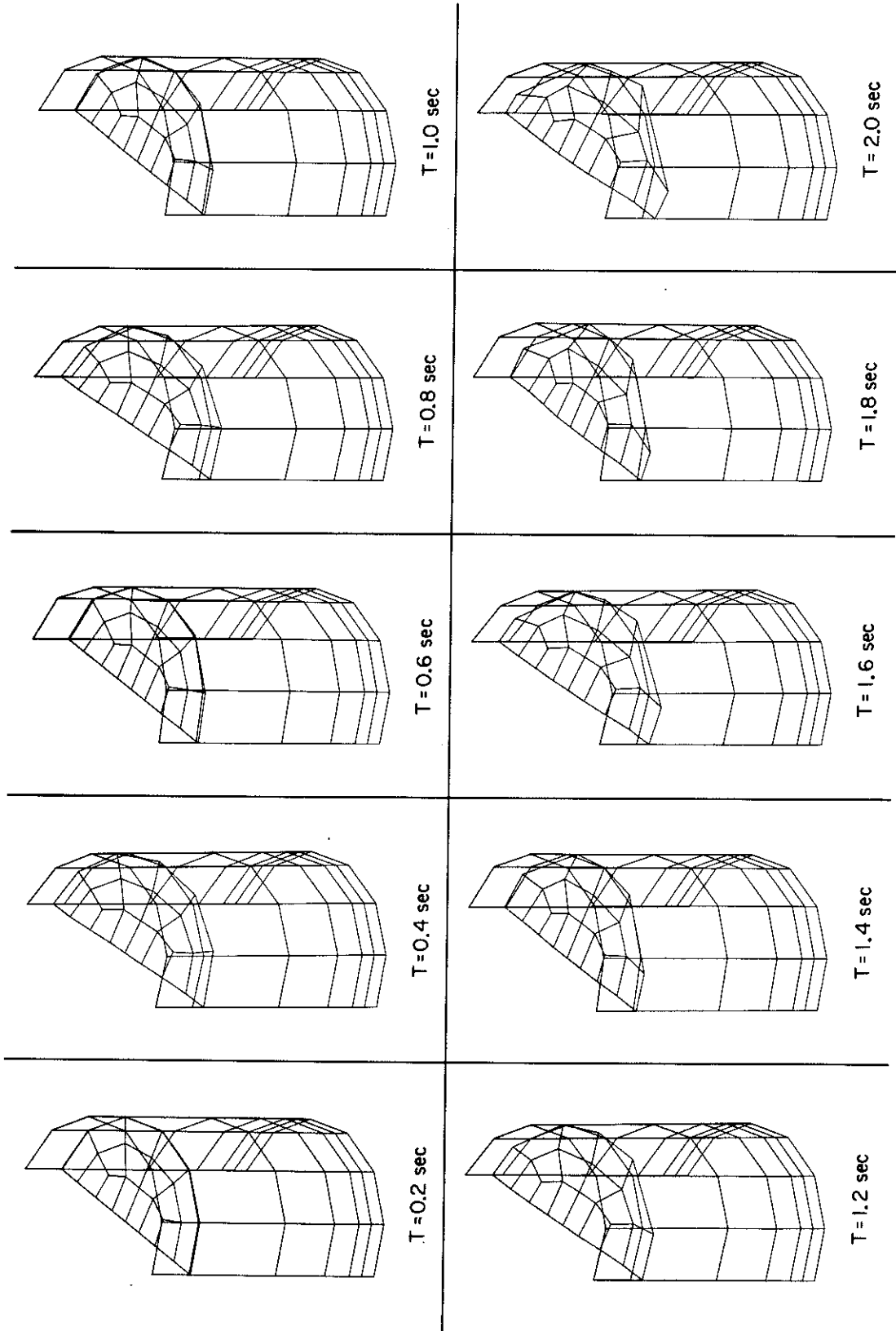


Fig. III D-2.

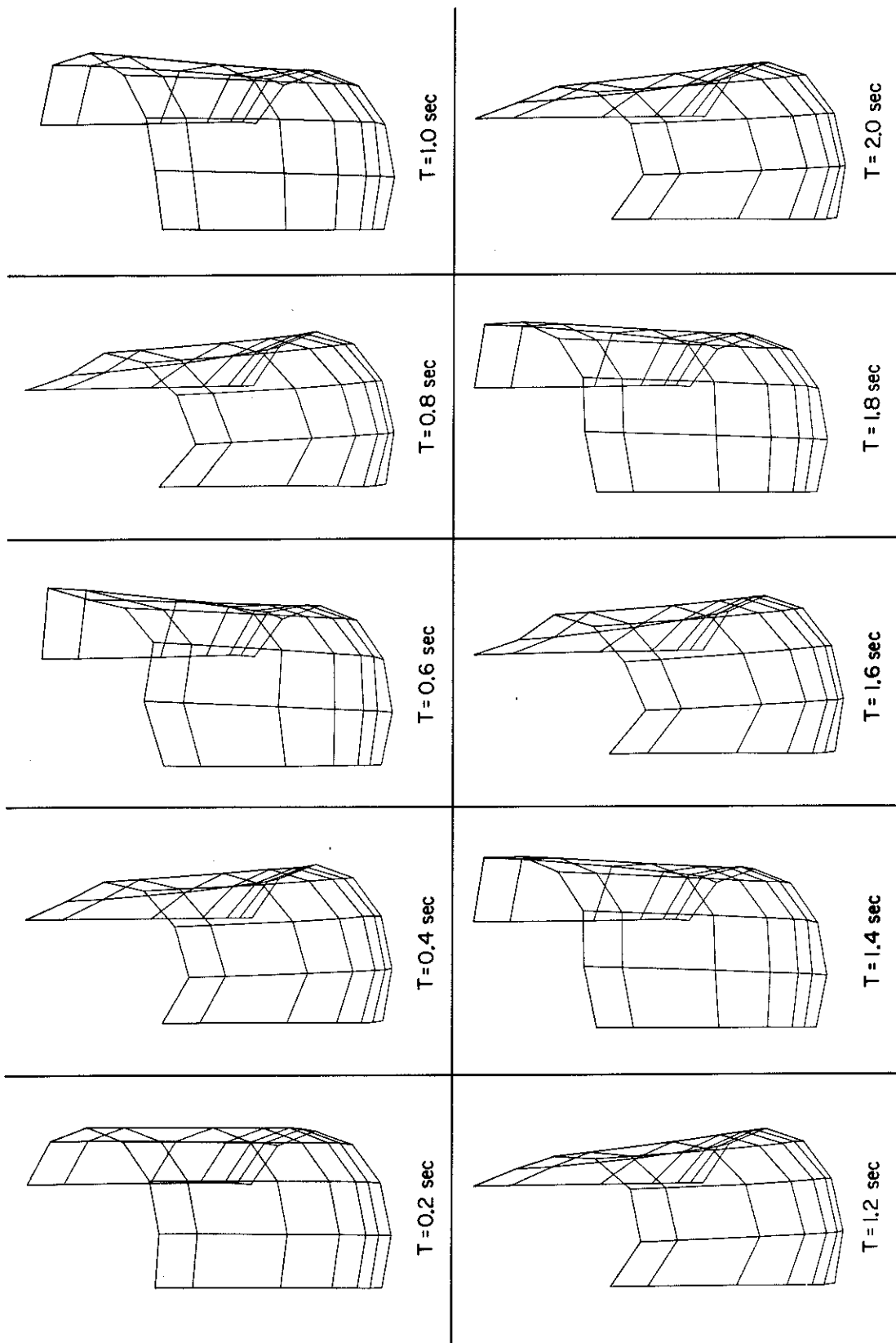


Fig. III D - 3.

$$\rho = 9.349 \times 10^{-5} \text{ lb sec/in}^4$$

$$g = 3.864 \times 10^2 \text{ in/sec}^2 \quad (\text{gravity})$$

The spring constant, k , of the contact elements is taken to be 4.44×10^{16} psi. The Newmark parameters are: $\beta = 0.5625$, $\gamma = 1.0$, and $\Delta t = 0.02$ sec. A linear implicit-nonlinear explicit operator splitting algorithm with one iteration is employed. A small deformation analysis option is used. The maximum computed stress occurring in the tank is less than σ_y even though the peak ground excitation is 1.5 g. The relative free surface motion as well as the relative tank displacement is within the small motion region. Therefore, no further analysis of this problem was performed. The computed acceleration, velocity, and displacement time histories of nodes B and C as well as the relative displacement between nodes B and A and between nodes C and A are shown in Figure IIID-1. It is expected that the fundamental mode is dominant for this kind of excitation; also nodes B and C are expected to respond in "phase." This phenomenon can be seen from the absolute displacement-time histories of nodes B and C in the figure.

The deformed shape of the tank and the free surface motion (with the input translational motion subtracted) are shown in Figure IIID-2 at a time interval of 0.2 seconds. The magnification factor of these plots is 7.81. Frequency responses higher than the fundamental sloshing frequency were observed. The sloshing period is approximately 6 seconds. Since the free surface motion is much larger than the tank deformation, plots of the tank response (with the input translational motion subtracted) are shown in Figure IIID-3, magnified by a factor of 76.31.

References

1. H. M. Westergaard, "Water pressure on dams during earthquakes," Trans. ASCE 98 (1933).
2. L. M. Hoskins and L. S. Jacobsen, "Water pressure in a tank caused by a simulated earthquake," Bull. SSA 24 (1934).
3. L. S. Jacobsen, "Impulsive hydrodynamics of fluid inside a cylindrical tank and of a fluid surrounding a cylindrical pier," Bull. SSA 39 (1949).
4. P. W. Werner and K. J. Sundquist, "On hydrodynamic earthquake effects," Trans. AM Geophys. Union 30 (1949).
5. L. S. Jacobsen and R. S. Ayre, "Hydrodynamic experiments with rigid cylindrical tank subjected to transient motions," Bull. SSA 41 (1951).
6. G. W. Housner, "Dynamic pressures on accelerated fluid containers," Bull. SSA 47 (1957).
7. G. W. Housner, "The dynamic behavior of water tanks," Bull. SSA 53, (1963).
8. A. S. Veletsos, "Seismic effects in flexible liquid storage tank," Proc. 5th World Conf. on Earthquake Eng. 1, 1974.
9. J. Y. Yang, "Dynamic behavior of fluid-tank systems," Ph.D. thesis, Rice University, Houston, Texas, 1976.
10. A. S. Veletsos and J. Y. Yang, "Dynamics of fixed-base liquid-storage tanks," Proc. U.S.-Japan Seminar on Earthquake Eng. Research with Emphasis on Lifeline Systems, Tokyo, Nov. 1976, pp. 317-341.
11. N. Edwards, "A procedure for the dynamic analysis of thin walled cylindrical liquid storage tanks," Ph.D. thesis, U. of Michigan, Ann Arbor, Mich., 1969.
12. C. I. Wu, T. Mouzakis, W. A. Nash, and J. M. Colonell, "Natural frequencies of cylindrical liquid storage containers," Dept. of Civil Eng., University of Massachusetts, June 1975.

13. S. H. Shaaban and W. A. Nash, "Response of an empty cylindrical ground supported liquid storage tank to base excitation," Dept. of Civil Eng., University of Massachusetts, August 1975.
14. M. A. Haroun, "Dynamic analysis of liquid storage tank," Ph.D thesis, California Institute of Technology, Dec. 1979.
15. D. G. Goring, "Tsunamis--The propagation of long waves onto a shelf," Ph.D. thesis, Report No. KH-R-38, California Institute of Technology, Nov. 1978.
16. S. P. Timoshenko and J. M. Gere, Theory of Elastic Stability (McGraw-Hill Book Co., New York, 1961).
17. C. Shih and C. D. Babcock, Jr., Private communication.
18. J. H. Argyris and P. C. Dunne, "Post-buckling, finite element analysis of circular cylinders under end load," Report 224, Institut für Statik und Dynamik der Luft und Raumfahrtkonstruktionen, University of Stuttgart, Germany, 1977.

Chapter 7

SUMMARY AND SUGGESTIONS FOR FURTHER DEVELOPMENT

In this thesis, finite element procedures for fluid-structure interaction problems have been developed. Different aspects of nonlinear methodologies have been studied. A working finite element method computer code [15], which will be discussed in a separate report, has been developed which may be applied to the dynamic, three-dimensional, nonlinear, inelastic analysis of ground-supported, cylindrical liquid storage tanks subjected to strong shaking, and various other fluid-structure phenomena. This is a significant step toward the development of a clean general purpose, modularized, fluid-structure interaction, finite element computer program that engineers will find helpful.

Future fluid-structure analysis developments will need to include improved transient algorithms, better fluid-structure interfacing techniques, and contact-impact techniques.

Automatic time stepping strategies based upon accuracy considerations [1,2], subcycling techniques [3-5], and effective iterative equation solvers [6-9] will be generalized and eventually included in this fluid-structure computer program. The presently developed, slightly compressible fluid formulation is a step towards the inclusion of a compressible formulation, although further studies are clearly required.

The mixed Lagrangian-Eulerian method seems to treat fluid-structure interaction problems with large motions of the structure naturally and economically. However, for large-deformation bubble

dynamics calculations [10] that occur, for example, in light water reactor systems, "continuous rezoning" of meshes, together with mixed Lagrangian-Eulerian methods are required. As rezoning is expensive and difficult to do adaptively, other techniques are called for. Hirt and Nichols [11] proposed a volume-of-fluid finite difference method (VOF) in which the boundary of the free surface is not specified directly, but instead is defined by the fraction of fluid in each cell. The fraction of fluid is treated as a cell variable and governed by a transport equation. This technique can permit the solution of very complicated free-surface problems (e.g., bubble dynamics, etc.). It is not yet clear how to develop VOF finite element methods due to the more general topology of finite element meshes compared with finite differences. A combination of VOF and mixed Lagrangian-Eulerian methods may be an effective compromise.

The contact/sliding element proposed here for fluid-structure interaction problems cannot be used directly for tanks lifting off from their foundations, and the resulting large-amplitude sloshing causing roof damage. This contact element, together with the contact-impact technique developed by Hughes et al. [12,13] and Hallquist [14] can serve the purpose and would be a worthwhile generalization.

Finally, a word of caution is in order regarding the ability of the present capabilities to solve general problems of fluid and structural response. Although a degree of confidence has been established in certain realms of phenomena, it should be emphasized that the present developments are incapable of solving many problems of

physical interest and application of these techniques in such circumstances is speculative at best. Areas which are particularly difficult and presently beyond the developed capabilities are (among others) high Reynolds' number flows and complex shell buckling. Much numerical research still needs to be done in these areas.

References

1. K. C. Park and P. G. Underwood, "A variable-step central difference method for structural dynamic analysis, Part I: Theoretical aspects," ASME Paper No. 79-PVP-120, presented at the Pressure Vessels and Piping Conference, San Francisco, CA, June 25-29, 1979.
2. P. G. Underwood and K. C. Park, "A variable-step central difference method for structural dynamics analysis, Part II: Implementation and performance evaluation," ASME Paper No. 79-PVP-121, presented at the Pressure Vessels and Piping Conference, San Francisco, CA, June 25-29, 1979.
3. T. Belytschko, H. J. Yen, and R. Mullen, "Mixed methods for time integration," *Computer Methods in Appl. Mech. and Eng.* 17/18, 259-275 (1979).
4. J. P. Wright, "Mixed time integration schemes," *Computers and Structures* 10, 235-238 (1979).
5. J. Isenberg, D. K. Vaughan, I. Sandler, "Nonlinear soil-structure interaction," EPRI NP-945, Project 810-2, Final Report, Dec. 1978.
6. M. A. Crisfield, "A faster modified Newton-Raphson iteration," *Computer Meth. in Appl. Mech. and Eng.* 20, 267-278 (1979).
7. M. A. Crisfield, "Iterative solution procedure for linear and non-linear structural analysis," TRRL Laboratory Report 900, Dept. of Transportation, 1979.
8. T.J.R. Hughes and J. M. Winget, "Symmetric and nonsymmetric equation solvers," to appear.
9. T.J.R. Hughes, "Implicit-explicit finite element techniques for symmetric and nonsymmetric systems," *Proc. Conf. on Nonlinear Problems in Mechanics*, University of Swansea, Swansea, U.K., Sept. 2-5, 1980.
10. J. Donea, P. Fasoli-Stella, S. Giuliani, J. P. Halleux, and A. V. Jones, "An arbitrary Lagrangian-Eulerian finite element procedure for transient dynamic fluid-structure interaction problems," paper No. B1/3, *Trans. 5th Internat. Conf. on Structural Mechanics*

- in Reactor Technology, Berlin, Germany, Aug. 13-17, 1979.
11. C. W. Hirt and B. D. Nichols, "Eulerian method with free boundaries," in Preprints of the 1st Internat. Seminar on Fluid Structure Interactions in LWR Systems, International Congress Center, Berlin, (West) Germany, Aug. 20-21, 1979 (T. Belytschko, ed.), pp. 29-42.
 12. T.J.R. Hughes, R. L. Taylor, J. L. Sackman, A. Currier, W. Kanoknukulchai, "A finite element method for a class of contact-impact problems," *Computer Meth. in Appl. Mech. and Eng.* 8, 249-276 (1976).
 13. T.J.R. Hughes, W. Kanoknukulchai and R. L. Taylor, "A finite element method for large displacement contact and impact problems," in Formulation and Computational Algorithms in Finite Element Analysis (M.I.T. Press, Cambridge, 1977).
 14. J. O. Hallquist, "A numerical treatment of sliding interfaces and impact," Computational Techniques for Interface Problems, AMD 30, ASME, 1978.
 15. W. K. Liu, "FLUSTR, A fluid-structure interaction finite element analysis computer program," User's manual, in preparation.